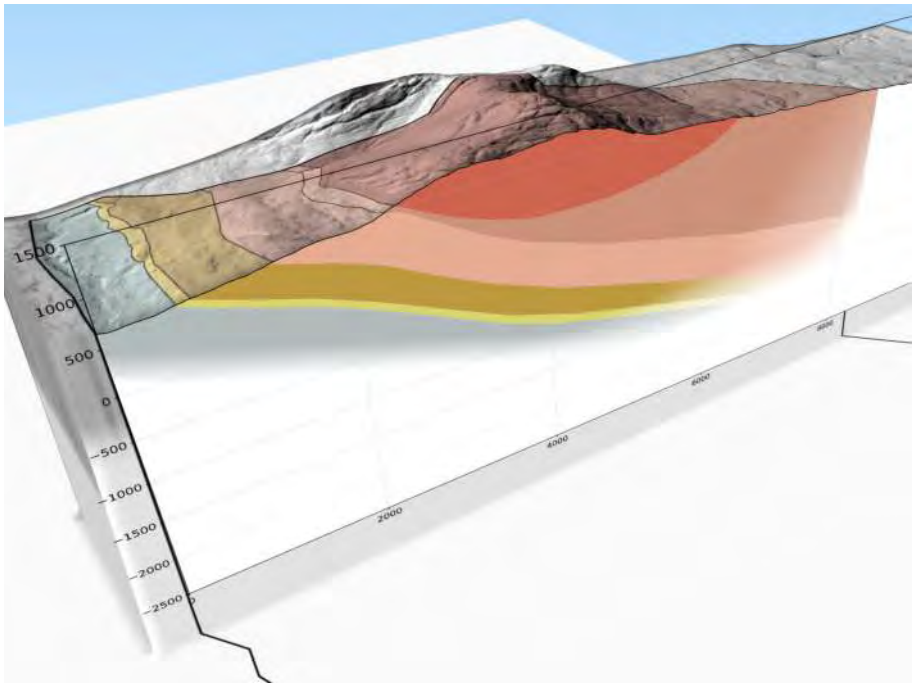
Understanding the West Jämtland nappe stack, Scandinavian Caledonides

Gustaf Larsson

2023



Whatever the outcome of these questions, the Jämtlandian section of the Scandinavian-Caledonian mountain zone, by virtue of the Törnebohmian theory, will likely be seen as classical ground for the type of mountain-building where thrust tectonics of gigantic proportions leaves its mark in the landscape.

Translated from
Högbom (1920)

Table of Contents

1 Introduction **5**

2 Geological Setting **7**
2.1 Opening and closure of the Iapetus Ocean 7

3 Architecture of the Scandinavian Caledonides **8**
3.1 Upper Allochton 8
3.2 Middle Allochton 8
3.2.1 Seve Nappe Complex 11
3.2.2 Upper Seve Nappes 11
3.2.3 Middle Seve Nappes 11
3.2.4 Lower Seve Nappes 12
3.2.5 Särv Nappes 12
3.2.6 Offerdal Nappes 12
3.3 Lower Allochton 13

4 Regional framework **13**
4.1 Naming conventions 15

5 Previous mapping of Åreskutan **15**
5.1 Metamorphic framework 23

6 Methods **23**
6.1 Field mapping 23
6.2 Map data processing 23
6.3 Sample selection and preparation 23

7 Results **28**
7.1 The nappe stack on Åreskutan 28
7.2 Åreskutan Nappe 28
7.2.1 Paragneiss 29
7.2.2 Felsic orthogneiss 35
7.2.3 Metabasite 36
7.2.4 Palaeosome, pegmatite and curiosities 42
7.2.5 Deformation history 44
7.2.6 Metamorphic history 57
7.3 Kall Nappe 62
7.3.1 Mörvikshummeln Formation 62
7.3.2 Calc-silicate gneiss 62
7.3.3 Amphibolite 68
7.3.4 Leucogranite 68
7.3.5 Marble 68
7.3.6 Rödkullen Formation 75
7.3.7 Amphibolite 75
7.3.8 Metasandstone 78
7.3.9 Micaschist 80
7.3.10 Deformation history 84
7.3.11 Metamorphic history 100
7.4 Särv Nappe 104
7.4.1 Metadolerite 104
7.4.2 Metasandstone 105
7.4.3 Micaschist 105
7.4.4 Deformation history 109

7.4.5 Metamorphic history . . . 113
7.5 Offerdal Nappe . . . 117
7.5.1 Metasandstone . . . 117
7.5.2 Semipelitic micaschist . . . 121
7.5.3 Deformation history . . . 121
7.5.4 Metamorphic history . . . 128
7.6 Jämtlandian Nappe Complex . . . 129
7.7 Tectonic Boundaries . . . 130
7.7.1 The Kall-Åreskutan Nappe boundary . . . 130
7.7.2 Internal boundary in the Kall Nappe? . . . 134
7.7.3 The Särv-Kall Nappe Boundary . . . 134
7.7.4 The Offerdal-Särv Nappe boundary . . . 135
7.7.5 The Lower-Middle Allochton boundary . . . 135
7.8 Geological maps and cross-sections . . . 135

8 Discussion **137**
8.1 Geological map . . . 137
8.2 Geometry of the nappe stack . . . 138
8.3 P-T path and assembly of the nappe stack . . . 146
8.3.1 Åreskutan Nappe . . . 146
8.3.2 Kall Nappe . . . 150
8.3.3 Särv and Offerdal Nappes . . . 153
8.3.4 Assembly of the nappe stack . . . 156
8.3.5 Boudinage of the Åreskutan Nappe . . . 164
8.4 Regional significance and implications . . . 165

9 Conclusions **166**

10 Proposals for future research **166**

11 References **167**

1 Introduction

Åreskutan in the Scandinavian Caledonides is a classic mountain in the tectonics research field ever since the recognition of older rocks thrust over younger formations, in the late 1800's. Thrust tectonics pioneer Törnebohm put forth his theory that the high-grade rocks of Åreskutan had been transported at least 100 km eastwards and were lying discordantly on top of low-grade, fossiliferous Silurian sediments following a traverse of the Scandinavian Caledonides from Östersund to Levanger Törnebohm, 1872; 1888; 1896). In the 150 years since the publication of Törnebohm's geognostic profile, the theory of thrust tectonics has merged with plate tectonic theory, which has provided a framework to identify the building blocks and formational processes of the Scandinavian Caledonides.

Törnebohm referred the lateral displacement of the high-grade rock units as the *Seve Group*, and this displacement is now estimated to exceed 300 km (Gee, 1975a; Gee et al., 1985; Greiling et al., 2023), with the upper nappes speculated to originate at least 1000 km off of the present coastline (Jakob et al., 2019). The Scandinavian Caledonides are now interpreted as being composed of four groups of thrust sheets, referred to as Allochtons, based on palaeogeographic position (Figure 1; see also Geological Setting). The Seve Group of Törnebohm is included in the Middle Allochton, and has been divided into individual nappes and nappe complexes. The transect through the Scandinavian Caledonides from Östersund to the Norwegian coast has been a key area in developing our understanding of the orogen, and Åreskutan has been pivotal due to the ease of access, and the exposure of multiple nappes of the Middle Allochton on its western flank.

Likely one of the most heavily researched singular mountains in Scandinavia in the 1900's, Åreskutan has received further attention in the past decade after indications of an overprinted ultra-high pressure metamorphic event and the discovery of metamorphic microdiamonds in the Åreskutan Nappe, the topmost nappe (Klonowska et al., 2014; Klonowska et al., 2017), together with seismic investigations of the regional nappe geometry and the COSC-1 project, drilling of a 2.5 km deep borehole on the eastern flank of the mountain (Gee et al., 2010; Lorenz et al., 2015). This renewed attention has sparked debates on the metamorphic history of certain nappe units (Li et al., 2020; Klonowska et al., 2021), refined timing of metamorphic events (e.g. Ladenberger et al., 2014; Li et al., 2021d), enhanced our understanding of the Scandian phase of the Caledonide orogeny, i.e. the collision of Laurentia and Baltica and the thrusting of the assembled allochtons onto the Baltoscandian platform (e.g. Majka et al., 2012; Bender et al., 2018; Giuntoli et al., 2018; Giuntoli et al., 2020), and given us a better idea of the subsurface geometry of the overthrust allochtons (e.g. Hedin et al., 2016).

Åreskutan seemingly lies on the western limb of the north-south-trending Åre Synform, with the topmost $\sim$ 500 m constituting a klippe of the highly migmatised granulite-facies Åreskutan Nappe, overlying the amphibolite-facies Kall Nappe which covers most of the synform (Figure 2). Between the high-grade nappes of Åreskutan and the basement and foreland sediments of the Mullfjället Antiform to the west are one or more greenschist-facies nappes, which may also crop out on the eastern side of the synform. Several mapping efforts have been made between Törnebohm's visit and the present. Over time the detail and interpretations of the geological maps have varied (*see section 5 on previous mapping efforts*). One question that still remains unanswered is the geometry of the nappe stack. In the last detailed mapping effort on Åreskutan, Helfrich (1967) noted an asymmetry of the high-grade nappes in the synform, a marked increase in thickness east of what appears to be the synform axis at Åreskutan. This asymmetry resulted in the COSC-1 project drilling 2.5 km through the Kall Nappe without reaching its intended target, the contact with greenschist-facies nappe below (Lorenz et al., 2015). Despite detailed seismic investigation in and around the COSC-1 borehole (Hedin et al., 2014; Hedin et al., 2016), the geometry of the nappe stack at Åreskutan remains unclear.

The aim of this thesis is to investigate and assess the geometry of the West Jämtland nappe stack on Åreskutan. How does the geometry change across the nappe stack with an apparent in-

verted metamorphic gradient, and can it be understood through geological field mapping? With several new geological maps and cross-sections of Åreskutan based on lithological and structural field data, a petrographic profile from base to summit and integration with current research, a model for the nappe geometry of Åreskutan is proposed.

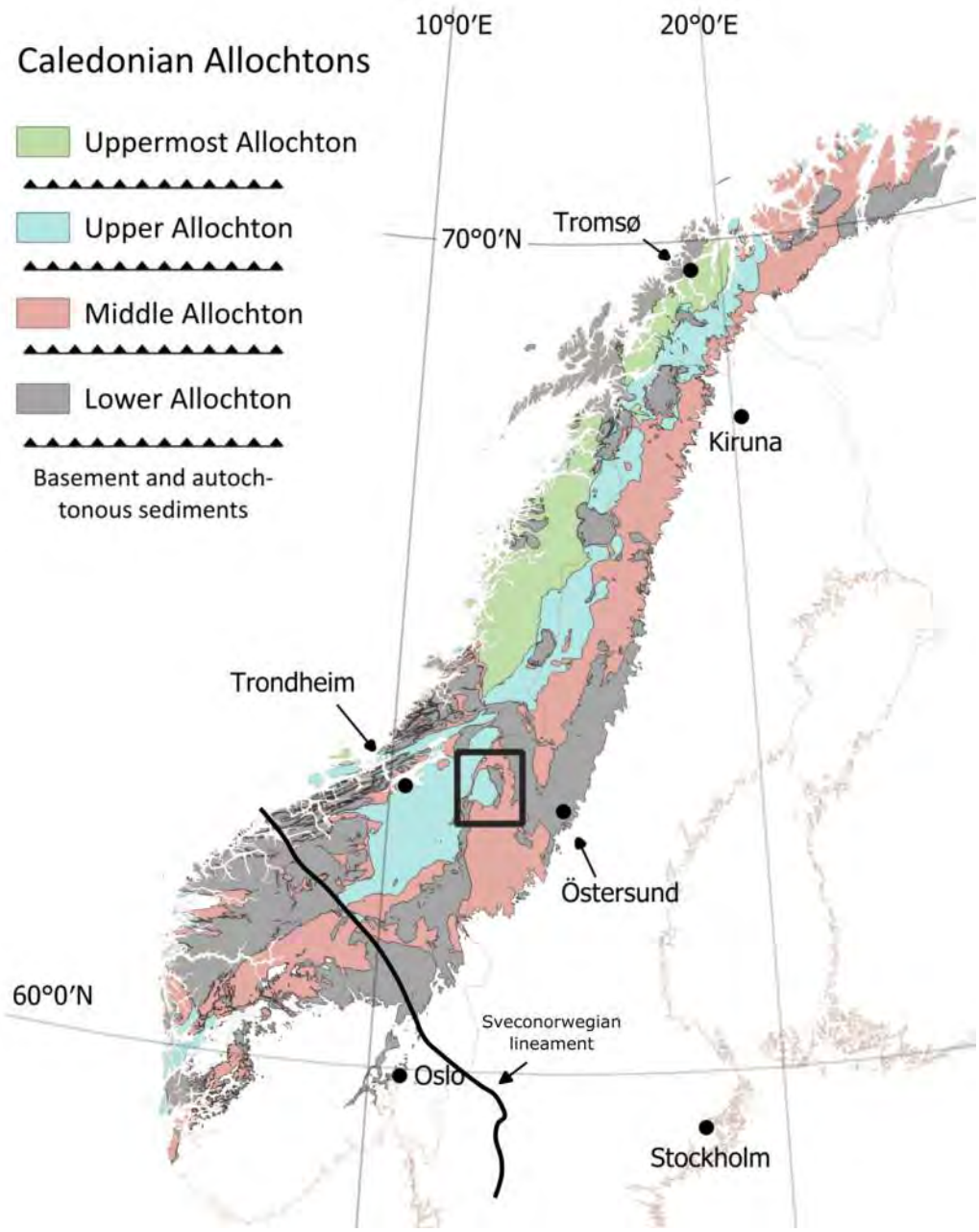


Figure 1: Tectonostratigraphic map of the Scandinavian Caledonides. Outlined square shows the location of Fig. 2. Map is based on tectonostratigraphic classification of the 1:50 000 – 1:250 000 and 1:1 000 000 bedrock geology datasets from SGU and the 1:250 000 bedrock geology dataset from NGU.

2 Geological Setting

The Caledonide Orogen in Scandinavia is a roughly 2500-km long belt stretching from Southern to Northern Norway, and through Northwestern Sweden. The orogen is attributed to the subduction of the Baltican plate beneath Laurentia in late Ordovician, closing the Iapetus ocean and ending in the Baltica-Laurentia collision. The Scandinavian Caledonides are characterised by wide and relatively thin thrust sheets, thrust over a wide foreland. The thrust sheets are grouped into four major allochtonous groups, each representing a separate palaeogeographic setting (Gee, 1975b; Roberts and Gee, 1985; Gee and Stephens, 2020b): (1) The Uppermost Allochton is the structurally highest nappe group, derived from the Laurentian margin. (2) The Upper Allochton is interpreted as derived outboard of Baltica, either the outermost part of the Laurentian margin or from domains within the Iapetus Ocean, including arcs and microcontinents. (3) The Middle Allochton represents the outer margin of Baltica. (4) The Lower Allochton represents Baltoscandian foreland, which transitions eastwards into platform facies sediments and Proterozoic basement slices imbricated with the sedimentary thrust sheets (Karis and Strömberg, 1998). This is of course an oversimplification, but it proves useful for distinctions of regional provenance and for discussing the broad dynamics of the closure of the Iapetus Ocean. There are also recent attempts to remake and diversify the classification of the Caledonide architecture (Jakob et al., 2022), though the discussion of alternate subdivisions is outside the scope of the present thesis.

2.1 Opening and closure of the Iapetus Ocean

Prior to the break-up of the supercontinent Rodinia, a long period of slow extension caused sedimentary basins to form at the margin of what became the Baltican plate (Andréasson et al., 1998; Nystuen et al., 2008; Kjøll, 2020). Syn-extensional Neoproterozoic sedimentation formed thick successions; those thrust onto the Baltoscandian platform are interpreted as up to 4-6 km thick (e.g. Kumpulainen, 1980; Nystuen, 1980), while basins in present-day Greenland accumulated at least 16-18 km of sediments (Nystuen et al., 2008). Both shallow-, deep-sea and terrestrial environments are recorded in the Lower and Middle Allochton (Karis and Strömberg, 1998; Siedlecka et al., 2004; Plink-Björklund et al., 2005; Be'eri-Shlevin et al., 2011). Cryogenian successions found across the Lower and Middle Allochtons (e.g. Kumpulainen, 1980; Thelander, 2009; Greiling et al., 2023) documenting sabkha conditions in evaporites and dolomites ((Thelander, 2009); Kjøll, 2020) which transitions into tillites from the Marinoan glaciation (Kumpulainen and Greiling, 2011). Rifting may also have caused slivers of continental crust to break off of Baltica to form microcontinents within the Iapetus, e.g. the proposed Jotun (Jakob et al., 2019) or Gula microcontinents (Hollocher et al., 2012). The late Cryogenian - Ediacaran rift magmatism in the Laurentian and Baltican basement and the extended Baltican margin signal the acceleration of rifting and the onset of seafloor spreading (Tegner et al., 2019).

The earliest sign of rift magmatism in the Baltican domain is the 616±3 Ma intrusion of a basaltic dyke swarm into the Sweconorwegian basement at Egersund (Bingen et al., 1998). South of the Sveconorwegian Lineament (Figure 1) are indications of a hyperextended magma-poor margin (e.g. Abdelmalak et al., 2015; Jakob et al., 2019; Andersen et al., 2022); in the central and northern Caledonides extensive magmatism is recorded in nappes representing the extended Baltoscandian margin. These intrusives were first called the Ottfjället Dolerites by Törnebohm (1877), now referred to as the Baltoscandian Dyke Swarm (Andréasson, 1987). The Baltoscandian Dyke Swarm can be traced along the entire Caledonides from roughly the Sveconorwegian lineament (Tegner et al., 2019) with intrusive ages of 610-595 Ma (Svenningsen, 2001; Root and Corfu, 2012; Baird et al., 2014; Barnes et al., 2019; Kjøll et al., 2019; Kumpulainen et al., 2021).

It is not determined when closure of the Iapetus commenced, but widespread late Cambrian arc magmatism in the Iapetus and Laurentian domains provide a lower constraint (Claesson et al., 1988; Stephens et al., 1993a; Slagstad et al., 2014; Carter et al., 2023). The Scandian phase of the closure is recorded from mid-Silurian to early Devonian, with a younging of Scandian

deformation ages from north to south (e.g. Barnes et al., 2022, *and references therein*) with out-of-sequence thrusting of the Upper Allochton over the Middle (Bender et al., 2018), and the Uppermost Allochton over the Upper (Saalmann et al., 2021), followed by Devonian collapse and extension of the orogen (Fossen, 2010), until the end of the Scandian orogeny at ca. 375 Ma (Tucker et al., 2004).

3 Architecture of the Scandinavian Caledonides

In the following section, descriptions of the Upper, Middle and Lower Allochtons will be provided and the architecture of the central Scandinavian Caledonides will be described from top to bottom. Summaries and descriptions of the Uppermost Allochton and its evolution can be found elsewhere (e.g. Corfu et al., 2014; *and references therein*) and is outside the scope of the thesis. In the following, the Western Gneiss Region, the Scandinavian Caledonides south of the Sveconorwegian lineament in Figure 1 as well as the northernmost segment, including the Kalak Nappe Complex, are also not described.

3.1 Upper Allochton

The Upper Allochton is a composite group of nappes exotic to Baltica, and likely originate from domains within the Iapetus (Stephens, 2020). In Sweden the nappes of the Upper Allochton are referred to as the Köli Nappe Complex after Törnebohm's Köli Group (Törnebohm, 1872), whereas in Norway the nomenclature is more varied. Three structural levels are recognized: Lower Köli, Middle Köli and Upper Köli (e.g. Saalmann et al., 2021). Nappes are composed of metamorphosed calcareous and siliciclastic sediments, and intrusive and volcanic rocks deposited or emplaced in island arc, fore-arc and back-arc environments (Gee, 1975b; Hollocher et al., 2012; Slagstad et al., 2014). Arc-related ophiolites are common at higher structural levels (Slagstad et al., 2014, *and references therein*), while a long trail of fragmented ophiolites in the otherwise arc-related lithologies of the basal Lower Köli lack arc components and are proposed to have formed part of the ocean floor outboard of the extended Baltoscandian margin (Grimmer and Greiling, 2012; Nilsson and Roberts, 2014). Nappes of the Upper Allochton are metamorphosed at greenschist to amphibolite facies and show a complex tectonothermal history (e.g. Stephens, 2020, *and references therein*). Models to account for events during the closure of the Iapetus propose multiple successions of subduction zones (e.g. Stephens and Gee, 1985; Brueckner and Van Roermund, 2007; Slagstad et al., 2014; Hollocher et al., 2022).

3.2 Middle Allochton

The Middle Allochton is composed of slices of the Baltoscandian margin accreted to the over-riding plate as Baltica was subducted. palaeogeographic reconstructions of the Baltica in the Proterozoic (e.g. ; Andréasson et al., 1998; Siedlecka et al., 2004; ; Jakob et al., 2019) show a heterogeneous passive margin affected by prior structures of the rifted crystalline basement (e.g. Kumpulainen and Nystuen, 1985; Pease et al., 2008; Nystuen et al., 2008; Andersen et al., 2022; Jakob et al., 2022). The Middle Allochton is further subdivided into several nappe packages, distinguished by palaeogeographic position, tectonostratigraphic position and metamorphic conditions. Each nappe group is broadly relatable though not always present along the whole orogen. Individual nappes in the Middle Allochton nappe groups are compiled in table 1. In this thesis, the nappe groups are named with the commonly used name of the nappes in Jämtland. See also section 4.1 on naming conventions.

Table 1: Tectonostratigraphy of the Middle Allochton in the Scandinavian Caledonides.

Structural group	South-Central Norway	Central Norway	West Jämtland
Seve Nappe Complex, without structural subdivision	Esandsjøen Nappe[8]; Blåhø Nappe[10]	Esandsjøen Nappe[9]; Skjøtingen Nappe[16]; Blåhø Nappe[20,22]	
Upper Seve Nappes			Täljstensvalen Complex[7]
Middle Seve Nappes			Åreskutan Nappe[6,31]; Snasahögarna Nappe[7]
Lower Seve Nappes			Kall Nappe[6,31]; Blåhammarfjället Nappe[7]
Särv Nappes	Sætra Nappe[4]; Hummelfjellet Nappe[10]	Upper Leksdal Nappe[2]	Särv Nappe[5]
Offerdal Nappes	Dagvolsjøen Nappe[10]; Rondane Nappe[10]; Åmotsdalen Nappe[10]; Valdres Nappe Complex[19]	Risberget Nappe[18]; Lower Leksdal Nappe[2]	Offerdal Nappe[17]; Tännäs Augen Gneiss[3]
Jämtlandian Nappe Complex	Osen-Røa Nappe Complex[19]; Synnfjell Nappe[24]	Osen-Røa Nappe Complex[19]	Jämtlandian Nappe Complex[27]
Alternative interpretations		The Blåhø Nappe is interpreted as a low structural unit of the Upper Allochton[29]	

Numbered references: 1: Zwart, 1974; 2: Andreasson, 1978; 3: Röshoff, 1978; 4: Krill, 1980; 5: Kumpulainen, 1980; 6: Arnbom, 1980; 7: Sjöström, 1983; 8: Gee et al., 1985; 9: van Roermund, 1985; 10: Nilsen and Wolff, 1989; 11: Zachrisson and Sjöstrand, 1990; 12: Dallmeyer et al., 1991; 13: Andréasson et al., 1992; 14: Andréasson and Albrecht, 1995; 15: Albrecht, 2000; 16: Nordgulen et al., 2002; 17: Plink-Björklund et al., 2005; 18: Hollocher et al., 2007; 19: Nystuen et al., 2008; 20: Robinson and Roberts, 2008; 21: Thelander, 2009; 22: Gee et al., 2015; 23: Klonowska et al., 2016; 24: Rice and Anderson, 2016, *and references therein*; 25: Greiling et al., 2018; 26: Andréasson et al., 2018; 27: Gee and Stephens, 2020b; 28: Andréasson, 2020; 29: Hollocher et al., 2022; 30: Greiling et al., 2023; 31: This study.

Table 1: (continued)

Structural group	North Jämtland and Västerbotten	Southern and Central Norrbotten	Northern Norrbotten
Seve Nappe Complex, without structural subdivision			
Upper Seve Nappes	Svartsjöbäcken Unit of the Western Belt[1]	Keddåive Nappe[12]	Kebne Dyke Complex[28]; Váivvančohkka Nappe[28]
Middle Seve Nappes	Lejaren and Avardo Units of the Ertseke Lens in the Central Belt[9]; Tjeliken Lens of the Sjouten Unit of the Eastern Belt[9]	Upper and Lower Units of the Tsäkkok Lens[21]; Grapesvarre nappe of the Vaimok Lens[15]	Mårma Terrane[28];
Lower Seve Nappes	Blåsjöälven Unit of the Central Belt[11]; Gakkafjället Unit and Sjouten Unit of the Eastern Belt[11]	Lillviken Nappe[22]	Mikka Nappe[12]; Leavasvaggi Gneiss[26]; Vássacorru Igneous Complex[28]; Vierručohkkha Amphibolite[26]
Särv Nappes	Referred to as the Särv Nappe	Kvikkjokk Complex[21]; Pieljekaise Nappe[14]; Skarja Nappe[12,13]	Laddjuvagge Nappe[26]
Offerdal Nappes	Stalon Nappe[25]; Danabergen Nappe[25]; Slussfors Nappe[25]; Åkerberget Nappe[25]; Sadenåive Nappe[25]; Ammarnäs Complex[25]; Fjällfjäll Nappe[25]	Akkajaure Nappe Complex[21]; Kabla-Stuor Tata Unit[21]; Rimobäcken Nappe[22]	Abisko Nappe[21]; Storriten Complex[21]
Jämtlandian Nappe Complex	Blaik Nappes[30]		
Alternative interpretations	The Tjeliken Lens and Sjouten Unit are both interpreted as part of the Lower Seve Nappes[23]	Sarektjåkkå Nappe is interpreted as the uppermost unit of the Seve Nappe Complex, and the Tsäkkok and Vaimok lenses are interpreted as different sections of a recumbent fold of a proposed Råvejávvre Nappe[28]	

3.2.1 Seve Nappe Complex

Töhrnebohm called all the nappes of the Middle Allochton the Seve Group (Törnebohm, 1888), but the Seve Nappe designation is now reserved for the uppermost high-grade nappes, derived from the outermost edge of the Baltoscandian margin. This complex of lithologically similar units largely consist of psammites, semi-pelites, marbles and proterozoic basement slices, all with mafic intrusions (e.g. Gee et al., 2020). Ultramafic lenses occur locally (e.g. Helfrich, 1967; Brueckner and Van Roermund, 2007). The Seve Nappe Complex is commonly divided into three nappe groups, the Lower, Middle and Upper Seve Nappes, though there is no formal definition. In northern Norrbotten, the Lower-Middle-Upper classification is not used (Andréasson et al., 2018).

The Seve Nappe Complex was originally placed as the basal unit in the Upper Allochton (e.g. Gee, 1975b), but based on Baltican affinity of detrital zircons (e.g. Williams and Claesson, 1987; Gee et al., 2014; Ladenberger et al., 2014; Gee et al., 2015; Kjøll, 2020), and the similarity in lithologies with the underlying Särv Nappes and abundant mafic intrusions of the same age (Svenningsen, 2001; Root and Corfu, 2012; Baird et al., 2014; Barnes et al., 2019) it is now included in the Middle Allochton (Gee et al., 2008).

3.2.2 Upper Seve Nappes

The Upper Seve Nappes are highly strained amphibolite facies units at the highest structural level of the Middle Allochton (e.g. Bender et al., 2018). So far, no pre-Scandian metamorphic ages have been published for the Upper Seve Nappes, which record major ductile deformation at 434 ± 6.4 Ma in Western Jämtland (Bender et al., 2019) and 5-10 Ma older ages in Västerbotten (see Bender et al., 2019 for comment on Rb-Sr ages in Grimmer et al., 2015). Shearing at lower grade continued until $\sim$ 416 Ma (Bender et al., 2019; Ma et al., 2022).

3.2.3 Middle Seve Nappes

The high-grade Middle Seve Nappes are often migmatitic, with ultra-high pressure metamorphism documented in nappes from Central Norrbotten to West Jämtland (e.g. Klonowska et al., 2017; Bukała et al., 2020b; Barnes et al., 2023). Peak temperatures decrease going north (Fassmer et al., 2021, *and references therein*). The tectonostratigraphy is complex, with multiple high-pressure or ultra-high-pressure units sandwiched between units of lower grade from Northern Jämtland to Norrbotten (e.g. van Roermund, 1985; Brueckner and Van Roermund, 2007; Root and Corfu, 2012; Fassmer et al., 2021).

The Middle and Lower Seve Nappes display similar lithologies (i.e. psammites, semipelites, calc-silicates, felsic orthogneisses, all intruded by rift-related mafic intrusions), but they distinctly differ in metamorphic grade, with the Middle Seve Nappes characterized by a significant degree of migmatization affecting all lithologies. High-pressure lithologies (e.g. eclogite) are preserved from Northern Jämtland and northwards, and a granulite-facies overprint is pervasive in West Jämtland (e.g. Bryhni and Andreasson, 1985, *and references therein*; van Roermund, 1985). Recent petrological studies using thermodynamic modelling and the discovery of metamorphic microdiamonds revealed pre-Scandian high- and ultra-high-pressure metamorphism, indicating deep subduction of the Middle Seve Nappes prior to the Laurentia-Baltica collision (West Jämtland: Klonowska et al., 2014; Rosén, 2014; Majka et al., 2014b; Klonowska et al., 2017; Klonowska et al., 2021; Slupski, 2023. Northern Jämtland and Västerbotten: Janák et al., 2013; Majka et al., 2014a; Grimmer et al., 2015; Klonowska et al., 2016; Fassmer et al., 2017; Petrík et al., 2019. Norrbotten: Bukała et al., 2018; Bukała et al., 2020a; Fassmer et al., 2021; Barnes et al., 2023.)

Geochronological work shows a younging of subduction-related prograde and peak metamorphic ages from north to south along the orogen, though a number of recent studies indicate the Middle Seve Nappes may have been concurrently subducted along the orogen at roughly 490-

480 Ma, with a second subduction event in the central Scandinavian Caledonides, i.e. Jämtland and southern Västerbotten, at ∼ 460-445 Ma (Figure 11B in Barnes et al., 2022, *and references therein*). In West Jämtland, significant partial melting and a granulite facies overprint occurred at 442-436 Ma (Williams and Claesson, 1987; Majka et al., 2012; Ladenberger et al., 2014; Klonowska et al., 2017; Bender et al., 2019; Walczak et al., 2022). Concurrent with the high-temperature event in Jämtland, the Scandian collision is recorded further north (Barnes et al., 2022). During the Scandian phase, protracted shearing is recorded in Jämtland at amphibolite facies conditions between 434-428 Ma (Ladenberger et al., 2014; Bender et al., 2019).

3.2.4 Lower Seve Nappes

The Lower Seve Nappes form the basal layer of the Seve Nappe Complex. In comparison with the much-studied Middle Seve Nappes, petrological and geochronological studies of the Lower Seve Nappes are lacking. The metamorphic conditions of the Lower Seve Nappes are generally estimated at amphibolite facies (e.g. Solyom et al., 1979; Arnbom, 1980; Bergman, 1993; Giuntoli et al., 2020; Jeanneret et al., 2022; Callegari et al., 2023), but there are also signs of an early high-pressure phase (Giuntoli et al., 2020; Jeanneret et al., 2022). Deformation is not as pervasive in northern Norrbotten, evident in the Sarek area where diamictites and stromatolites are preserved (Kjøll, 2020). Metamorphic ages are broadly comparable to the Middle Seve Nappes, with indications of an early Ordovician tectonothermal event in the Jämtland area (Glodny et al., 2017; Giuntoli et al., 2020; (Li et al., 2021d)). In the Jämtland area, the Scandian phase is recorded at progressively lower temperatures at 432-417 Ma (Dallmeyer et al., 1985; Glodny et al., 2017; Bender et al., 2019; Giuntoli et al., 2020; Jeanneret et al., 2022).

3.2.5 Särv Nappes

The Särv Nappes represent the distal segment of the rifted Baltoscandian margin (e.g. Gee et al., 2020), and are lithologically similar to the underlying Offerdal Nappes. It is distinguished by voluminous intrusions of the Baltoscandian Dyke Swarm, which are absent from the underlying nappes and basement. The connection between the Offerdal and Särv Nappes was revealed when similar dolerite dykes were found to intrude the western continuation of the Risberget Nappe and basement gneisses in the Western Gneiss Region, a key to the hypothesis of rift basins forming at the Baltican margin (e.g. Hollocher et al., 2007). The Särv Nappes are dominated by siliciclastic Neoproterozoic sediments (i.e. felspathic sandstones) though minor shales, conglomerates and dolomites may also be found (Krill, 1980; Kumpulainen, 1980; Kumpulainen and Nystuen, 1985). Deformation of the Särv Nappe is highly variable, ranging from thin mylonitic layers to several km thick relatively undeformed sequences with preserved primary structures (Krill, 1980). Detrital zircons in the Särv Nappes in the central Caledonides show Sveconorwegian and Svecofennian basement as primary sources (Be'eri-Shlevin et al., 2011; Gee et al., 2014; Gee et al., 2015).

No thermodynamic modelling studies have focused on metamorphism of the Särv Nappes, though they are generally described as greenschist-facies based on index minerals (Arnbom, 1980; Gilotti and Kumpulainen, 1986; Gilotti, 1989). Dating of the Särv-Seve shear zone in Jämtland (samples taken in the Lower Seve Nappes) indicate shearing at progressively lower temperatures between 434 ± 4 Ma and 426.3 ± 3.2 Ma (Bender et al., 2019); brittle-to-ductile deformation can be inferred to have progressed between 417-400 Ma (Giuntoli et al., 2020).

3.2.6 Offerdal Nappes

The Offerdal Nappes are considered the basal units of the Middle Allochton , representing proximal basins and basement of the Baltican margin (Gee et al., 2020). The Offerdal Nappes consist of allochtonous basement slices and Neoproterozoic, mainly siliciclastic, sedimentary cover sequences (i.e. conglomerates, fine-grained feldspathic sandstones, turbidites and pelitic schists) (Stephens et al., 1993a; Plink-Björklund et al., 2005). Primary structures are locally

well preserved (Stephens et al., 1993b; Greiling et al., 2018). Like the Särv Nappes, petrological or geochronological studies focused on metamorphism of the Offerdal Nappes are lacking, but the peak is generally estimated at mid to upper greenschist facies conditions (Plink-Björklund et al., 2005). Ages of deformation of metamorphism in the Scandian phase may be inferred from overlying nappes and the foreland successions of the Lower Allochton (e.g. Greiling et al., 2013; Greiling et al., 2018; Greiling et al., 2023).

3.3 Lower Allochton

The Lower Allochton comprises the platform and foreland successions of the orogen and large parts of exposed basement. There are preserved Cryogenian and Ediacaran syn-rift sedimentary successions in parts of the Lower Allochton, e.g. the Risbäck Group, but most of the presently exposed extent consists of Phanerozoic formations (Karis and Strömberg, 1998). The sedimentary successions are often referred to as the Jämtland Supergroup, or Jämtlandian Nappe Complex, (Gee, 1975a; Gee and Stephens, 2020a). Basement slices are occasionally imbricated with the sedimentary rocks. Also included in the Lower Allochton is the allochtonous basement exposed in windows along the orogen, e.g. the Western Gneiss Region and the Grong-Olden Culmination (Gee and Stephens, 2020a). In the Jämtland-Härjedalen area, the lithologies, stratigraphy and biostratigraphy of the Lower Allochton has been extensively mapped by Karis and Strömberg (1998).

There is a large range of metamorphic conditions recorded in the Lower Allochton during the Scandian phase, from nearly unaltered sediments along the Caledonian Front (Karis and Strömberg, 1998), to coesite- and diamond-grade ultra-high pressure metamorphism in the Western Gneiss Region of western Norway (e.g. Smith, 1984; March et al., 2022). The Jämtlandian Nappe Complex can be traced in windows across the orogen into the hinterland with increasing metamorphic grade going west(Andreasson and Lagerblad, 1980, Robinson, 1995). In the central Caledonides, the approach of the orogenic wedge which subsequently overthrust the Lower Allochton can be constrained to Llandovery - early Wenlock (Greiling et al., 2013), dated to 434.6 ± 6.9 Ma in West Jämtland (Bender et al., 2019). Protracted shearing is recorded until ca. 414 Ma (Bender et al., 2019).Concurrently, the Western Gneiss Region of the Lower Allochton was deeply subducted, experiencing peak ultra-high-pressure metamorphism at ca. 410 - 401 Ma (DesOrmeau et al., 2015). Exhumation of the Western Gneiss Region to crustal levels was likely finished by ca. 390 Ma (Kylander-Clark et al., 2008).

4 Regional framework

In West Jämtland, the nappes of the Upper, Middle and Lower Allochtons are gently folded and exposed in orogen-parallel north-south-trending open synforms, separated by basement-cored antiforms. The non-cylindrical nature of the large-scale fold structure is evident from the uneven distribution of synforms and antiforms (Figure 2). In the Tännforsen synform to the west, a klippe of the Köli Nappe Complex lies over the nappes of the Middle Allochton, seemingly excising them towards the basement-cored Mullfjället antiform (Beckholmen, 1978; Sjöström et al., 1991), though this contact may also be interpreted as an extensional fault (e.g. Gee and Stephens, 2020b). In the Åre Synform east of Mullfjället, Åreskutan forms a klippe of the the Åreskutan Nappe at the hinge, overlying the Kall Nappe and one or more of the Särv and Offerdal Nappes. The majority of the synform consists of the eastern limb, dipping towards Åreskutan. On the eastern edge, the Seve Nappe Complex excises the lower nappes and is direct contact with the Lower Allochton (Strömberg et al., 1984). Alternatively, a thin mylonite zone of the lower nappes of the Middle Allochton separate the two (Helfrich, 1967). Like the eastern end of the Tännforsen Synform, this contact is sometimes interpreted as an extensional fault (Gee and Stephens, 2020b). East of the synform, the complex fold-thrust belt of the Jämtlandian Nappe Complex stretches to the erosional front of the Scandinavian Caledonides.

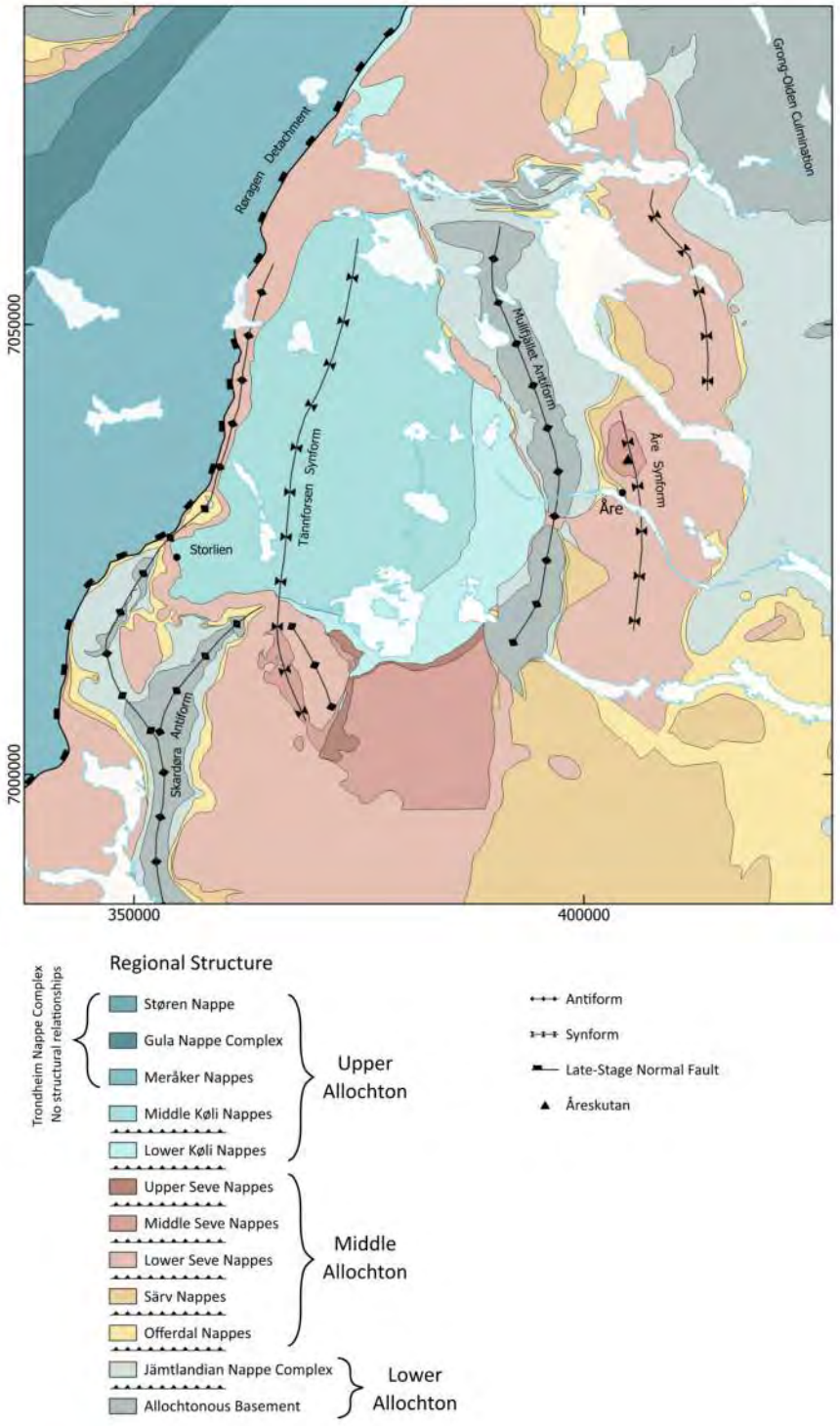


Figure 2: Regional framework of West Jämtland. Structures are based on structural data from Sjöstrand (1999) and Strömberg et al. (1984). Note the location of Åreskutan and the axis of the Åre Synform, showing the asymmetry of the nappe stack. For further description of the nappe units, see section 3, Geological Setting. Sweref 99 TM is used for map projection and reference grid.

4.1 Naming conventions

The nappe-group subdivisions within the Middle Allochton are informal names meant to simplify correlation in the Scandinavian Caledonides. Following SGU guidelines to geological nomenclature, the traditional practice of geographical names should be used to refer to individual nappes (Kumpulainen, 2017). This practice is rarely used in recent studies, e.g. where a nappe unit belonging to the Seve Nappe Complex is simply referred to as the Lower Seve Nappe (REF). While this may facilitate understanding of the structural context of the study, there is also a risk of false correlation over large distances as the same name is used for nappe units from West Jämtland to Norrbotten. In the context of this field study of Åreskutan, the geographical name convention will be used: the Offerdal and Särv Nappe will be used to refer to equivalents on Åreskutan, given they can reasonably be assumed to have the same origin. The lower nappe of the Seve Nappe Complex will follow the name of Yngström, i.e. the Kall Nappe, while the topmost nappe will be referred to as the commonly used Åreskutan Nappe (after Arnbom, 1980), eschewing the less specific Åre Nappe of Helfrich (1967).

5 Previous mapping of Åreskutan

On Åreskutan, Törnebohm noted already in the 1800's that high-grade rocks were lying discordantly above low-grade shale and fossiliferous limestone formations ((Törnebohm, 1872); Figure 3). Since then, Åreskutan has been mapped several times, both at larger and smaller scale. Identification of nappe units on Åreskutan has varied with mappers, particularly at lower structural levels.

The earliest cross-sections of the Åreskutan massif pictured the high-grade overthrust nappes as a basement window, surrounded by 'primordial shale' (Hisinger, 1819; reproduced in figure 1 in Törnebohm, 1872). After Törnebohm's cursory description, a more detailed description is provided by Högbom (1909) wherein he describes crossing from the fossiliferous sediments of the Jämtlandian Nappe Complex through a zone of mylonitic schists to what he calls the Åre Schists (Figure 4). The Kall Nappe, as mapped by later studies, is described as composed of granulite-facies gneisses (term used is granulitic), mica-schists and amphibolites, which is succeded upwards by coarse-grained cordierite- and sillimanite-bearing migmatitic gneisses, and later by migmatitic amphibolites and gabbroid rocks. Högbom (1909) also notes the synformal structure of Åreskutan, and the resemblance of the migmatitic gneiss to Archean gneisses elsewhere.

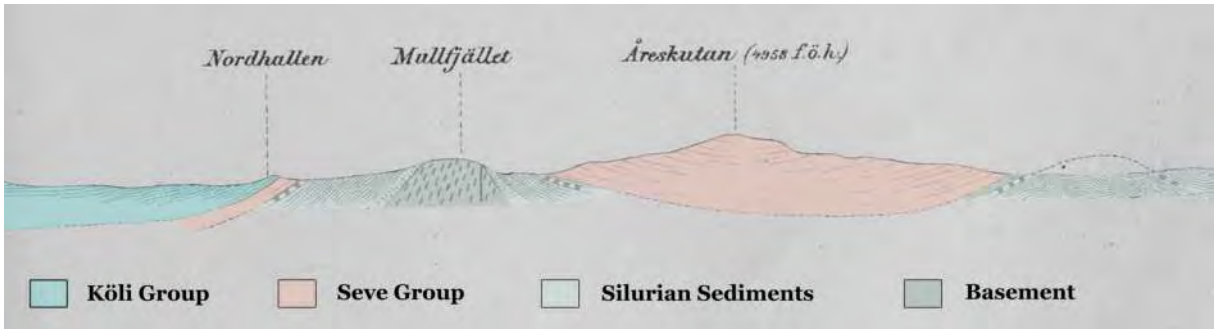


Figure 3: Figure 3: Part of Törnebohm's geognostic profile, transecting from the Tännforsen Synform through the Mullfjället antiform and the Åre Synform, from West to East. Note the crinoid-bearing limestone layer close to the basal thrust of the Seve Group, marked by a wide black-and-white line. The biostratigraphy and regional structure led Törnebohm to subsequently develop his theory of thrust tectonics Törnebohm (1896). Modified from Törnebohm (1872).

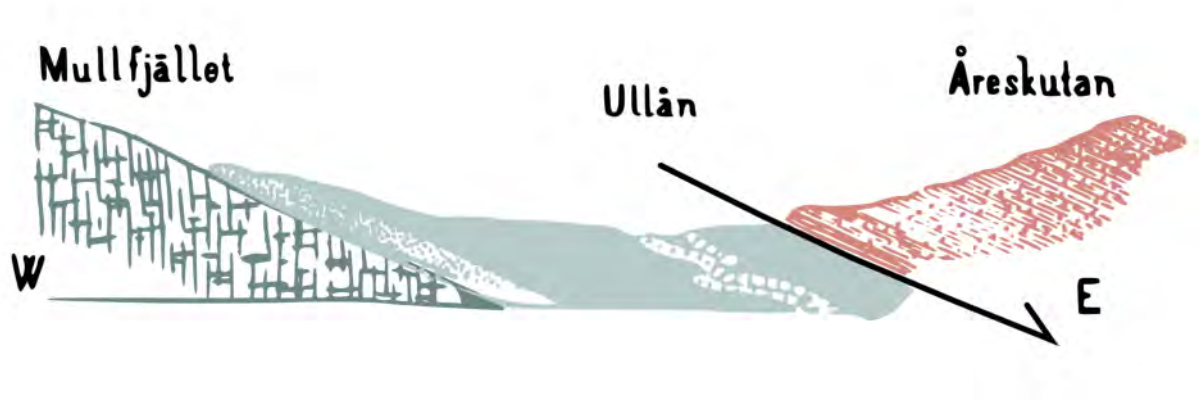


Figure 4: Stylised cross-section from the basement of Mullfjället (dark grey), across Cambrian to Silurian sediments (light grey), showing the basal thrust of the Seve Group (red) on the western slope of Åreskutan. The sediments of the Lower Allochton are increasingly mylonitised approaching the contact, and a mylonite zone at the base of the Seve Group transitions upwards into the Åre Schists. Modified from Högbom (1909)

Åreskutan is only briefly mentioned in the description to the SGU national bedrock map Ba 16, together with subdivision of the Seve Group of Törnebohm into individual nappes (Magnusson et al., 1962). The Jämtlandian Nappe Complex is interpreted as overlain by a thin and highly deformed slice of the Särv Nappe, followed by what is referred to as the Seve Proper. The gneisses of the Seve Proper are not described in any detail, but it is mentioned that deformational structures in parts of the nappe are discordant with the younger Caledonian fabric (Asklund, 1962). Not long after, Helfrich (1967) published what may be the most detailed mapping effort until now of Åreskutan and the Åre Synform (Figure 5). Helfrich (1967) documented five separate nappes overlying the Jämtlandian Nappe Complex. The Mylonite Nappe is equated with the Offerdal Nappes and the Imbrication Zone, consisting of greenschist-facies metasandstones and metadolerites, is equated with the Särv Nappes. Helfrich (1967) focuses on the Seve Nappe Complex, which is subdivided into the amphibolite-facies Amphibolite-schist Nappe at the base of the complex, the calc-silicate-dominated Fröå-Bjelke Nappe which constitutes the vast majority of the synform, and the topmost granulite-facies Åre Nappe. In particular, Helfrich (1967) looks at the asymmetrical distribution of the Kall Nappe in the synform, as it dips towards Åreskutan across most of the cross-section which places the hinge of the synform close to the western edge. This is explained through internal thrusting and imbrication of the upper calc-silicate rich part of the Kall Nappe, which would account for the dramatic difference in thickness of the nappe from west to east (Figure 5).

A widely cited work by Yngström (1969) is not available for review online, nor in any library. Neither this nor any subsequent work can be found, and the author is not listed in the registry of PhD theses at Stockholm University. He is however cited as the main mapper in the Åre area by Karis and Strömberg (1998), lending credence to a comment by Arnbom (1980) that Yngström (1969) divided the rocks of the Middle Allochton on Åreskutan into the Åreskutan Nappe, the Kall Nappe and the Särv Nappe. According to Arnbom (1980), the Kall Nappe according to Yngström (1969) is related to the Lower Seve Nappes, and Yngström identified an upper unit of calcareous metasediments and amphibolite, and a lower unit of metasandstone and amphibolite. As the thesis can not be found, no further review can be made.

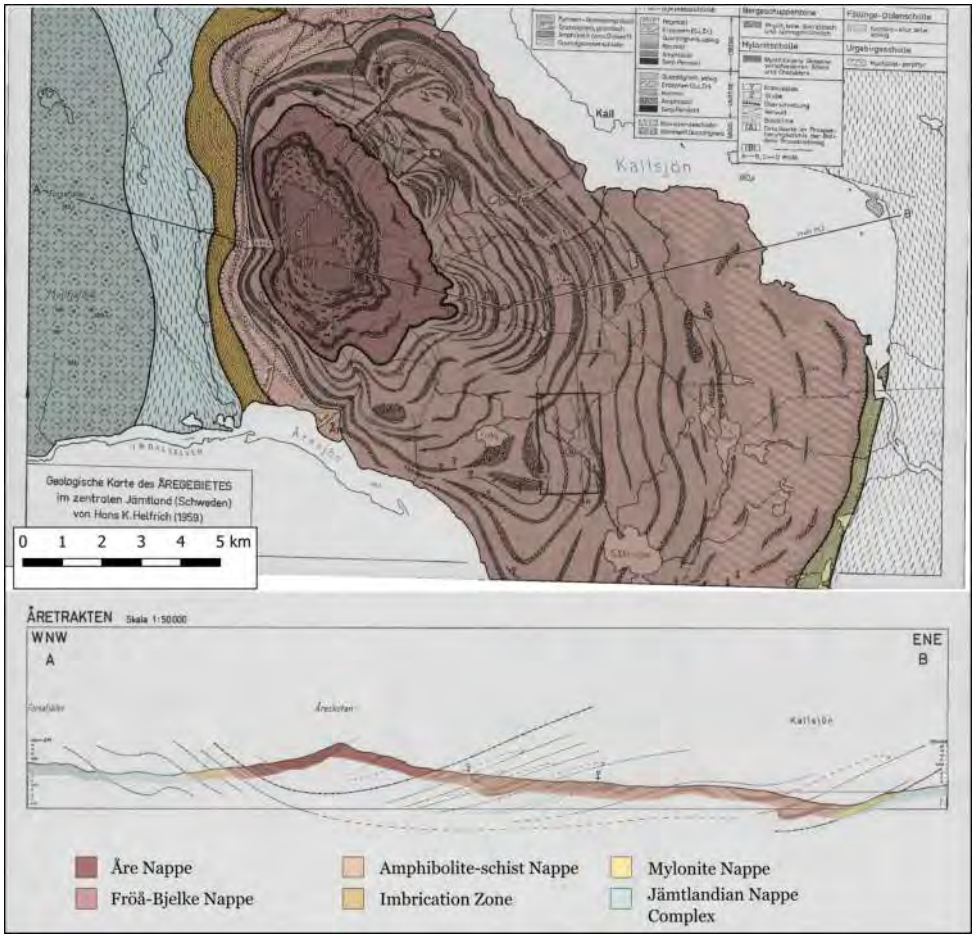


Figure 5: Geological map and cross-section modified from Helfrich (1967), colouring the interpreted tectonic units for increased clarity. The Seve Nappe Complex is divided into three separate nappes, underlain by the Imbrication Zone in the west (equated with the Särv Nappes), and the Mylonite Nappe to the east (equated with the Offerdal Nappes). Note the difference in thickness of the Fröå-Bjelke Nappe from West to East, explained through imbrication of internal thrusts. The maximum thickness of the Fröå-Bjelke Nappe is estimated at 1200 m at the eastern slopes of Åreskutan. Note also the internal thrusts marked in the Åre Nappe, one of which separates a unit of garnet-pyroxene amphibolite from the underlying garnet gneiss. Map is georeferenced in Sweref 99 TM.

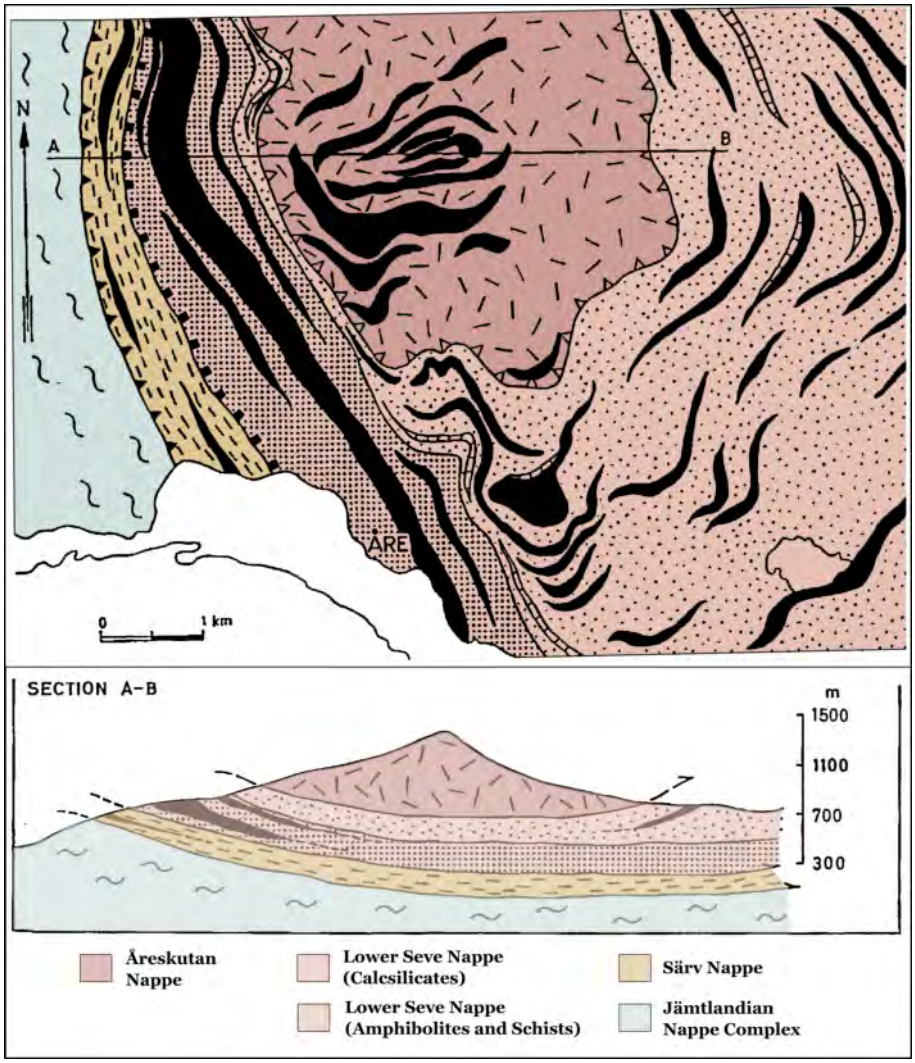


Figure 6: Geological map and cross-section of Åreskutan modified from Arnbom (1980). Tectonic units are colourised for increased clarity. The geological map is similar to that of Helfrich (1967), emphasising the asymmetry of the nappes. The cross-section however disregards this asymmetry, and estimates the thickness of the Fröå-Bjelke Nappe to 400 m at the deepest point of the synform. The geological map is georeferenced to Sweref 99 TM

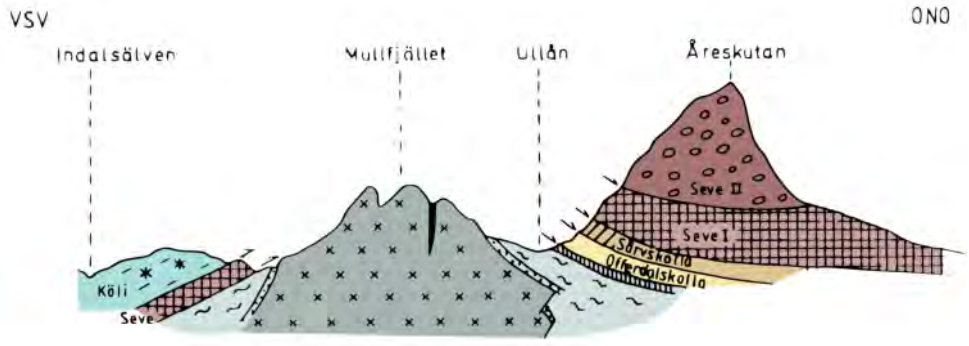


Figure 7: Tectonostratigraphic cross-section of the Mullfjället Antiform and Åre Synform, colourised for clarity. Legend as in figure 2. Modified from Karis and Strömberg (1998).

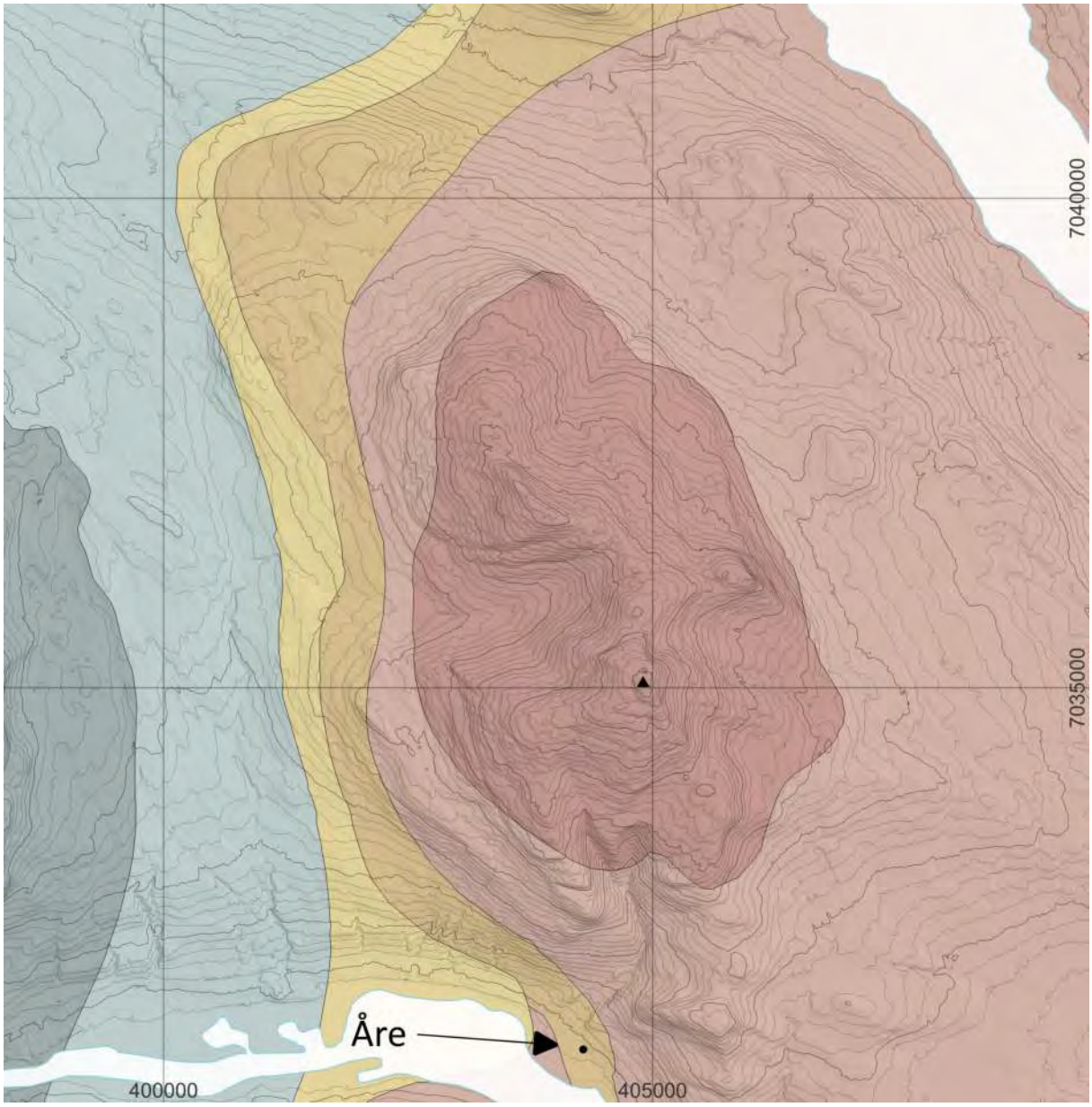


Figure 8: Tectonostratigraphic map based on data from the current geological map provided by SGU, which is based on the regional map of Jämtland by Strömberg et al. (1984). Note how, when displayed with contours and a detailed hillshade, it is evident the nappe boundaries don't follow the morphology of the mountain. Legend as in figure 2

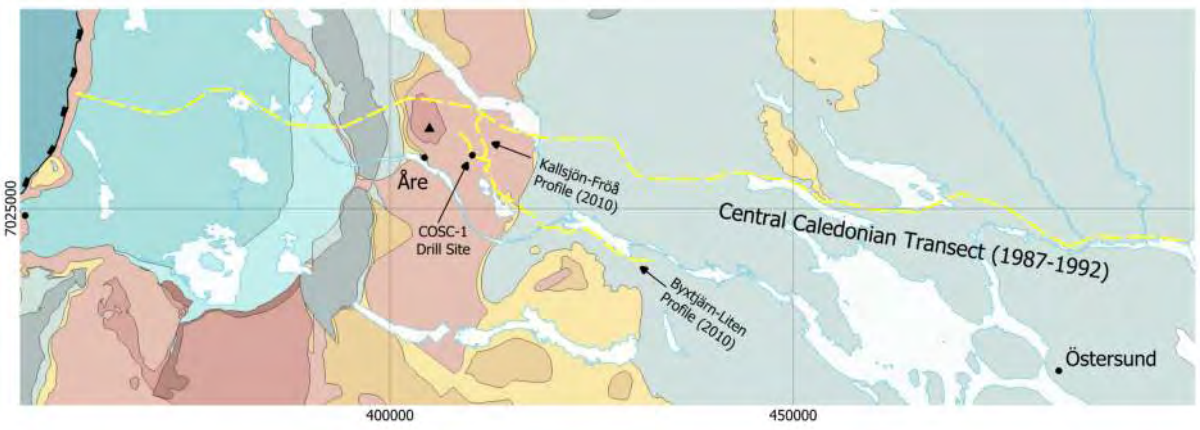


Figure 9: Geological map of West Jämtland showing the Swedish section of the Central Caledonian Transect (e.g. Juhojuntti et al., 2001), as well as the seismic profiles made in preparation for the COSC drilling project (Hedin et al., 2012). Legend as in Figure 2. Sweref 99 TM is used for map projection and reference grid.

Subsequent surface mapping studies are either focused on regional mapping, or with mapping as a minor component of e.g. petrological or structural analysis. A detailed small-scale structural investigation to identify fold generations was performed by Ghosh et al. (1979), identifying multiple generations of isoclinal folds in the high-grade nappes. A comment by Arnbom (1980) questions the usefulness of the five fold categories of Ghosh et al. (1979), which are all related to Scandian thrusting; while they are a bit generalised and simplified they may be applied to the Kall Nappe, however, the style and orientation of folds in the Åreskutan Nappe often fall outside of the proposed classifications.

In Gee and Kumpulainen (1980), parts of the field journal document localities on or around Åreskutan. Below the northern slope of Åreskutan, S.A. Tirén documents a profile crossing eastwards from the Jämtlandian Nappe Complex through thin slices of the Offerdal and Särv Nappes to the Seve Nappe Complex. J.-O. Arnbom describes several localities on Åreskutan, from the summit going south and along a river cut on the western slope, where he passes from the migmatitic gneisses of the Åreskutan nappe, through the Kall Nappe and the underlying Särv Nappe to reach the Jämtlandian Nappe Complex to the west, identifying nappe contacts along the way (Gee and Kumpulainen, 1980). Arnbom (1980) subsequently published a comprehensive petrological study of the nappe stack on Åreskutan, quantifying the metamorphic gradient by garnet-biotite geothermometry, accompanied by a simple tectonostratigraphic map and cross-section (Figure 6). Åreskutan is again only briefly described in Karis and Strömberg (1998) following the publication of the regional geological map of Jämtland (Strömberg et al., 1984), with a simple tectonostratigraphic cross-section (Figure 7, Figure 8). Instead, Karis and Strömberg (1998) focus on the Lower Allochton and the lower nappes of the Middle Allochton.

In a regional structural study, Bender et al. (2018) incorporate the structure of the nappe stack at Åreskutan in an analysis of thrust mechanics during the assembly of the Caledonian nappes and thrusting onto the Baltoscandian platform. The Seve Nappe Complex was found to have been exhumed through synthrusting vertical ductile thinning before emplacement on the Särv and Offerdal Nappes, and out-of-sequence thrusting of the Upper Allochton during the collisional phase of the orogen, greatly affecting the geometry of the Middle Allochton (Bender et al., 2018).

Contrasting the decreased geological field mapping in recent research, West Jämtland, and Åreskutan in particular, has been the stage for multiple sub-surface surveys, including the COSC-1 drilling project. The Central Caledonian Transect, performed between 1987 and 1992 in Jämtland, investigated the regional structure of the Caledonide Allochtons and the autochtonous basement below (e.g. Palm, 1991; Juhojuntti et al., 2001). A higher-resolution profile was made in preparation for the COSC project, including a profile connecting to the Central Caledonian

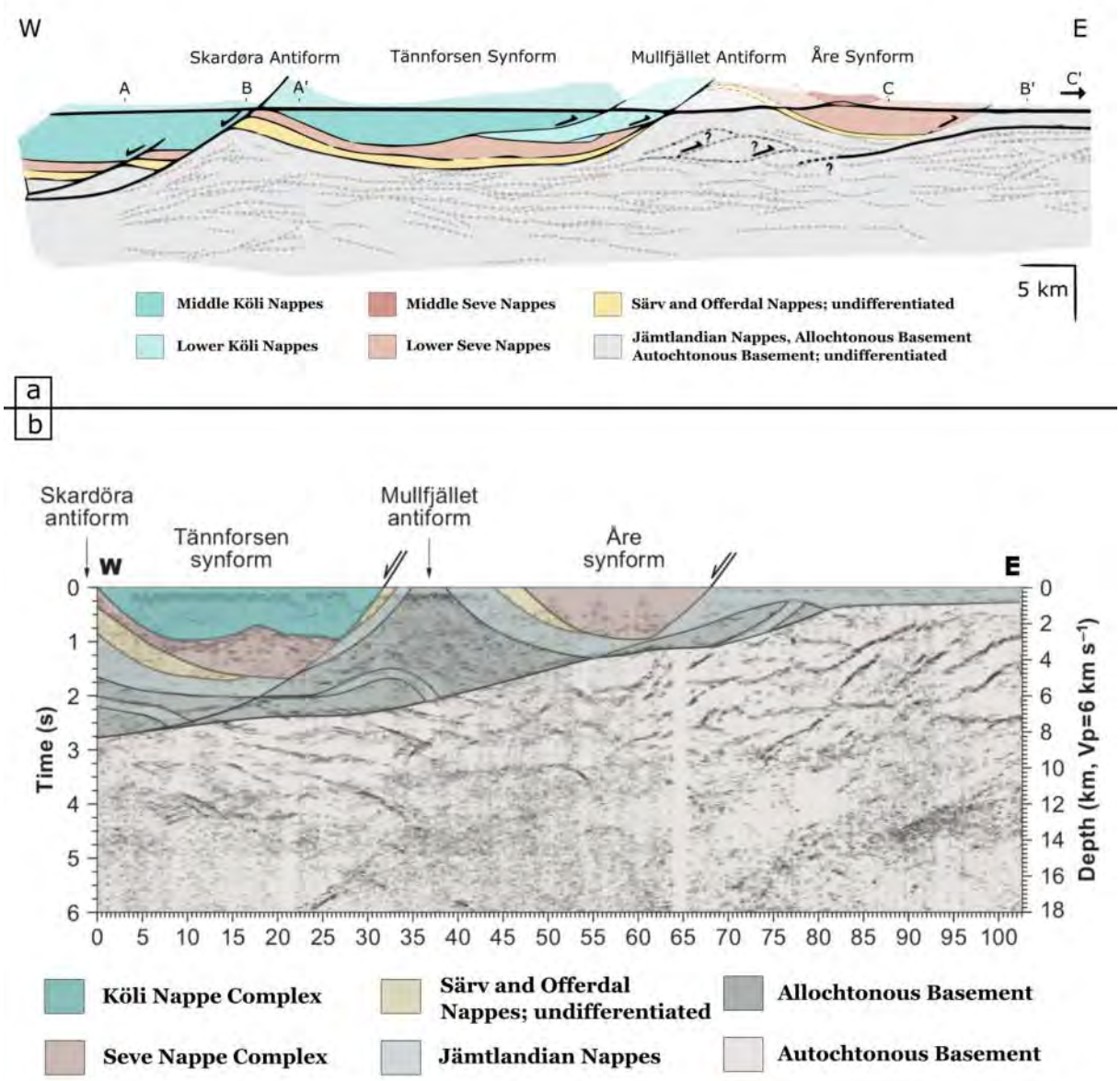


Figure 10: (a.) Interpreted seismic cross-section from the Skardøra Antiform to the Åre Synform, modified from Bender et al. (2018). The late-stage extensional Røragen Detachment flanks the Skardøra Antiform on the western side; see also the Røragen Detachment in Figure 2. The attenuated lower nappes in the Tännforsen and Åre Synform are interpreted to have been excised by higher units. Especially, the excising effect of out-of-sequence thrusting of the Upper Allochton can be seen at the Mullfjället Antiform. Profiles used by Bender et al. (2018) are marked (Hurich et al., 1989, A-A'; Palm, 1991, B-B'; Juhlin et al, 2016, C-C'). Geological interpretation of Bender et al. (2018) based on Palm (1991) and Hurich and Roberts (1997). (b) Interpreted seismic cross-section from the Tännforsen Synform to the Åre Synform, modified from Gee and Stephens (2020b). In an alternative interpretation, the geometry of the Caledonian nappes are controlled by normal faults at the eastern edge of the Tännforsen and Åre Synforms. Seismic profile and geological interpretation of Gee and Stephens (2020) based on combination of Palm (1991) and Juhojuntti et al. (2001).

Transect (Hedin et al., 2012; Figure 9). Interpretations of these profiles by Bender et al. (2018) and Gee and Stephens (2020b) are shown in Figure 10. The COSC-1 drill site was located at the foot of the eastern slope of Åreskutan, with the aim of reaching the top of the Jämtlandian Nappe Complex, to investigate effect of the apparent inverted metamorphic grade on the nappes below the Seve Nappe Complex. The Lower Allochton was speculated to be separated from the Seve Nappe Complex by a thin layer of the Särv and Offerdal Nappes in the center of the synform (Hedin et al., 2014), or possibly directly overlain by the Seve Nappe Complex (Hedin et al., 2012). Despite not reaching the base of the Kall Nappe, 2 500 m of continuous drill core was collected and analysed (Lorenz et al., 2015; Sjöqvist et al., 2015; see Lorenz et al., 2019 for full data set). The bottom 800 m showed a high degree of mylonitisation and retrogression, which was interpreted as a wide basal shear zone (Lorenz et al., 2015). Subsequent high-resolution seismic investigation in and around the COSC-1 borehole resulted in a 3-D seismic model, showing that two additional west-dipping nappe units below the Kall Nappe pinch out at the center of the synform, possibly representing the lower nappes of Åreskutan (Hedin et al., 2016; Figure 11).

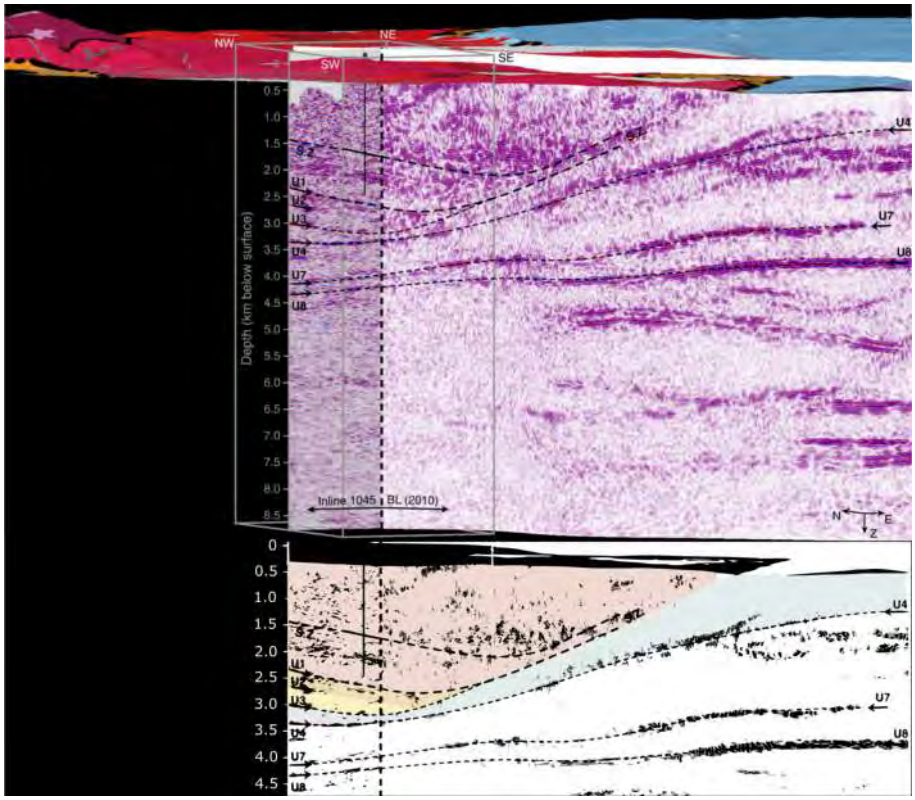


Figure 11: Inline 1045 of 3-D seismic model based on investigation in and around the COSC-1 drill hole (Hedin et al., 2016), combined with the Byxtjärn-Liten profile (Hedin et al., 2012). Inline 1045 trends east, while the Byxtjärn-Liten profile trends south-east (see Figure 7). Below is an interpreted profile based on analysis by Hedin et al. (2016), pointing out the possibility of one or two nappe units of the Middle Allochton pinching out east of the synform center (reflectors U2 and U3), in this thesis interpreted as either the Särv and Offerdal nappes, or both. The top of the basal shear zone of the Seve Nappe Complex is marked by S.Z., and the reflector U1 interpreted as the contact with the underlying nappes. Modified from Hedin et al. (2016).

5.1 Metamorphic framework

There is a general consensus that he metamorphic grade of the nappe stack rises from lower greenschist facies at the base of the mountain to granulite facies in the Åreskutan Nappe. Pressure-Temperature (P-T) estimates for various phases of the metamorphic history of the nappe units on Åreskutan are compiled in table 2. The first major jump in metamorphic grade comes at the transition from the Särv Nappe to the Kall Nappe, from greenschist facies- to amphibolite facies metamorphism, overprinted at base of the Fröå Nappe by greenschist-facies fabrics during Scandian thrusting (e.g. Giuntoli et al., 2020). The next jump occurs going up to the Åreskutan Nappe, with highly migmatised granulite-facies lithologies. The high-temperature fabric of the Åreskutan Nappe pervasively overprints a proposed ultra-high-pressure metamorphic event, now only visible through micro-diamond inclusions (Klonowska et al., 2017; Klonowska et al., 2021) and nano-granitoid melt inclusions (Slupski, 2023), though this ultra-high-pressure stage is disputed (Li et al., 2020; Klonowska et al., 2021; Li et al., 2021c).

6 Methods

6.1 Field mapping

A study area was chosen stretching from Ullån in the west to the Fröå Road in the east, and from lake Åresjön to the Tväråvalvet cirque, an area of roughly 42 km^2. From west to east, the study area covers the uppermost section of the Lower Allochton in Ullådalen, crossing the summit of Åreskutan and all present nappes of the Middle Allochton on the way. Field mapping was performed using FieldMove to record data (Petroleum Experts, 2020), while orientation of structures were measured using a magnetic compass for greater accuracy and to reduce the risk of faulty electronic equipment. In forested areas without roadcuts or streams, potential areas of interest were identified using orthophotos and LiDar datasets from Lantmäteriet. Previous geological maps of the area were consulted to identify potential locations of tectonic contacts. The study area is located both below and above the treeline, in an area affected by glacial erosion and deposition (Blomdin et al., 2021).

6.2 Map data processing

Field data was imported and processed in QGIS. Outcrop polygons were simplified and merged where multiple outcrops of the same rock type were sufficiently close. Drawing of lithologies was done primarily based on outcrops. Where no outcrops could be used for interpolation, lithology extent was extrapolated based on structural data, and morphology seen by LiDar and ortophotos. The elevation profile for the cross-section was extracted from the DEM using the QGIS plugin qprof. Structural measurements were projected onto the profile in order to extrapolate subsurface structure. Boundaries and fields were inter- /extrapolated where deep Quaternary deposits cover the bedrock, as inferred from the geomorphology seen in the DEM.

6.3 Sample selection and preparation

In total, 170 rock samples were collected from representative lithologies, as well as curious or rare outcrops to both get a representation of the dominant rock types of the area and information on events which are generally not seen everywhere. Orientation of foliation and lineation of collected samples was recorded where possible. Samples were cut at Stockholm University, perpendicular to foliation and parallel to the lineation where possible. Initially 40 samples were chosen as prospective thin section candidates, with 20 ultimately chosen for preparation, representing a rough traverse from the top of the Lower Allochton to the summit of Åreskutan. Thin sections were prepared by Thin Section Lab in Nancy (thinsectionlab.com). The thin sections were processed to 30 μm thickness and polished. Many other samples not chosen for thin section preparation were cut for observation of planar surfaces, which gives a better view of texture and fabric than rough surfaces.

Table 2: Summary of estimates of metamorphic conditions of the West Jämtland nappe stack on Åreskutan. Mineral abbreviations from Whitney and Evans (2010), WM: white mica.

Author	Unit	Lithologies	Metamorphic facies	P (kbar)	T (°C)	Method	Index Minerals	Stage	Inferred process
Ghosh et al., 1979	Åreskutan Nappe		Granulite facies	-	-	Qualitative assessment based on index minerals	Hbl + Opx + Cpx + Pl ± Grt (metabasite)	Peak metamorphic conditions	-
Arnbom, 1980	Åreskutan Nappe	Garnet-sillimanite paragneiss, quartzo-feldspathic paragneiss, metabasite, felsic orthogneisses, skarn rocks, pegmatites		-	660 - 785	Grt-Bt geothermometry			
			Granulite facies	> 5-7	> 650	Qualitative assessment based on index minerals	Sil + Ky + Crd + Grt (~30% Prp) (paragneiss); Opx + Cpx + Hbl + Spl (metabasite)	Peak metamorphic conditions	-
			Upper amphibolite facies	-	-	Qualitative assessment based on index minerals	Grt + Bt + WM + Ky (paragneiss)	Overprinting of granulite-facies rocks.	Exhumation
			Amphibolite facies	-	-	Qualitative assessment based on index minerals	Stability of Grt + Bt + Sil + Ky + WM + Pl (basal mylonite)		Emplacement of the Åreskutan Nappe on top of the Kall Nappe
	Kall Nappe	Calc-silicates, amphibolites, pegmatites, peridotites, amphibolites (lower formation?), Qz-Fsp gneisses, micaschists		-	560 - 580	Grt-Bt geothermometry		Peak metamorphic temperature	-
			Amphibolite facies	2-5 kbar	~550	Qualitative assessment based on index minerals	Bt + St + Grt ± WM	Peak metamorphic conditions	-

Table 2: (continued)

Author	Unit	Lithologies	Metamorphic facies	P (kbar)	T (°C)	Method	Index Minerals	Stage	Inferred process
			Greenschist facies	-	-	Qualitative assessment based on index minerals	WM + Czo (micaschist); Chl + Cb (amphibolite); WM + Czo + Chl (calc-silicates)	Retrogression in mylonites and shear zones	Development during Scandian thrusting
	Särv Nappe	Phyllonites, greenschists, feldspathic sandstones	Upper greenschist facies (biotite zone)	-	-	Qualitative assessment based on index minerals	Amp (Tr-Act) + Bt	Peak metamorphic conditions	-
			Lower greenschist facies (chlorite zone)	-	-	Qualitative assessment based on index minerals	Chl + WM	Retrogression	-
	Jämtlandian Nappe Complex	Phyllites	"Only slightly metamorphosed"	-	-	Qualitative assessment based on index minerals	WM + Czo		-
Klonowska et al., 2014	Åreskutan Nappe	Paragneiss, leucogranites, metabasite	Eclogite facies (Ultra-High Pressure)	26-32	600-720	Equilibrium phase diagram		Peak pressure conditions	Deep subduction
			Granulite facies	~ 12	700-820	Equilibrium phase diagram		Decompression, partial melting	Exhumation
			Granulite facies	~ 5	800-820	Equilibrium phase diagram		Peak temperature conditions	Exhumation
			Granulite facies	< 5	750-800	Equilibrium phase diagram		Final phase of exhumation	Exhumation
Klonowska et al., 2017	Åreskutan Nappe	Paragneiss, leucogranites, metabasite	Eclogite facies (Ultra-High Pressure)	41-42	830-840	Equilibrium phase diagram	Metamorphic diamond	Peak pressure conditions	Deep subduction
			Granulite facies	10-11	850-870	Equilibrium phase diagram		Peak temperature conditions	Exhumation
			Granulite facies	-	$\tilde{8}75$	Ti-in-Qz geothermometry		Peak temperature conditions	Exhumation

Table 2: (continued)

Author	Unit	Lithologies	Metamorphic facies	P (kbar)	T (°C)	Method	Index Minerals	Stage	Inferred process
Giuntoli et al., 2018	Kall Nappe	Amphibolites (investigated lithology in drill core)	Amphibolite facies	7.5-9.7	600	Amphibole-plagioclase thermobarometry	Amp + Pl	Development of mylonitic foliation in amphibolites	Shearing during the Scandian collisional phase
Giuntoli et al., 2020	Kall Nappe	Amphibolites, micaschists (investigated lithologies in drill core)	Blueschist facies	10-13	400-500	Equilibrium phase diagram	Cores of WM, Grt, Ab	Early high-pressure event	Subduction
			Upper amphibolite facies	8	600-650	Amphibole-plagioclase thermobarometry	Amp + Pl	Incipient development of mylonitic foliation in amphibolites	Shearing during the Scandian collisional phase
			Lower amphibolite facies - upper greenschist facies	5-8	450-550	Equilibrium phase diagram		Development of mylonitic foliation in micaschists	Shearing during the Scandian collisional phase
			Lower greenschist facies	3	300-350	Chlorite + white mica + quartz + H20 thermobarometry	Chl + WM	Late brittle-to-ductile shearing	Shearing during the Scandian collisional phase
Li et al., 2020	Åreskutan Nappe	Paragneiss (investigated sample)	Amphibolite facies	8-8.5	600	Equilibrium phase diagram	Inclusions in Grt (Chl + WM + Bt + Stt + Qz + Rt + Ilm)	Prograde conditions	Shallow subduction beneath island arc
			Amphibolite facies	8	616 ± 21	Zr-in-rutile geothermometry		Prograde conditions	
			Upper amphibolite facies - granulite facies	8-8.5	700	Equilibrium phase diagram	Grt, Cores of WM, Grt inclusions (WM + Bt + Ky + Pl + Qz + Rt)	Peak P-T conditions before exhumation at high temperature	Continuous isobaric heating beneath island arc

Table 2: (continued)

Author	Unit	Lithologies	Metamorphic facies	P (kbar)	T (°C)	Method	Index Minerals	Stage	Inferred process
			Upper amphibolite facies - granulite facies	8.5	693 ± 13	Zr-in-rutile geothermometry		Peak P-T conditions before exhumation at high temperature	
			Granulite facies	6.5	725	Equilibrium phase diagram		Peak temperature conditions	Exhumation as extrusion wedge, channel flow
Jeanneret et al., 2022	Kall Nappe		Upper greenschist facies	6-7.3	460-500	Titanium-in-quartz geothermometry + quartz-in-garnet elastic geobarometry		Conditions in Grt cores, incipient growth	Subduction
			Upper greenschist facies - lower amphibolite facies	7.5-8.5	490-520	Ti-in-Qz geothermometry + Qz-in-Grt elastic geobarometry		Conditions in Grt mantles, continued Grt growth	Subduction
			Upper amphibolite facies	11.3-11.8	590-610	Ti-in-Qz geothermometry + Qz-in-Grt elastic geobarometry		Peak metamorphic conditions	Peak metamorphic conditions during subduction
			Upper amphibolite facies	9.3	581	GBMP geobarometer	Grt + Bt + WM + Pl	Peak metamorphic conditions	
			Amphibolite facies	7.8-10	570-610	Equilibrium phase diagram		Peak metamorphic conditions	
Slupski, 2023	Åreskutan Nappe	Paragneiss (investigated sample)	Eclogite facies (Ultra-High Pressure)	40-45	850-900	Re-homogenization of nano-granitoid inclusions in garnet		Peak metamorphic conditions	Anatexis at ultra-high-pressure conditions during deep subduction

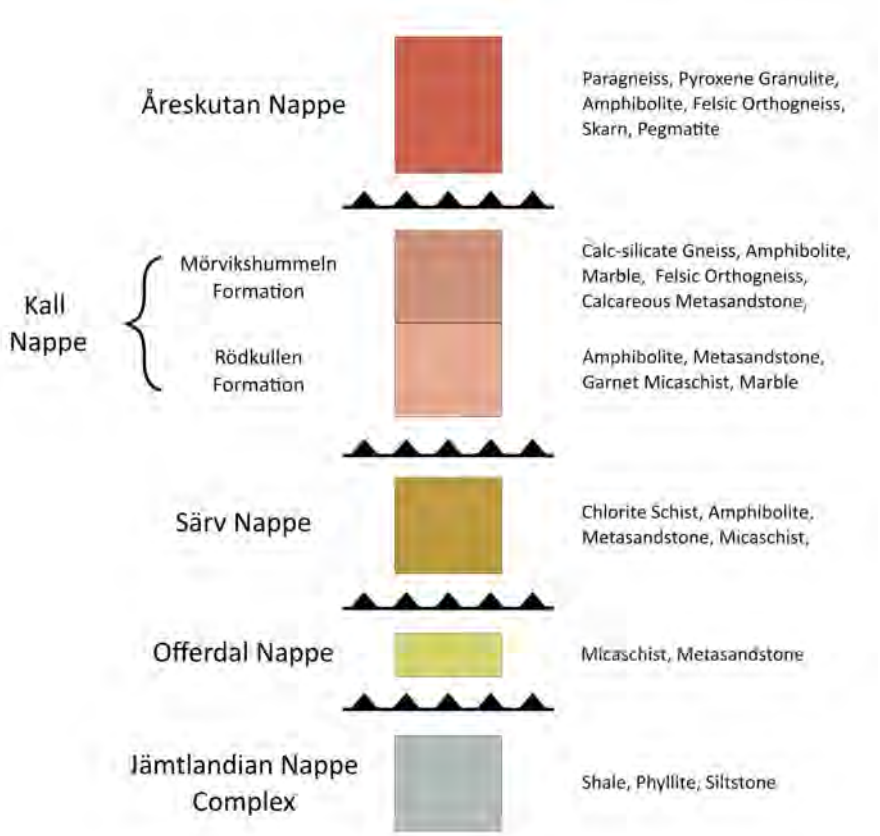


Figure 12: Tectonostratigraphic column of the nappe units on Åreskutan

7 Results

7.1 The nappe stack on Åreskutan

After extensive field mapping over three months in the study area, four distinct nappes were identified in the Middle Allochton, with the Kall Nappe subdivided into the Mörvikshummeln and Rödkullen formations (Figure 12). In the following section the nappe stack will be described in the observational order from top to bottom where the main lithologies, deformation history and metamorphic history will be covered for each nappe unit. Where minerals are marked in figures, abbreviations follow Whitney and Evans (2010).

7.2 Åreskutan Nappe

The Åreskutan Nappe makes up the top $\sim$ 500 m of Åreskutan, at the center of the Åre Synform. The maximum thickness is estimated at $\sim$ 1000 m. It is mostly composed of paragneiss, felsic orthogneiss and metabasite, predominantly pyroxene amphibolite, at a distinct granulite-facies metamorphic grade. Partial melting is pervasive throughout the nappe, though with some relatively preserved domains of metabasite. Strain is unevenly distributed with distinct shear zones between more chaotically deformed domains. The tectonic contact with the underlying Kall Nappe is well exposed at many locations around the mountain, and is discussed further in the section on tectonic boundaries. Each lithology is highly variable in composition, degree of partial melting and deformation. A wedge-shaped retrogression zone is found in the lower part of the Åreskutan Nappe, thickest on the eastern slope and attenuating to the west. Multiple late shear zones also cut the nappe in many orientations, either cutting lithologies, presenting as large folds or in zones of rheological contrast.

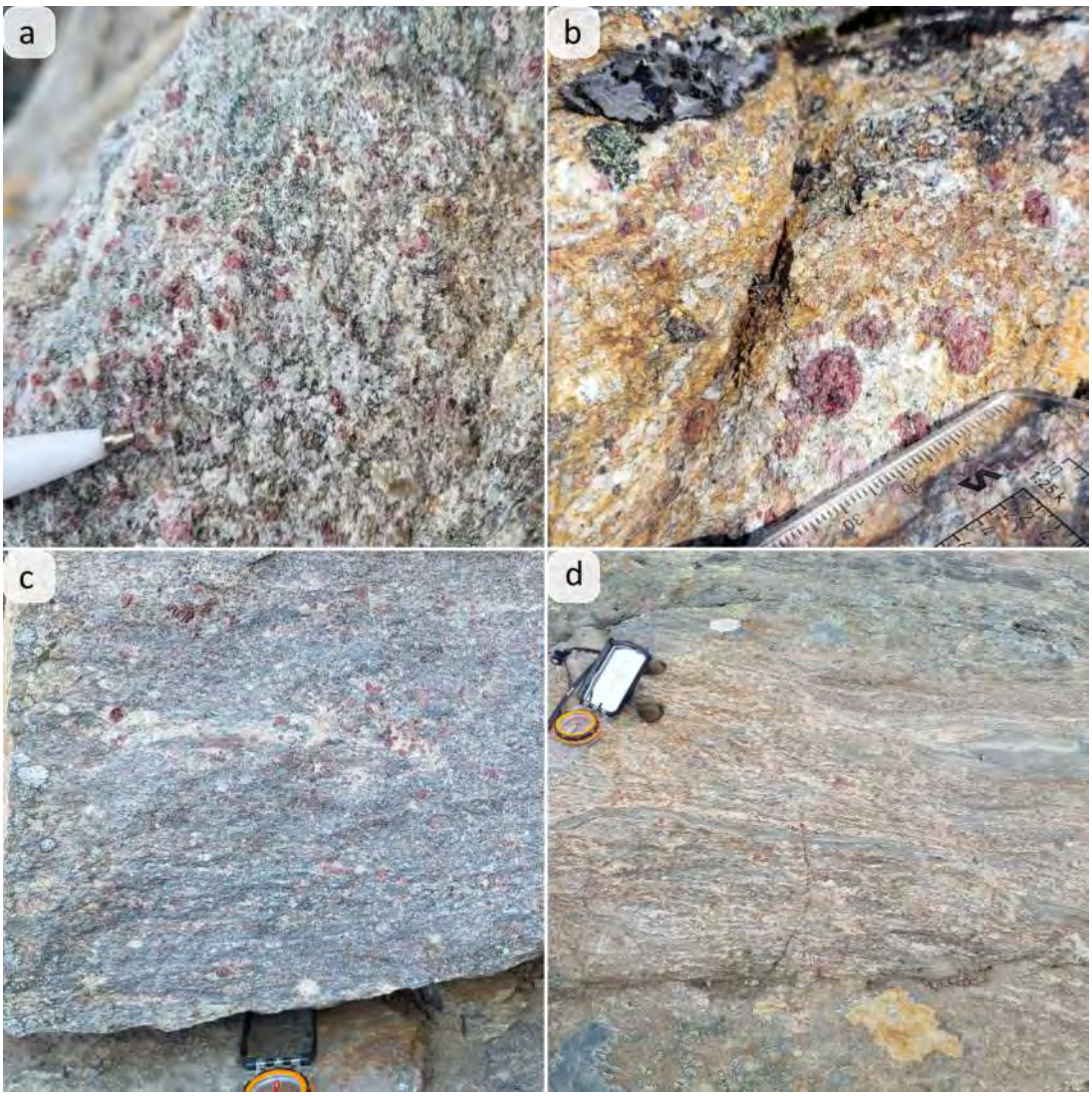


Figure 13: Photos of different varieties of paragneiss. Pen for scale. (a) Weathering surface of kyanite- and sillimanite-rich leucocratic paragneiss. (b) Rusty weathering surface of leucocratic paragneiss with large garnets. (c) Fresh surface of mesocratic paragneiss at blasted outcrop, just by the top of the cable car. Note the large garnets in the leucosome, indicating growth at the peritectic. (d) Weathering surface of garnet-rich mesocratic paragneiss with metabasite pods.

7.2.1 Paragneiss

Garnetiferous paragneiss is the dominant lithology of Åreskutan with a large range of composition and deformation style. The paragneiss can first be classified as either leucocratic or mesocratic, with two broad categories based on composition: biotite ± sillimanite-rich and biotite + sillimanite + kyanite-rich (Figure 13, Figure 14). The general composition is quartz, plagioclase, k-feldspar, garnet, biotite, ± sillimanite, ± kyanite, ± white mica, with accessory ilmenite and rutile. The paragneiss is highly migmatitic, though the exact degree of partial melting is difficult to gauge (see discussion in P-T path of the Åreskutan Nappe). Leucosomes are quartzofeldspathic and often contain peritectic garnet. Where melanosomes can be distinguished, they are rich in biotite. Leucocratic and mesocratic paragneiss is often transitional with each other, with no observed distribution pattern across the nappe. Paragneiss restite where significant melt extraction of quartz is evident is observed at all structural levels in the nappe, with the main assemblage plagioclase + biotite + garnet (Figure 15).

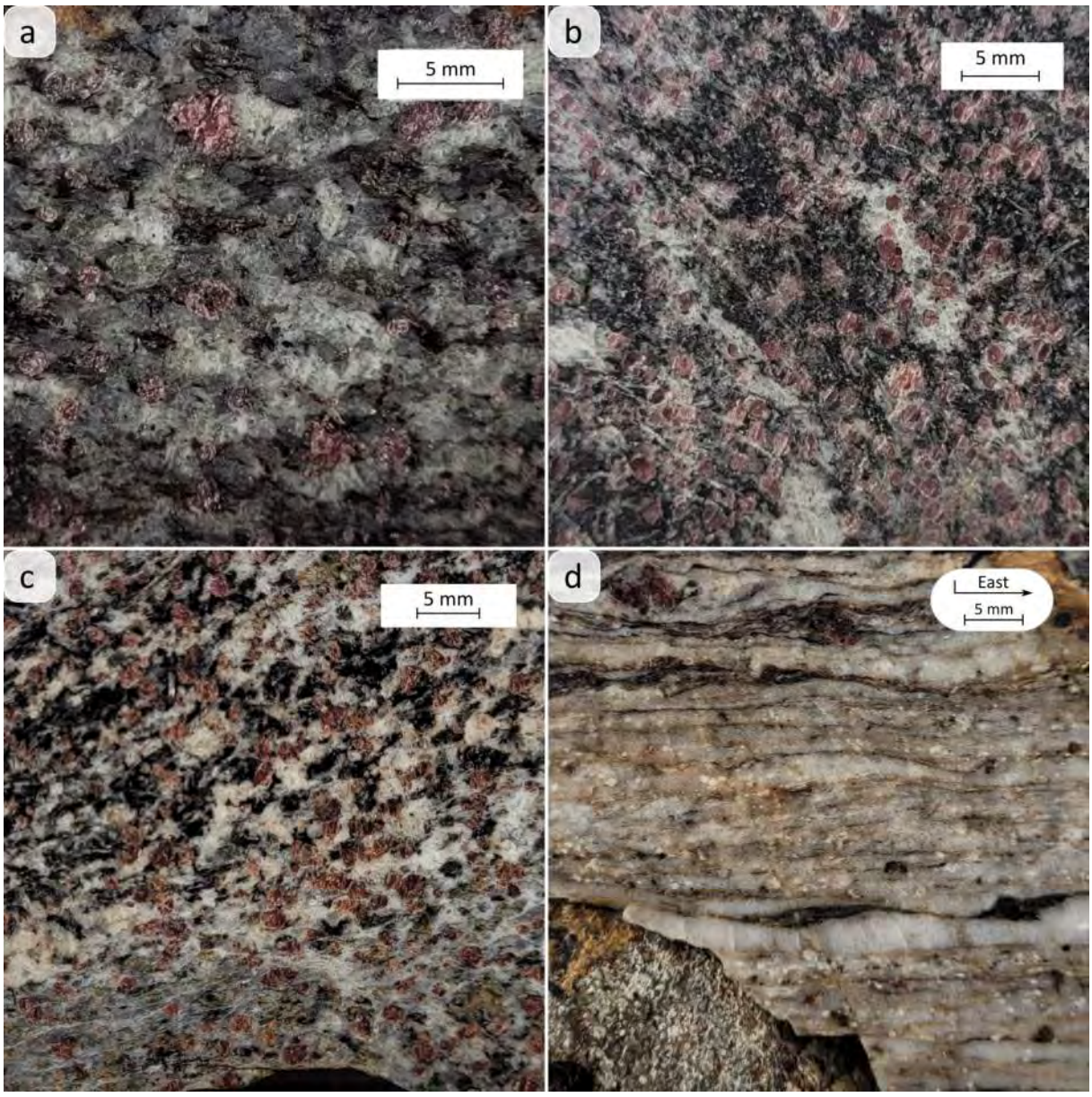


Figure 14: Photos of cut paragneiss samples. (a) Leucocratic paragneiss with quartz-rich matrix and no aluminosilicates. (b) Mesocratic paragneiss rich in biotite, garnet and sillimanite. Note sillimanite needles randomly oriented with respect to the foliation plane marked by white leucosome. (c) Paragneiss straddling the line between leucocratic and mesocratic. Matrix is poor in quartz and rich in sillimanite. Note transition from the lower domain almost exclusively consisting of sillimanite, garnet and unknown aggregates to the upper domain with a markedly lower mode of sillimanite, and abundant biotite and feldspar. (d) Leucocratic paragneiss leucosome with a low mode of ferromagnesian minerals. This rock is referred to as felsic orthogneiss in this thesis ((see below).

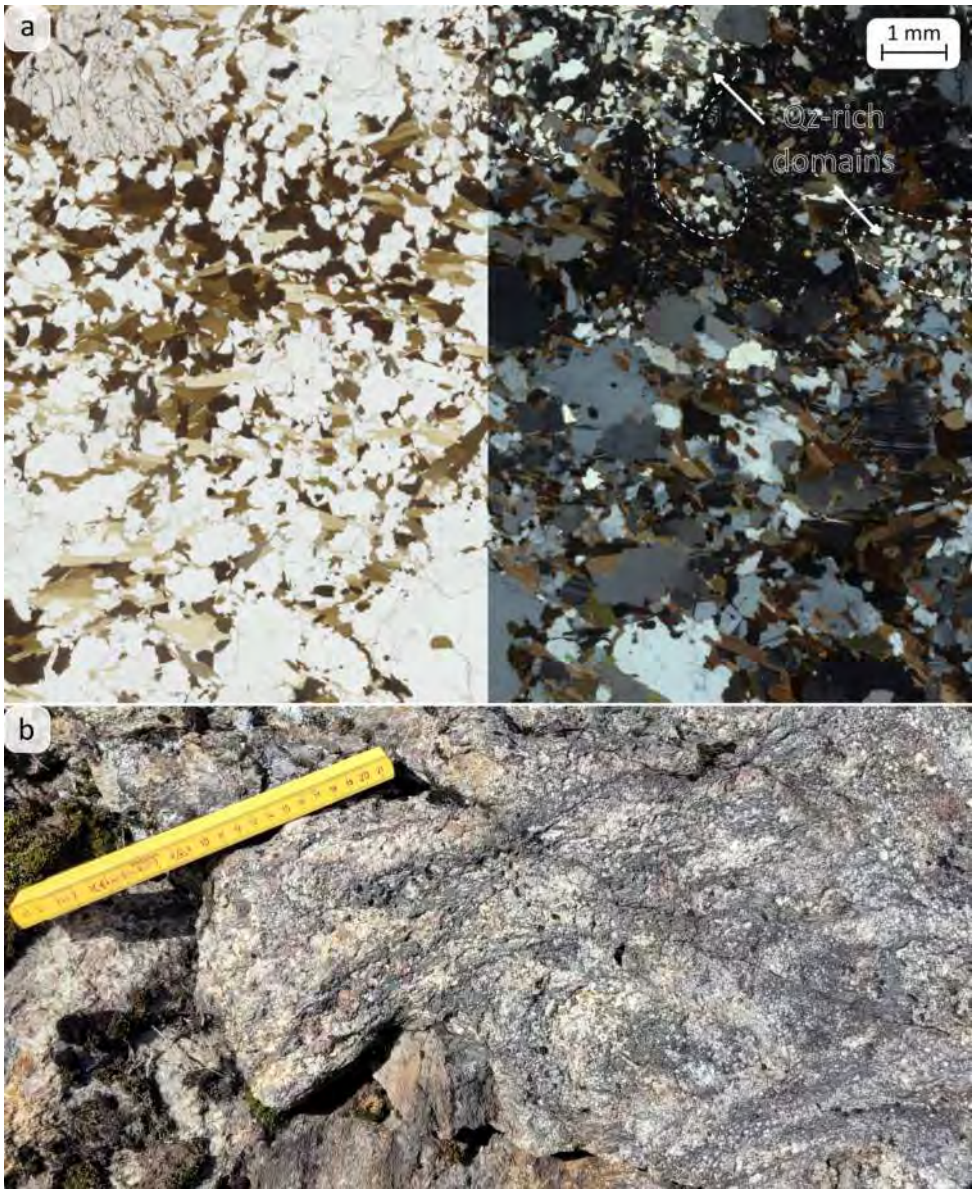


Figure 15: Thin section scan and outcrop photo of paragneiss restite. (a) Scan of thin-section from the unoriented paragneiss restite sample MS23104. Left side is displayed in plane-polarized light, right side in cross-polarized light. Three domains can be seen in the restite sample: in the lower half the composition is dominated by large plagioclase grains surrounded by bands of biotite, in the upper half the composition is dominated by biotite and garnet with smaller plagioclase grains. In the upper half two quartz-rich domains are marked, where extraction did not occur. (b) Outcrop with biotite- and feldspar-rich paragneiss restite. The fabric is marked by thick bands of bioite separating felsic patches.

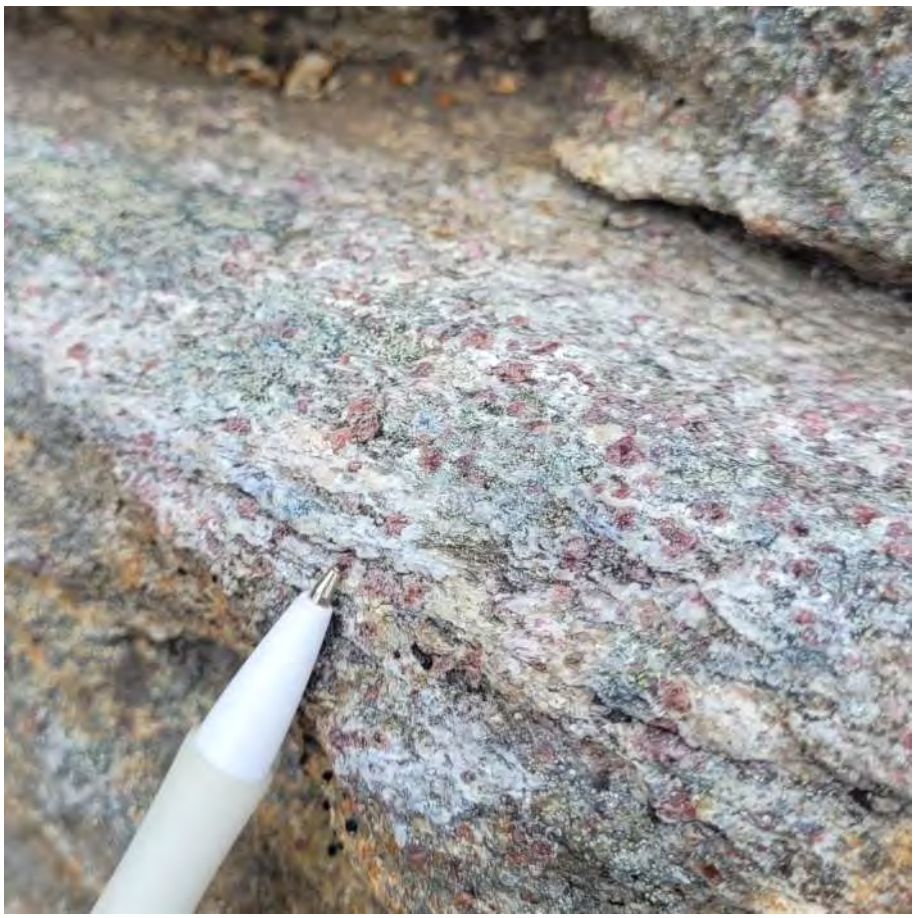


Figure 16: Photo of kyanite marking the foliation in leucocratic paragneiss.

Leucocratic paragneiss has a rusty yellow to light grey or white weathering surface, fresh surfaces are light grey to light purplish grey. Grain size is variable from fine- to medium-grained, with garnet porphyroblasts generally around 1-2 mm, but ranges from < 0.5 mm to ~ 10 mm. The distinction between leucocratic paragneiss and felsic orthogneiss is often hard to make in the field, as they can be similar in appearance. Leucocratic paragneiss however has a higher mode of biotite $\pm$ aluminosilicates, i.e. are more aluminous.

Mesocratic paragneiss often has a rusty brown weathering surface, fresh surfaces are dark purplish grey. Leucocratic bands mark the foliation at outcrop-scale. It is fine- to medium-grained with a larger range of garnet porphyroblast size, from < 0.5 mm to > 10 mm not being uncommon.

Paragneiss restite has a rusty dark grey weathering surface, and a dark fresh surface. Fine- to medium-sized grains, with coarse garnet and feldspar porphyroblasts. The matrix is weakly foliated, marked by the preferred orientation of biotite. Large biotite-rich bands defines the mesoscale fabric (Figure 15b).

The foliation of leucocratic and mesocratic paragneiss is slightly to very well developed, depending on composition and strain, marked by compositional bands, biotite and sillimanite $\pm$ kyanite (Figure 16). Thin sections made of paragneiss samples MS2305, MS2310, MS2314A, MS2320, MS2332C, MS23104 and MS23150 are described in table 3.

Table 3: Summary of sample thin sections from the Åreskutan Nappe and the tectonic boundary with the Kall Nappe. Location of samples can be seen in appendix A. Mineral abbreviations from Whitney and Evans (2010), WM: white mica. Minerals are listed in the estimated order of decreasing abundance. Inclusions are presented in the format Host (Inclusion).

Sample	**Lithology**	**Minerals**	**Marking foliation**	**Inclusions**	**Reactions**	**Pseudomorph aggregates**	**Zoned**	**Discordant foliation**	**Notes**
MS2305	Mylonitic paragneiss	Qz + Grt + Pl + Kfs + Bt + Sil + Ky + Ilm + WM + Rt	Bt, Qz bands, Sil, Ky	Grt (Ilm, Bt, Qz, Rt); Kfs (Qz, Ilm, Sil)	Ky → Sil; Ky → Bt; Grt → Bt; Sil → Bt; Fsp → WM; Rt → Ilm		Fsp	WM	Some Grt are replaced with large Bt, discordant with the main foliation. A significant portion of Fsp (Pl + undifferentiated) are fractured and contain abundant iron oxide.
MS2310	Paragneiss	Qz + Grt + Pl + Kfs + Bt + Sil + WM + Ilm + Rt	Bt, Sil, Qz bands	Grt (Qz, Bt, WM, Ilm, Rt)	Fsp → Sil; Grt → Sil; Grt → Bt; Sil → Bt; Rt → Ilm	Sil (fibrous and euhedral) + WM	Fsp	Bt	Rutile only present as inclusion in Grt. Sample displays apparent shear fabric of Sil, heavily replaced by Bt, but sample is not oriented.
MS2314A	Mylonitic paragneiss	Qz + Grt + Bt + Sil + Fsp (Pl + undifferentiated)+ WM + Ilm + Rt	Qz bands, Sil, Bt (partially)	Grt (Qz, Bt, Ilm, Rt, altered aggregates); Fsp (Bt)	Ky → Sil; Grt → Sil; Sil → Bt; Rt → Ilm		Fsp, Bt		Grts are generally poikiloblastic or idoblasticwith few inclusions.
MS2318	Ultramylonite	Qz + Cpx + Kfs + Pl + Ttn + WM + Ep + Ilm	Compositional bands, alignment of elongated Cpx, Ttn.	Cpx (Qz, Ilm)					Ultramylonitic calc-silicate gneiss judged by assemblage. Recrystallised Cpx different colour than original grain in PPL.
MS2320	Mylonitic paragneiss	Qz + Grt + Bt + Sil + Pl + Kfs + Ky + WM + Ilm + Rt	Bt, Sil	Grt (Qz, Bt, Ilm, Rt, (Grt?); altered aggregates)	Ky → Sil; Grt → Sil; Sil → Bt, Sil → WM; Rt → Ilm	WM + Ky + Sil + Bt + Qz	Bt, WM, Pl, Kfs	WM, Bt	Collected in the same location as MS2314

Table 3 (continued)

Sample	Lithology	Minerals	Marking foliation	Inclusions	Reactions	Pseudomorph aggregates	Zoned	Discordant foliation	Notes
MS2321	Felsic orthogneiss	Qz + Sil + Grt + Fsp + Bt + Ilm + Rt + WM	Elongate Ilm	Grt (Qz, Bt, Ilm)	Fsp → Sil; Grt → Sil; Grt → Bt; Sil → Bt; Rt → Ilm	Sil + Bt		Bt	Abundant Sil pseudomorphs after Fsp, often partially replaced by Bt.
MS2332C	Paragneiss	Qz + Grt + Sil + Ky + Pl + Kfs + Bt + Ilm + WM + Rt	Sil, elongate aggregates	Grt (Qz, Bt, Rt, Ilm, altered aggregates); Qz (Sil); Kfs (Wm, Qz, Pl)	Ky → Sil; Grt → Sil; Sil → Bt; Grt → Bt; Ky → WM; Sil → WM	Wm + Ky + Sil + Bt + Qz	Pl, Kfs, Bt	Bt, Wm	Pl are typically fractured, sericitised along fractures. Grt are also highly fractured. In one Grt, Wm fills a wide fracture. Bt generally appears as large flakes in aggregates and replacing Grt, often discordant with the main foliation.
MS23104	Paragneiss restite	Pl + Bt + Grt + Qz + Ilm	Bt	Grt (Qz, Pl, Bt, Ilm)	Grt → Bt		Bt		Paragneiss with probable melt extraction of Qz. Bt colour is different than than the vibrant red-brown found in other Åreskutan Nappe rocks, instead it's pleochroic between pale yellow through greyish brown to very dark brown. Grt are highly fractured and rich in inclusions (primarily Qz).
MS23145	Pyroxene amphibolite	Amp + Opx + Bt + Pl + Ilm + Oxides	Bt, Compositional bands, alignment of elongated Px, Amp	Amp (Ilm, Pl, Bt, (Px?)), Pl (Bt)				Bt	Different compositional domains in sample, Px-Amp-Pl and Bt-Pl, with minor mixing. The two domains display different foliation orientation. Bt colour is not quite as vibrantly red-brown as the typical Bt colour in the Åreskutan Nappe samples.
MS23150	Mylonitic paragneiss and amphibolite	Paragneiss: Qz + Fsp (Pl + undifferentiated) + Grt + Bt + Wm + Sil; Amphibolite: Amp + Pl + Ep + Ilm	Bt, Amp, compositional bands	Grt (Bt, Ilm, Qz); Fsp (Bt)	Grt → Bt; Fsp → Wm; Sil → Bt; Amp + Pl → Ep		Bt		Different compositional domains, paragneiss and amphibolite. High Fsp mode in paragneiss, potentially some melt extraction of Qz. Amp and Pl in the amphibolite are surrounded by Ep coronas.



Figure 17: Photo of sharp contact between felsic orthogneiss and rusty paragneiss in a large fold. note sharp folds in paragneiss. Faint folds can be seen in the felsic orthogneiss as well, but are diffuse due to poorly marked foliation.

7.2.2 Felsic orthogneiss

Felsic orthogneiss, also referred to as leucogranite (e.g. Ladenberger et al., 2014), is compositionally transitional with paragneiss. The correct term would be leucocratic veins or layers of neosome (following Sawyer, 2008), as the felsic orthogneiss is shown to likely be cogenetic with the migmatitic paragneiss (Ladenberger et al., 2014). However, the term felsic orthogneiss will be used to identify the less aluminous felsic lithologies not obviously emplaced in the original rock, especially as they in places appear similar to foliated granite. In the field, sharp contacts are generally observed between paragneiss and felsic orthogneiss (Figure 17). Rusty yellow to light grey or white weathering surface, fresh surfaces are light grey. Fine- to medium-grained, occasionally coarse-grained, with a low mode of garnet porphyroblasts (Figure 14d). Composition is dominated by quartz, with biotite, garnet, feldspars, ± sillimanite, ± white mica. At the microscale, the quartz matrix show significant recrystallisation, and subhedral to anhedral feldspars are mostly replaced, forming pseudomorph aggregates of fibrous sillimanite (Figure 18). Thin section made of felsic orthogneiss sample MS2321 is described in table 3.



Figure 18: Scan of thin-section from the unoriented felsic orthogneiss sample MS2321. Upper left plane-polarized light, lower right cross-polarized light. Matrix is quartz-dominated with fibrous aggregates of sillimanite in pseudomorphs and small but pristine subhedral garnets.

7.2.3 Metabasite

Metabasite is common throughout the Åreskutan nappe as xenoliths or layers in migmatitic paragneiss, and as larger coherent domains with a varying degree of partial melting. Further investigation is needed to provide a detailed description of the different metabasite lithologies, as only two thin sections were made. The most common lithology is pyroxene amphibolite, which predominantly appears in two large coherent domains on Åreskutan: on the upper southwest ridge and face below the cable car top station, and around the summit. Smaller domains are scattered throughout the nappe, from mafic pods only a decimeter thick to layers and bodies tens of meters thick. The weathering surface is rusty and dark, fresh surfaces are blue-green-hued black to pitch black (Figure 19a-b). Fine- to medium-grained, often with a granular texture. The composition of the metabasite varies depending on degree of partial melting and retrogressive reactions. The most common assemblage consists of amphibole, orthopyroxene, plagioclase, ± garnet. Peritectic garnet is common in partially melted metabasite, and garnets observed in the matrix may have formed after the main assemblage. Metasomatically altered metabasite xenoliths are occasionally oberved in paragneiss (Figure 19c). The foliation is marked by compositional bands, as well as foliaton-parallel bands of leucosome in strained regions (Figure 19d). The degree of migmatisation varies from none or minor stromae parallel to the foliation to almost complete melting with isolated rafts (Figure 20a-e). The leucosome consists of plagioclase and minor quartz, plus pyroxene, amphibole, ± garnet, with amphibole replacing pyroxene (Figure 20f). Mafic selvedges, melanosomes and restite are rich in pyroxene. Mingling of metabasite leucosome with apparent migmatitic paragneiss is often observed, which complicates distinction between paragneiss and metabasite rocks (Figure 21). At the microscale, pyroxene amphibolite can be seen interlayered with possible paragneiss restite (Figure 22. Thin sections made of metabasite samples MS23145 and MS23150 are described in table 3.

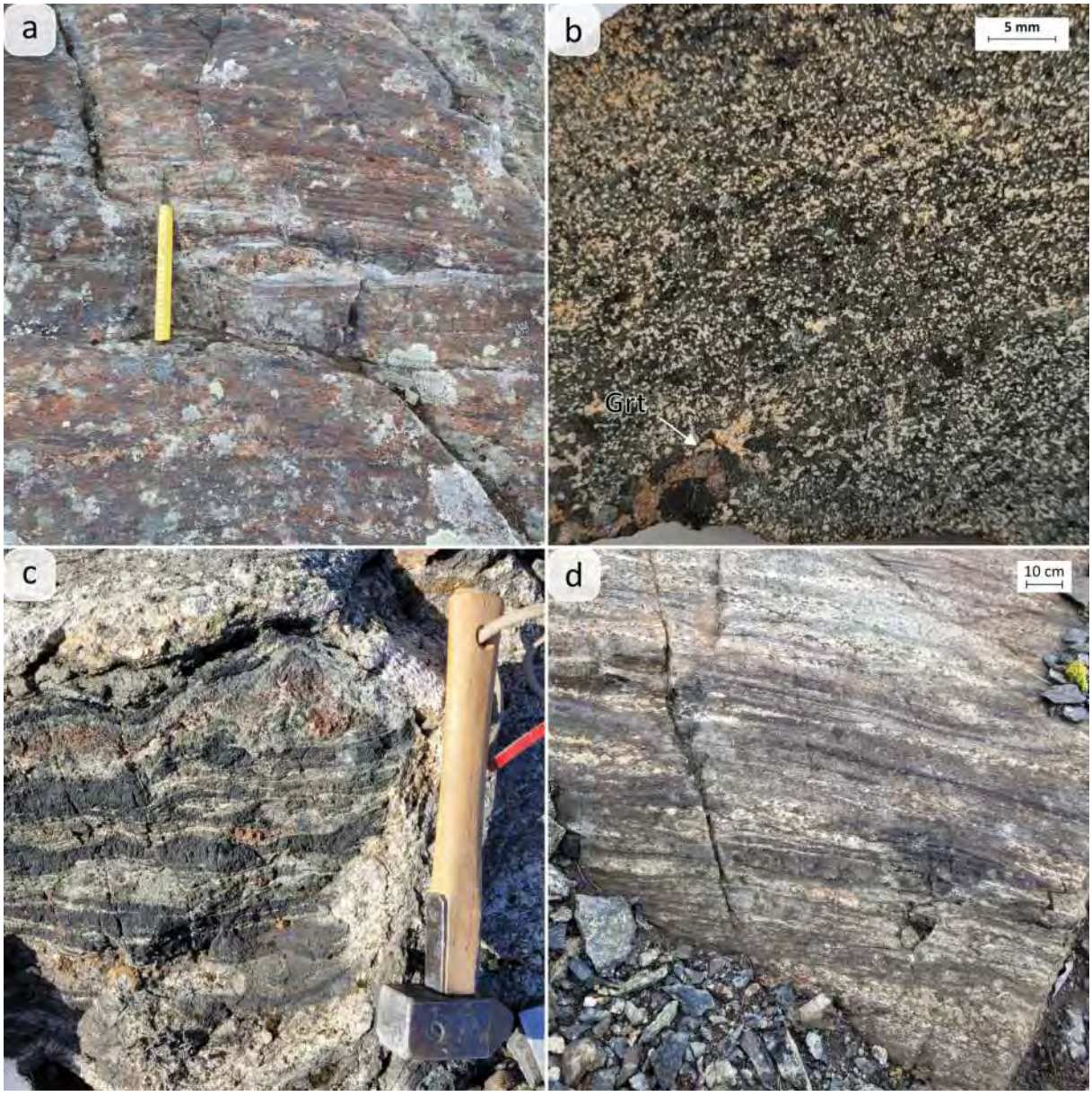


Figure 19: Photos of metabasite outcrops and cut sample. (a) Rusty weathering surface of mylonitic highly migmatised pyroxene amphibolite with skarn pods. Outcrop-scale foliation marked by leucocratic and melanocratic bands. (b) Cut surface of pyroxene amphibolite. Note garnet in lower left corner, being replaced by pyroxene and plagioclase. (c) Pyroxene- and garnet-rich pod of metasomatically altered metabasite hosted in metabasite leucosome. (d) Weathering surface of mylonitic highly migmatised pyroxene amphibolite, similar to (a), but with a fresher surface. Large pyroxene and amphibole porphyroblasts are clearly visible in the leucosome.

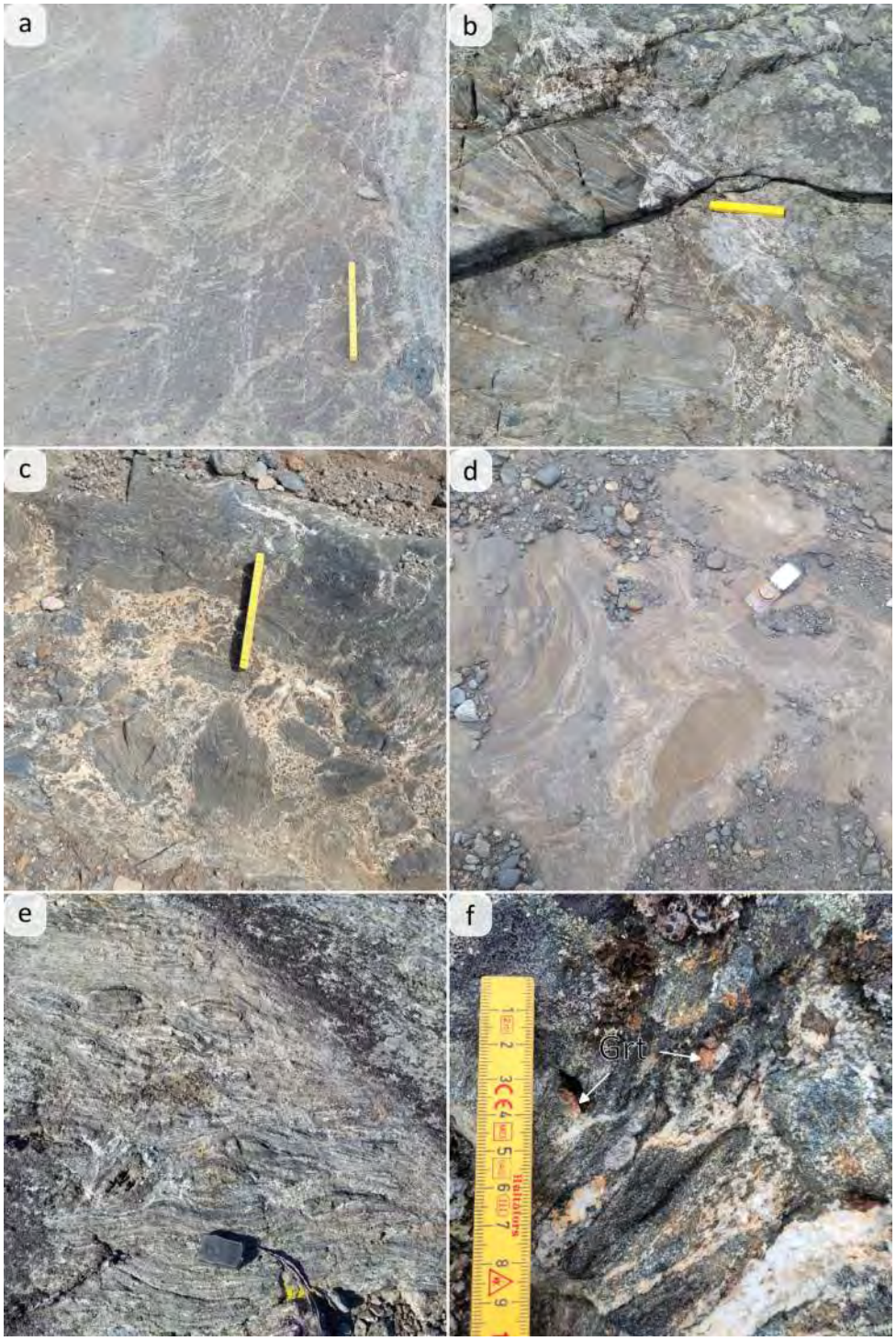


Figure 20: Photos of migmatised metabasite rocks display different degrees structures of anatexis. (a) Pyroxene amphibolite with folded stromatic leucosomes. In lower right, next to ruler, a dark patch of possible restite can be seen. (b) Pyroxene amphibolite with both net-structured and stromatic leucosome. Rafting of angular blocks of the host rock is seen in larger melt patches. Note the large triangular melt patch below the ruler. (c) Raft-structured pocket of melt in pyroxene amphibolite, rafting angular to sub-angular blocks of host rock. Net-structured and stromatic leucosome is visible in the host rock. (d) Rounded and folded metabasite rafts in a highly melted outcrop. (e) Restite or skarn pods in pyroxene amphibolite with minor stromatic to net-structured leucosome. (f) Garnets in or in contact with leucosome in pyroxene amphibolite.



Figure 21: Mixed outcrop of mesocratic paragneiss and metabasite rock, contact below ruler. Note gradual decrease of garnet mode going downwards in the left half of the photo, and increase in small light grey metabasite pods. The light grey lithology appears to be a partial melt derifed from the black melanosomes or restite to the right.

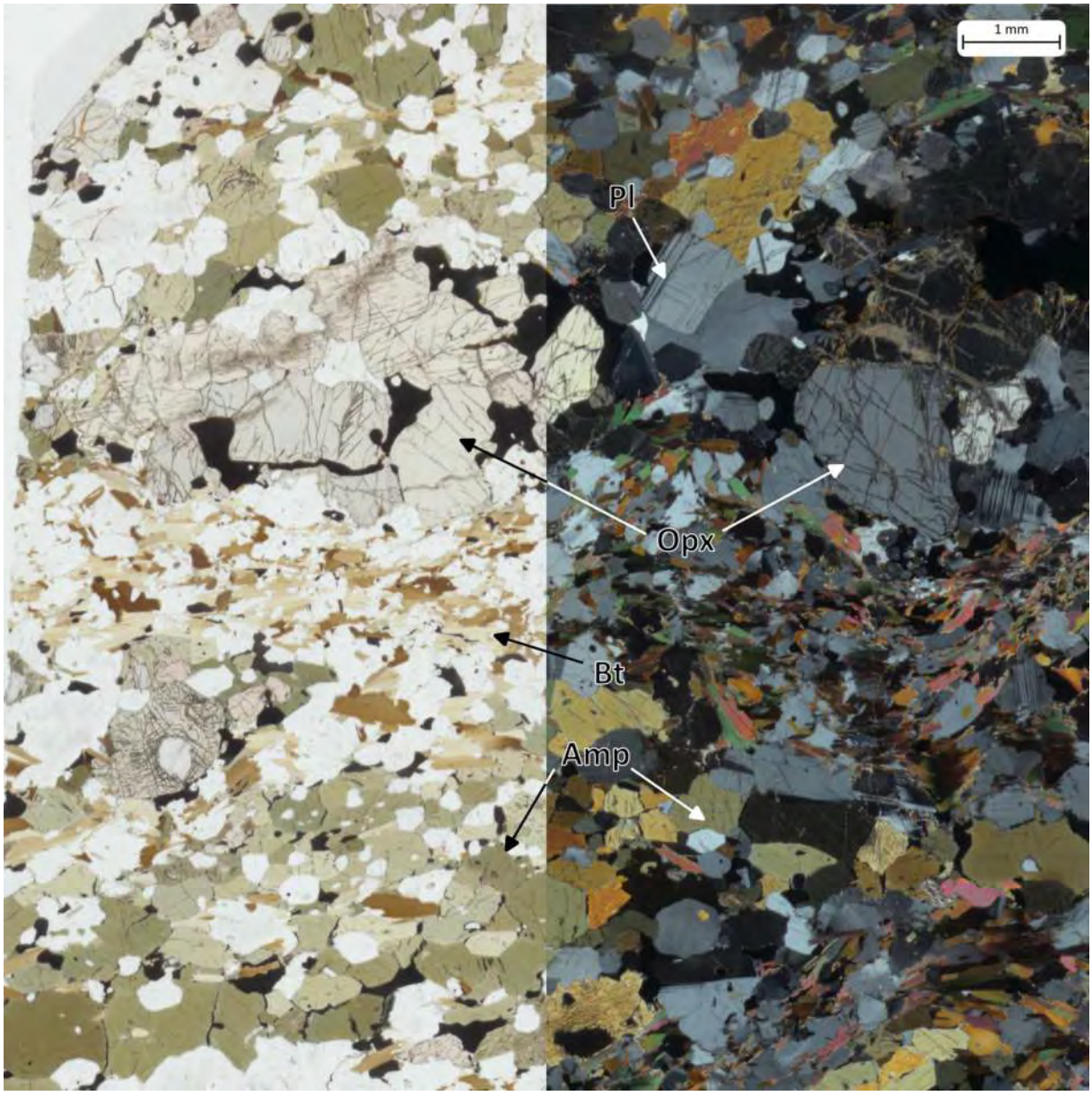


Figure 22: Scan of thin section from metabasite sample 145, with interlayered pyroxene amphibolite and biotite-rich layers wich may represent paragneiss restite. The amphibole grains in the sample are interpreted as primary, indicated by the sharp boundaries and lack of visible replacement reactions. The left side is displayed in plane-polarised light, the right in cross-polarised light.

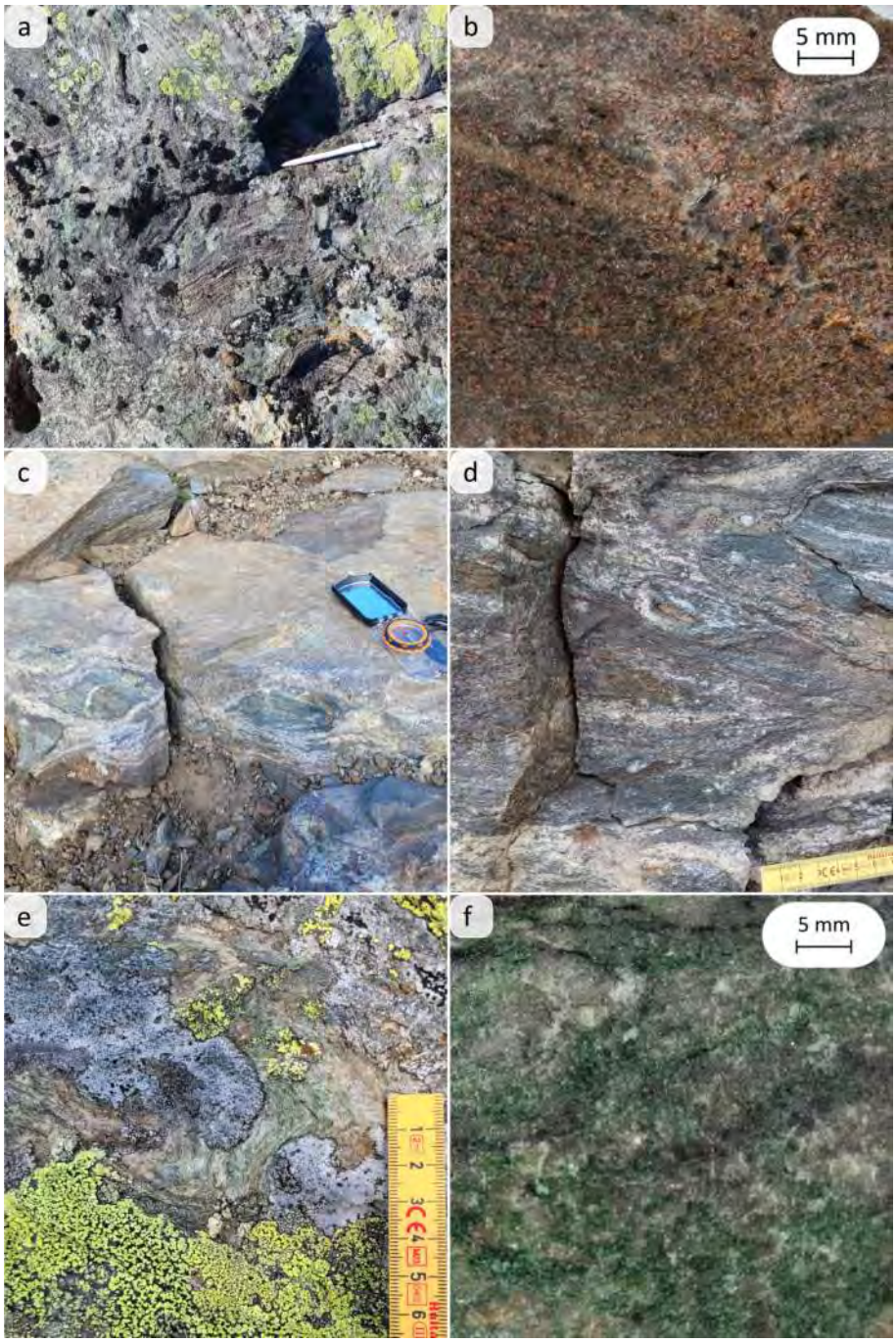
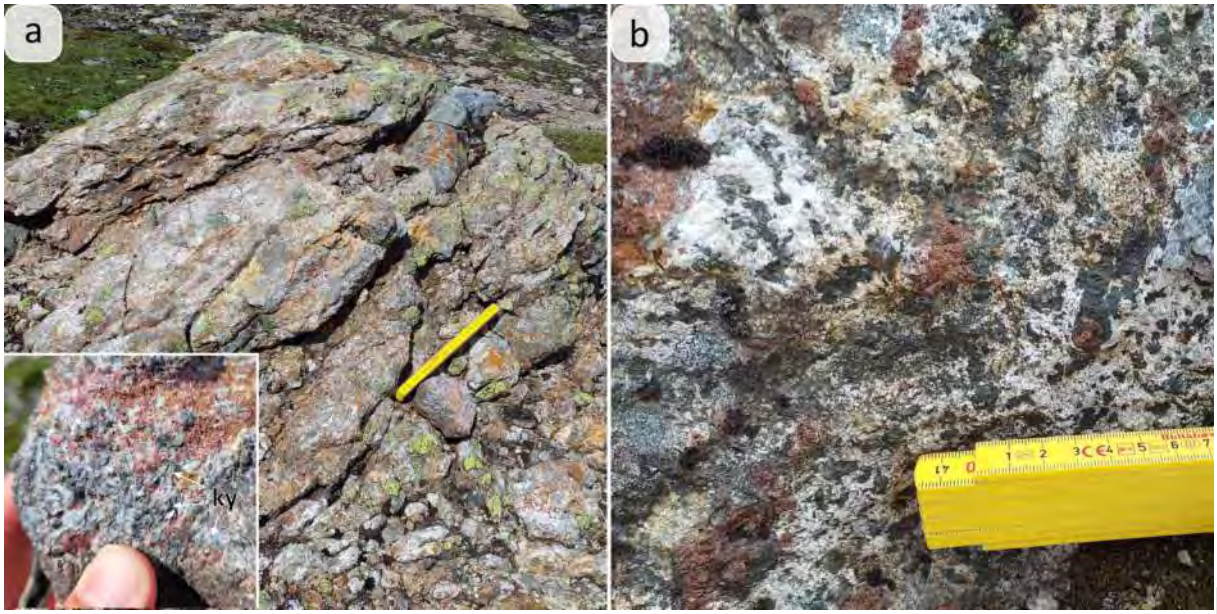


Figure 23: Photos of curious rocks that need further attention in the future. (a) Apparent paragneiss palaeosomes in kyanite-sillimanite-rich leucocratic paragneiss. (b) cut surface of pod from (a), revealing a fine-grained quartz- and garnet-rich matrix. (c) Blue-hued pods of unknown palaeosome, with apparent mafic selvedges. (d) Small skarn pod and metabasite pods in a relatively low-strain paragneiss domain. (e) Xenolith rich in unknown green minerals. (f) Cut sample from loose boulder of unknown lithology with green minerals. Colour may indicate chromium-rich minerals.

7.2.4 Palaeosome, pegmatite and curiosities

Detailed descriptions and analysis of xenoliths, palaeosomes and pegmatite fall outside the scope of this thesis, but may prove important for future research. As such, they are only briefly described in this section. Pods of palaeosome or resister lithologies are occasionally seen in paragneiss. These display a relict foliation, predating that of the main foliation (Figure 23a-b). Examples of xenolith or palaeosome lithologies are garnetiferous metasandstone, skarn pods of varying composition, blue-tinted to dark grey metasandstone and quartz- or amphibole-rich pods with abundant green crystals of unknown type, possibly chromium-rich (Figure 23c-f).



[h]

Figure 24: Photos of lithologies that require further attention. (a) Outcrop of kyanite-garnet-rich lithology, small figure shows sample lying just below ruler. (b) Lithology of unknown paragenesis with large, fractured garnets appearing to be replaced by pyroxene. The feldspathic matrix is quite coarse-grained, with large patches of quarts, visible on the right edge of the photo, above the ruler.

Close to the summit of Åreskutan, sandwiched between two larger domains of pyroxene amphibolite, is an area of difficult to describe rocks rich in garnet, kyanite and possibly pyroxene (Figure 24a). This domain is speculated to represent high-grade paragneiss melanosome, but further investigation is needed to correctly identify the paragenesis. Also requiring further investigation is a layer cutting the foliation in pyroxene amphibolite, consisting of feldspar, quartz and abundant garnet and pyroxene, which replaces garnet (Figure 24b). The assemblage is reminiscent of garnet granulite, but the relationship to the surrounding pyroxene amphibolite is not known.

Pegmatites are occasionally observed cutting the foliation of all lithologies, but are also observed parallel to the main foliation (Figure 25). Composition is quartz, feldspar and biotite, ± garnet, ± white mica. The pegmatite sometimes shows incipient to well developed foliation, marked by the preferred orientation of biotite.



Figure 25: Photos of the relationship between foliation and pegmatite. (a) Pegmatite cutting the foliation of pyroxene amphibolite. The pegmatite consists of quartz, feldspar and large books of biotite, which do not show any preferred orientation. Sketch to the right outlines the pegmatite in the host rock. (b) Pegmatite intruding paragneiss, intrusive contact visible in center of photo where foliation of a wedge of paragneiss is cut. The pegmatite consists of quartz, feldspar and large books of biotite which mark a weak foliation concordant with that of the outrop, i.e. the main foliation. Sketch to the right outlines the pegmatite in the host rock.

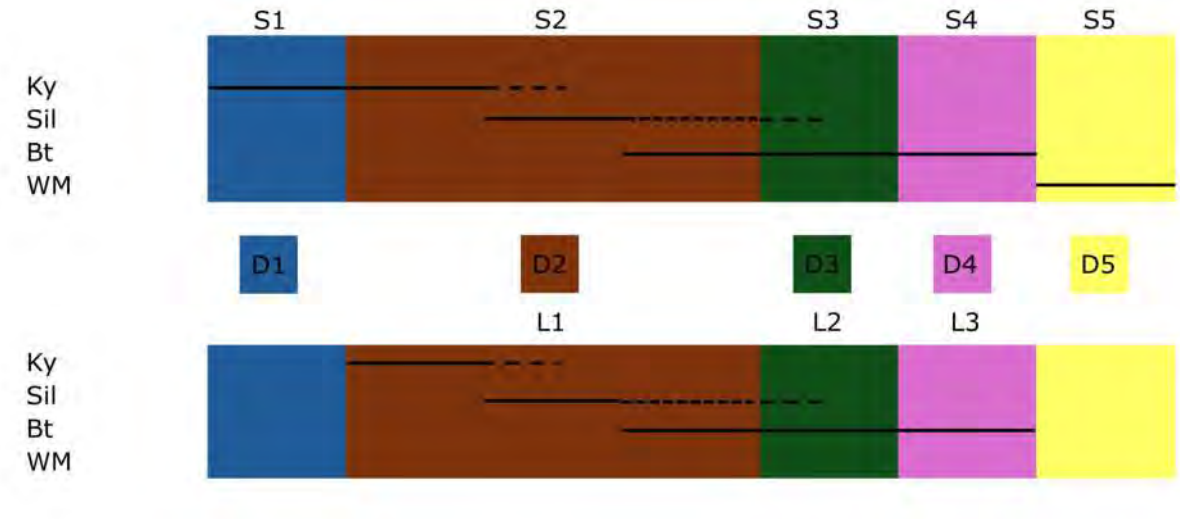


Figure 26: Summary of the deformation history of the Åreskutan Nappe. Deformational events D1-D5 are identified and shown based on the succession of minerals marking foliation and stretching lineation.

7.2.5 Deformation history

The Åreskutan Nappe shows a long deformational history with five deformational phases, D1-D5, identified in the field and in thin sections. The deformational phases are summarised in figure 26. The earliest observable deformation event in the Åreskutan Nappe, D1, can be seen in the foliation S1 in preserved domains of metabasite, and in xenoliths and palaeosome (Figure 23a-c). Folds can be observed in the relict foliation, but further investigation is needed to identify deformational structures postdating S1 but predating partial melting during D2 and the development of the migmatitic main foliation S2. Strain during anatexis is difficult to gauge due to protracted deformation. However, unstrained melt pockets are observed, mainly in metabasite lithologies, indicating at least a partitioning of strain. The main foliation S2 of the Åreskutan Nappe separates domains of random migmatitic folding. It developed contemporaneously with the folded domains, as indicated by the succession of minerals marking the foliation, kyanite, sillimanite and biotite. Strain was partitioned in internal high-grade shear zones both thick and thin with continual development of the main foliation through cooling, as indicated as above by the succession of minerals marking foliation, which is also concordant with the basal retrogression zone (See metamorphic history). Stretching lineation is generally well developed throughout the nappe, stronger in domains parallel to the main foliation, and show a consistent east-west trend (Figure 27). High-grade stretching lineation L1 is marked by mineral aggregates and the succession of kyanite, sillimanite and bitotite (Figure 28a-c). The most developed stretching lineation is marked by mineral aggregates and the preferred orientation of prismatic sillimanite. Migmatitic zones outside of S2 are sometimes distinguished by random or radial orientation of sillimanite on the foliation plane (Figure 28d). At the microscale, the rocks of the Åreskutan Nappe has a diffuse shear fabric geometry (Figure 29, Figure 30), but abundant mesoscale structures are observed in outcrops. High-grade shear sense indicators dominantly show top-to-the-east shear (Figure 31). Coeval shear bands indicating top-to-the-west shear are observed in high-grade lithologies of the nappe, particularly at upper structural levels, together with, and likely conjugate with, top-to-the-east indicators (Figure 32).

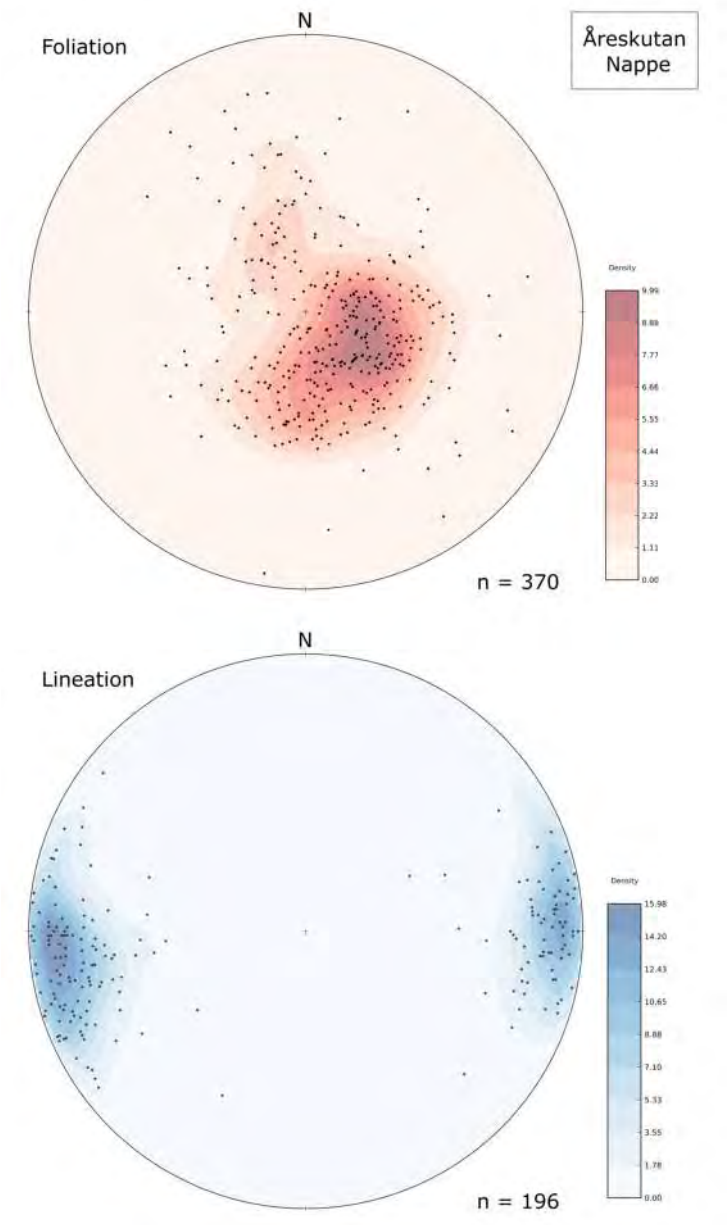


Figure 27: Structural measurements of the Åreskutan Nappe within the study area, projected in lower hemisphere equal-area stereograms. The foliation is dominantly dipping gently towards northwest, and the stretching lineation shows a clear east-west trend. Contours marking the observation density are constructed using Fisher probability distribution in the projection program OpenStereo.

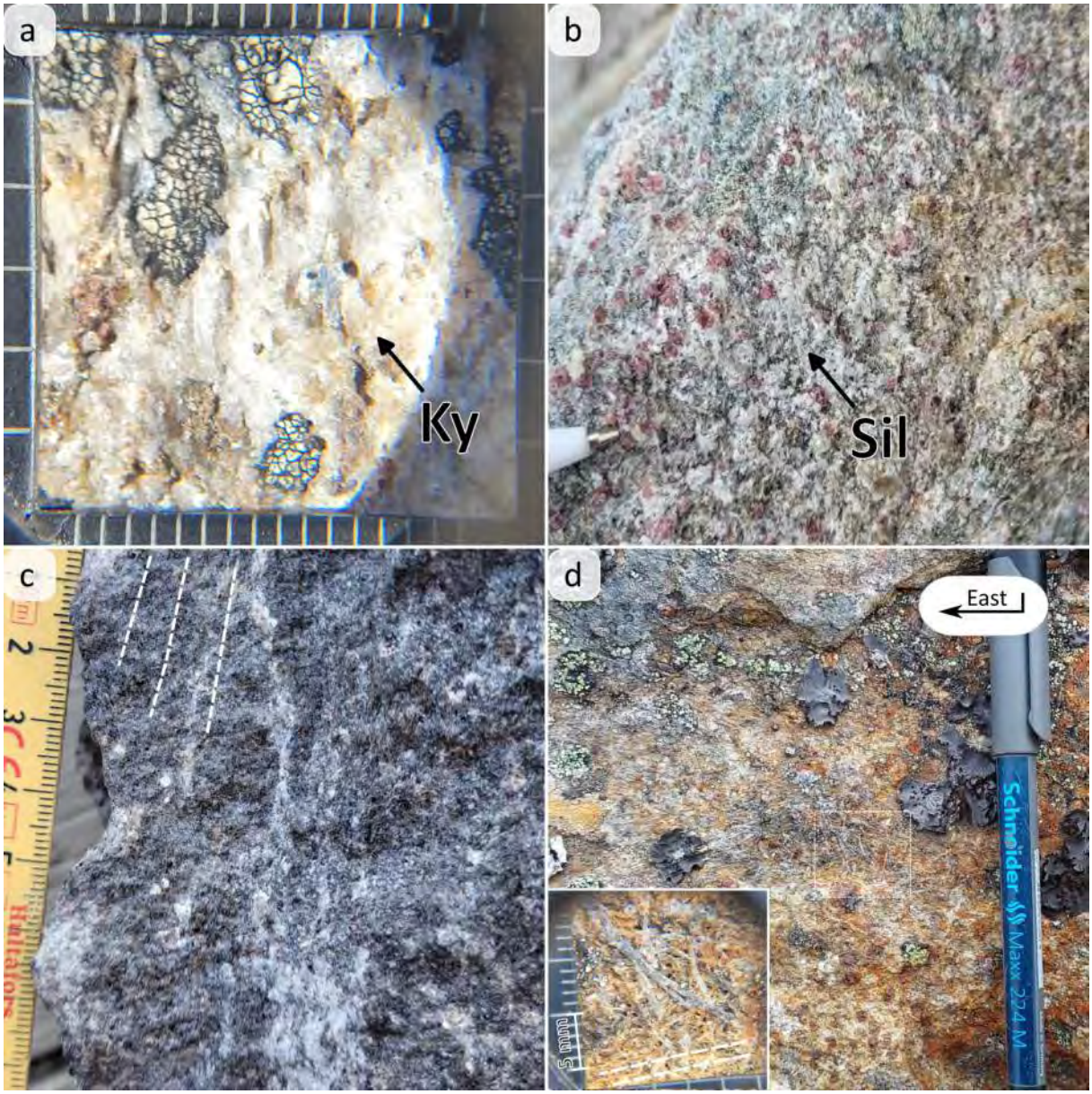


Figure 28: Photos of stretching lineation markers in paragneiss. (a) Stretching lineation marked by quartzofeldspathic aggregates and kyanite, partially replaced by sillimanite. (b) Stretching lineation marked by quartzofeldspathic aggregates and sillimanite. (c) Stretching lineation faintly marked by biotite. Indicated by striped lines. (d) Random orientation of sillimanite on foliation plane. A faint stretching lineation marked by quartzofeldspathic aggregates and sillimanite is indicated by striped lines.

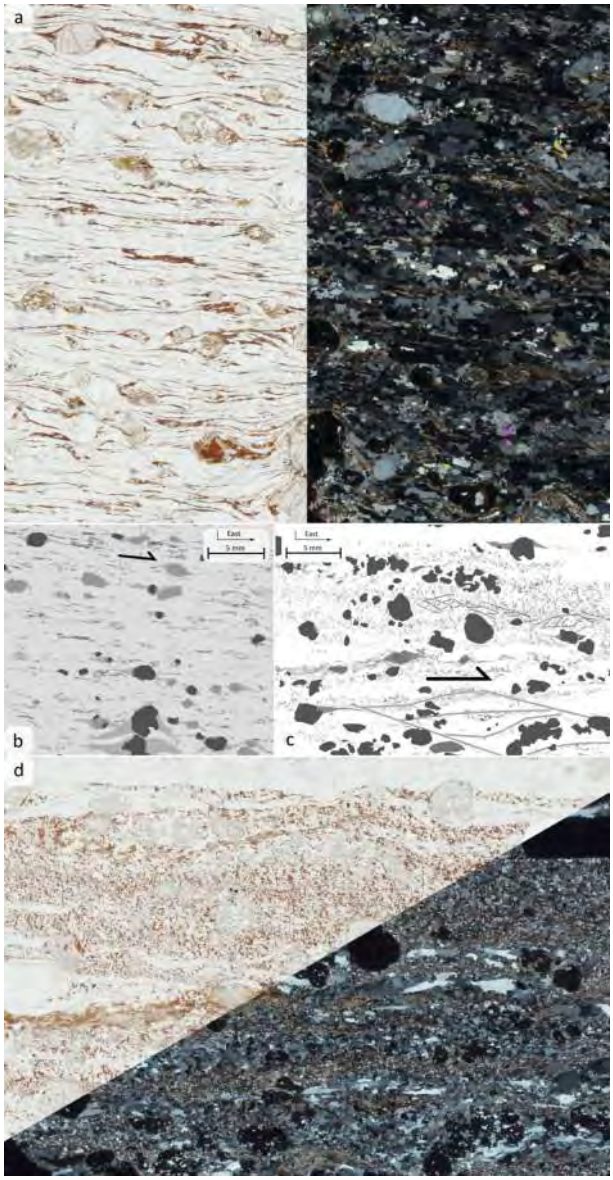


Figure 29: Thin section scans of paragneiss and sketches showing the shear fabric. (a) Thin section of mylonitic paragneiss sample MS2305. Left half is displayed in plane-polarized light, right half in cross-polarized light. (b) Sketch showing the deformational fabric of (a).There is no distinct shear fabric, but delta- and sigma-shaped tails around garnet and feldspar faintly indicate top-to-the-east shear. (c) Sketch showing the deformational fabric of (d). Faint shear bands indicating top-to-the-east shear are marked by biotite, and tails around garnet and feldspar are nearly symmetrical. (d) Thin section of mylonitic paragneiss sample MS2314A. Upper left is displayed in plane-polarized light, lower right in cross-polarized light.

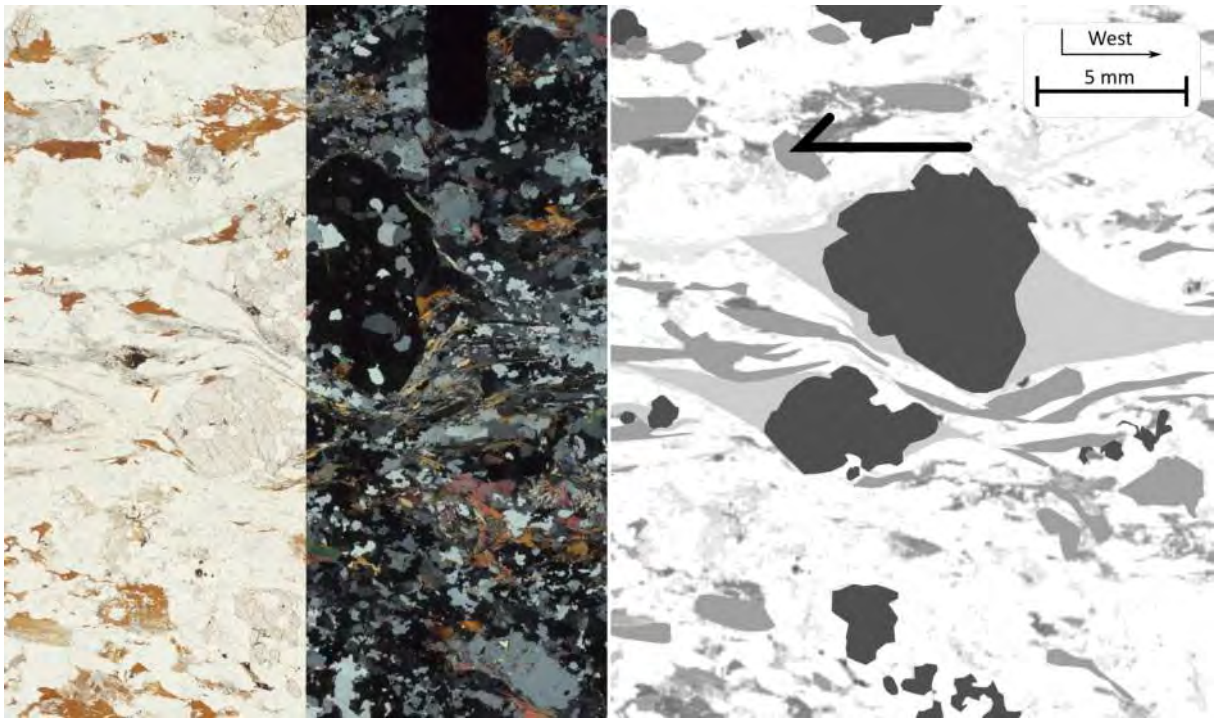


Figure 30: Thin section scan of paragneiss sample MS2332C to the left, and a sketch showing the shear fabric to the right. Left half on the thin section is displayed in plane-polarized light, the right half in cross-polarized light. The sketch highlights asymmetric grain tails indicating top-to-the-east shear.

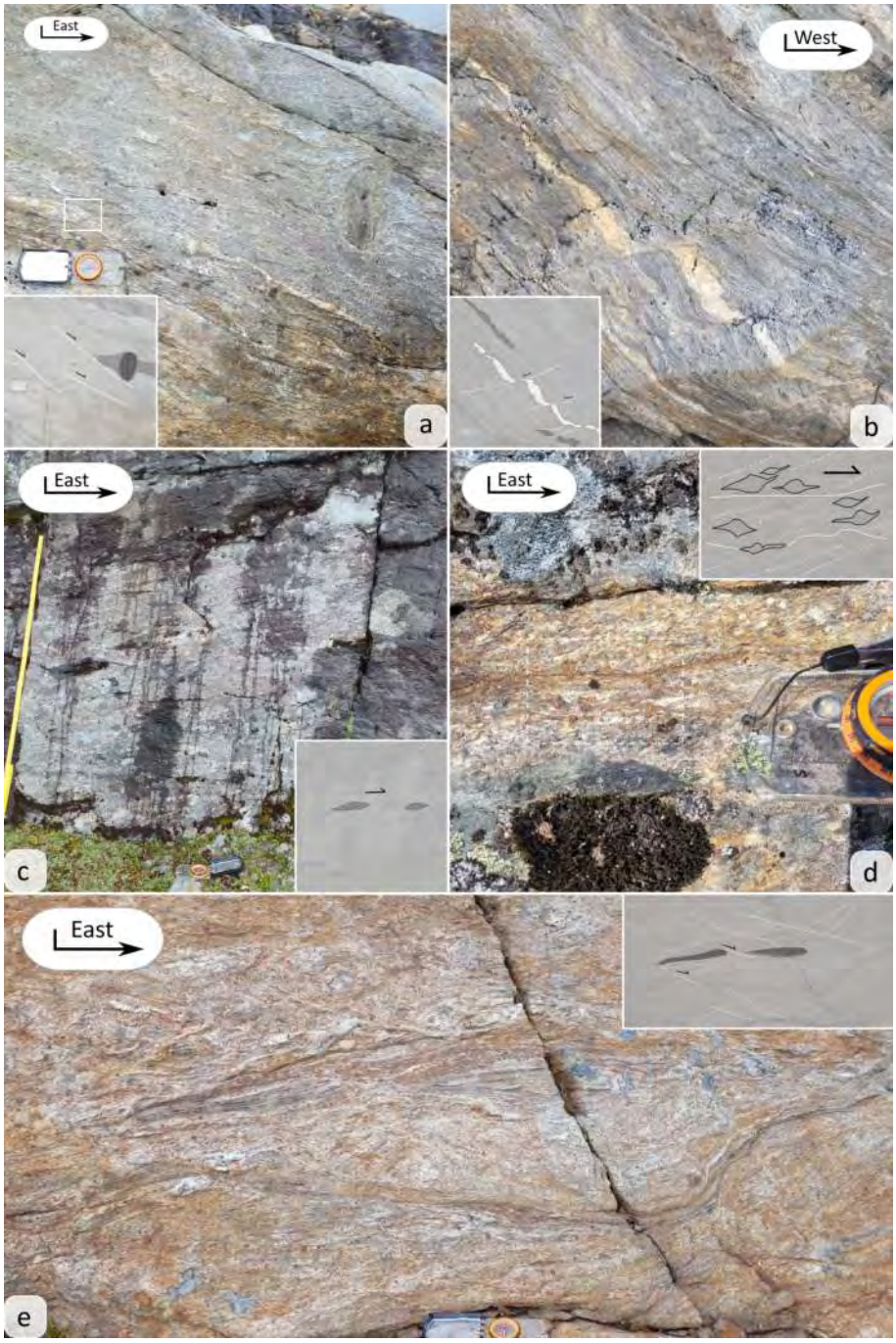


Figure 31: Photos of meso-scale shear sense indicators, and sketches highlighting the deformational fabric. All photos are taken parallel to the stretching lineation, with the trend shown. All photos show outcrops with top-to-the-east shear indicators. (a) Shear bands in mesocratic paragneiss. Note the pod on the right with symmetric strain shadows. (b) Shearbands cutting wide leucosome bands in mesocratic paragneiss. (c) Sigmoid pods in mesocratic paragneiss. (d) Rare S-C fabric in paragneiss. White rectangle shows the extent of the sketch. (e) Shear bands and boudinaged mafic pods in garnet-rich mesocratic paragneiss

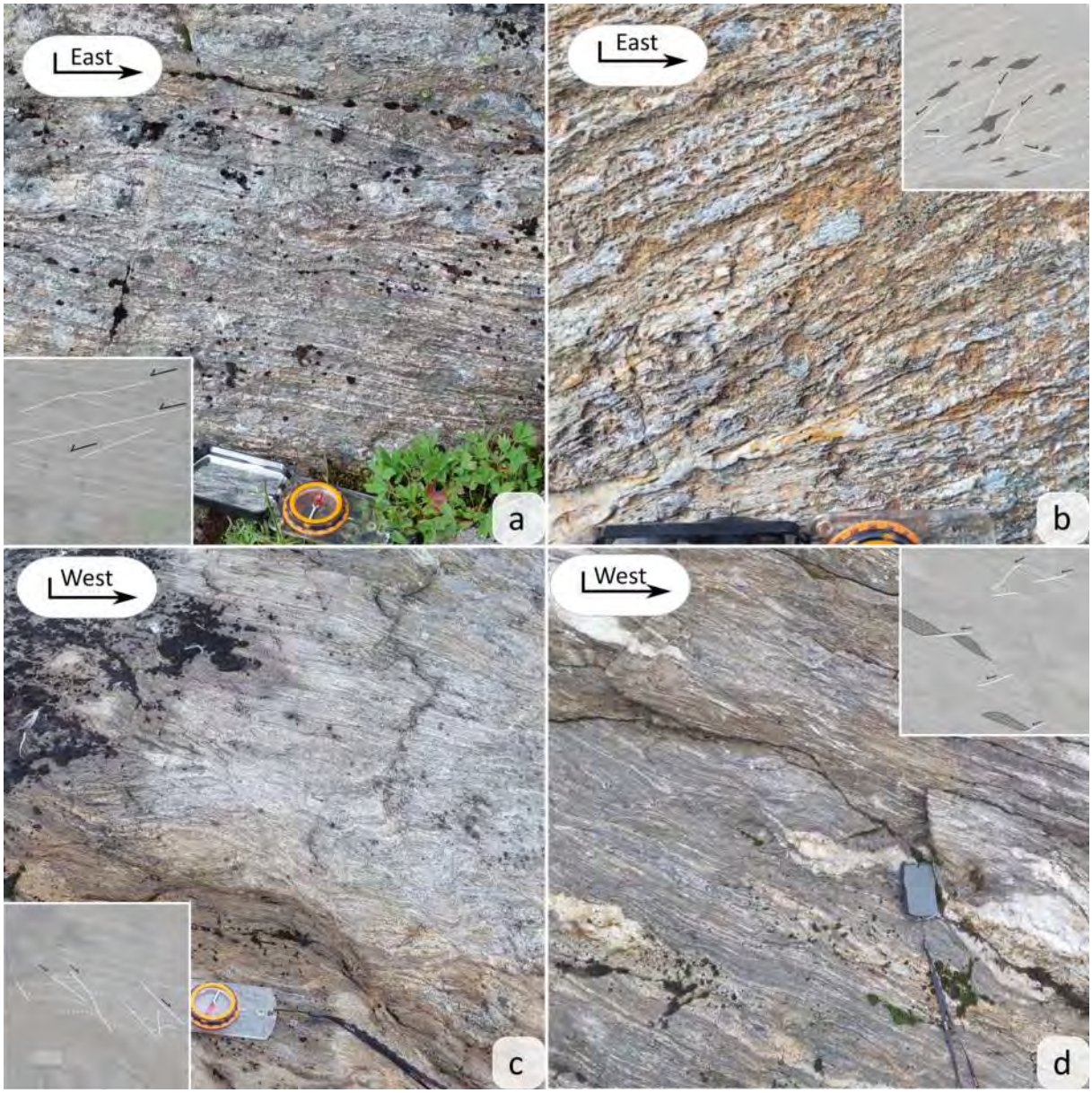


Figure 32: Photos of meso-scale shear sense indicators, and sketches highlighting the deformational fabric. All photos are taken parallel to the stretching lineation, with the trend shown. (a) Shear bands and noticable buckling of the foliation in mesocratic paragneiss, indicating top-to-the-west shear. (b) Shear bands indicating top-to-the-east shear, conjugate shear bands indicating top-to-the-west shear and grain-tail complexes in paragneiss with distinct leucosome layers. Grain-tail complexes are symmetric or show top-the-east shear. (c) Shear bands indicating top-to-the-west shear in mesocratic paragneiss with clear leucocratic segregations. (d) Shear bands indicating top-to-the-east shear a few meters from (c).

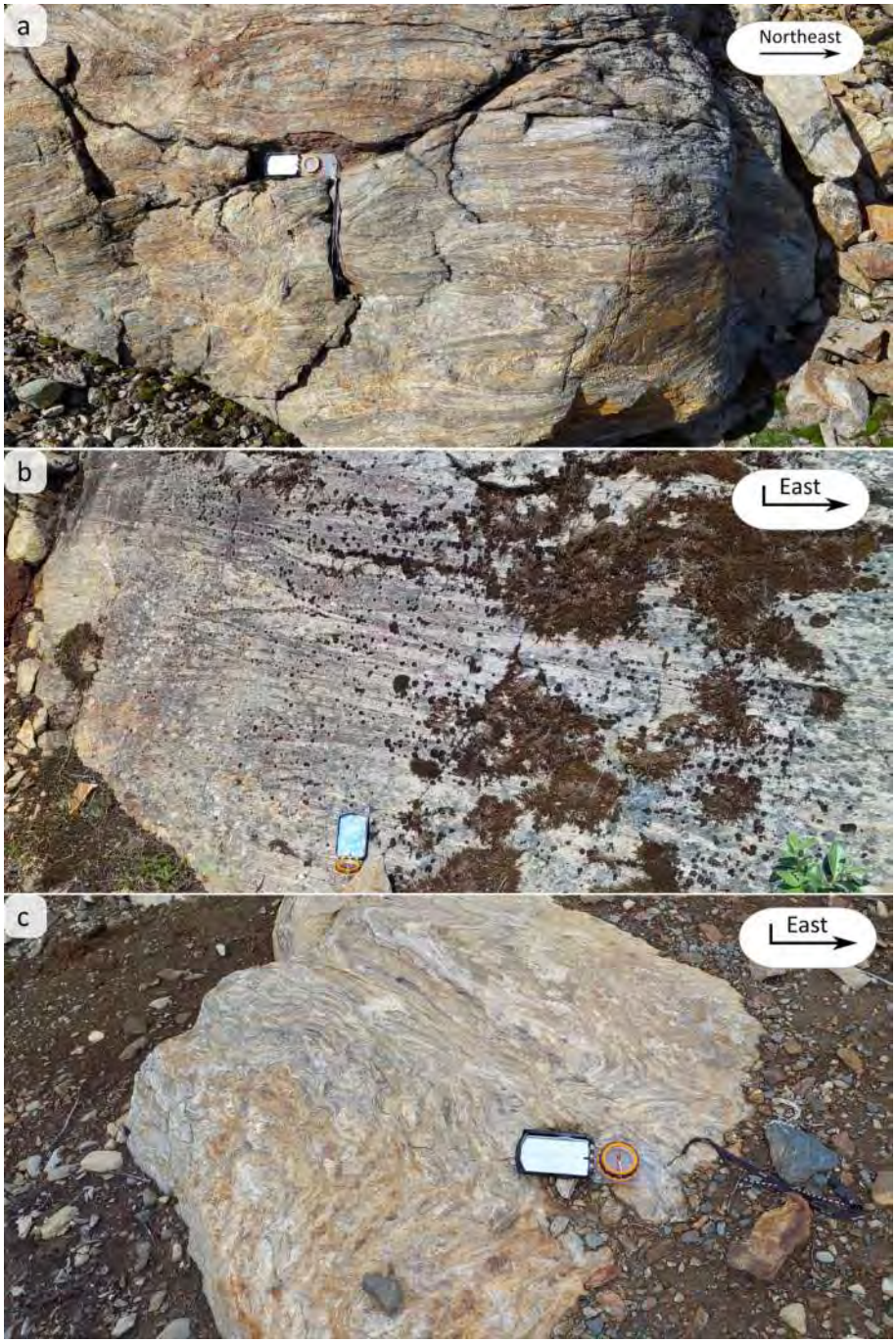


Figure 33: Photos of isoclinal folds. (a) Isoclinal folds in mylonitic pyroxene amphibolite. Photo taken oblique to stretching lineation. (b) Sharp isoclinal folds in paragneiss close to the base of the nappe, within 50 m of the tectonic boundary with the Kall Nappe. Photo taken parallel to the stretching lineation. (c) Complex fold structure in paragneiss.



Figure 34: Photo of garnet-rich vein filling a brittle fracture, cutting the foliation of metabasite close to the lower tectonic boundary.

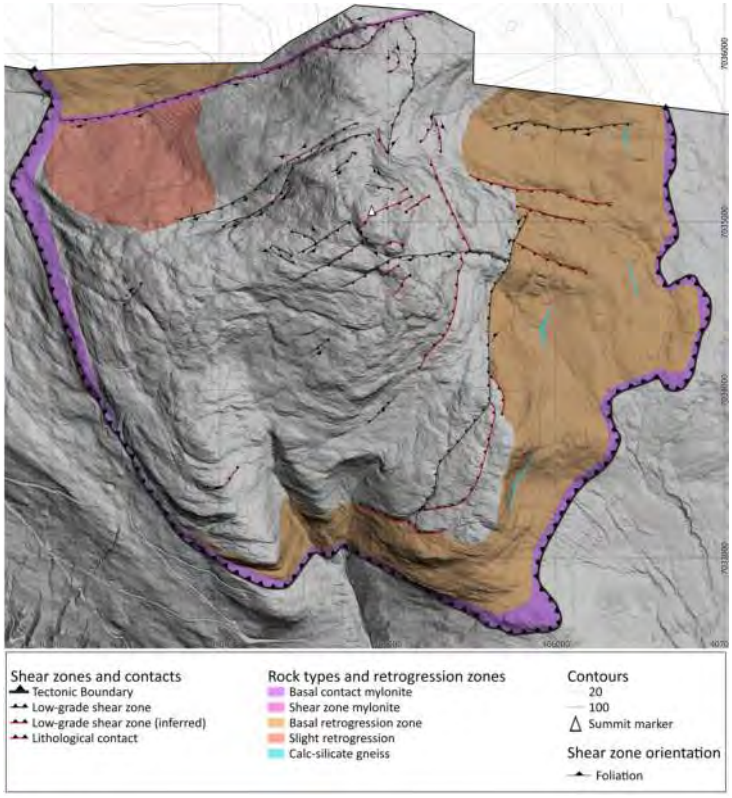


Figure 35: Map of late shear zones and areas affected by retrogression in the Åreskutan Nappe. Observed shear zones are marked with black lines and their extent extended along the depression or shelf formed by erosion. The inferred shear zones are based on morphology shown in the DEM, where the grooves or canyons marked show orientation similar to those observed. Large retrogression zones can be found towards the base of the nappe, seemingly bounded by late shear zones. Within the basal retrogression zone several outcrops of calc-silicate gneiss similar to that in the Kall Nappe are marked.

Strain shadows of xenoliths and porphyroblasts are symmetrical to asymmetrical, also indicating a significant pure shear component. In domains concordant with the main foliation isoclinal folds are common and display fold axes perpendicular to the stretching lineation, while discordant domains show a more complex fold structure (Figure 33). The main foliation is partially discordant with the basal contact with the Kall Nappe, marked by the foliation S3, which developed during the deformational phase D3. Description of the stretching lineation of the S3 foliation and the L2 stretching lineation is found in the section on the tectonic boundary between the Kall and Åreskutan Nappe. A brittle fracture filled with a garnet-rich vein cuts the main foliation close to the lower boundary of the nappe, indicating brittle deformation at a high metamorphic grade, likely related to D3 (Figure 34).

The deformational phase D4 is characterized by late ductile shear zones (S4) that cut the nappe at high angles. The relationship between D3 and D4 is not entirely certain, though the lack of displacement of the tectonic contact with the Kall Nappe indicates the do not cross to the lower nappes (Figure 35). They are referred to as late shear zones in this thesis to distinguish from shear zones related to the development of the main foliation. Mylonite in the late shear zones is found wrapping over higher-grade outcrops or in zones of rheological contrast, such as between two lithologies (Figure 36). Occasionally the surrounding rock can be observed being deflected into the shear zone (Figure 38). The shear zones are typically $\sim$ 10-100 cm thick, though the largest, following the valley floor of Tväråvalvet is estimated to 10-20 m thick. The late shear zones are distinguished from high-grade shear zones by the often high dip angle, and the retrogression of the sheared lithologies. The weathering surface is a dull rusty brown, and the surface is often broken through by more competent rocks (Figure 36a).

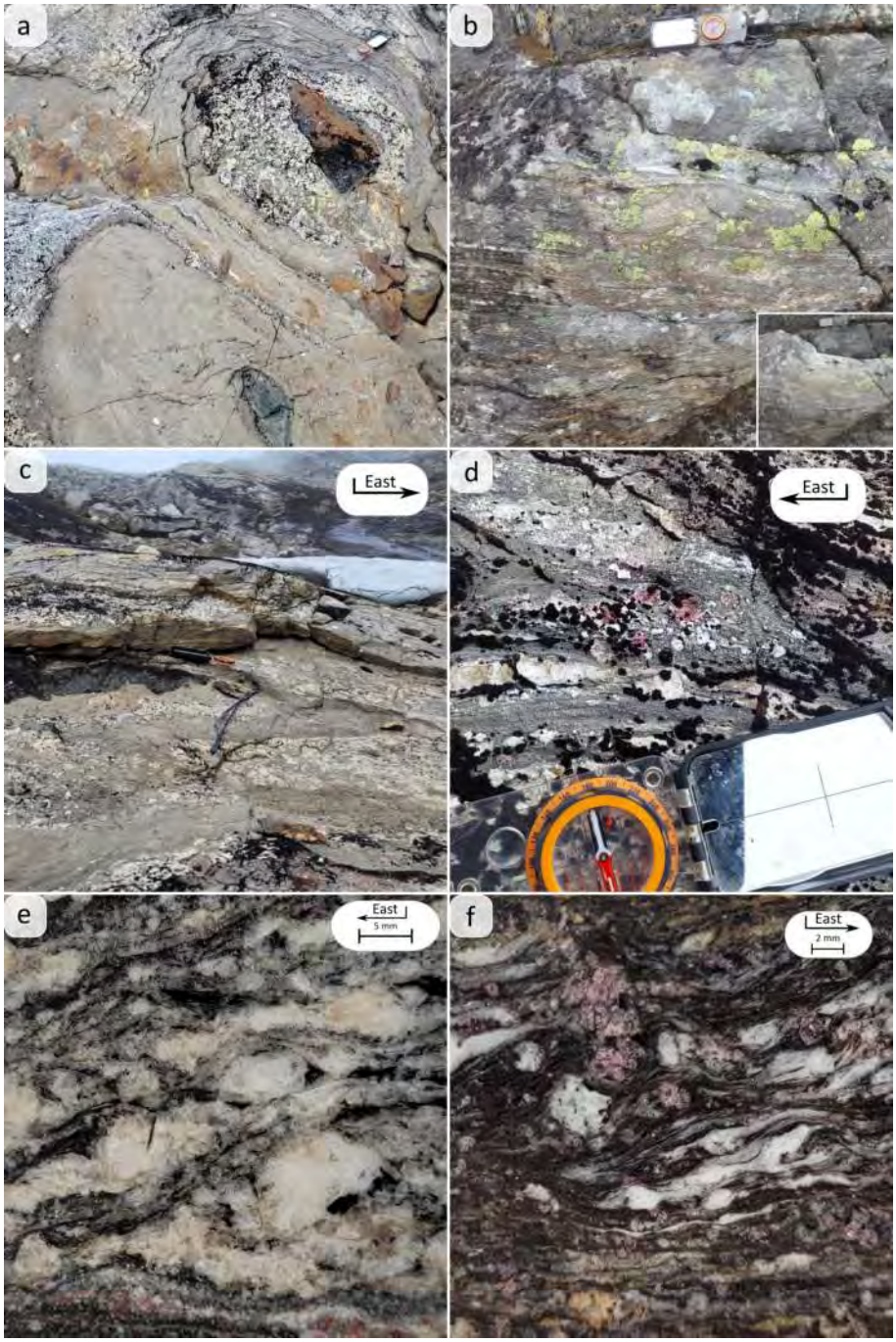


Figure 36: Photos describing the late shear zones in the Åreskutan Nappe. (a) Dull gray paragneiss and spotted white pegmatite reworked in a late shear zone, wrapping over competent metabasite rocks. (b) Mylonite at the contact between competent pyroxene amphibolite above and less competent paragneiss below. Sketch outlines the gradual transition into the shear zone going upwards in paragneiss, with a sharp contact to the overyling pyroxene amphibolite. (C) Photo taken parallel to the stretching lineation, showing isoclinal folds marked by layers of paragneiss and pegmatite reworked in a late shear zone. (d) Large garnets with quartz rims in reworked paragneiss, showing low degree of decomposition. (e) Cut surface of reworked proto-mylonitic pegmatite with large rounded clasts of feldspar. (f) Cut surface of reworked mylonitic paragneiss rich in biotite. Note relative competency of feldspar clasts compared to the elongated polycrystalline quartz bands.

Observed lithologies in the shear zones are fine-grained biotite-rich mylonitic paragneiss with garnet porphyroclasts, and what appears to be proto-mylonitic pegmatite with large rounded feldspars surrounded by thin bands of biotite and recrystallised felsic minerals. Occasional layers of retrogressed metabasite are also observed. The fresh surface of the retrogressed mylonitic paragneiss is a dull purplish brown, while the proto-mylonitic pegmatite is black-brown spotted with white porphyroclasts. The mylonitic foliation S4 is marked by compositional bands and biotite, and the shear fabric is well developed at hand-sample scale. Feldspar clasts show significant rounding while quartz appears as elongated polycrystalline bands, and garnets show no clear signs of retrogression (Figure 36d-f). The stretching lineation L3 is moderately to well developed and marked by biotite. The trend of the stretching lineation in late shear zones is consistent with measurements outside of shear zones in the Åreskutan Nappe, and shear-sense indicators show top-to-the-east shear. Syn-thrusting vertical displacement occurred along steep to moderately dipping shear zones dipping south- to southeast (Figure 36, Figure 37, Figure 38). Contemporaneously, thrusting occurred along shallower west-dipping shear zones. Further shear zones developed due to rheological contrast, predominantly between rigid amphibolite and less competent paragneiss. Brittle deformation related to the deformation phase D5 is recorded following the ductile stages, in slickensides and fractures related to top-to-the-east thrusting in the brittle regime. Slickenside surfaces are coated in white mica, marking the foliation S5.



Figure 37: Depressions cutting into in the northern slope of Åreskutan shows the location of south-dipping late shear zones. The hanging wall of shear zones is marked by lines in the lower picture, together with orientation of foliation and stretching lineation.



Figure 38: Photo of south-dipping late shear zone cutting the valley floor in Blåstensvalvet. Foliation traces are shown in the sketch below. The foliation of the outcrop to the right is deflected downwards into the shear zone, and the foliation in the outcrops to the left is slightly deflected and abrubtly terminated.

7.2.6 Metamorphic history

The metamorphic history recorded in the rocks of the Åreskutan Nappe is long and complex. Detailed description of palaeosome and odd pods are outside the scope of this thesis, but the high mode of garnet in metasandstone palaeosome point to a high-grade event, M1, prior to anatexis. Garnet replacement by pyroxene and plagioclase in pyroxene amphibolite also indicates a transition from higher to lower pressure. That this event took place at ultra-high pressures is contradicted by the high mode of biotite present in paragneiss restite and by the high mode of primary amphiboles in pyroxene amphibolite. Significant partial melting, M2, of paragneiss and pyroxene amphibolite is pervasive in the nappe, though there are metabasite domains that appear largely untouched, e.g. around the summit. Paragneiss lacks white mica in the matrix predating retrogression, pointing to dehydration of muscovite as the primary melting reaction. The main foliation was developed at progressively lower pressure and temperature, subdivided into the metamporphic phases M2-M4. Kyanite related to M2 is common in paragneiss at all structural levels, with different degrees of sillimanite replacement (Table 3). Elongated aggregates of kyanite and replacement minerals mark the main foliation, which wraps around garnets (Figure 39), as well as the stretching lineation L1. Sillimanite is ubiquitous in the paragneiss and characterizes M3, continued deformation at lower pressure and/or higher temperature. Sillimanite primarily marks the main foliation and stretching lineation as prismatic crystals, but is also present as fibrous aggregates replacing kyanite, garnet and feldspar (Figure 40). Replacement of sillimanite by biotite related to M4 is variable but always present. In some domains sillimanite is almost completely replaced by biotite. Biotite appears both as smaller grains marking the main foliation or as large grains discordant with the foliation. White mica can be seen replacing kyanite and feldspar, growing discordant with the main foliation and also observed as fracture filling in garnets. In summary, the main foliation and stretching lineation of the Åreskutan Nappe is marked by the succession of kyanite, sillimanite and biotite in migmatitic paragneiss, whereas paragneiss restite is characterized by the assemblage biotite-garnet-feldspar (dominantly plagioclase).

At the base of the Åreskutan Nappe a large retrogression zone has been identified, related to M5 (Figure 35). It is defined by a markedly lower mode of garnet and aluminosilicates in paragneiss and felsic orthogneiss, likely due to replacement by biotite. An often high degree of oxidation gives a rusty appearance, and a relative lack of mafic bodies are observed. There are patches of preservation in the retrogression zone, where paragneiss appears largely unaffected. The weathering surface is generally rusty yellow or brown, fresh surfaces range from coated in rust to fresh and dark grey (Figure 41a-b). Fine- to medium-grained, dominantly composed of quartz, feldspars, biotite, ± garnet, ± sillimanite (Figure 41c-d)). Close to the base of the nappe, on both the western and eastern slopes, a layer of calc-silicate gneiss similar to that of the Kall Nappe (see below) is sandwiched between layers of retrogressed paragneiss. Just above Döda Fallet in the northeast a large body of amphibolite is found together with the calc-silicate gneiss, also similar to that found in Mörvikshummeln Formation of the Kall Nappe. The calc-silicate gneiss layer is found at multiple locations on the east side of the mountain, thickest at the foot of Hällfjället in the southeast, and on the the west side calc-silicate gneiss is found as two 50-100 cm thick layers at different structural positions.



Figure 39: Photo of kyanite marking the foliation wrapping around garnet in paragneiss.

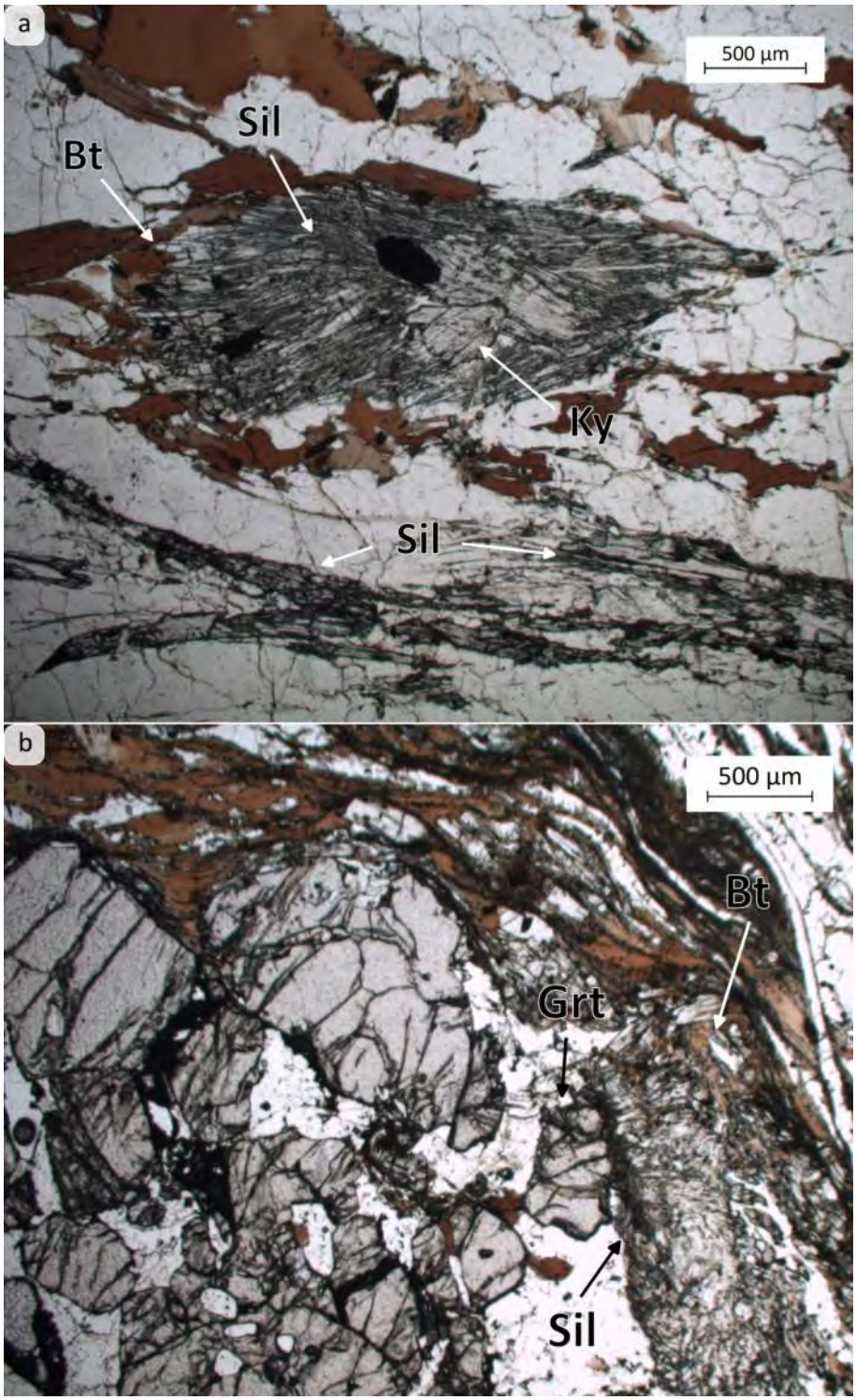


Figure 40: Photomicrographs of metamorphic replacement reactions in paragneiss. (a) Kyanite is being replaced by sillimanite, which in turn is being replaced by biotite. Sample MS2332C. (b) Garnet being replaced by sillimanite, which in turn is being replaced by biotite. Sample MS2310.

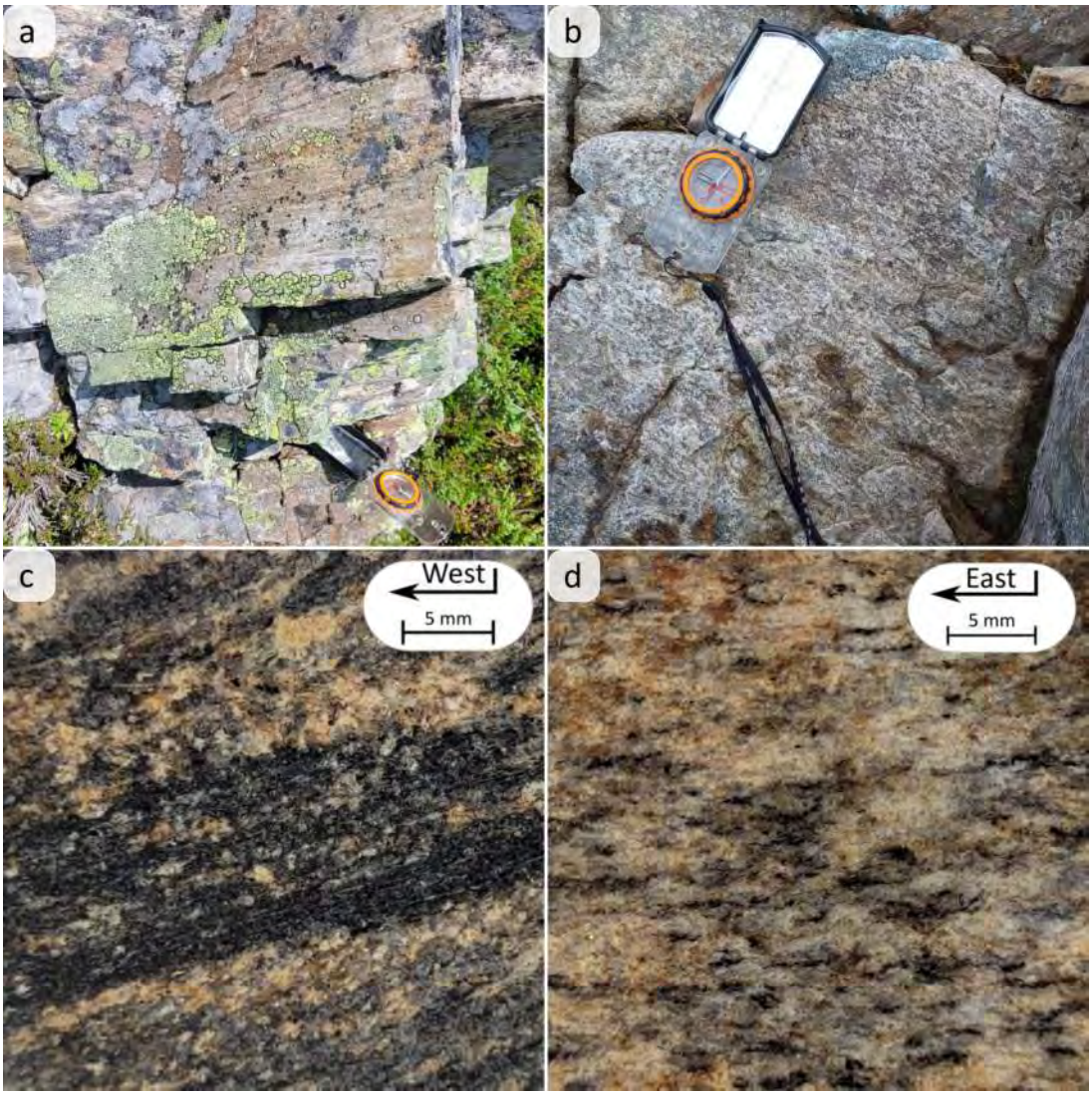


Figure 41: Photos of outcrops and cut samples of retrogressed paragneiss and felsic orthogneiss. (a) Weathering surface of retrogressed mylonitic paragneiss immediately above the tectonic contact on Mörvikshummeln. (b) weathered foliation surface of retrogressed paragneiss. (c) Cut surface of biotite-rich retrogressed paragneiss sample. Sillimanite needles are still present in the biotite bands. The garnet mode is markedly lower than the typical paragneiss of the Åreskutan Nappe. (d) Cut surface of retrogressed felsic orthogneiss sample.

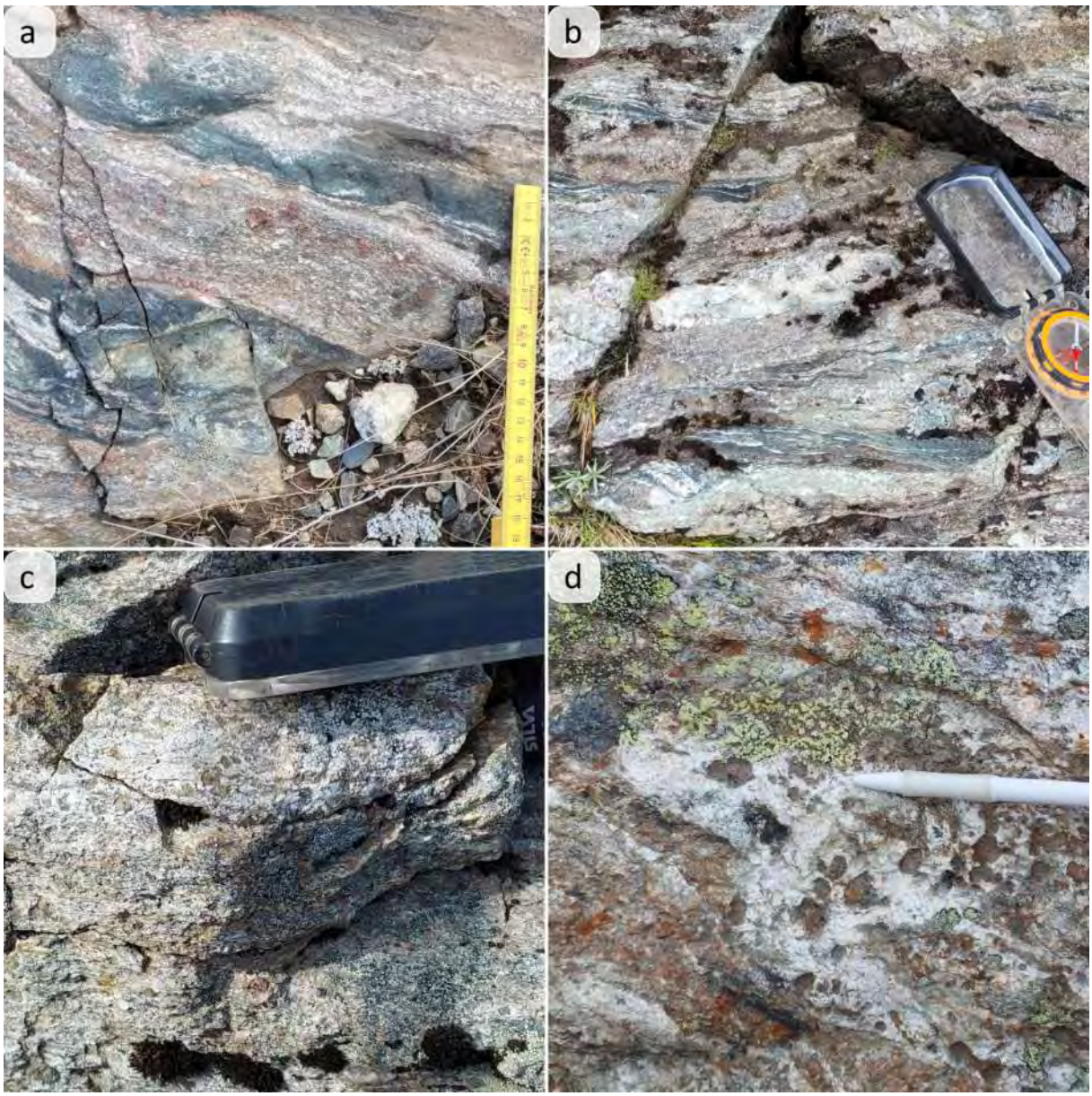


Figure 42: Photos of retrogression in the Åreskutan Nappe. (a) Mylonitic retrogressed paragneiss and metabasite rock close to the top of the retrogression zone marked 'slight retrogression' in figure 35. Only traces of sillimanite is left in the paragneiss and the metabasite is distinctly green-toned (see sample MS23150 in table 3. (b) the same lithologies as in (a) deflected into the wide south-dipping shear zone on the floor of Tväråvalvet.

A less conspicuous zone of retrogression is found on the north-western slope of Åreskutan, also related to M5, from approximately the top of the Tväråvalvet ski lift to the wide late shear zone at the floor of Tväråvalvet (Figure 35). metabasite and paragneiss are mylonitic to protomylonitic, with garnet porphyroblasts (or -clasts) in the paragneiss. Paragneiss generally tends towards mesocratic, with aluminosilicates almost completely replaced by biotite. Metabasite is dominantly green amphibolite (Figure 42a-b). In the amphibolite, a compositionally different layer can be observed, with epidote rims around plagioclase and amphiboles (Figure 43). The late shear zones show complete replacement of aluminosilicates by biotite, and fracturing of garnet coupled with minor biotite replacement (Figure 36d-f). The late shear zones can be related to M6, characterized by the rounding of competent feldspar porphyroclasts, while quartz is finely recrystallised in ductile bands. Further retrogression occurred in isolated patches in the high-grade region of the nappe, tentatively identified as M7, where chlorite replacement of garnets is observed (Figure 42c-d).

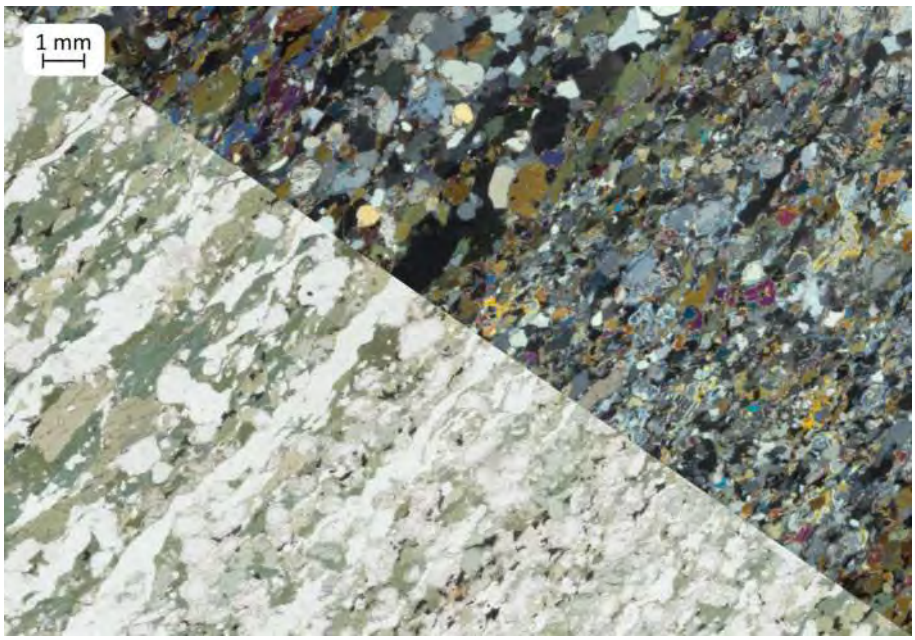


Figure 43: Thin section scan of mylonitic metabasite in sample MS23150. Lower left is displayed in plane-polarized light, upper right in cross-polarized light. Epidote coronas surround amphibole and plagioclase to the right in the figure.

7.3 Kall Nappe

The Kall Nappe is the lower of the two units of the Seve Nappe Complex on Åreskutan, and of a markedly lower metamorphic grade than the Åreskutan Nappe. Helfrich (1967) identified two different nappes, the upper calc-silicate-rich Fröå-Bjelke Nappe and the lower Amphibolite-schist Nappe. Subsequent investigations (e.g. Arnbom, 1980) put these in the same nappe unit, named the Kall Nappe by Yngström (1969); the name adopted by this study. Extensive fieldwork in this study and a review of the data available for the COSC-1 drill core (Lorenz et al., 2019) point to a need to distinguish the upper and lower part of the Kall Nappe, but that no tectonic boundary can be identified (see section on tectonic contacts). In this study, the upper formation will be referred to as the Mörvikshummeln Formation and the lower as the Rödkullen Formation based on prominent exposures at these locations, following SGU naming conventions (Kumpulainen, 2017).

7.3.1 Mörvikshummeln Formation

The Mörvikshummeln Formation makes up the upper part of the Kall Nappe, and is dominated by calc-silicate gneiss with amphibolite interlayers and boudins. Subordinate marble is often found as thin layers in the calc-silicate gneiss, and leucogranite intrudes all lithologies. Pelitic micaschist is completely absent in outcrops, with the exception of garnetiferous biotite schist in a roadcut at Mörvikshummeln. The Mörvikshummeln Formation has a highly asymmetric distribution in the synform, only a thin sliver in the western limb, $\sim$ 50 m thick, and covering the whole extent of the study area in the eastern limb.

7.3.2 Calc-silicate gneiss

Calc-silicate gneiss defines the Mörvikshummeln Formation, and is ubiquitous in outcrops. Texture and fabric varies from ultramylonitic and highly strained to coarse grained with deformation visible at outcrop scale, but only weakly in hand samples.

Greyish weathering surface with often differential weathering due to high carbonate content. Fresh surfaces are white to pale green or purple, with more or less prominent foliation marked by compositional bands of e.g. clinopyroxene and calcic garnets and the the preferred orientation



Figure 44: Photos of calc-silicate gneiss. (a) Mylonitic calc-silicate gneiss above and below a layer of altered amphibolite and intensely sheared pegmatitic leucogranite. Where the calc-silicate gneiss contains biotite foliation is well marked, otherwise it's diffuse and seen through compositional layers. (b) Compositional layering in folded calc-silicate gneiss with greenish, reddish and white layers. (c) Metasomatic rim around amphibolite in isoclinally folded calc-silicate gneiss.

of biotite (Figure 44). The biotite-rich layers could possibly represent previous metapelite layers, now altered by metasomatism. It is possible to differentiate amphibolite layers where the amphibolite is not yet altered, surrounded by a metasomatic rim of calc-silicate minerals (Figure 44c). The calc-silicate character of the nappe is strongest in the highly strained domain in the western limb of the synform. In the easternmost sector of the study area towards Fröå and the COSC-1 drill site calc-silicate minerals are still abundant in the rocks, but outcrops tending towards calcareous metasandstone are also observed. Grain size ranges from ultramylonitic (i.e. practically no grains visible by the eye) to medium-grained with coarse garnet and amphibole porphyroblasts (Figure 45). The calc-silicate gneiss is compositionally varied, but generally composed of quartz, feldspars, clinopyroxene, carbonate and biotite ± garnet. At the microscale, significant grain-size reduction is apparent in the mylonitic foliation, as well as weak shear fabric marked by biotite. In strained domains, reaction rims surround large garnet grains, something not seen in low-strain, garnet-rich domains (Figure 46). Thin section of calc-silicate gneiss sample LS23161A is summarized in table 4.

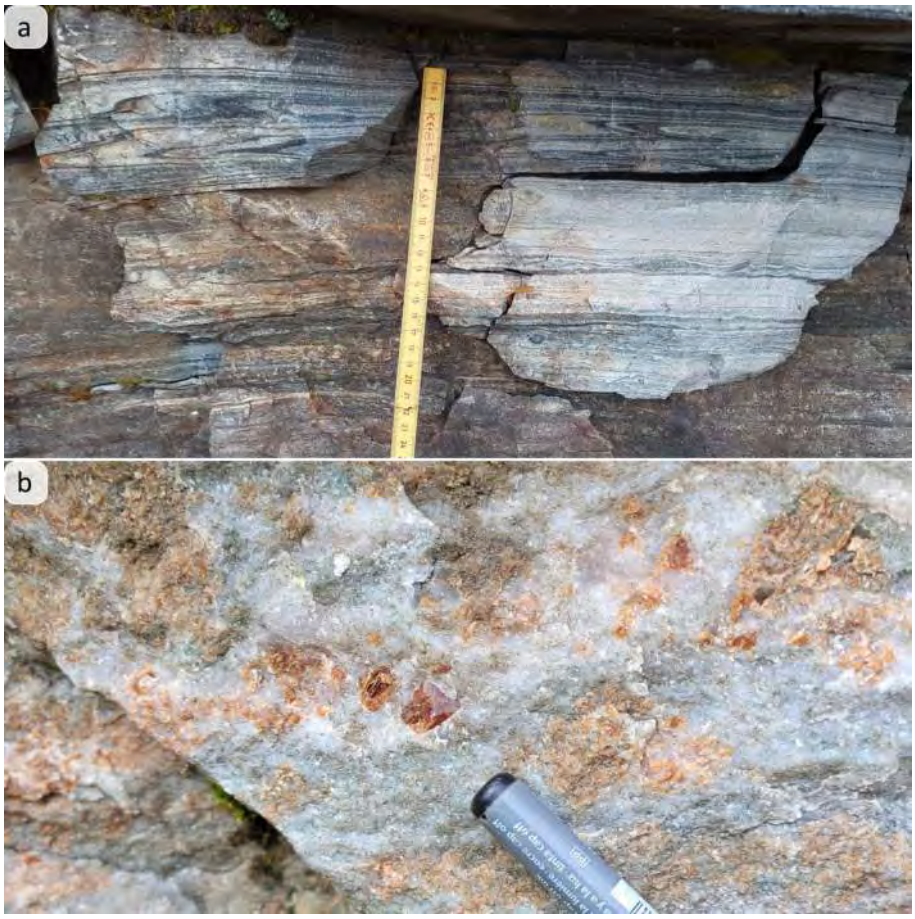


Figure 45: Photos of variation in grain size in calc-silicate gneiss. (a) Ultramylonitic calc-silicate gneiss close to the tectonic boundary with the Åreskutan Nappe on Mörvikshummeln. Sample LS23161 is the big block to the right of the ruler. (b) Large garnet porphyroblasts in patches in weakly foliated calc-silicate gneiss, 50 m in elevation below and 300 m east of (a).

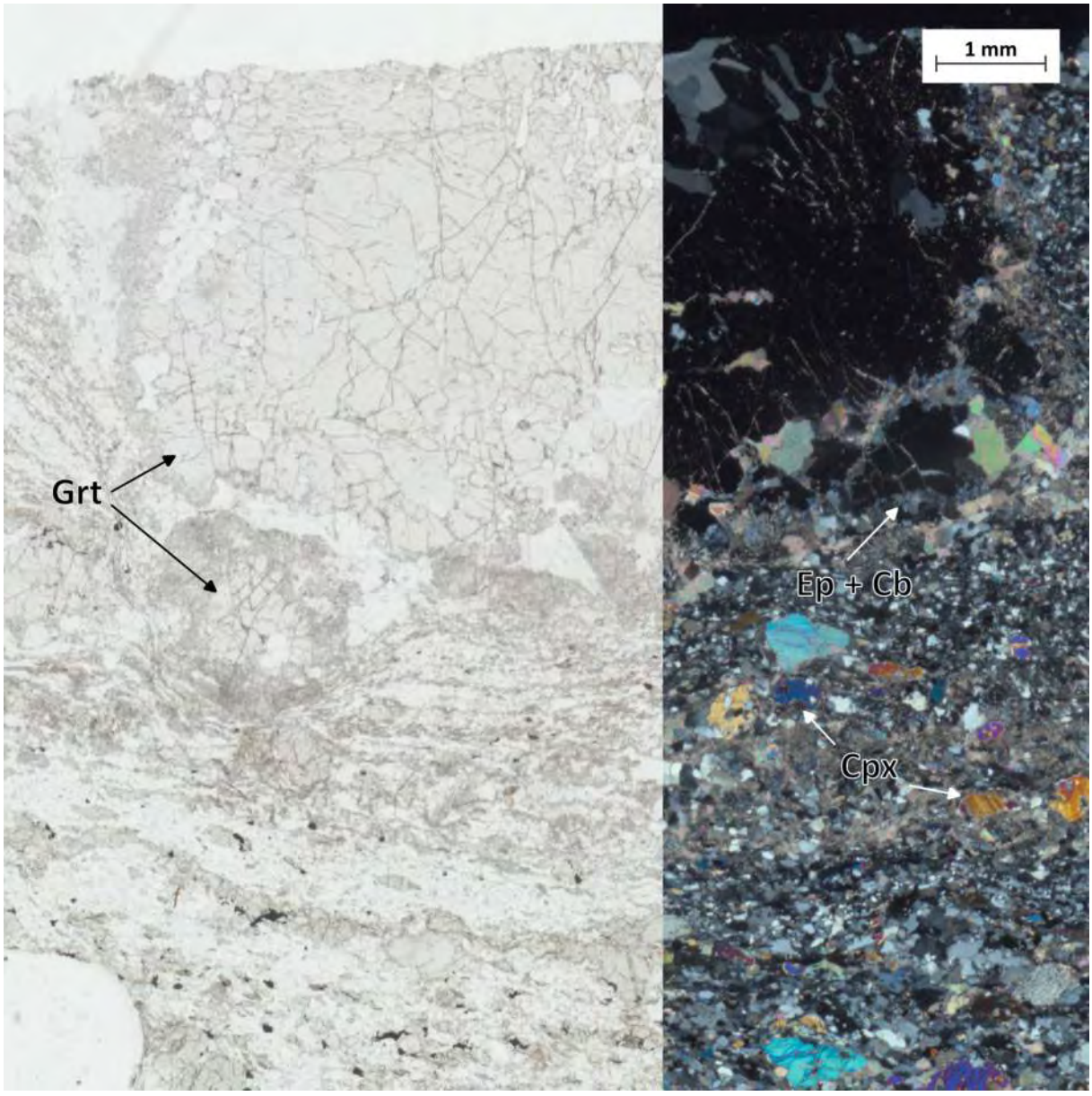


Figure 46: Corona of epidote and carbonate around decomposing garnet in scan of thin section LS23161A. The left side is displayed in plane-polarized light, right in cross-polarized light.

Table 4: Summary of sample thin sections from the Kall Nappe. Location of samples can be seen in appendix A. Mineral abbreviations from Whitney and Evans (2010), WM: white mica. Minerals are listed in the estimated order of decreasing abundance. Inclusions and internal foliation are presented in the format Host (Inclusion).

Sample	Lithology	Minerals	Marking foliation	Inclusions	Internal foliation	Reactions	Zoned	Discordant foliation	Notes
LS2389	Mylonite with layers of amphibolite, micaschist and metasandstone	Amphibolite: Amp + Grt + Bt + Qz + Pl + Chl + Ilm Micaschist: Qz + Fsp (Pl + undifferentiated) + Bt + Amp + St + WM + Chl + Pl + Ilm Metasandstone: Qz + Fsp + Bt + St + WM + Ilm	Bt, Qz bands, smaller elongated Amp, St, Ilm	Grt (Qz, Amp, Bt, Pl, Ilm, Chl); Amp (Ilm); Fsp (Bt, Ilm)	Grt (Qz, Bt, Ilm, Chl); Fsp (Bt)	Grt → Bt; Amp → Bt; Grt → Chl; Bt → Chl;	Fsp, Bt		Grt is observed in both the micaschist and metasandstone in hand sample. Grt is highly fractured and seemingly being replaced by Chl. Chl inclusions in Grt are likely internal replacements of Bt inclusions along fractures. Grt → Chl replacement is unclear. Internal foliation in Fsp is faint.
LS2392	Feldspathic semipelitic micaschist	Fsp (Pl + undifferentiated) + Bt + WM + Qz + Grt + Chl + Ep + Ilm	WM, Bt, Chl	Fsp (Bt, Qz, Ep (?), Ilm); Gt (Qz, Ilm)	Fsp (Bt, Ep)	(Grt → Bt); (Ms → Bt); Bt → Chl	Fsp	Bt	Fsp display zoning, sometimes prominently. Occasional large Bt flakes are discordant with the main foliation, observed in possible pseudomorph aggregates with Qz and Ms. Ms in these aggregates mark S folia.
LS2395	Garnet-biotite micaschist	Bt + Grt + Qz + Amp + Fsp + Rt + Ilm	Bt, Amp, Ilm, thin Qz-bands, fractured Rt	Grt (Qz, Ilm, Rt, Bt, Fsp); Fsp (Bt	Grt (Ilm)	Amp → Bt; Grt → Bt; Bt → Chl; Rt → Ilm	Pl		Rt seems fractured and granulated, occurs abundantly in matrix and rarely as inclusions in Grt. A few Grt display an apparent internal foliation marked by Ilm, possibly also by Rt.

Table 4: (continued)

Sample	Lithology	Minerals	Marking foliation	Inclusions	Internal foliation	Reactions	Zoned	Discordant foliation	Notes
LS2397	Calcareous amphibolite	Amp + Pl + Ep + Cb + Qz + Rt + Ilm	Amp, ribbons of Qz ± Pl ± Cb, Rt, Ilm	Pl (Amp, Qz, Ep, (Rt ?), Ilm); Amp (Ep, Ilm)	Pl (Amp, Ep, Ilm)	Rt → Ilm	Bt		Orientation mark is placed in lower right corner instead of upper right corner.
LS23103	Metagabbro / Amphibolite	Amp + Pl + Bt + WM + Mrg + Oxides	Bt (faintly)	Amp (Ilm, Pl)			Ms, Amp		Compositionally different pale green zones contain Ms, Bt, Amp, Pl. Oxides are dark red, remain to be identified.
LS23122	Garnet micaschist	WM + Qz + Grt + Ep + Bt + Chl + Rt + Ilm (+ Fsp?)	WM, Qz bands, Bt, Chl, Ilm	Grt (WM, Qz, Ilm, (Fsp?))	Grt (Ilm)	Grt →Bt; Bt → Chl; Grt → Chl, Rt → Ilm			Isolated Ms grains are discordant with the main foliation, clastic grains or late? Ms (?) with low interference colours to the right in thin section.
LS23161A	Mylonitic calcsilicate gneiss	Qz + Cpx + Bt + Grt + Cb + Pl + Kfs + Ep + Ttn + Ilm	Bt, Qz bands, alignment of elongate Cpx and TTn, Ilm	Grt (CB, Qz, Pl); Cpx (Bt, Ilm)		Grt → Cc + Ep; (Cpx → Bt ?)			Calcic Grt has wide corona of calcite and epidote, which possibly also forms a debris trail in the strain shadow of a heavily fractured Grt.

7.3.3 Amphibolite

The amphibolite of the Mörvikshummeln Formation has a distinctive appearance compared to the amphibolite of the lower Rödkullen Formation. The weathering surface has a black-grey salt-and-pepper texture, fresh surface is similar but darker or practically black (Figure 47). Medium-grained and with a weak to moderate foliation. Composition is dominantly black amphiboles with subordinate biotite and plagioclase. At the microscale, brown amphibole is weakly aligned to the main foliation, which is also weakly marked by the preferred orientation of biotite (Figure 48). Amphibole, biotite and compositional bands mark the foliation in high strain domains. Rare patches of green white mica occur in a few outcrops (Figure 47b, Figure 48). In a few outcrops there are textural signs of incipient partial melting, which could also have been caused by intrusion of hydrothermal fluids (Figure 49). Metasomatic products at the boundary between calc-silicate gneiss and amphibolite are common (Figure 44c, Figure 50). Leucocratic veins are common in larger, low-strain bodies. Boudinage of amphibolite layers is observed in most calc-silicate gneiss outcrops (Figure 51). Amphibolite is often prominently visible in the typical isoclinal folds of the unit, especially at the hinge, where the thickness ranges from < 1 cm to > 10 m (Figure 50b). A large domain of amphibolite is found on and around Totthummeln and Getvalen, which is interpreted as a boudin at least 100 m thick. Thin section of amphibolite sample LS23103 is summarized in table 4.

7.3.4 Leucogranite

Leucogranite can be observed in calc-silicate gneiss and amphibolite outcrops across the study area. In weathered and highly strained outcrops leucogranite is inconspicuous, but it is highly visible in roadcuts and along scoured stream beds. The weathering surface is pale yellow, fresh surfaces are white with large black biotite grains and agglomerates. Composition is quartz, feldspars, biotite and rare garnet and amphibole. Foliation is marked by the preferred orientation of biotite. Intrusive contacts in calc-silicate outcrops are difficult to see due to the high amount of strain and similar orientation of the main foliation of both lithologies. However, the host rock foliation can be observed being cut by leucogranite with a slightly discordant foliation, though the discordance may also be caused by boudin rotation (Figure 52a). The intrusive nature of the leucogranite is clearer in amphibolite (Figure 52b). The intrusive nature of the leucogranite is covered by Li et al. (2021d).

7.3.5 Marble

Marble layers are common in layers up to a few meters thick in outcrops of calc-silicate gneiss, often with a higher degree of deformation and weathering compared to the surrounding gneiss (Figure 53). The composition is dominantly quartz and carbonates.

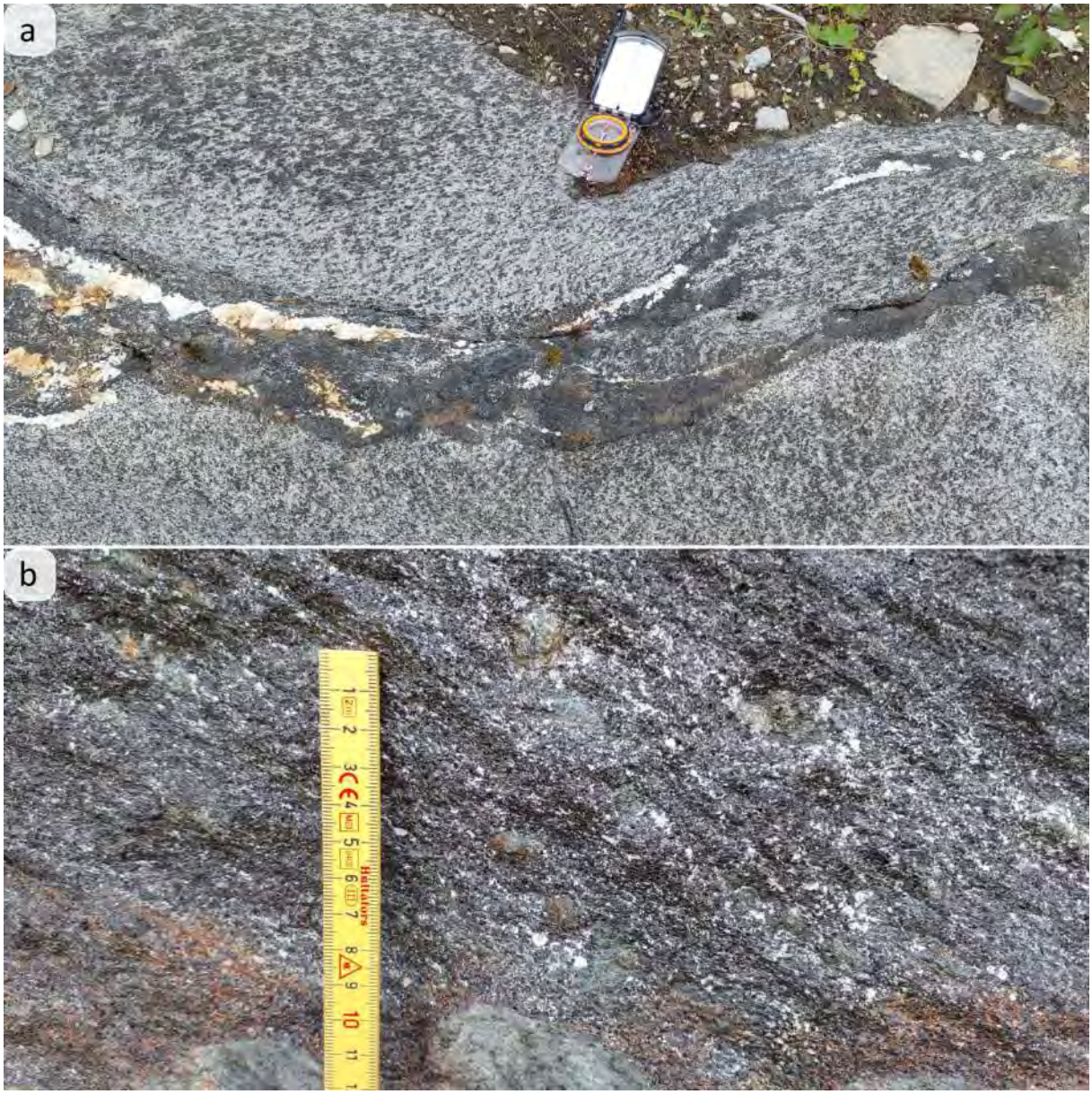


Figure 47: Photos of amphibolites from the Mörvikshummeln Formation. (a) Grey and black weathering surface of amphibolite outcrop almost at the eastern edge of the study area, close to the Fröå copper mine and the site of the COSC-1 drill core. Note the leucocratic and melanocratic segregations. (b) Fresh surface of weakly foliated amphibolite with green patches of white mica on the north-west slope of Totthummeln, an outcrop of a large coherent amphibolite domain on Totthummeln and Getvalen.

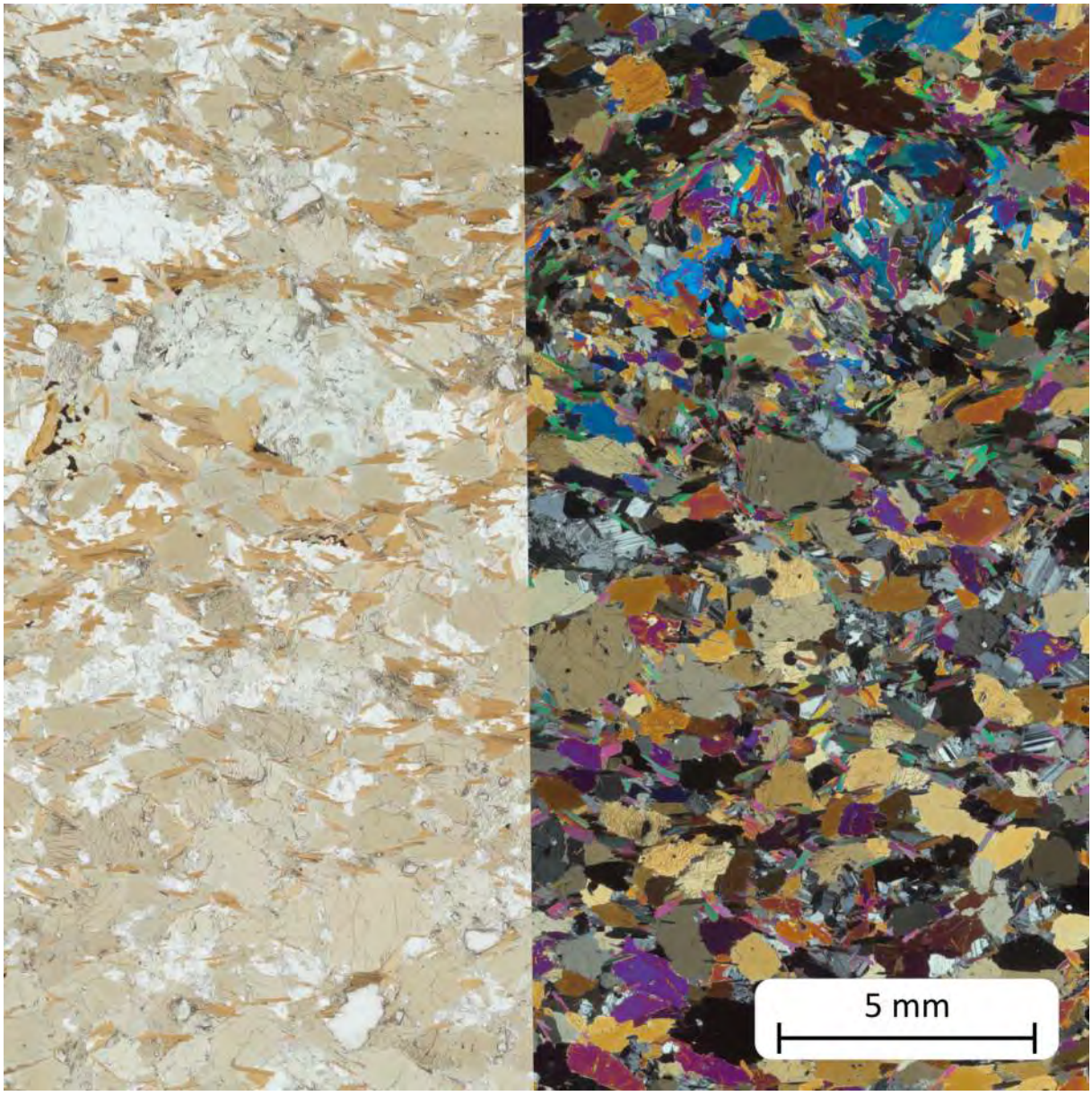


Figure 48: Scan of thin section from the amphibolite sample LS23103, taken from the outcrop shown in figure 47b. The left side is displayed in plane-polarized light, right in cross-polarized light. Brown amphiboles are only weakly aligned along the main foliation, which is marked by the preferred orientation of biotite. The pale green patch on the upper left side is rich in zoned white mica, also seen in the upper right in cross-polarized light.

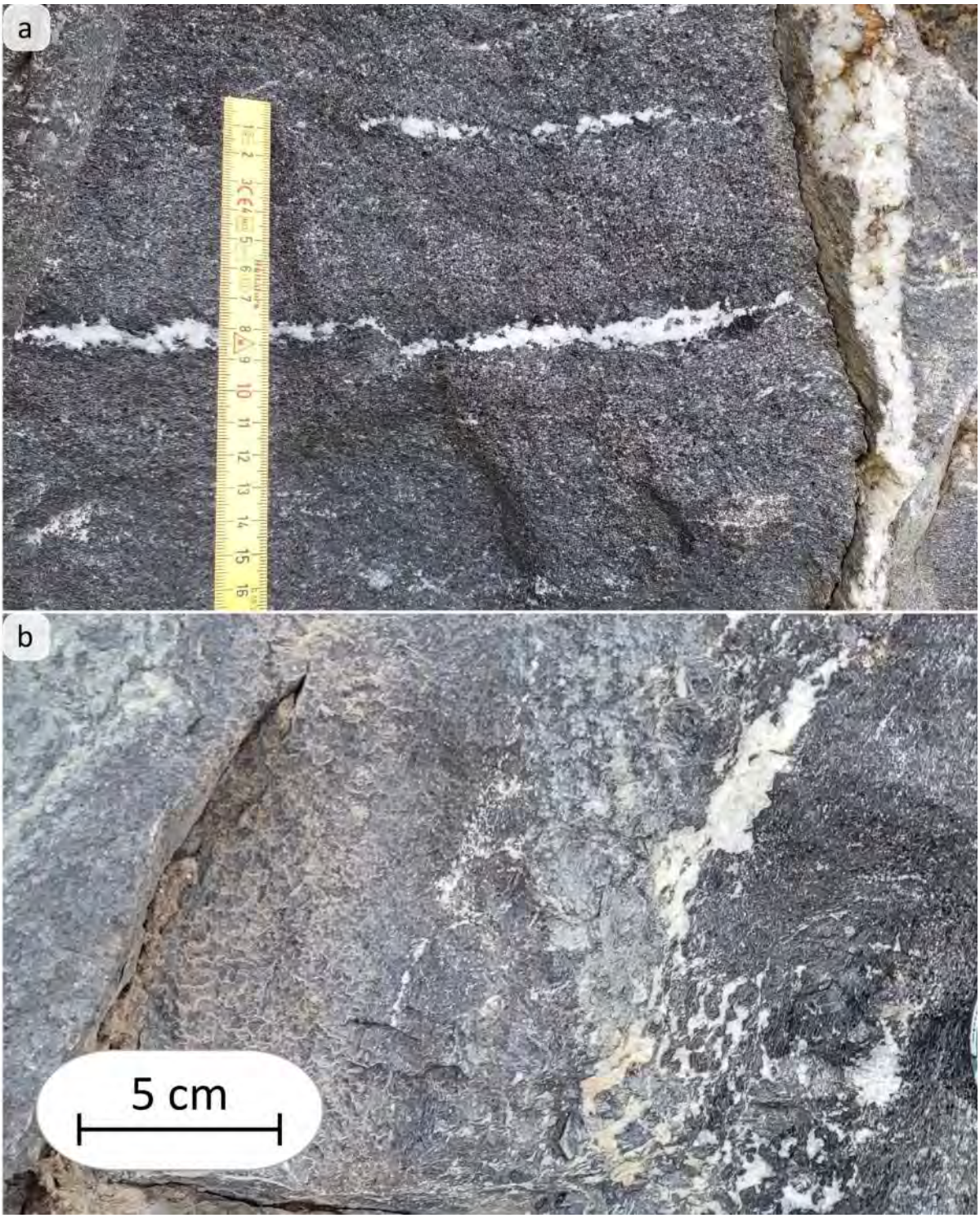


Figure 49: Felsic veins of unclear origin in amphibolite outcrops, either hydrothermal or signs of incipient partial melting. (a) Foliation-parallel veins in the same amphibolite outcrop as figure 47b. Note the dark border around the veins. (b) Foliation-parallel veins in an amphibolite outcrop higher up in the Totthummeln-Getvalen amphibolite domain. Large amphibole crystals in the veins can be seen in the lower part of the photo.

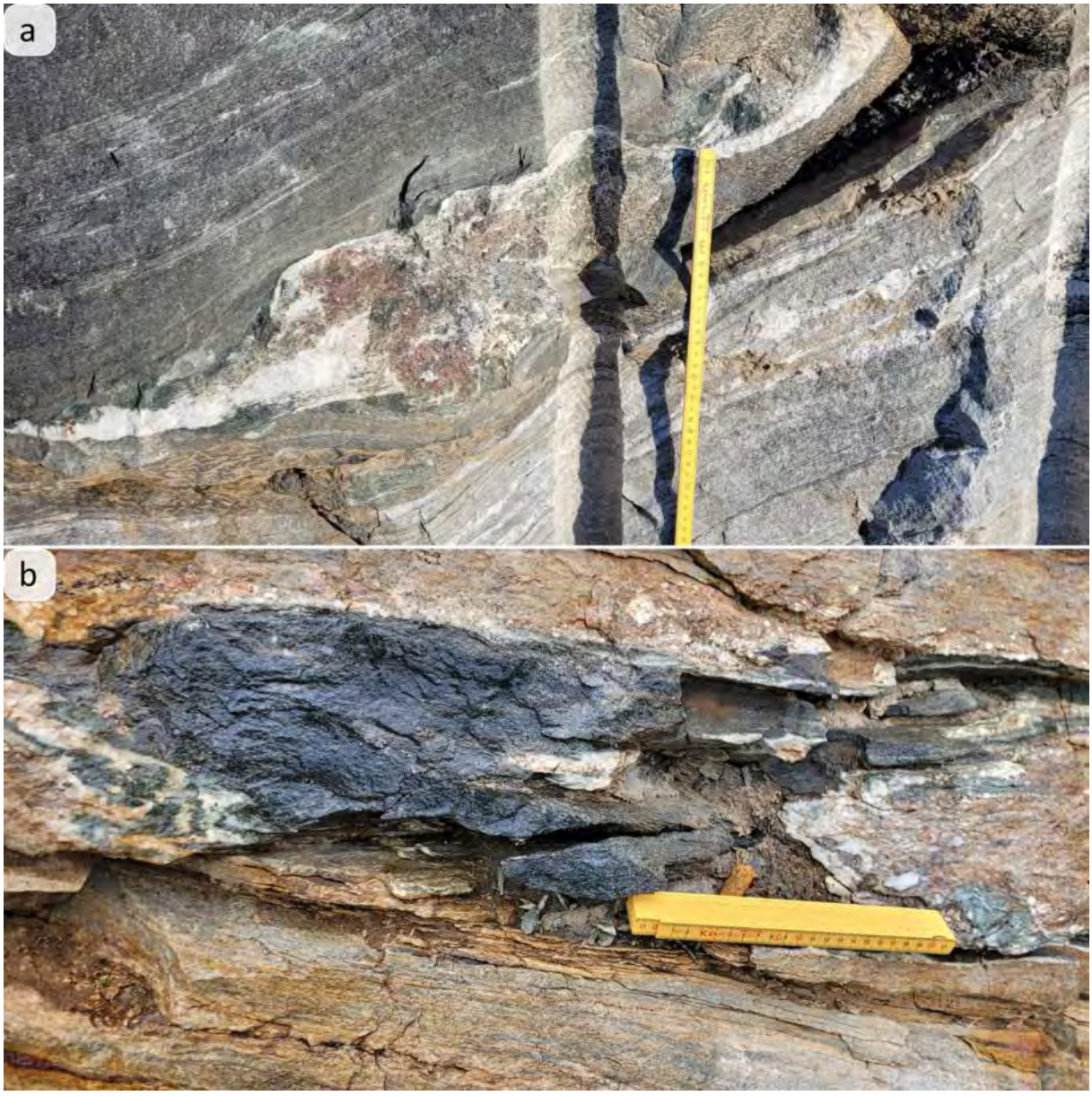


Figure 50: Photos of metasomatism at the contact between amphibolite and calc-silicate gneiss. (a) Garnet-rich metasomatic patchat the boundary between amphibolite and calc-silicate gneiss in outcrop along E14. (b) Green-hued bands of metasomatic products surround amphibolite in the fold hinge of an isoclinal fold. Note also the apparent thinning of amphibolite in the limbs of the fold.

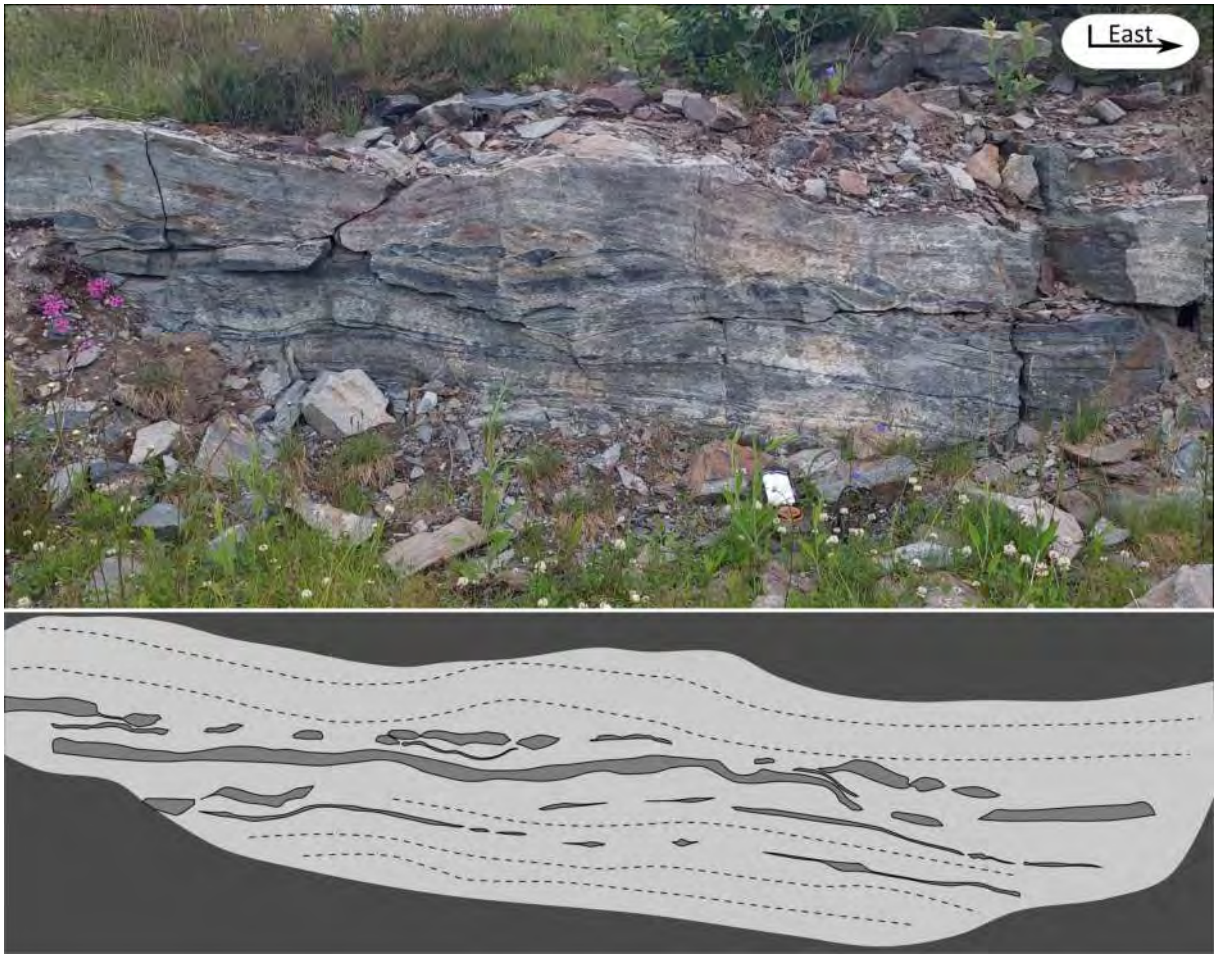


Figure 51: Photo and sketch showing an example of boudinage of amphibolite in calc-silicate gneiss. Note the ductile asymmetric deformation of sheared boudins.

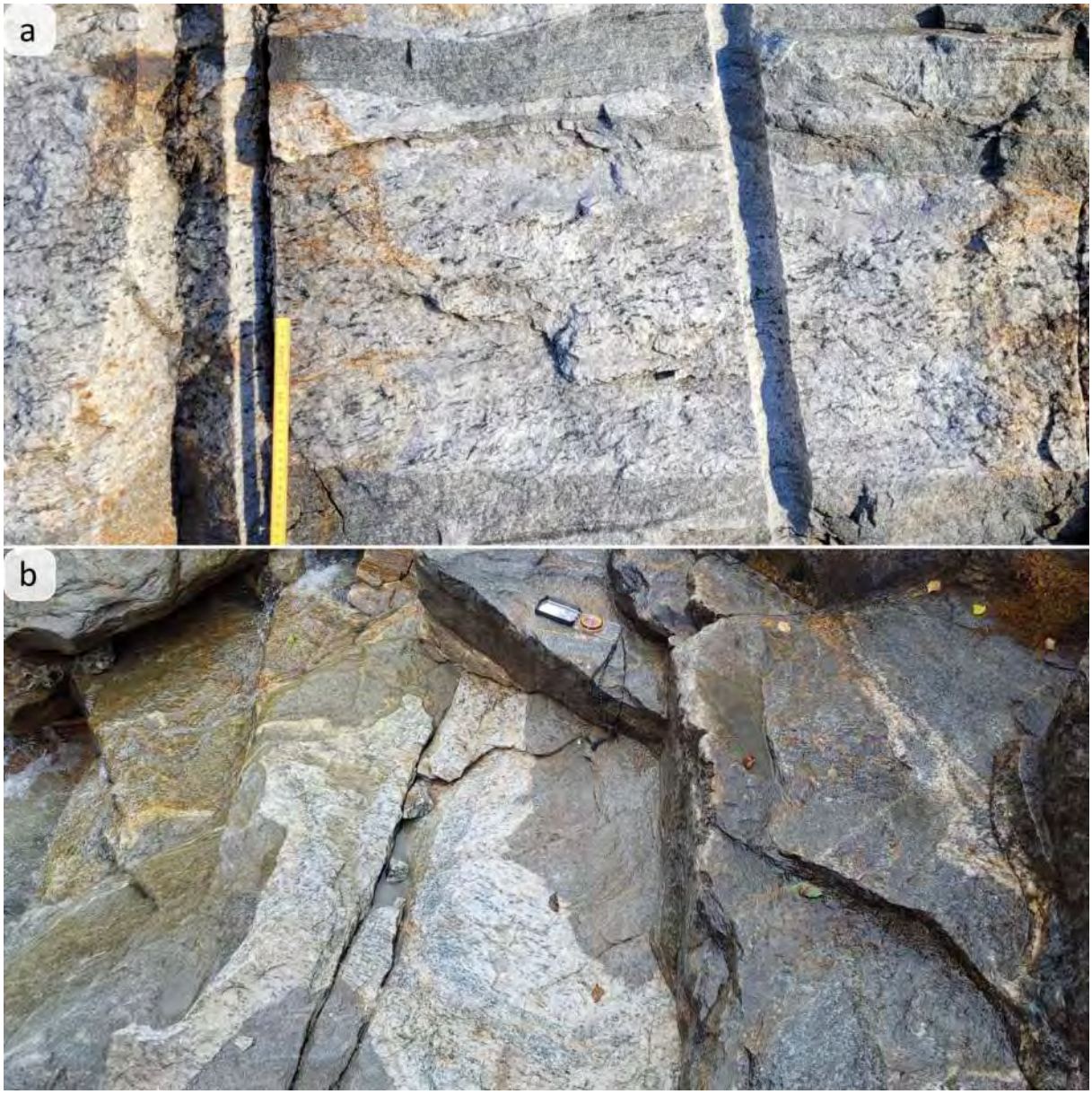


Figure 52: Photos of leucogranite intruding calc-silicate gneiss and amphibolite. (a) Leucogranite with large biotite grains cutting the foliation of calc-silicate gneiss. The foliation of the leucogranite is slightly discordant with the main foliation of the calc-silicate gneiss. The texture becomes more fine-grained towards the top of the leucogranite body but not towards the bottom. (b) Leucogranite cutting the foliation of amphibolite, but display concordant foliation.



Figure 53: Photo displaying highly deformed quartz marble, which is often interlayered with the calc-silicate gneiss.

7.3.6 Rödkullen Formation

The Rödkullen Formation makes up the lower part of the Kall Nappe, and is distinguished from the Mörvikshummeln Formation by the general lack of calc-silicate gneiss and marble, different texture and mineralogy of amphibolites, the common presence of garnetiferous pelitic-semipelitic micaschists and a difference in deformation style. Rare marble layers have been observed in the formation. Outcrops are typically composed of interlayered or massive amphibolite and sandstone, often with thin layers of micaschist. The thickness of the Rödkullen Formation is estimated at $\sim$ 450 m, and it is only found in the western limb of the synform, where it dips eastwards towards the synformal hinge.

7.3.7 Amphibolite

Amphibolite may be the dominant lithology of the Rödkullen Formation but as it is generally interlayered with metasandstone and micaschist the proportions at a large scale are difficult to determine (Figure 54). At Rödkullen on the western slope of Åreskutan, the base of the formation consisist of mylonitic amphibolite, transitioning to interlayered lithologies further up. The weathering surface is rusty gray-brown or dark bluish grey, and fresh surfaces are black, with a blue-green hue (Figure 55). The grain size is finer than amphibolite in the Mörvikshummeln Formation, and plagioclase porphyroclasts around 1 mm are common. Composition is dominantly green amphibole, plagioclase, carbonate and quartz, occasionally with garnet and biotite (Figure 56). Foliation is well developed, marked by compositional bands and the preferred orientation of amphibole and bands of fractured ilmenite and rutile. Thin sections of amphibolite samples LS2389 (amphibolite layer in composite sample) and LS2397 are summarized in table 4.

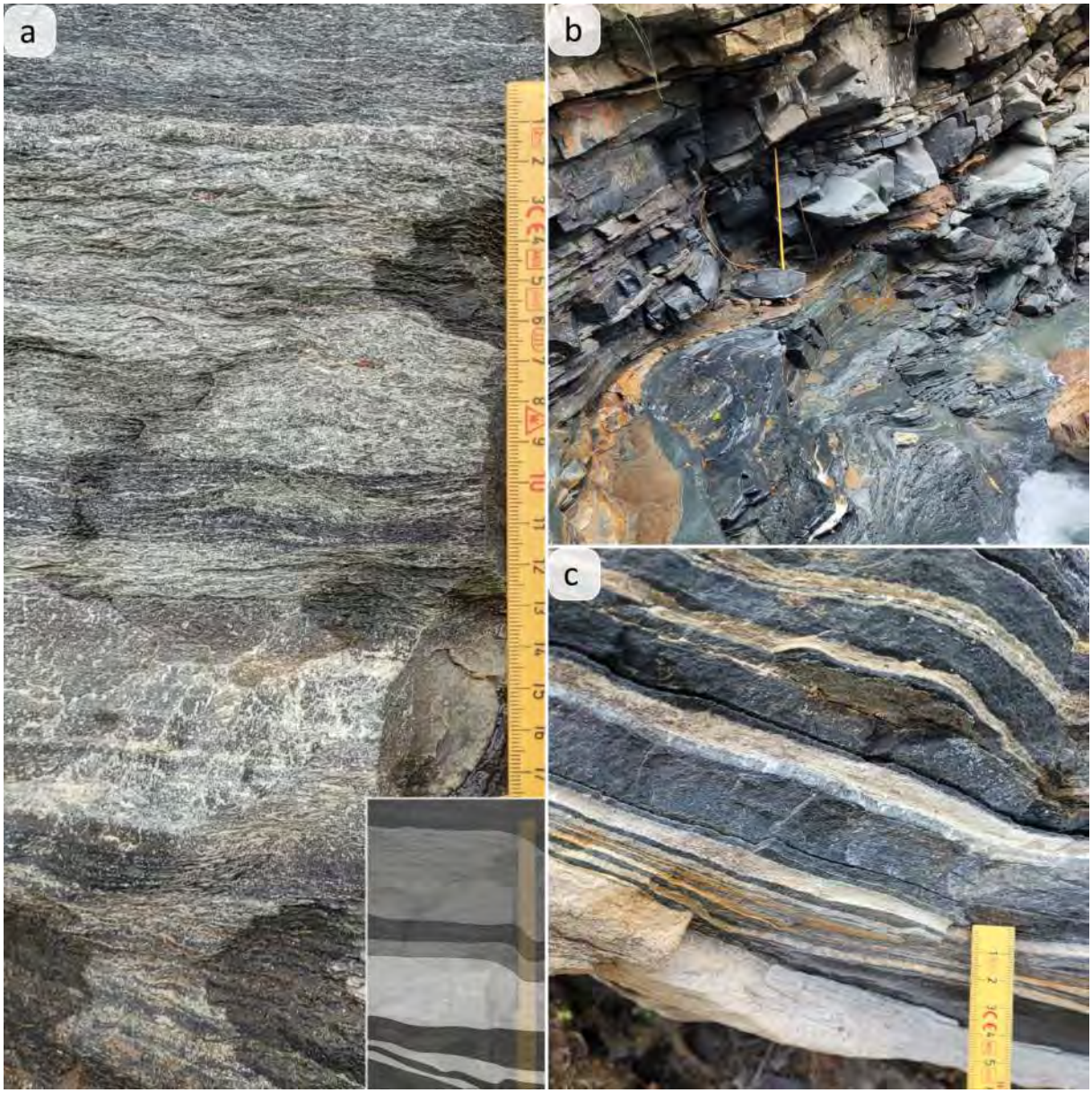


Figure 54: Photos showing the typical interlayering of other litologies with amphibolite. (a) Interlayered amphibolite, micaschist and metasandstone in roadcut along E14. The small sketch highlights the boundaries of amphibolite (black), micaschist (dark grey) and metasandstone (light grey). (b) Water-scoured outcrop along the stream Susabäcken, of 0.5 to 1 m thick layers of amphibolite alternating with metasandstone layers a few centimeters to several meters thick. (c) Alternating amphibolite and metasandstone layers down to a few millimeters thick.



Figure 55: Weathering surface of blue-green porphyroclastic amphibolite close to the lower tectonic boundary of the nappe at Rödkullen.



Figure 56: Garnets in mylonitic amphibolite close to the lower tectonic contact of the nappe. Garnets are typically rare in amphibolite of the Rödkullen Formation. Scan of thin-section from mylonitic sample LS2389, containing interlayered amphibolite, micaschist and metasandstone. The lower left is displayed in plane-polarized light, upper right in cross-polarized light.



Figure 57: Photos of metasandstone outcrops from the bottom and top of the Rödkullen Formation. (a) Mylonitic metasandstone within 10 m of the Särv - Kall Nappe tectonic boundary. Note amphibolite layer at the left foot of the outcrop. (b) Mylonitic metasandstone just below the transition from the Rödkullen to the Mörvikshummeln Formation. The lower part of the outcrop consists of blue-hued amphibolite. Note the large feldspar clasts below the compass, which may be primary, metamorphic or highly boudinaged leucogranite.

7.3.8 Metasandstone

Metasandstone in the Rödkullen Formation is generally devoid of calc-silicate minerals, though there is a small transitional zone close to the boundary (see section on lithological boundary in the Kall Nappe). Metasandstone is high in feldspathic content, and range from purely quartzofeldspathic to transitional with micaschist. Weathering surfaces are typically yellowish, and fresh surfaces may vary from yellow, to bluish green, to light or darker grey, depending on composition (Figure 54, Figure 57). Darker grey metasandstone may be confused with amphibolite at first glance. Composition is dominantly quartz, feldspar, white mica and biotite, ± garnet, ± staurolite. Large feldspar porphyroclasts or porphyroclast agglomerates occur, but it is not clear whether these originate in the metasandstone protolith, are metamorphic or highly boudinaged intruding leucogranite (Figure 57, Figure 58). Foliation and shear fabric is well developed to mylonitic, marked by compositional bands and the preferred orientation of biotite, white mica and bands of ilmenite, occasionally also by staurolite (Figure 59). Thin section of metasandstone layer in sample LS2389 is summarized in table 4.



Figure 58: Large feldspar clasts visible in metasandstone along the stream Tvärån, close to the transition to the Mörvikshummeln Formation. Arrows point out feldspar clasts at least 3 cm in size. The weathering surface and water did not allow for a detailed description of the rock, which may also be a pegmatitic leucogranite intrusion.

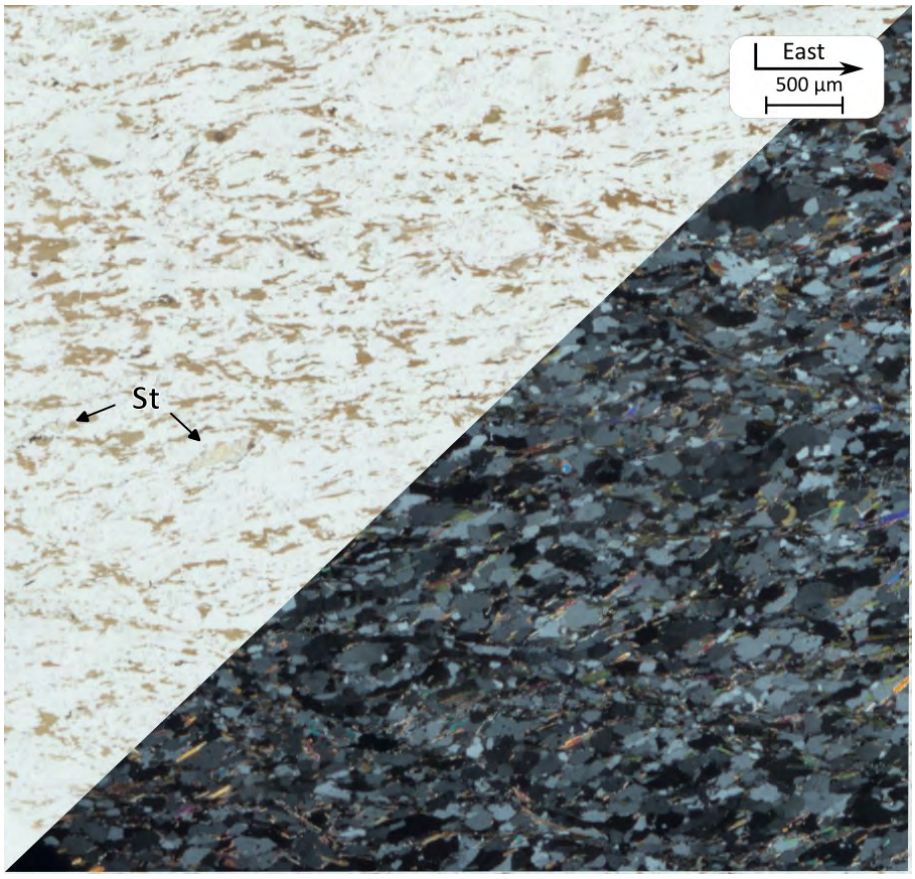


Figure 59: Mylonitic metasandstone with euhedral fractured staurolite grains oriented with the long axis parallel to the folitaion, which is marked by biotite. Scan of thin-section from mylonitic sample LS2389, containing interlayered amphibolite, micaschist and metasandstone. The lower left is displayed in plane-polarized light, upper right in cross-polarized light.



Figure 60: Mixed lithology outcrop along E14 showing the differential weathering pattern of micaschist One highly weathered micaschist layer is marked by the ruler. Note also boudinage of the competent amphibolite layers.

7.3.9 Micaschist

Micaschist is common in the Rödkullen formation as 1-50 cm thick layers in mixed outcrops, often more weathered than the surrounding layers (Figure 60). Weathering surfaces are often rusty brown, and where stream-scoured brown to dark grey. Fresh surfaces are light to dark grey. The micaschist is compositionally varied, from semipelitic schist with large plagioclase porphyroclasts to completely dominated by white mica or biotite, with or without garnet and staurolite (Figure 61). Garnet porphyroblasts range in size from < 1 mm to > 10 mm (Figure 62). Foliation and shear fabric is well developed, and marked by compositional bands and by the preferred orientation of biotite, white mica, the occasional chlorite or staurolite and elongated or fractured ilmenite and rutile. An isolated pod rich in randomly oriented kyanite blades has been observed enclosed by micaschist at Rödkullen (Figure 63). Thin sections of micaschist samples LS2389 (micaschist layer in composite sample), LS2392, LS2395 and LS23122 are summarized in table 4.

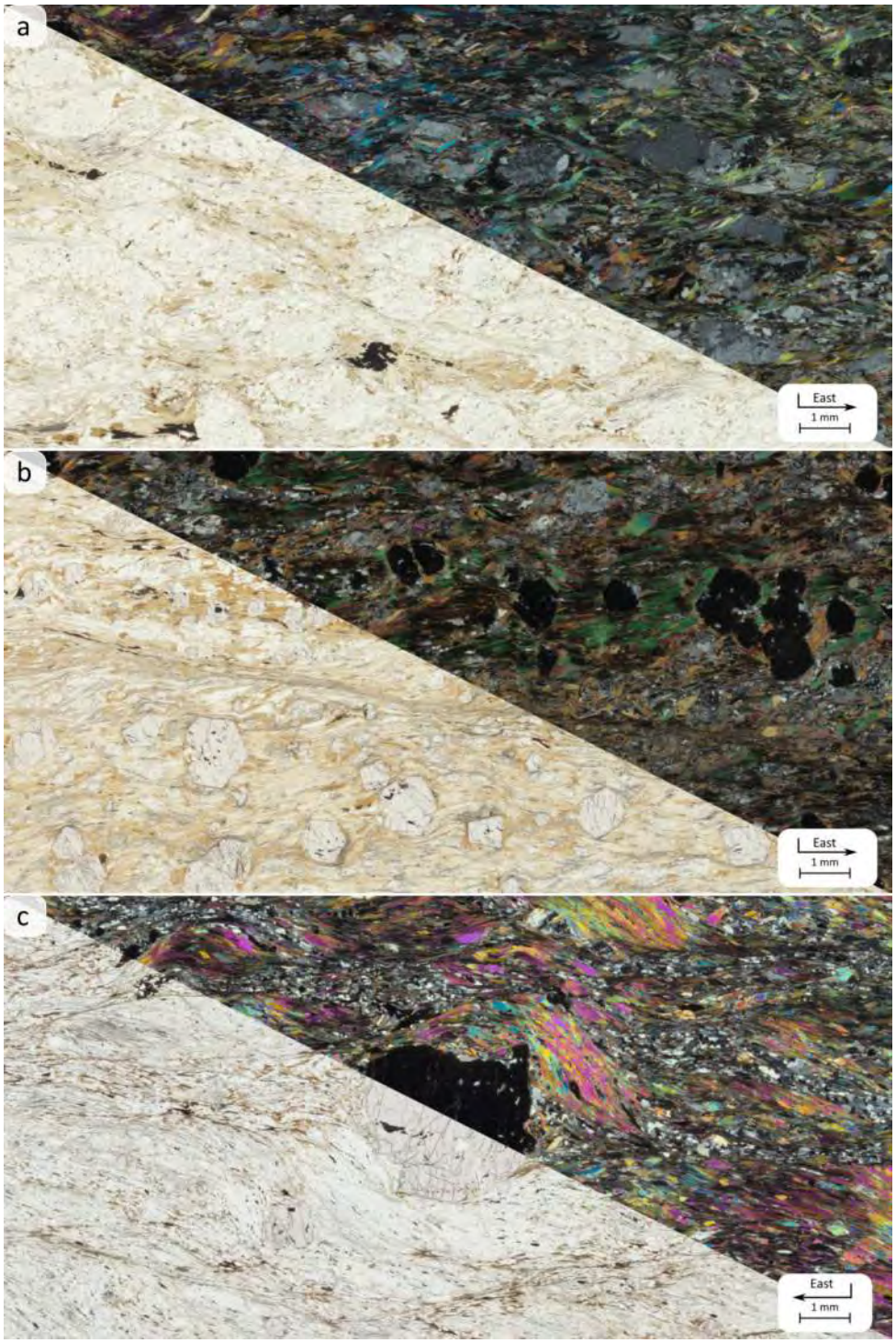


Figure 61: Thin section scans of micaschist samples showing the great compositional range of micaschists in the Rödkullen Formation. (a) Micaschist with abundant feldspar porphyroblasts in a matrix rich in both biotite and white mica, with well developed anostomosing shear fabric. Sample LS2392. (b) Biotite micaschist with a high mode of euhedral garnets. In the biotite matrix are scattered green amphibole being replaced by biotite. A shear band marked by significant grain size reduction cuts through the middle of the figure. Sample LS2395. (c) Micaschist with a matrix dominated by white mica and quartzofeldspathic microlithons, which wraps around unevenly sized garnets. Well developed S-C fabric. Sample LS23122.



Figure 62: Large garnets in interlayered micaschist, metasandstone and amphibolite close to the base of the nappe. Garnets are distributed throughout all three lithologies. Site of multi-lithology sample LS2389. Arrows mark the stretching lineation.

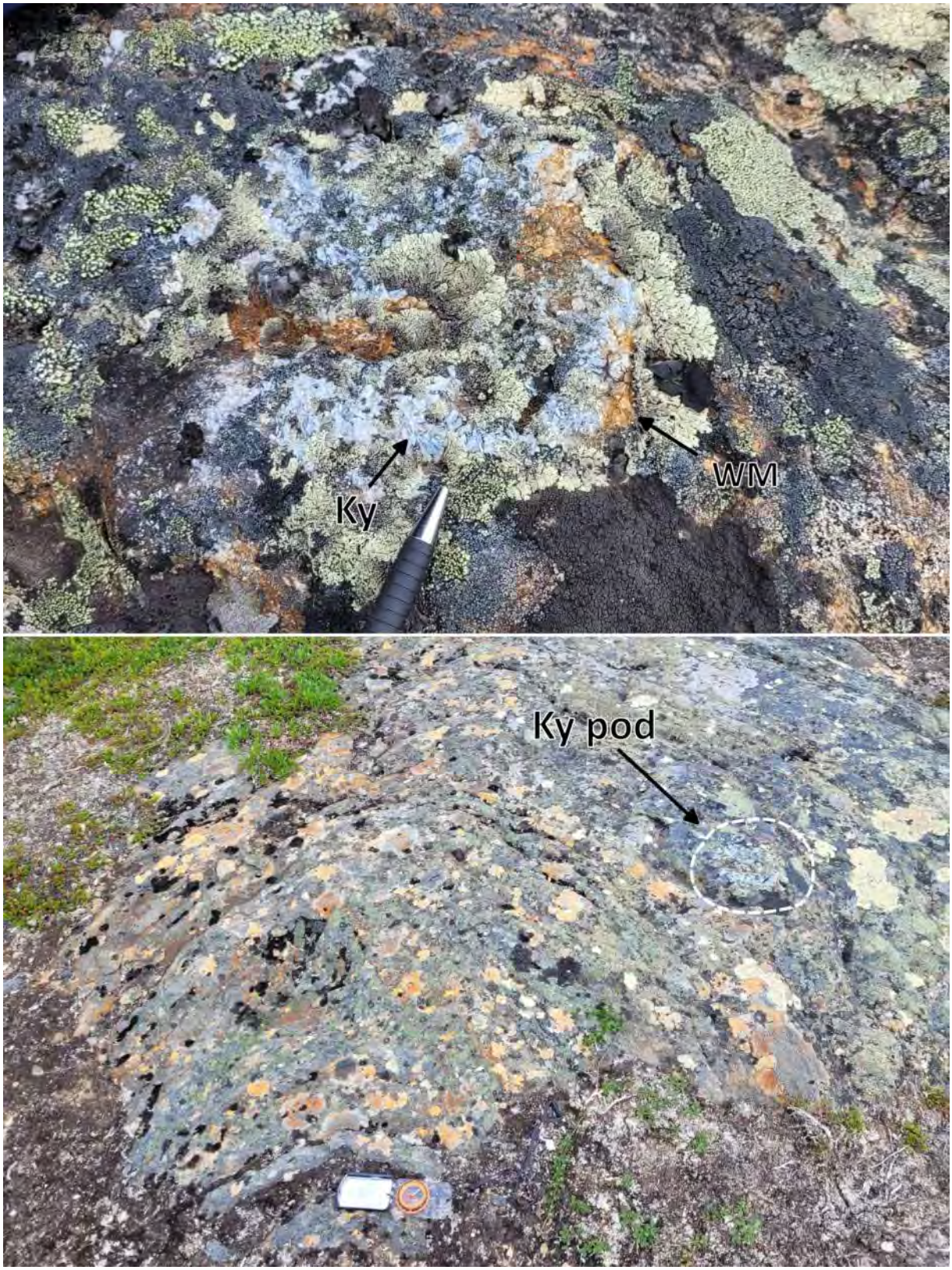


Figure 63: Photo of kyanite-rich pod in micaschist. (a) Close-up photo of pod with blue-white blades of kyanite. Whitening towards the rims of the blades may be a retrogressive phase. The pod itself is rimmed by a layer of white mica. (b) Pod location in outcrop. No similar pods have been found elsewhere.

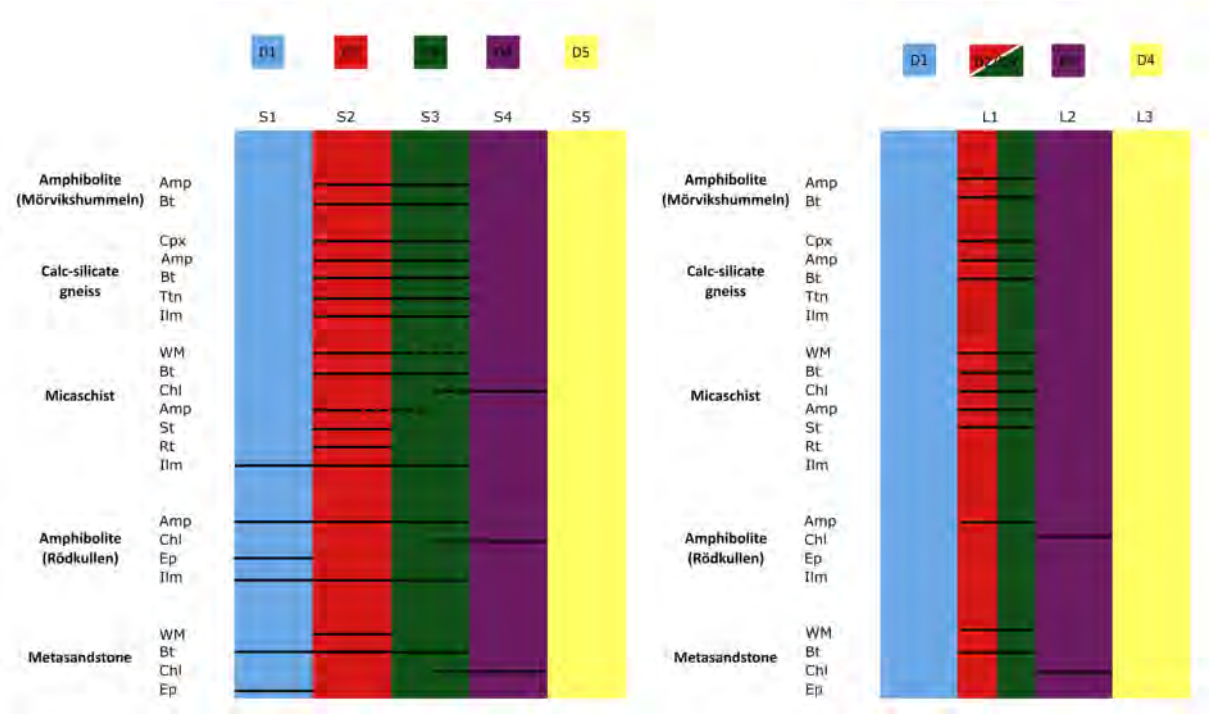


Figure 64: Summary of the deformation history of the Kall Nappe. Deformational events D1-D5 are identified and shown based on the succession of minerals marking foliation and stretching lineation.

7.3.10 Deformation history

Five deformational phases has been identified in the Kall Nappe, D1-D5 (Figure 64. The high degree of strain in the Kall Nappe has largely erased prior structures. The earliest recorded event in the Kall Nappe, D1, is seen in the relict foliation S1, marked by rotated internal foliation in porphyroblasts in the Rödkullen Formation (Figure 65). The original intrusive relationship between amphibolite and the host rocks has been erased, and amphibolite is seen either as layers parallel to the main foliation or as boudins. The foliation S2, developed during the phase D2, is seen at the meso- and microscale in S-planes of the reworked shear fabric characterising D3. The shear fabric S3 is seen in C and C'-planes, and defines the main foliation of the Kall Nappe. The mylonitic foliation grows stronger when approaching the lower tectonic boundary and is also interpreted as S3, most prominent in mylonitic to ultramylonitic interlayered amphibolite, metasandstone and micaschist (Figure 57a, Figure 62), In lithologies where a clear shear fabric is not developed, S2 and S3 can not be differentiated. In addition, the stretching lineations could not be differentiated between D2 and D3 in the field and share the designation L1. However, two sets of stretching lineation of roughly similar trend can be observed in a porphyroclast-rich layer close to the base of the Mörvikshummeln Formation, which may represent a slight difference between the two deformation phases (Figure 66). In the Mörvikshummeln Formation the stretching lineation L1 is primarily marked by mineral aggregates and rarely by the preferred orientation of large clinopyroxene porphyroblasts. In the Rödkullen Formation, L1 is marked by mineral aggregates and the preferred orientation of green amphiboles, biotite, white mica. Mesoscale folding and boudinage related to D3 is ubiquitous in the nappe, particularly in the extremely plastically deformed Mörvikshummeln Formation (Figure 67, Figure 68), but the main foliation is concordant with the synform shape at a large scale. In the Mörvikshummeln Formation, compositional layering has been folded and refolded in tight isoclinal folds, reflecting the highly ductile deformation mode (Figure 50, Figure 67). Folds are highly non-cylindrical, the fold axes are perpendicular or parallel to the stretching lineation (Figure 69). The Rödkullen Formation is likewise highly folded with abundant amphibolite boudins.

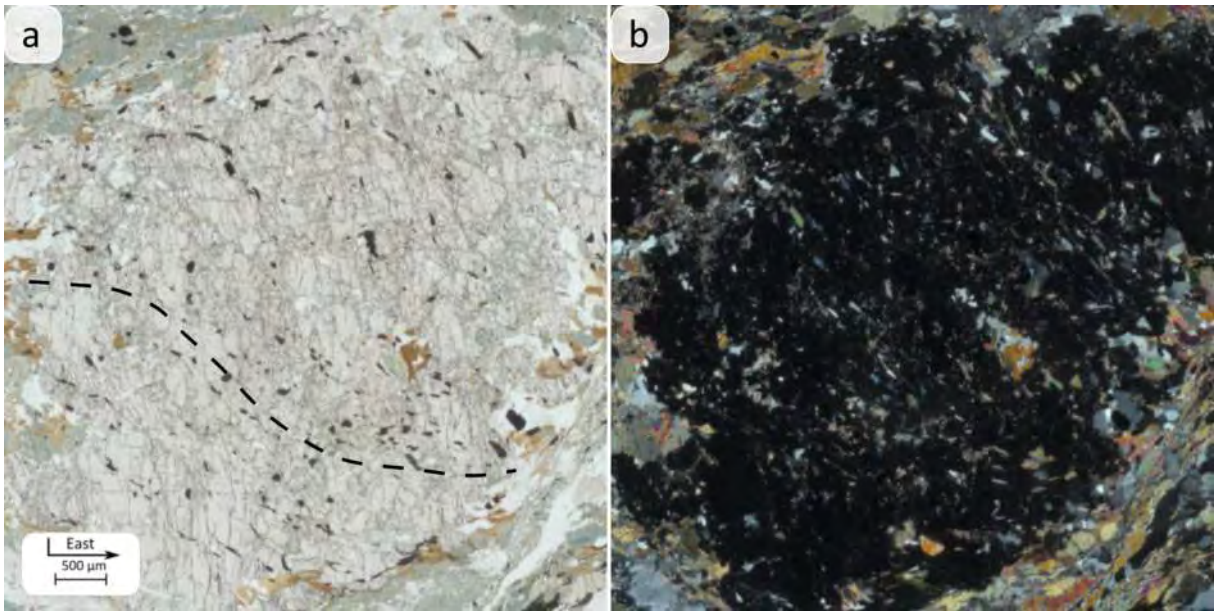


Figure 65: Rotated inclusion trail in garnet. Foliation is traced by striped line in left figure. Scan of thin-section from mylonitic sample LS2389, containing interlayered amphibolite, micaschist and metasandstone. Left figure is displayed in plane-polarized light, right figure in cross-polarized light.



Figure 66: Two sets of stretching lineation seen on a steeply dipping layer rich in feldspar porphyroclasts, in a calc-silicate gneiss outcrop.

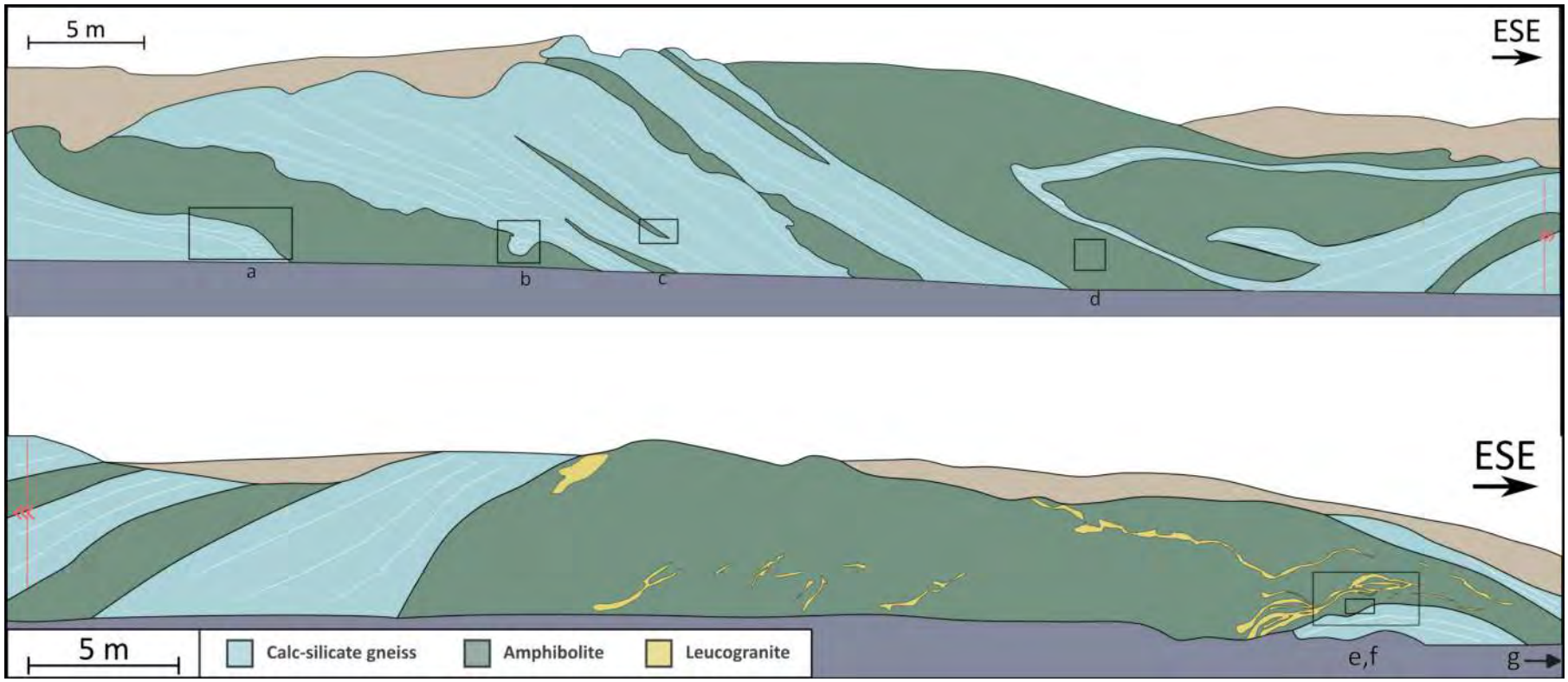


Figure 67: Sketch of long outcrop along E14, blasted and wire-sawed in the summer of 2023. The two sketches are continuos, joined at the red line to the right and to the left of the outcrop, respectively. The highly ductile mode of deformation is evident both at outcrop scale and close up. Rectangles mark close-up photos, a, b, d and e in figure 68, c in figure 44a, f (small rectangle) in figure 50a and g, which is located of to the right of the sketched outcrop, is seen in figure 52a. Outcrop-scale foliation is marked in the calc-silicate gneiss, which wraps around amphibolite boudins and is interfolded with amphibolite layers. The foliation of amphibolite is faint, mainly visible through compositional layering, shown in figure 68d. Even though the proportions of calc-silicate gneiss and amphibolite are quite evenly matched in the outcrop, the highly ductile calc-silicate gneiss defines the deformation. leucogranite can be seen in the outcrop and adjoining outcrops as thinned layers parallel to the foliation veins and patches (c; figure 44a), veins intruding amphibolite, wrapping around broken-off blocks of the host rock (e; figure 68e) and as larger patches (g; figure 52a).

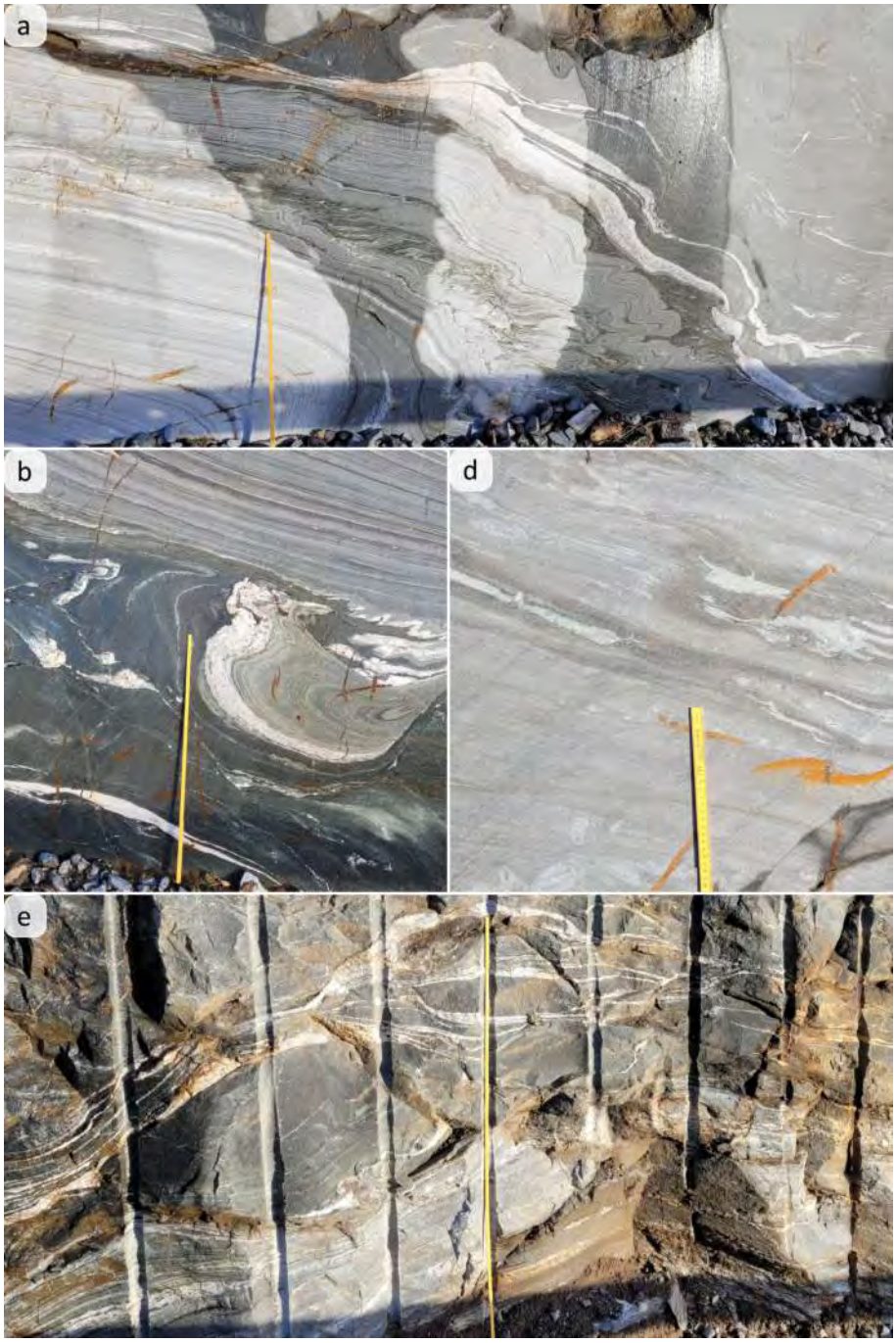


Figure 68: Close-up photos marked using the same letters in figure 67. (a) Folded sequence of calc-silicate gneiss, with dm-scale S-C fabric visible above the ruler. Ruler is 1 m. (b) Patch of refolded calc-silicate gneiss bounded by leucogranite in amphibolite layer, illustrating the highly ductile nature of the calc-silicate gneiss. Ruler is 1 m. (d) diffuse compositional layering in amphibolite. Note the apparent metasomatic domains surrounding leucocratic layers and patches. (e) Intrusive veins of leucogranite in amphibolite. Layering appears concordant with the main foliation. Ruler is 1.8 m.



Figure 69: Photos of isoclinal folds in calc-silicate gneiss. (a) Isoclinal folds with the axis parallel to the stretching lineation in calc-silicate gneiss on the southern slope of Mörvikshummeln. The outcrop is immediately above the transition from the Rödkullen Formation. The rusty layer above the compass contains large feldspar clasts, possibly originating in pegmatitic leucogranite. (b) Isoclinal folds in calc-silicate gneiss along the stream Tvärån, with the axis parallel to the stretching lineation. Photo is taken perpendicular to the stretching lineation. (c) Tight isoclinal folds in calcsilicate gneiss, in an outcrop immediately above the transition from the Rödkullen Formation. Though at the same structural level as (a), the outcrop is situated 500 m northwest and 130 m of elevation higher, where the Mörvikshummeln is significantly thinner.

Leucogranite intrusion appears contemporaneous with the development of S2, though the exact age relationship is difficult to distinguish; leucogranite can be found in thin bands interlayered with calc-silicate gneiss and amphibolite, but also as larger boudinaged bodies cutting the main foliation S3, with a slightly discordant internal foliation.

Approaching the base of the nappe and the contact with the underlying Särv Nappe, outcrops of the Rödkullen Formation displays increasing deformation related to D4, distinguished by chlorite marking C and C' planes parallel to S3, and C-planes of finely recrystallised white mica in the fabric S4 (Figure 70). The related stretching lineation L2 is marked by chlorite in the affected lithologies. No difference in trend has been observed between L1 and L2 in the field.

The large-scale structure of the Kall Nappe marks the geometry of the Åre Synform, with an inflection point from eastward to westward dip (i.e. the hinge of the synform) roughly in the area of Susabäcken at the southern base of the Åreskutan Nappe. However, the synform hinge line appears to move eastwards at lower structural levels, apparent in east-dipping roadcuts along E14 situated east of the hinge at structurally higher levels and in projections of structural measurements (Figure 71, Figure 72). The orientation of the stretching lineation is slightly dispersed, but dominantly trend east-west (Figure 72). Top-to-the-east shear-sense indicators are observed across the nappe, both at the meso- and microscale (Figures 73, 74, 75, 76, 77, 78). Brittle deformation related to the deformation phase D5 is observed towards the base of the nappe, where meso-scale faults cut across foliation and fractures in rock samples show top-to-the-east thrusting (Fig 79).

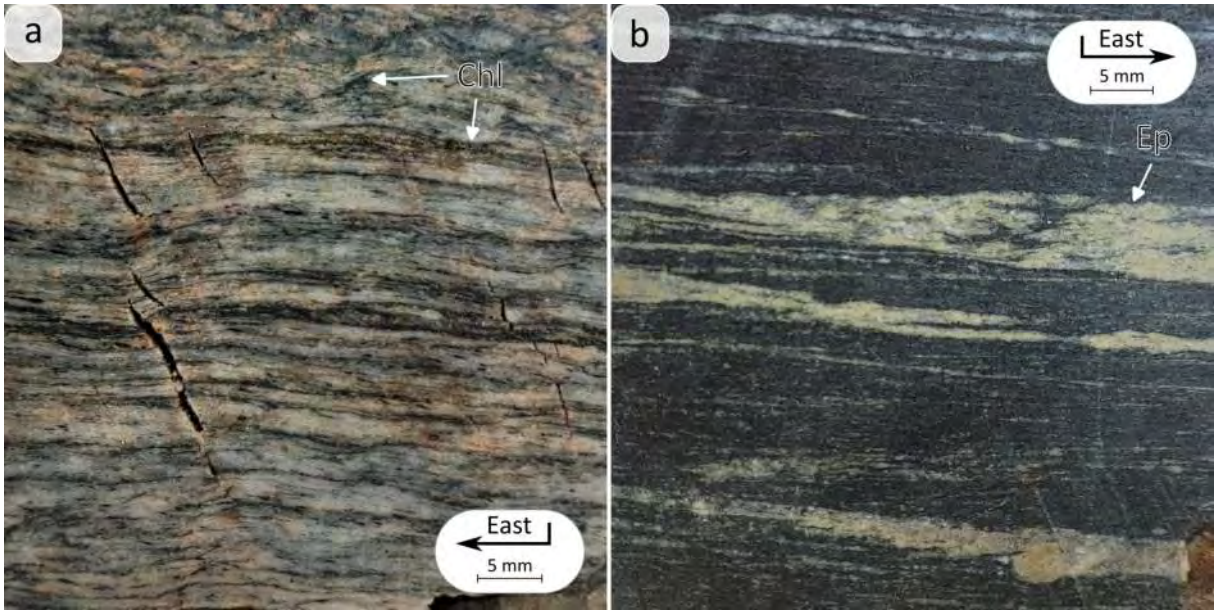


Figure 70: Cut surfaces of mylonitic samples from within 10-20 m above the tectonic contact with the Särv Nappe, cut parallel to the stretching lineation. (a) Mylonitic amphibolite with significant epidote alteration of quartzofeldspathic layers. (b) Mylonitic metasandstone with incipient fractures related to thrusting in the brittle regime.

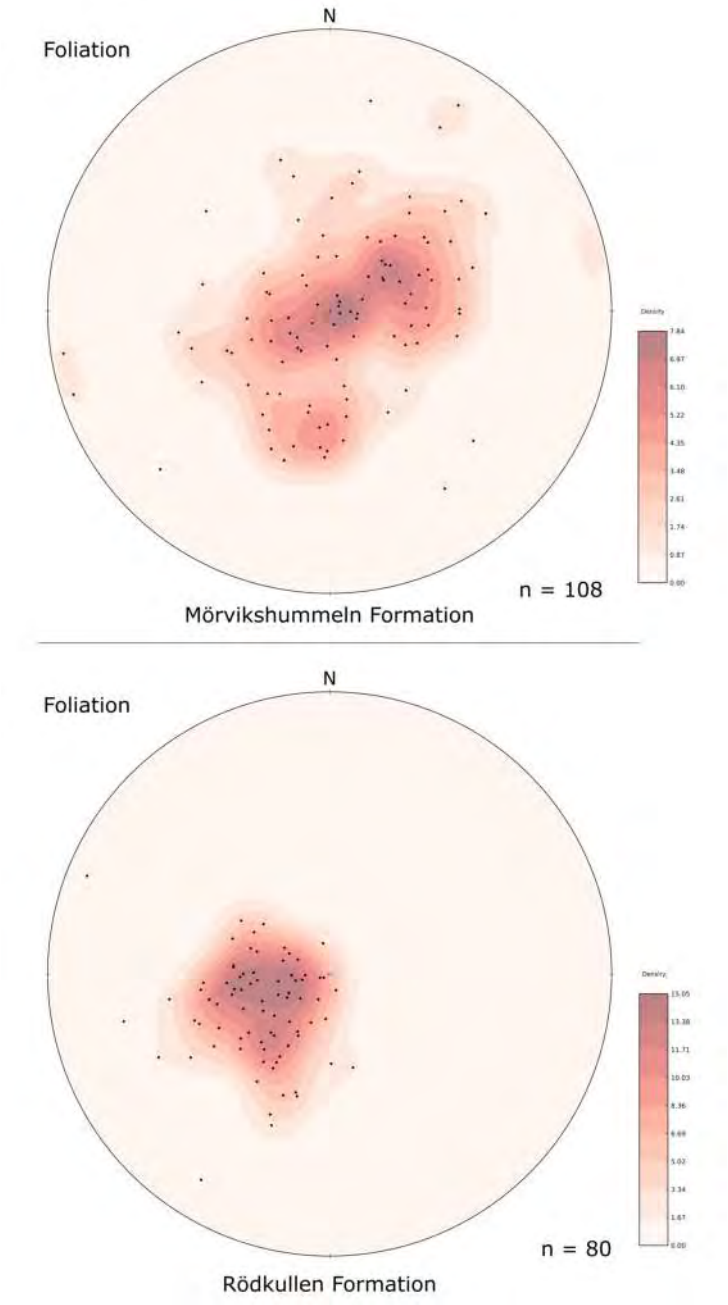


Figure 71: Difference in orientation of foliation measured in the Mörvikshummeln and Rödkullen Formations within the study area, projected in separate lower hemisphere equal-area stereograms. The dip of the foliation of the Mörvikshummeln formation is generally sub-horizontal to gentle, with dip direction distributed around the center of the projection, as expected when mapping two limbs of a synform. By contrast, measurements from the Rödkullen formation show a consistent eastward dip direction. Contours marking the observation density are constructed using Fisher probability distribution in the projection program OpenStereo.

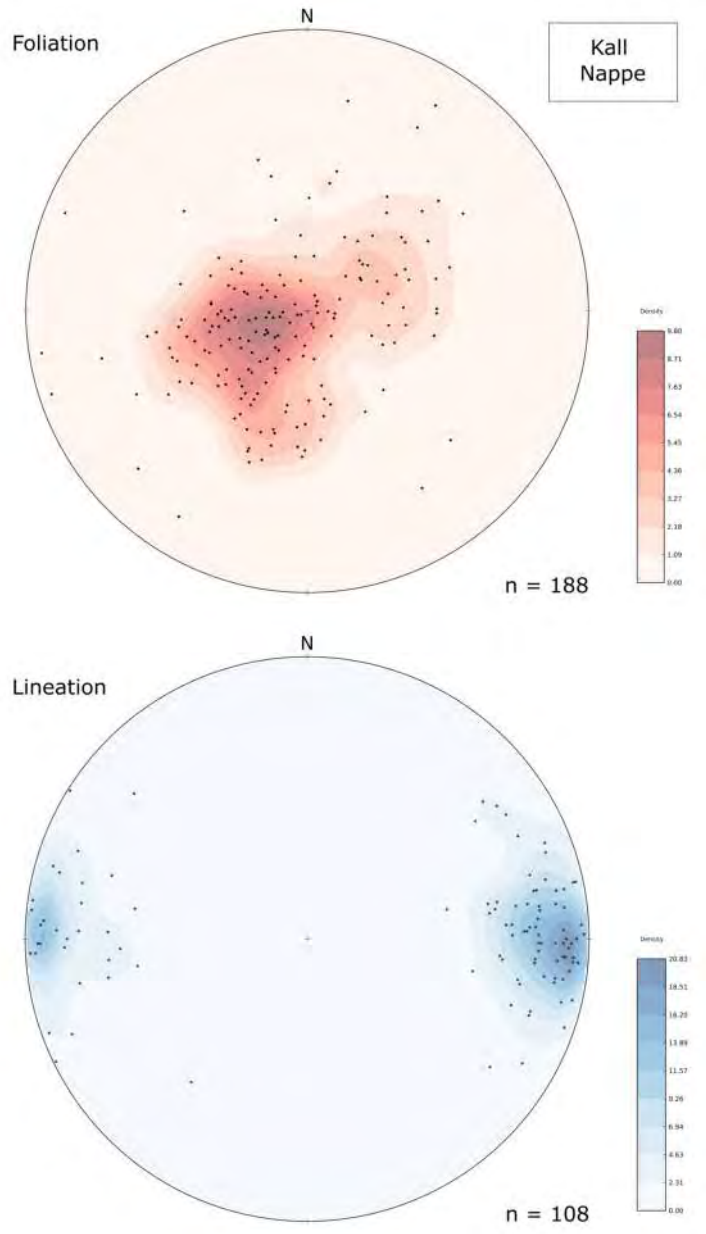


Figure 72: Projection of the foliation orientation and stretching lineation measurements of the Kall Nappe within the study area. The distribution of foliation measurements shows subhorizontal to gentle dip towards north and east dominate the structure of the nappe around Åreskutan. The stretching lineation dominantly trends east-west. Contours marking the observation density are constructed using Fisher probability distribution in the projection program OpenStereo.



Figure 73: Rotated and sigmoid mafic pods in calcsilicate gneiss from the Mörvikshummeln Formation showing a top-to-the-east shear sense. Photo taken parallel to the stretching lineation.



Figure 74: C-C' fabric showing a top-to-the-east shear sense, marked by biotite, in scan of thin section from calc-silicate sample LS23161. The left side is displayed in plane-polarized light, right in cross-polarized light. To the right is a sketch highlighting the deformational fabric.

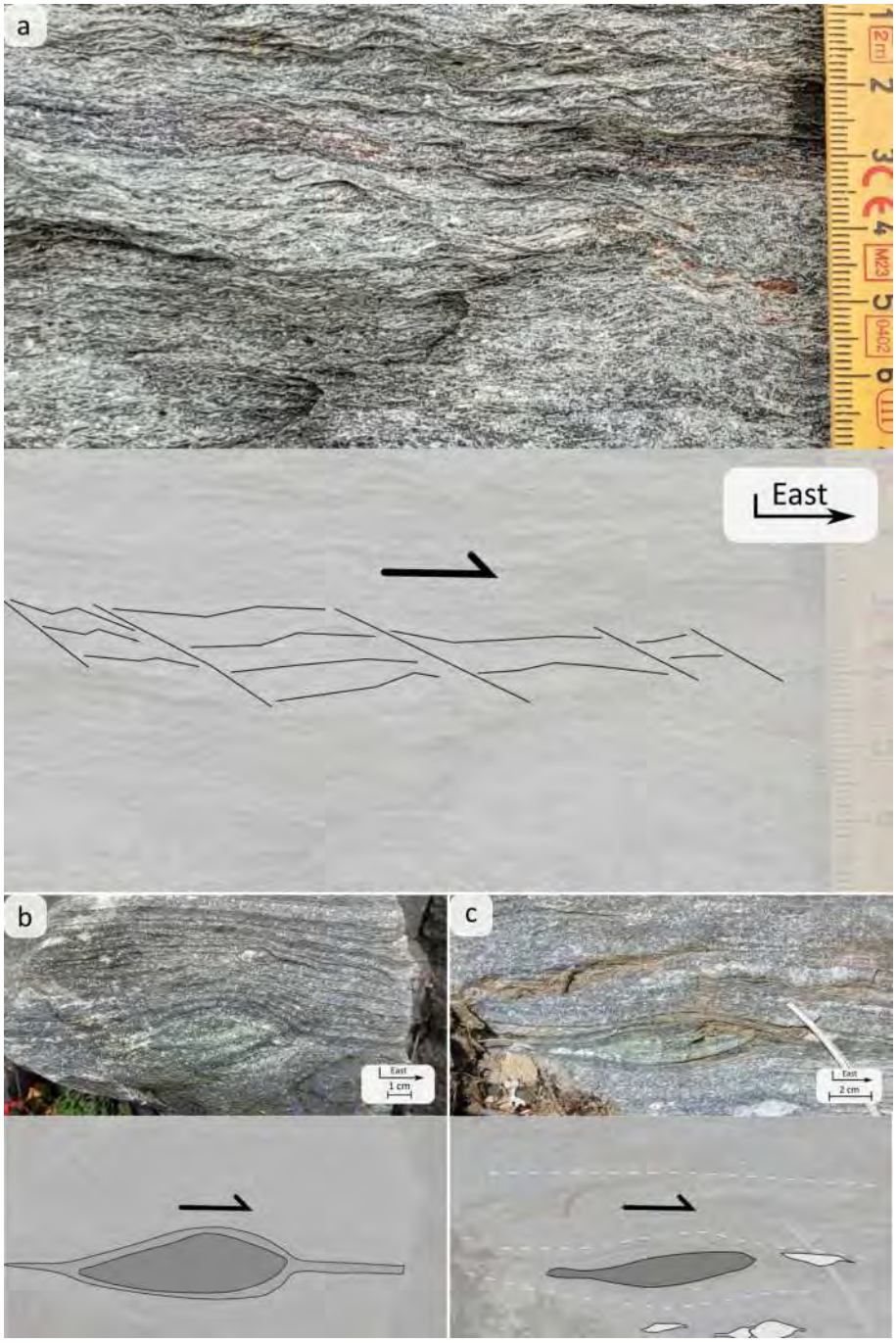


Figure 75: Photos of shear sense indicators from the Rödkullen Formation, with sketches highlighting the fabric or structure. Photos taken parallel to the stretching lineation. (a) C-C' fabric in micaschist showing a top-to-the-east shear sense. Photo is a close-up of the micaschist seen in figure 54a. (b) and (c) Sigmoid mafic pods in metasandstone showing a top-to-the-east shear sense. Both photos are taken at the same outcrop, the transitional metasandstone at the top of the Rödkullen Formation shown in figure 57b.

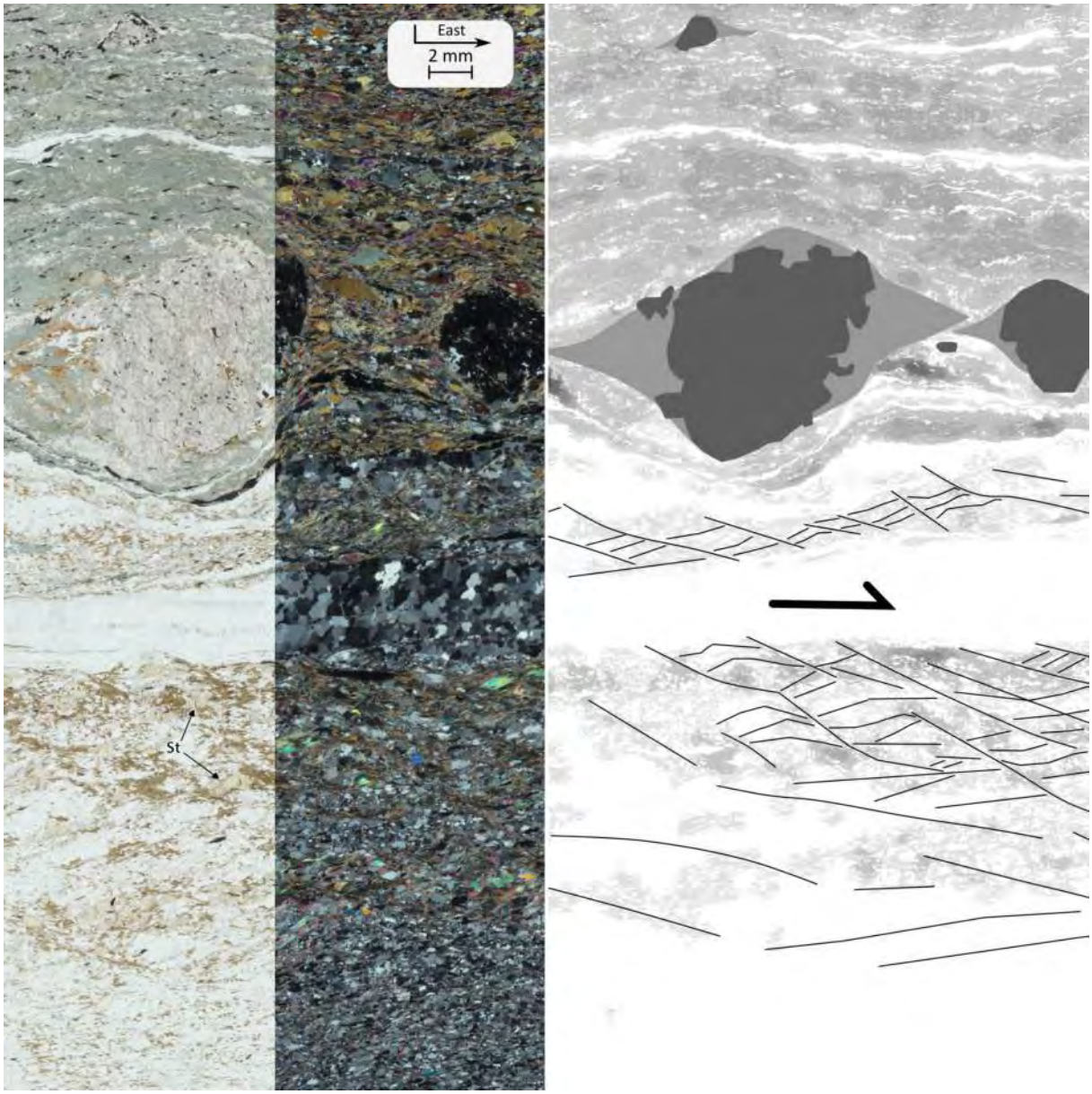


Figure 76: C-C' fabric in micaschist and strain shadows around garnet in amphibolite shows a top-to-the-east shear sense, in scan of thin section from sample LS2389. The left side is displayed in plane-polarized light, right in cross-polarized light. To the right is a sketch highlighting the deformational fabric. The C-C' fabric is primarily marked by white mica and biotite, with chlorite occasionally marking the C'-plane. Note also the long axis of staurolite grains marking the foliation.

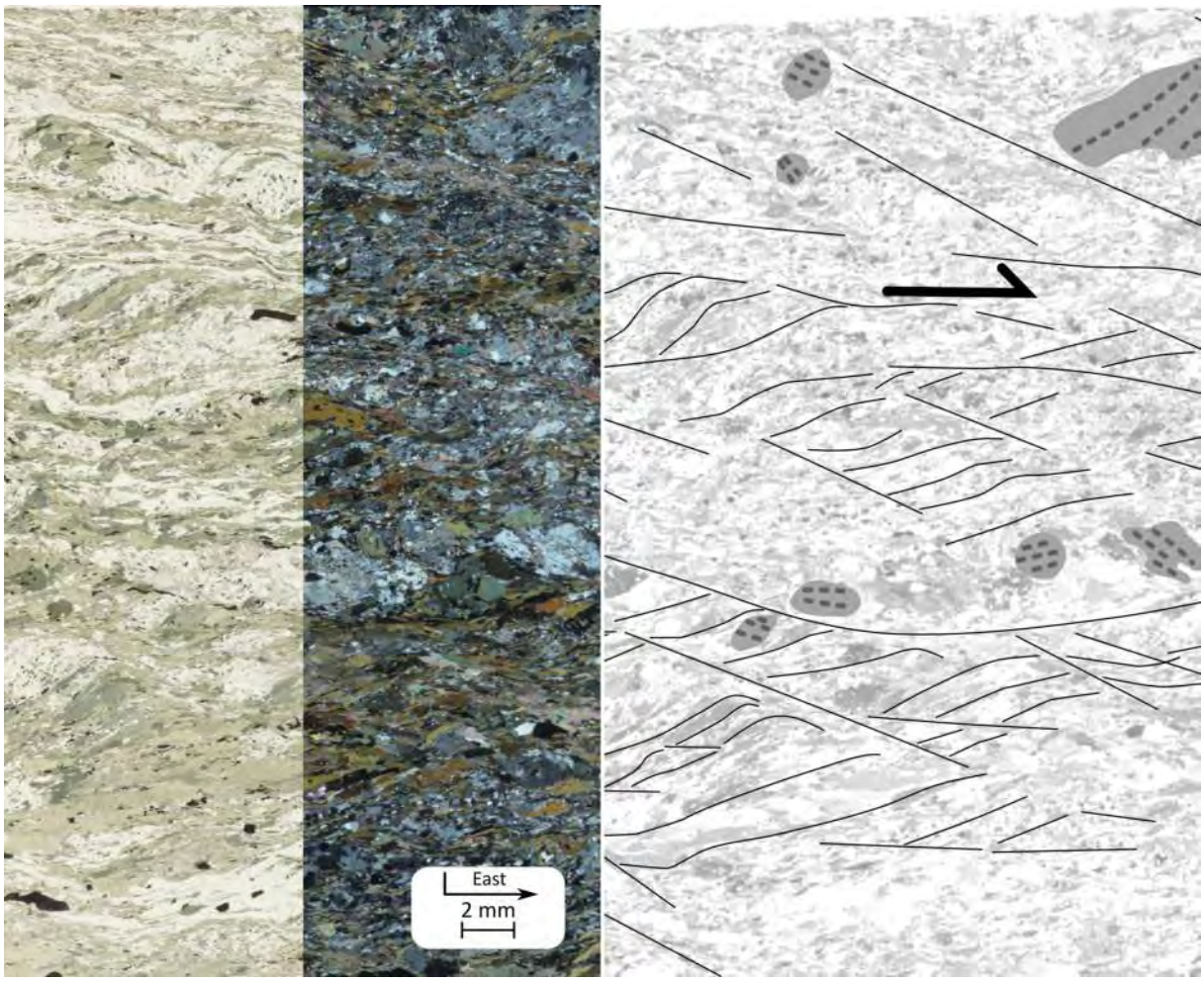


Figure 77: C-C' and S-C fabric showing a top-to-the-east shear sense, marked by green amphibole, in scan of thin section from amphibolite sample LS2397. The left side is displayed in plane-polarized light, right in cross-polarized light. To the right is a sketch highlighting the deformational fabric.

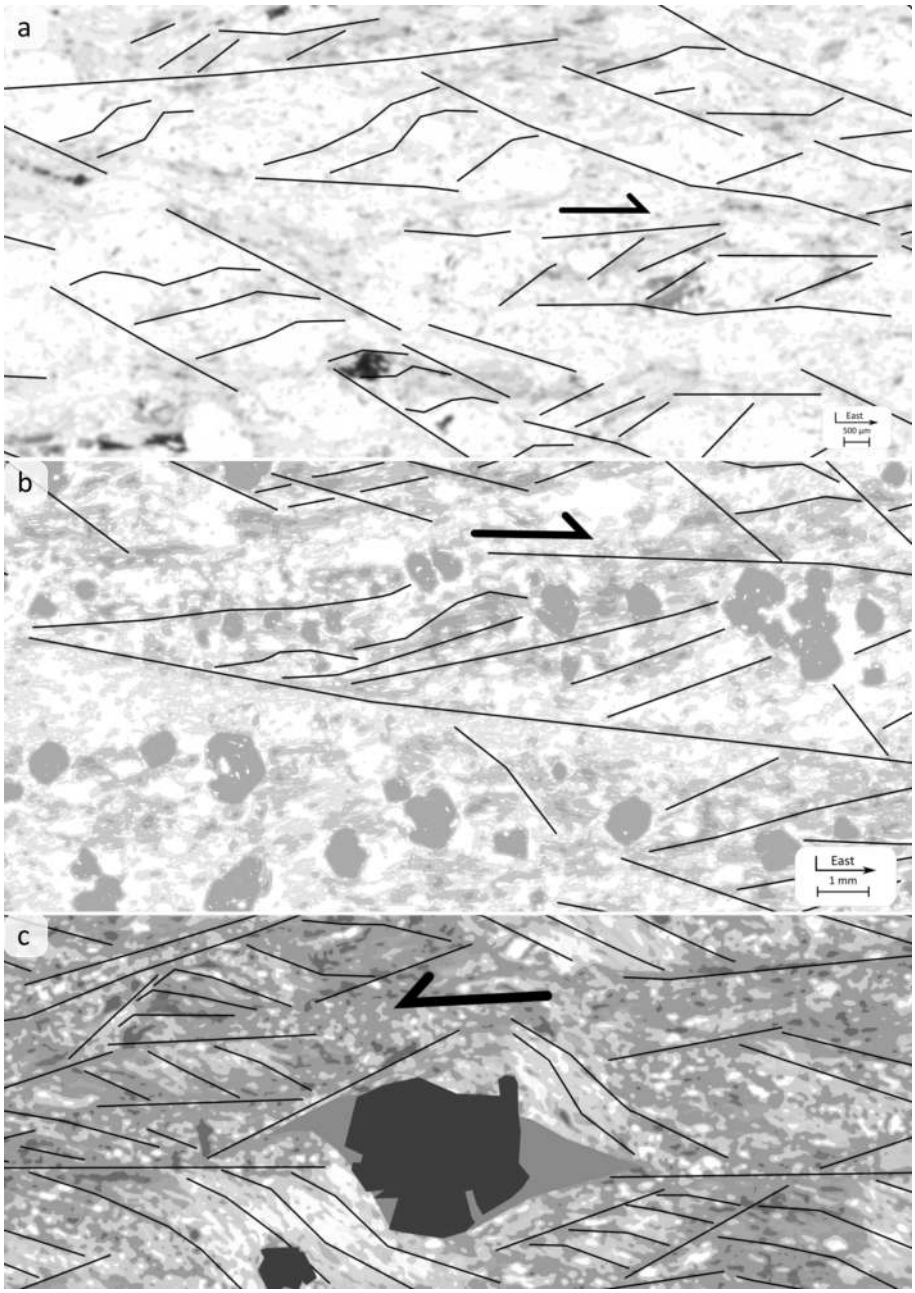


Figure 78: Sketches highlighting the deformational fabric of the thin section scans of micas-chist shown in figure 61. All samples show a top-to-the-east shear sense. (a) LS2392 shows a diffuse S-C and C-C' fabric wrapping around feldspar porphyroblasts. S-planes are primarily marked by white mica, C-planes by biotite and C'-planes by biotite and chlorite. (b) LS2395 shows a C-C' fabric marked by biotite. The C' plane cutting through the middle of the figure shows significant grain-size reduction. (c) LS23122 shows a distinct S-C fabric and weak C-C' fabric, as well as a strain shadow around the central garnet. S-planes are primarily marked by white mica, C-planes by white mica, biotite and chlorite, and C' planes are marked by biotite and chlorite.

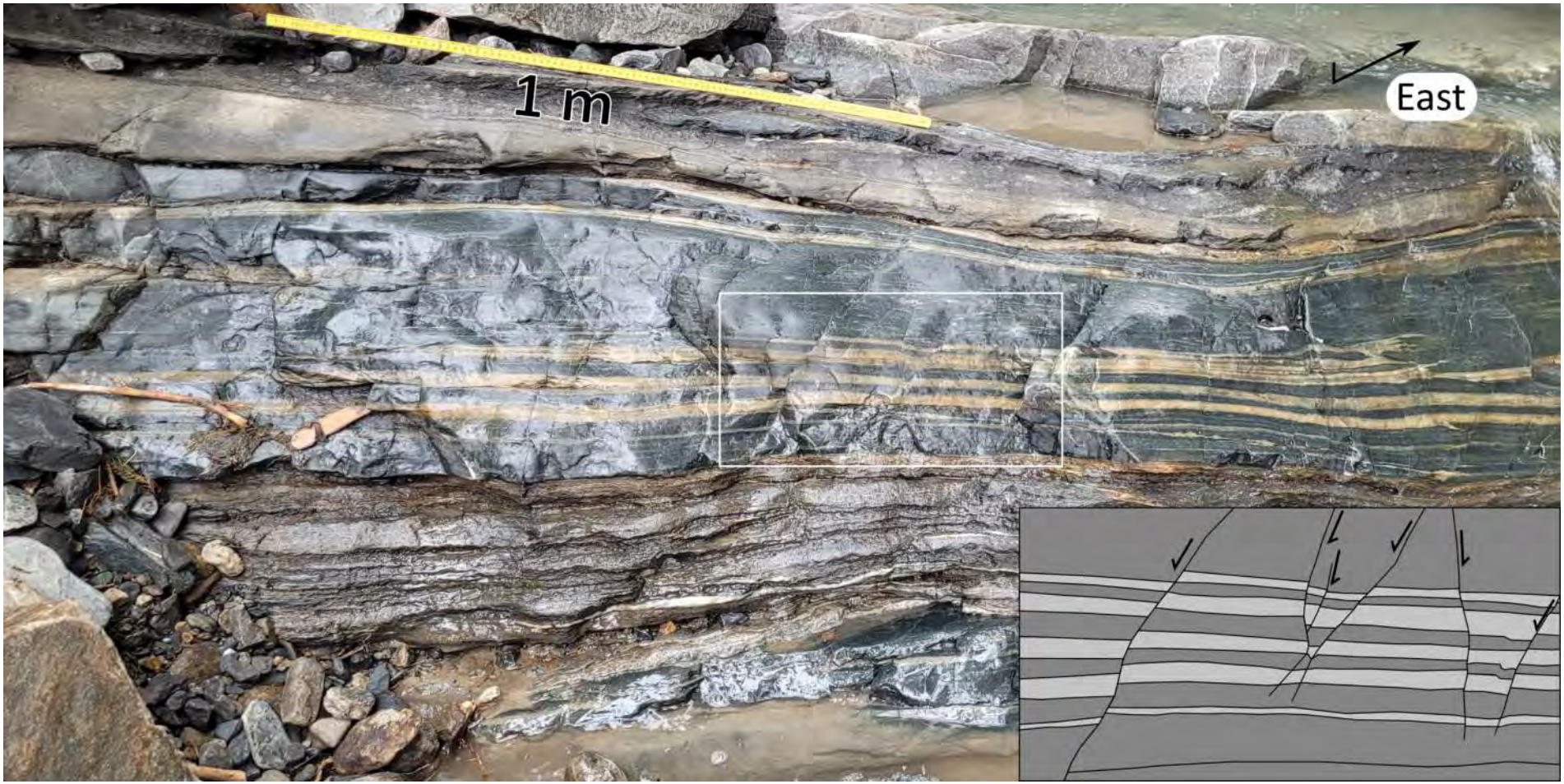


Figure 79: Photo and sketch of brittle deformation in interlayered mylonites close to the base of the Kall Nappe. The white rectangle shows the extent of the sketch. The minor vertical displacement is highlighted by light layers of mylonitic metasandstone. Fractures can be traced into the micaschist layers below the sketched area, but displacement is difficult to distinguish.

7.3.11 Metamorphic history

The earliest observable event in the Kall Nappe, M1, can be seen in inclusions and internal foliation in garnet. Rotated inclusion trails are syntectonic with top-to-the-east shear, but further investigation is needed to describe this event. M2 is defined by the distinct amphibolite-facies assemblages garnet-staurolite-biotite at the base of the nappe and diopside and calcic garnet towards the top. The Kall Nappe did not seem to reach the partial melting field, indicated by the widespread presence of white mica and lack of melt segregations. Veins in amphibolite close to the contact with the Åreskutan Nappe are equivocal, and may be attributed to intrusion of hydrothermal fluids. Leucogranite intrusions are also affected by M2, indicated by the presence of garnet. Progressive retrogression occurred during M3 and M4, evidenced by replacement of garnet by biotite, followed by replacement of biotite and garnet by chlorite (Figure 80). Chlorite marks shear bands at all structural levels in the Rödkullen formation, and chlorite or epidote alteration increases significantly towards the base of the nappe (Figure 81). The basal retrogression is either completely related to D4, or indicating the development of the basal mylonitic foliation during D3 partially occurred at lower metamorphic grade.

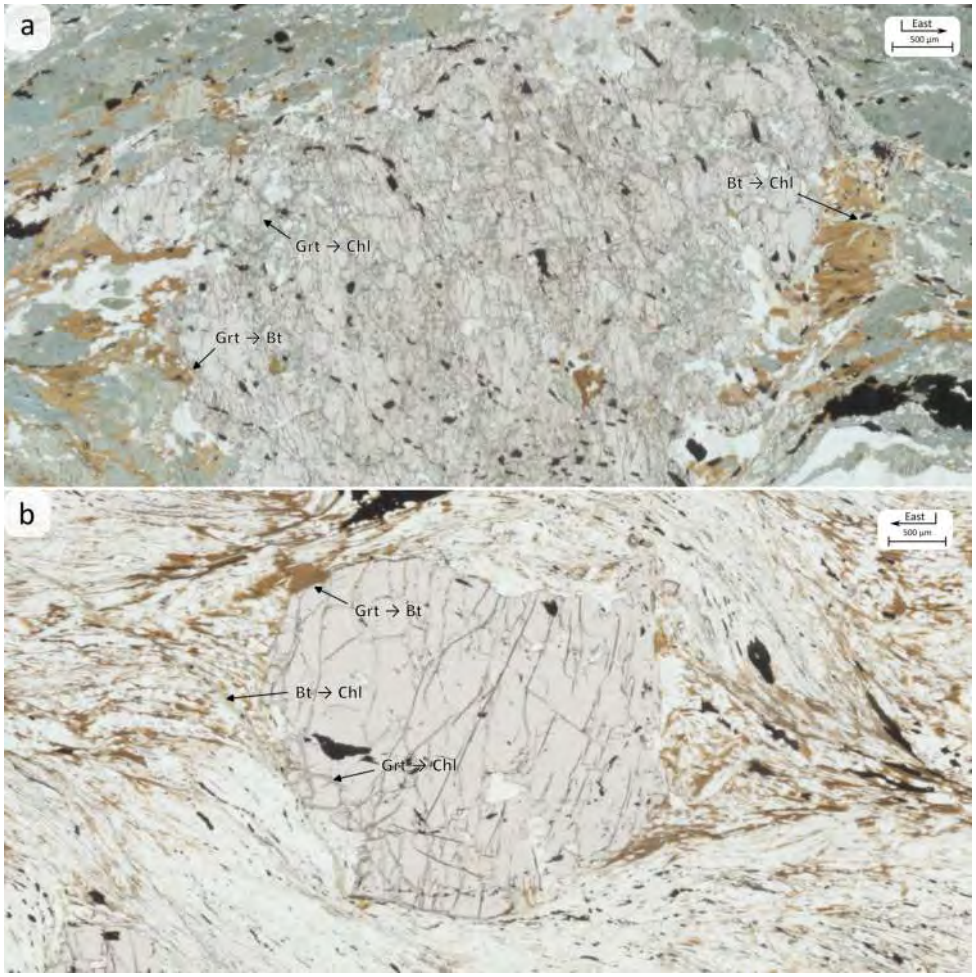


Figure 80: Scans of thin sections showing replacement reactions during retrogression, displayed in plane-polarized light. (a) In sample LS2389 replacement of garnet in amphibolite by biotite and chlorite, and replacement of biotite by chlorite is observed. (b) The same reactions are also seen in micaschist sample LS23122.



Figure 81: Photo of mixed outcrop with interlayered amphibolite and metasandstone, showing significant epidote alteration of metasandstone.

Close to the tectonic contact with the Särv Nappe some amphibolite outcrops are almost completely altered to mylonitic chlorite schist. Close to the transition from the Rödkullen to Mörvikshummeln Formation, an intrusion has brecciated an outcrop of amphibolite. The intrusive rock consists of a fine groundmass of epidote and large anhedral quartz clasts, together with dispersed angular amphibolite fragments (Fig 82). Further investigation is needed to fully identify the timing of this intrusion. Additional signs pointing to circulation of hydrothermal fluids are what appears to be white amphibole needles are found filling fractures in the upper Rödkullen and the Mörvikshummeln Formations, fractures cutting the main foliation (Figure 83).

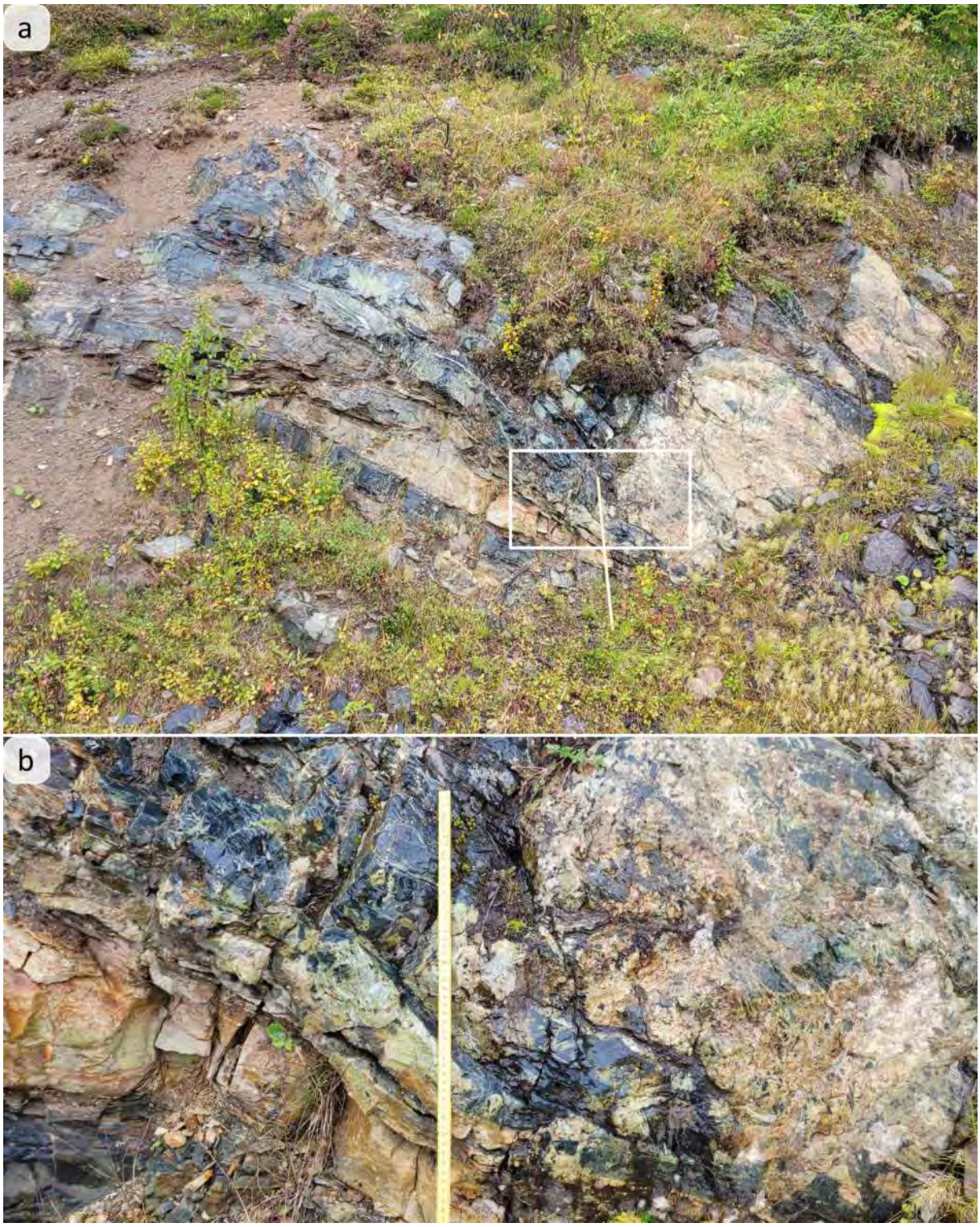


Figure 82: Photos of hydrothermal vein intruding a mixed outcrop exposed towards the top of the Rödkullen Formation on Mörvikshummeln. (a) Overview photo of the outcrop. To the left bright green epidote can be seen on fracture surfaces in amphibolite. Ruler is 1 m. (b) close-up, marked by the white rectangle in (a). Angular fragments of amphibolite can be seen in the epidote-dominated groundmass. The thickness of the exposed vein decreases from right to left.



Figure 83: Photo of white amphibole needles growing radially in a fracture in calc-silicate gneiss. The same fracture filling can also be found at high structural levels in the Rödkullen Formation. Note also the differential weathering of the marble layer by the ruler.

7.4 Särv Nappe

A ∼ 300-400 m thick unit of dolerite-intruded metasandstone and micaschist of the Särv Nappe, underlying the Rödkullen formation of the Kall Nappe, make up a sizeable portion of the lower western slope of Åreskutan. A low metamorphic grade distinguishes it from the amphibolite-facies Kall Nappe above. The transition from the overlying Kall Nappe as well as the underlying Offerdal Nappe is not exposed, and the distinction is made based on metamorphic grade and deformation style of lithologies. Metadolerite of varying alteration grade and feldspathic metasandstone dominate the Särv Nappe, with subordinate micaschist.

7.4.1 Metadolerite

Metadolerite of the Särv Nappe is observed in a variety of shapes: in massive outcrops several meters thick, interlayered with metasandstone in mixed outcrops and as highly strained < 1 cm layers in mylonite (Figure 84). The alteration of metadolerite is highly variable, from negligible to full chloritisation, which is also related to degree of mylonitization. The weathering surface is black to pale bluish green depending on chlorite content, with fresh surfaces black to dark green. The texture varies from aphanitic to porphyroclastic with plagioclase porphyroclasts generally 1 mm, up to 4 mm (Figure 85). Composition is dominantly green or black amphibole, variable plagioclase and chlorite, plus minor sulphide and carbonate. Foliation is well to very well developed, marked by compositionally different layers of amphibole and plagioclase, as well as by the preferred orientation of chlorite and elongated plagioclase and sulphide grains.

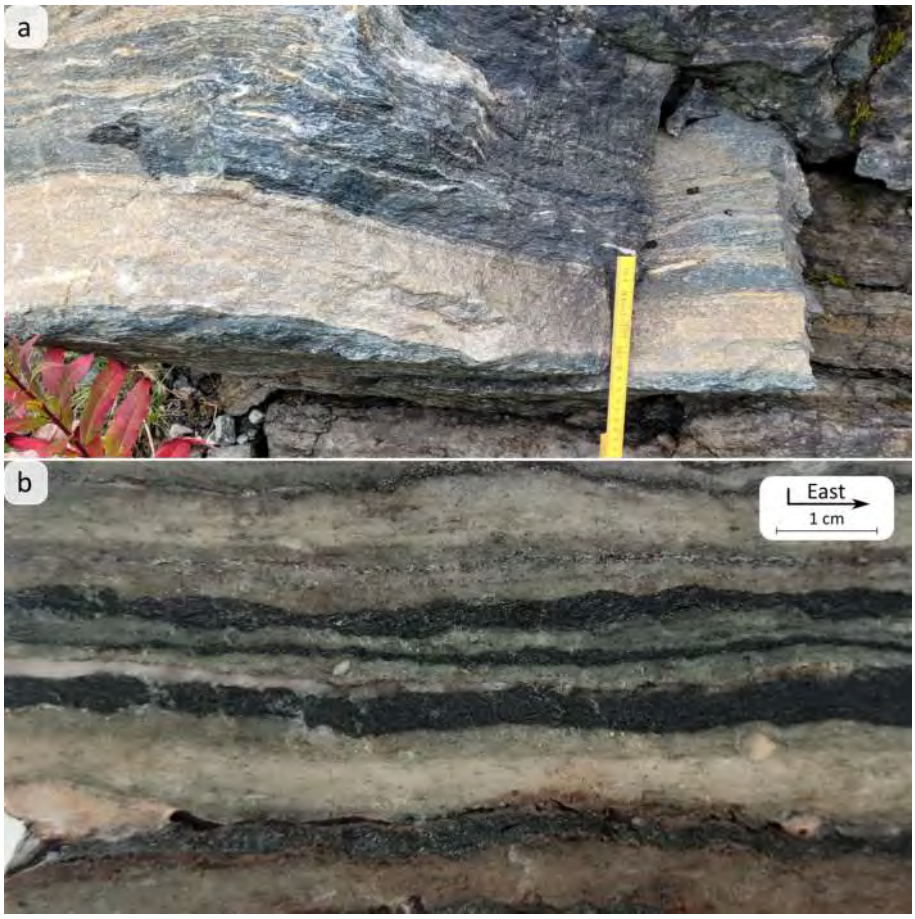


Figure 84: Photos of different varieties of metadolerite. (a) Porphyroclastic and aphanitic metadolerite interlayered with weakly foliated metasandstone. (b) Cut surface of mylonite sample, cut parallel to the stretching lineation. Metadolerite is completely altered to chlorite schist, interlayered with mylonitic metasandstone.

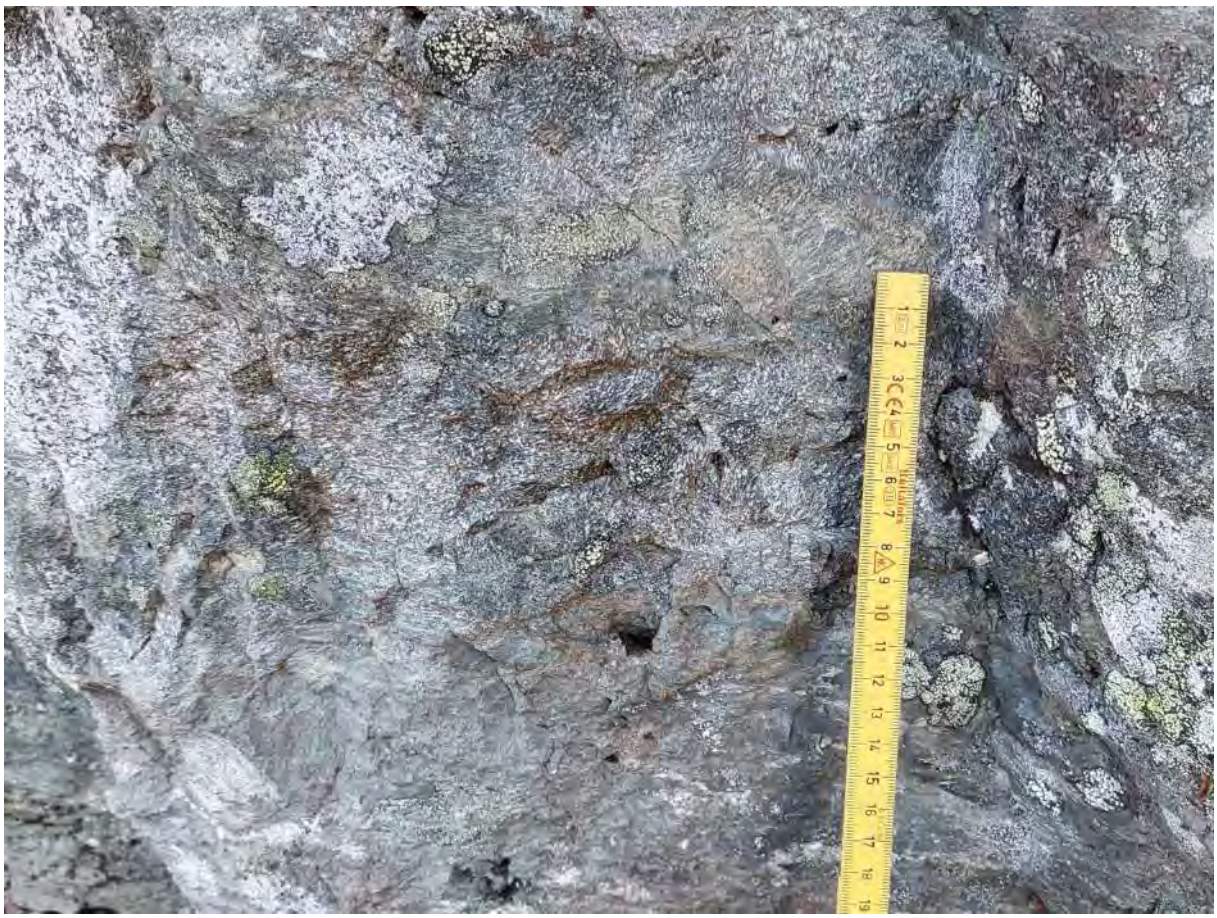


Figure 85: Photo of metadolerite with elongated plagioclase porphyroclasts marking the foliation.

7.4.2 Metasandstone

In addition to metadolerite, feldspathic metasandstone makes up the bulk of the Särv Nappe. The weathering surface is pale brown, fresh surfaces are light to dark grey, sometimes with a yellowish hue (Figure 86). Grain size varies from very fine grained to medium grained, with feldspar porphyroclasts 0.5-1 mm, up to 5 mm. Composition is variable, from quartzofeldspathic with only minor micas, to significant content of, biotite, white mica, green amphiboles, epidote and sulphides, all of which also marks foliation. In less homogeneous metasandstone, carbonate content is typically also high (Figure 87). Thin section of metasandstone sample SV23118 is summarized in table 5.

7.4.3 Micaschist

Micaschist is typically interlayered with metasandstone, and may be difficult to distinguish from metadolerite chlorite schist in the field. Weathering surfaces and fresh surfaces are grey, and a distinguishing feature is coarse and flakey white mica grains or agglomerates, giving a fish-scale appearance on the foliation plane (Figure 88). Small plagioclase porphyroclasts are common (Figure 90). Composition is dominantly white mica, plagioclase, sulphide, epidote, biotite and quartz. Foliation is well developed and marked by the preferred orientation of white mica, elongated sulphide grains and partially by biotite. Thin section of micaschist sample SV23116 is summarized in table 5.

Table 5: Summary of sample thin sections from the Offerdal and Särv Nappe. Location of samples can be seen in appendix A. Mineral abbreviations from Whitney and Evans (2010), WM: white mica. Minerals are listed in the estimated order of decreasing abundance. Inclusions and internal foliation are presented in the format Host (Inclusion). Discordant is abbreviated from discordant with the main foliation.

Sample	Lithology	Minerals	Marking foliation	Inclusions	Internal foliation	Reactions	Zoned	Discordant foliation	Notes
OF2334	Semipilitic micaschist	Qz + WM + Ep + Chl + Grt + Fsp + Bt + Oxides	Qz microlithons, WM, Chl, Bt	Grt (Qz, Ep)		Grt → Chl			Minor amounts of green Bt. Crenulation of Ms observed on right side of sample. Possible faint kink bands cut the foliation at a high angle.
SV23116	Micaschist, calcareous Metasandstone	Qz + WM + Fsp + Bt + Cb + Ep +Ilm + Rt + Oxides	Qz aggregates, WM, Bt	Fsp (Qz, Ep, Oxides)	Fsp (Qz, Ep, Oxides)	Rt → Ilm + Bt	Fsp	Bt	Fsp often display Carlsbad twinning, no distinction can be made between Pl and Kfs. Bt greyish brown, pleochroic between to almost black. Rare large Bt flakes are discordant with the main foliation. Sample is folded (visible in cut hand sample), TTW shear sense is likely overturned shear criteria due to folding.
SV23118	Micaceous, feldspathic, calcareous amphibole Metasandstone	Qz + Fsp (Pl + undifferentiated) + Amp + Cb + Bt + Ep + Rt + Oxides	Amp, Bt, Ribbons of Qz ± Pl ± Cb, Elongated Oxides	Fsp (Ep, Bt, Qz, Oxides); Amp (Rt)	Fsp (Ep, Bt, Qz, Oxides)	(Amp → Bt ?)	Fsp		Pl display twin lamellae, undifferentiated Fsp are untwinned. Internal foliation in Fsp is curved, indicating syndeformational growth.

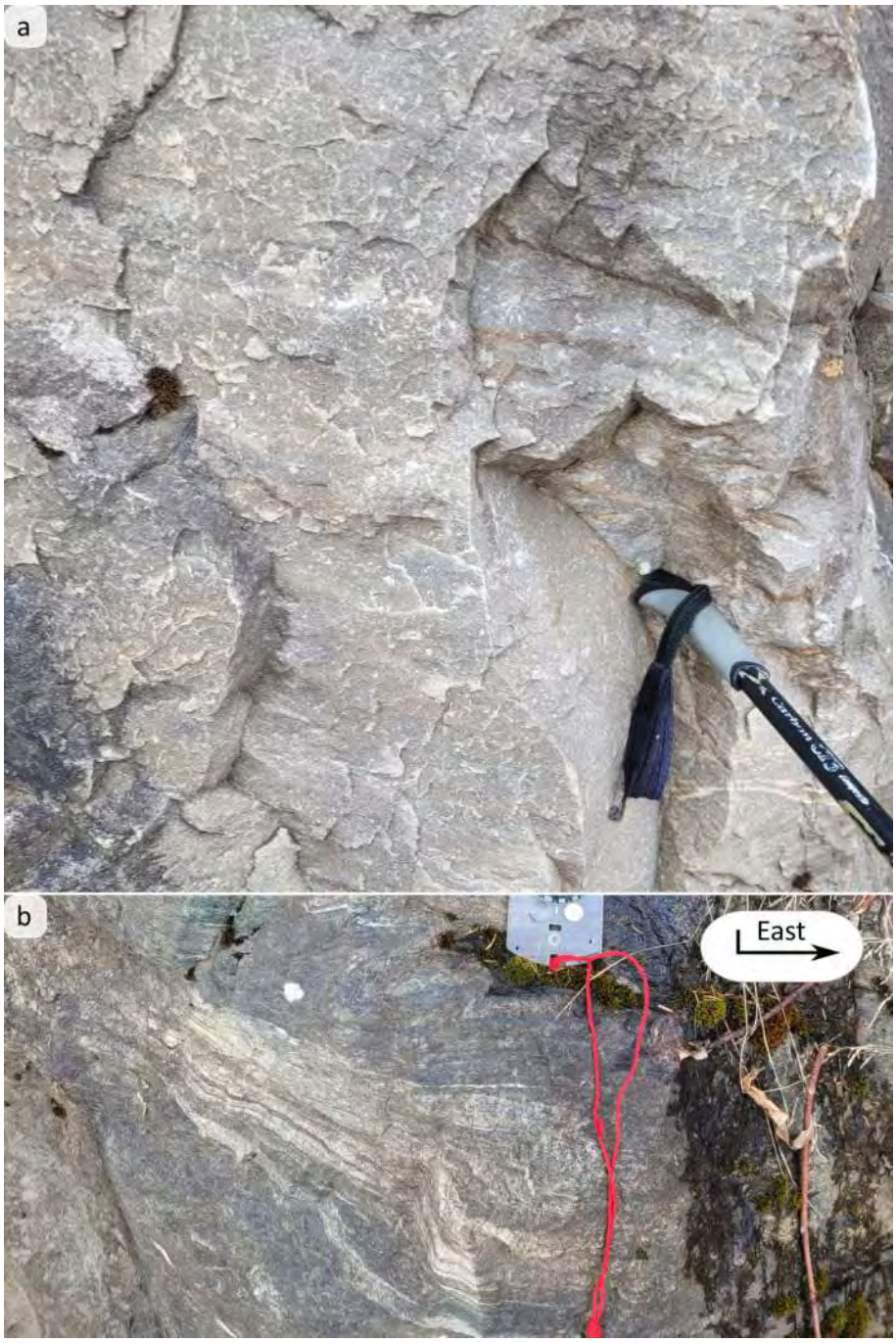


Figure 86: Photos of metasandstone outcrops. (a) Massive, weakly foliated metasandstone. Pole for scale. (b) Metasandstone interlayered with folded metadolerite. The foliation in the metasandstone is marked by thin layers of metadolerite.



Figure 87: Scan of thin section from calcareous metasandstone sample SV23118. Lower left is displayed in plane-polarized light, upper right in cross-polarized light. The sample contains a high mode of carbonate with significant deformation twinning. Sparse green amphibole and biotite marks the foliation.



Figure 88: Photo of crenulated micaschist. Photo taken roughly perpendicular to the stretching lineation. The foliation is marked by large aggregates of white mica, which resemble fish scales on the foliation plane.

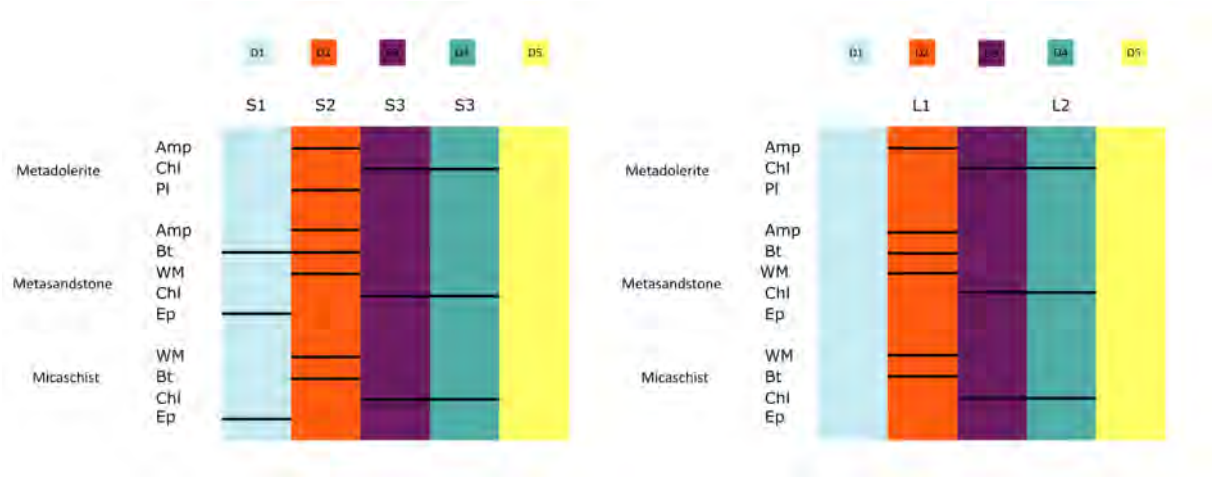


Figure 89: Summary of the deformation history of the Särv Nappe. Deformational events D1-D4 are identified and shown based on the succession of minerals marking foliation and stretching lineation.

7.4.4 Deformation history

Five deformation phases can be distinguished in the Särv Nappe, summarised in figure 89. Large parts of the nappe is proto-mylonitic and folded, but the strain appears markedly lower than the overlying Kall Nappe. The earliest deformational event, D1, recorded in the Särv Nappe can be seen as internal foliation, S1, in plagioclase. The internal foliation is rotated with respect to the main foliation S2 (Figure 90).

The main foliation is developed during D2, and is well defined in all but massive metasandstone. The related stretching lineation L1 is marked by amphibole, biotite and white mica. S2 is reworked in S-planes of the faint shear fabric S3, which is characterised by C-planes marked by biotite in micaschist. Development of S3 is likely contemporaneous with crenulation and folding of the main foliation during the deformation phase D3. Crenulation is observed both in metadolerite and micaschist; in metadolerite the fold axis trends perpendicular to the stretching lineation, while crenulation of micaschist appears more complex (Figure 88, Figure 91). Folds related to D3 range from gentle crenulation to tight or isoclinal, with fold axes perpendicular and parallel to the stretching lineation (Figure 92). The deformation phase D4 is observed in a locally well developed shear fabric, S4, associated with extensive chloritisation of metadolerite. A rheological contrast can be seen between metadolerite in S-planes and chlorite in C or C' planes, which are occasionally also marked by quartz veins. The stretching lineation L2 is related to D4, and is marked by chlorite.

A possible isolated deformation phase D5 is identified at the lower tectonic boundary, where the main foliation is reworked in isoclinal folds with roughly east-west trending axes (Figure 92b). Folded metadolerite layers are fully chloritised, interlayered with fine-grained metasandstone and apparent microcrystalline quartz layers.

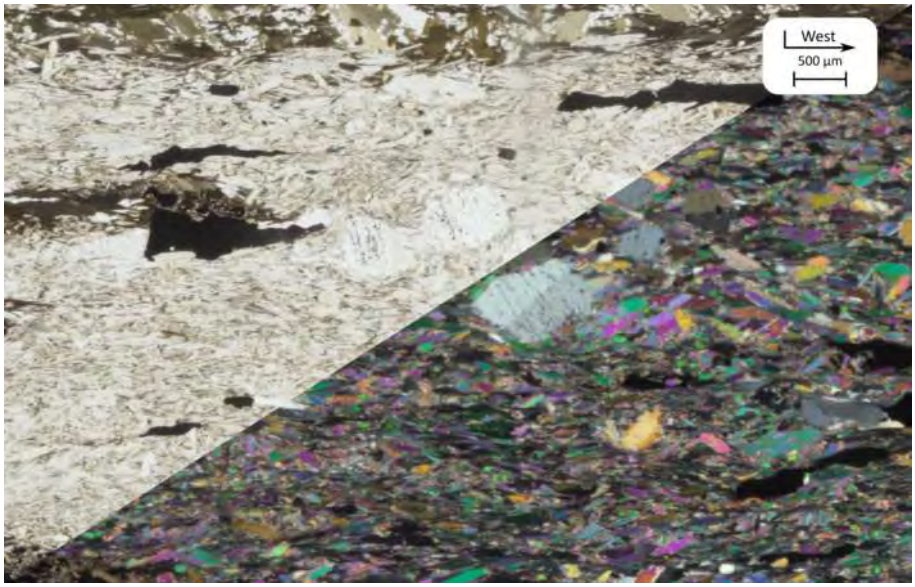


Figure 90: Planar internal foliation of twinned plagioclase porphyroblasts is micaschist close to the upper boundary of the nappe. Scan of thin section from folded micaschist sample SV23116. Upper left is displayed in plane-polarized light, lower right in cross-polarized light.

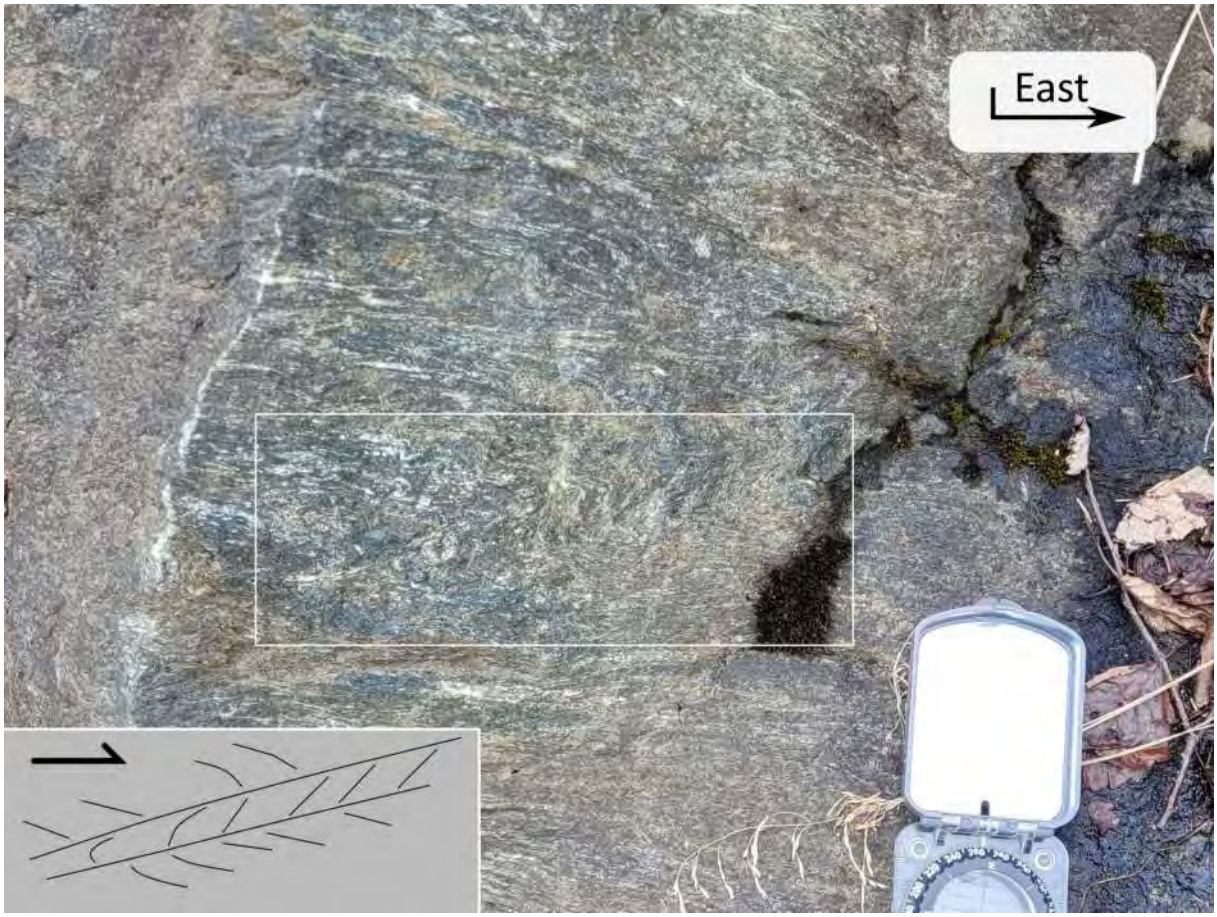


Figure 91: Crenulation surfaces visible in folded metadolerite close to the uppper boundary of the nappe. Sketch highlights the crenulation plane. Photo taken parallel to the stretching lineation.

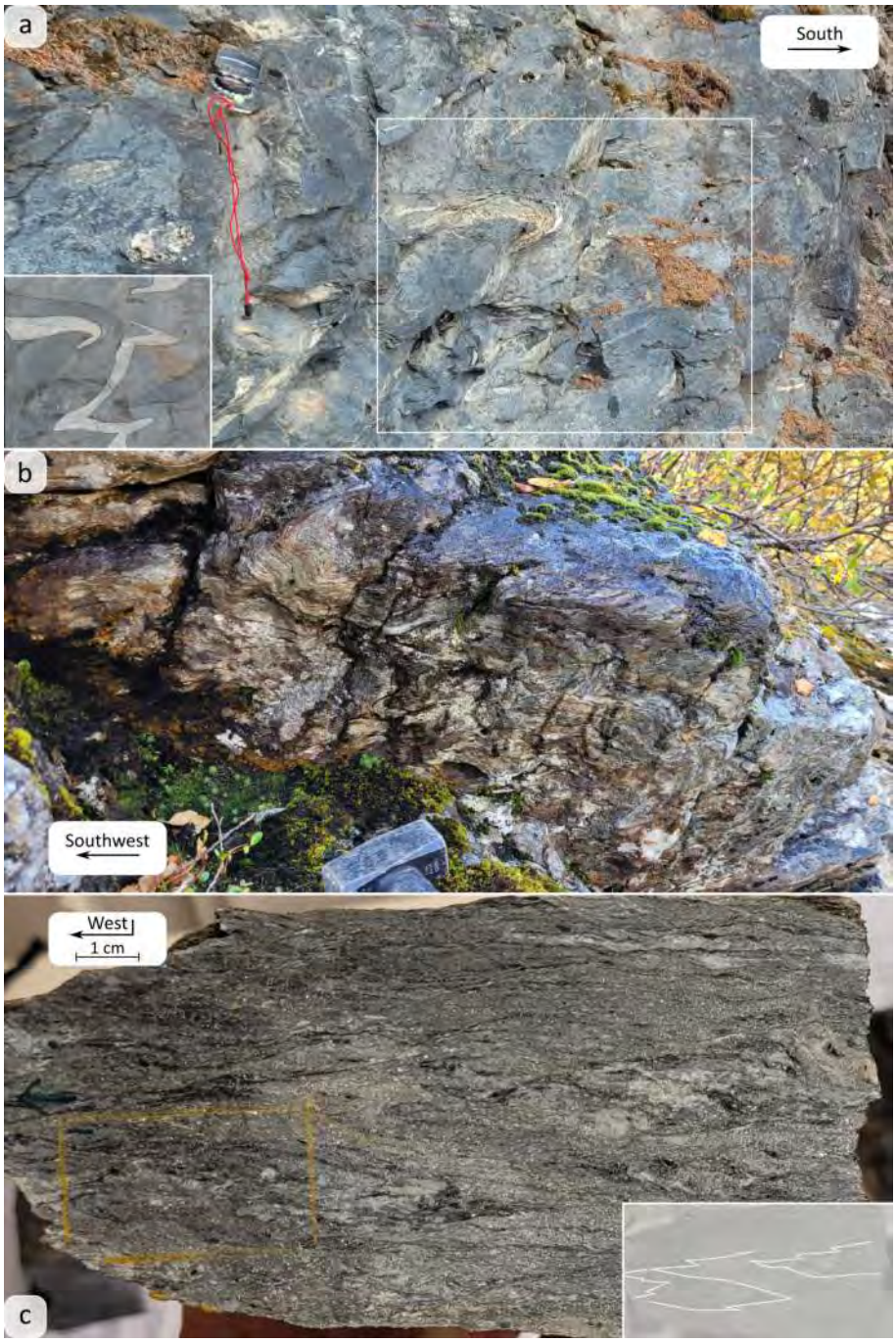


Figure 92: Photos of isoclinal folds in the Särv Nappe. (a) Tight to isoclinal folds primarily visible in light metasandstone layers, in outcrop dominated by metadolerite close to the upper boundary of the nappe. The axes of the folds are parallel to the stretching lineation, indicated by the direction of the compass. (b) Complex folds at the base of the nappe, in outcrop with thin alternating layers of metasandstone and metadolerite.

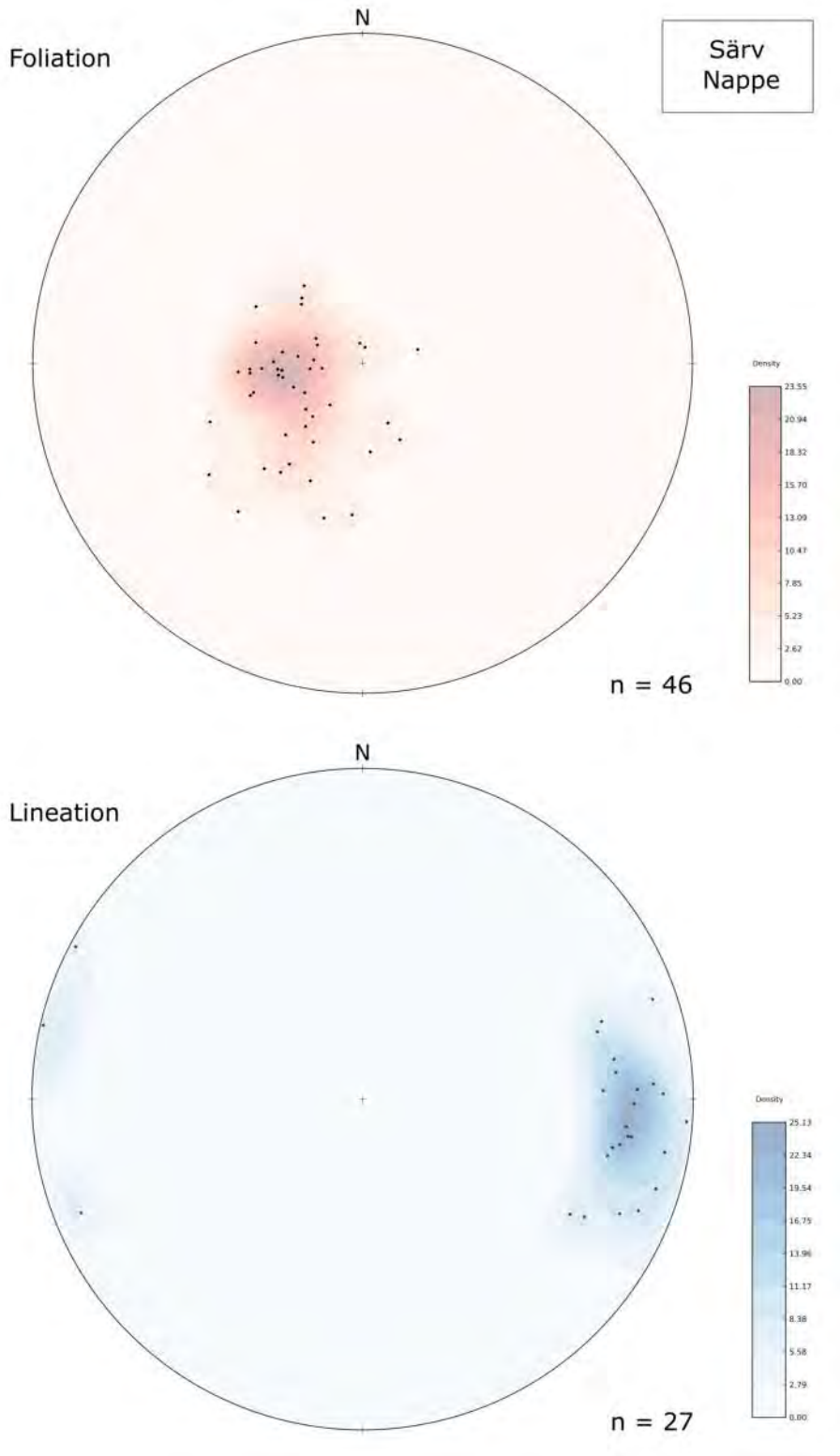


Figure 93: Foliation orientation and stretching lineation measurements of the Särv Nappe within the study area, projected in lower hemisphere equal-area stereograms. The distribution of foliation measurements shows subhorizontal to gentle dip towards the east. The stretching lineation dominantly trends east-west. Contours marking the observation density are constructed using Fisher probability distribution in the projection program OpenStereo.

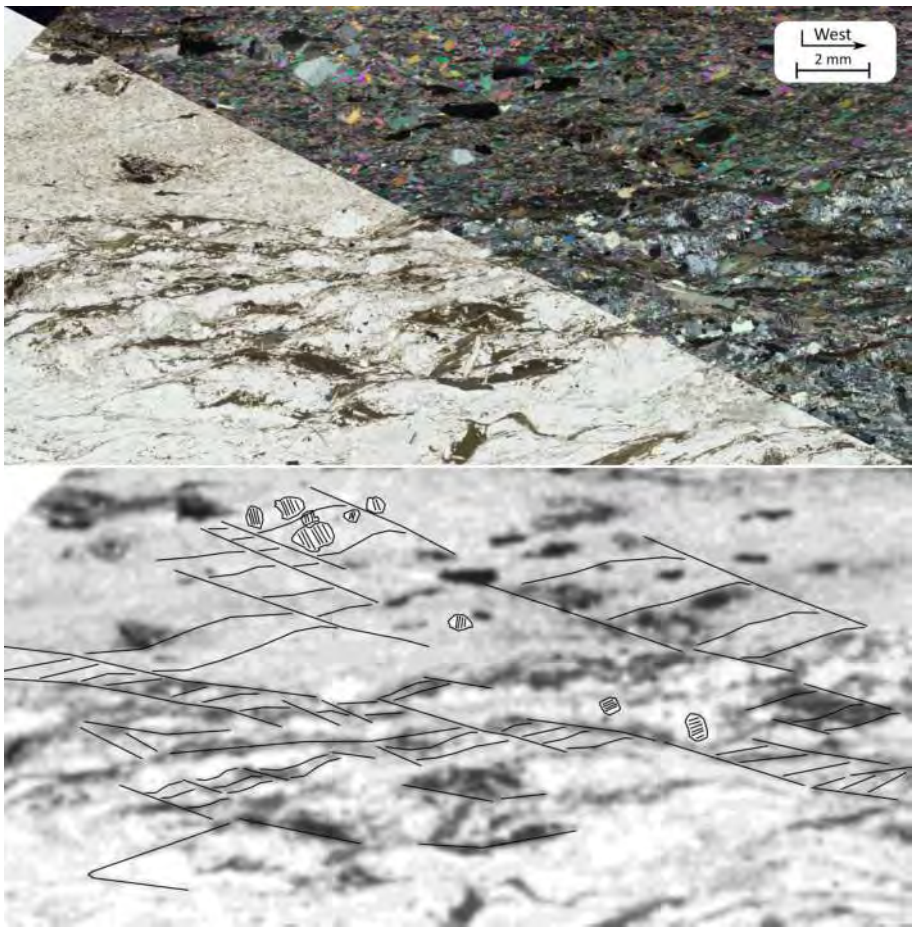


Figure 94: Thin section scan and sketch of epidote-rich micaschist with S-C and C-C' fabric indicating a top-to-the-west shear sense. Scan of thin section from folded micaschist sample SV23116. Lower left is displayed in plane-polarized light, upper right in cross-polarized light. The sketch below highlights the deformation fabric.

The Särv nappe is exposed on the western slope of Åreskutan and dips east towards the center of the Åre Synform (Figure 93). The stretching lineation trends east-west with no distinction between L1 and L2. At the microscale, sample SV23-116 of interlayered and tightly folded metasandstone and micaschist shows a top-to-the-west shear sense (Figure 94). Mesoscale shear sense indicators are sparse and show a top-to-the-east shear sense (Figure 95, Figure 96). Ductile shearing was followed by brittle deformation during the last recorded deformation phase D5, visible through slickensides on fault surfaces. Orientation of displacement is not known, due to diffulties to reach observed fault surfaces. Slickensides related to D5 are also observed on the foliation surface of chlorite schist immediately below the Kall - Särv Nappe boundary, indicating brittle top-to-the-east thrusting.

7.4.5 Metamorphic history

The earliest recorded event in the Särv Nappe, M1, is the growth of the internal foliation of plagioclase porphyroblasts, which primarily consists of elongated epidote grains. Crenulation of internal foliation in plagioclase porphyroblasts indicate syntectonic growth (Figure 97). The Särv Nappe did not appear to reach garnet-zone metamorphism, the peak assemblage is characterised by biotite in metasediments in the M2 stage. Widespread retrogression, M3, is evidenced by the common occurrence of chlorite schist, where chlorite has replaced amphibole as the primary mafic mineral in affected metadolerite.

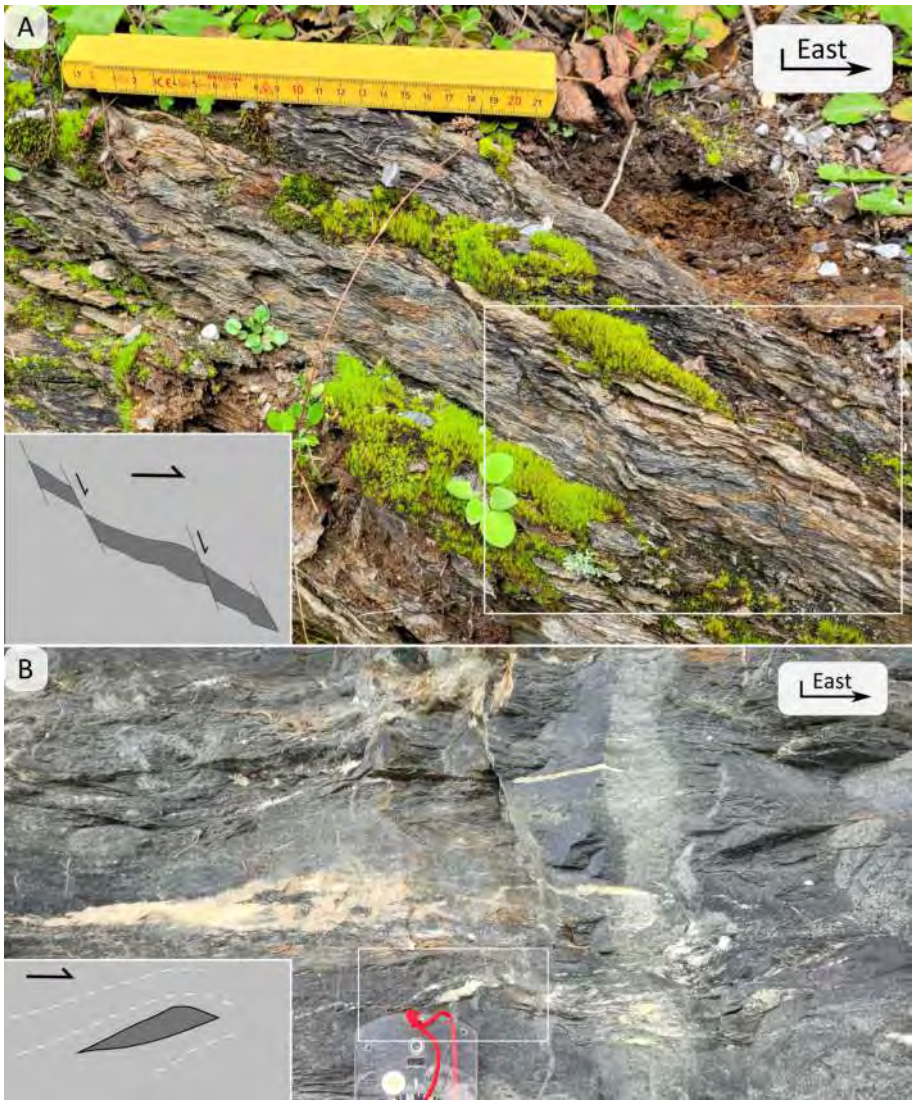


Figure 95: Photos of shear sense indicators in the Särv Nappe. Photos are taken parallel to the stretching lineation. (a) D4 shear bands displacing metadolerite layers in a mixed lithology outcrop, showing a top-to-the-east shear sense and a brittle-ductile deformation mode. (b) Sigmoid shape of metasandstone patch shows a top-to-the-east shear sense. White rectangle shows extent of sketch.

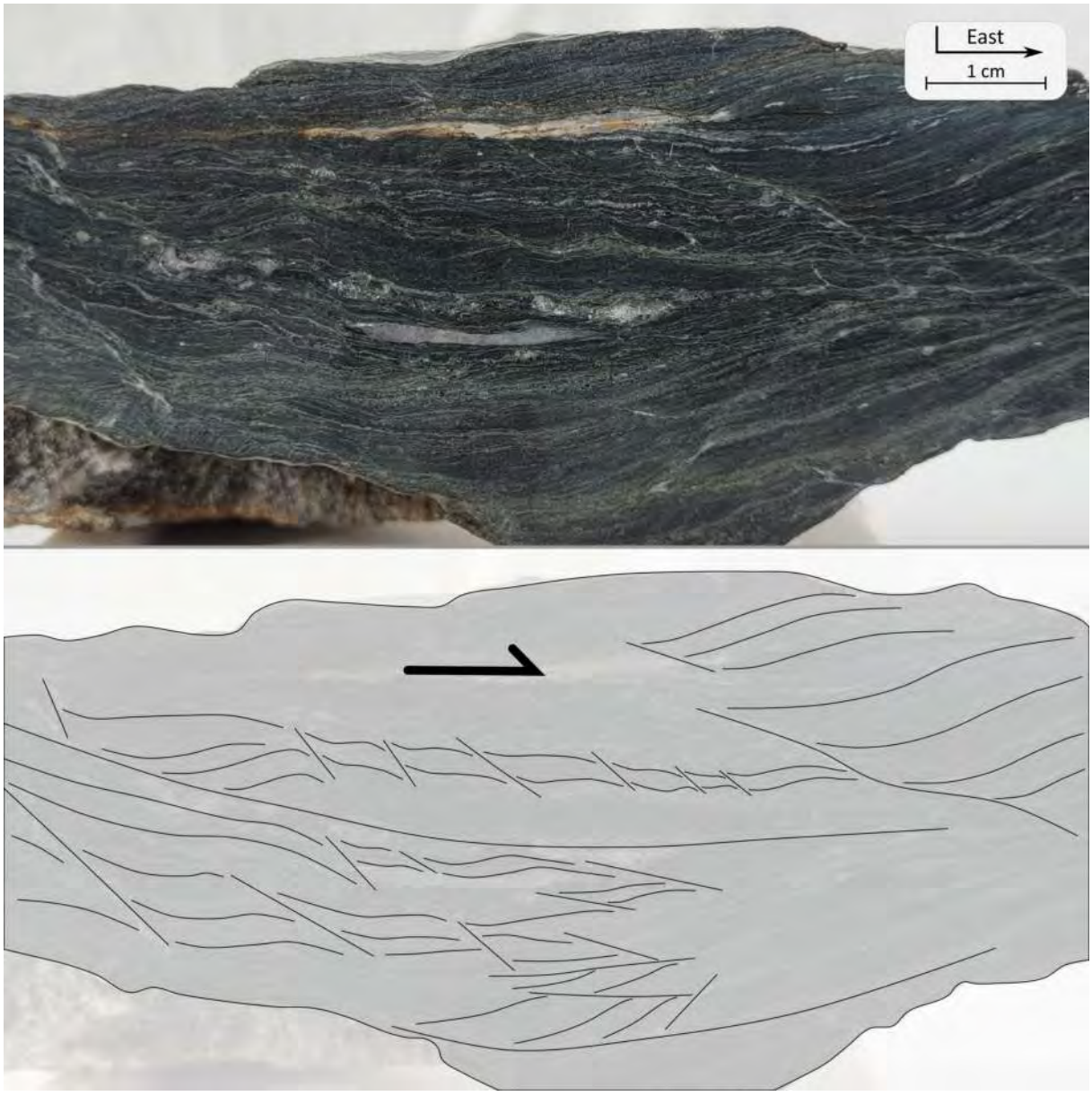


Figure 96: Cut surface of metadolerite sample with significant chlorite alteration, cut parallel to the stretching lineation. The sample shows a distinct S-C and C-C' fabric marked by chlorite layers, indicating a top-to-the-east shear sense.

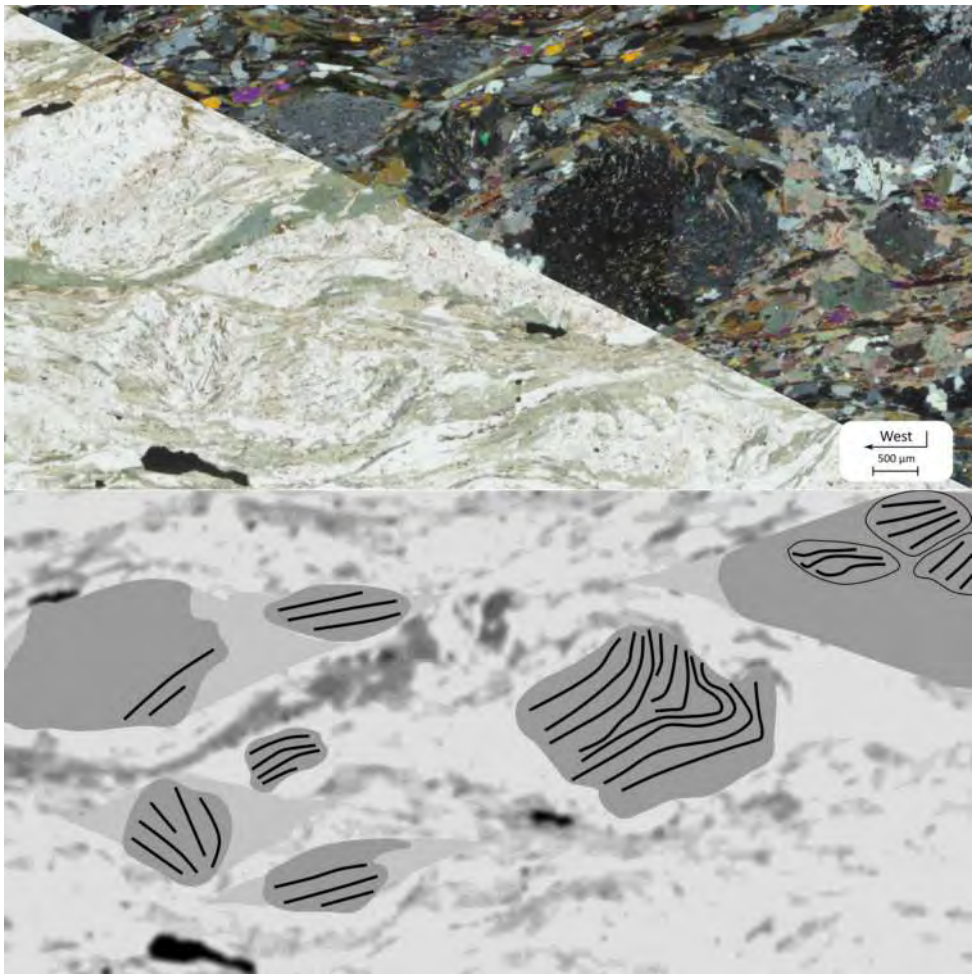


Figure 97: Feldspar porphyroblasts with crenulated internal foliation. Thin section scan from metasandstone sample SV23118. lower left displayed in plane-polarized light, upper right in cross-polarized light. The sketch below highlights the foliation trace of the inclusions. Note discordance of internal foliation between different grains, indicating rotation after growth. Faint strain shadows are marked in the sketch, indicating a top-to-the-east shear sense. Sample is collected in the same outcrop as sample SV23116, which indicates a top-to-the-west shear sense.

7.5 Offerdal Nappe

Directly overlying the dark mylonitic shales of the Jämtlandian Nappe Complex is a $\sim$ 50 m thick unit of mylonitic metasandstone and semipelitic micaschist of the Offerdal Nappe. The lower contact is visible at multiple locations (see section on tectonic boundaries below), but most prominently by a large waterfall in the river Tvärån. The metasediments lack dolerite intrusions and garnets have been observed in semipelitic micaschist.



Figure 98: Photos of weathering surfaces of metasandstone outcrops in the Offerdal Nappe. (a) Outcrop of folded fine- to medium-grained metasandstone at a high structural level in the nappe. Quartzofeldspathic layers alternate with thin more micaceous layers, visible through differential weathering in the outcrop. Where the surface is not covered by the ubiquitous lichen found on outcrops at lower elevations, the weathering surface is a rusty light brown. (b) Exposed patch of weathering surface in outcrop where the boundary to the Lower Allochton is visible.

7.5.1 Metasandstone

Feldspathic metasandstone dominates the Offerdal Nappe, with a high variability in composition and deformation style. The weathering surface is light red-brown to grey, fresh surfaces are vari-

able in colour (Figure 98). The matrix is fine-grained to very fine-grained with occasional coarse clasts. Darker more micaceous layers are interlayered with purely quartzofeldspatic (Figure 99).

Directly above the contact with the Lower Allochton is a highly deformed, very fine-grained metasandstone with thin micaceous layers and small euhedral pyrite crystals (Figure 100). Foliation is marked by folded brown micaceous layers, up to 2 mm thick. The hue of the matrix is weakly blue-green with lenses and layers of white quartz. Going south along strike folding decreases in intensity, and the metasandstone is finely laminated with planar foliation (Figure 100c).

Structurally higher up, metasandstones are occasionally more massive and display only slight mesoscale folding (Figure 98a, Figure 101). The weathering surface is grey to brown, with intercalated dark micaceous layers. Fine to medium grain size, and lower mica content. Foliation is marked by micaceous layers and compositional differences in the metasandstone. Layer thickness is highly variable, from 1-50 cm observed in the field. Micaceous layers are generally 1-2 cm thick.



Figure 99: Commonly observed fine- to very fine-grained layered metasandstone of the Offerdal Nappe. The light layers are quartzofeldspathic, while the dark layers are rich in quartz and micaceous minerals. Note asymmetric fold in lower left corner.

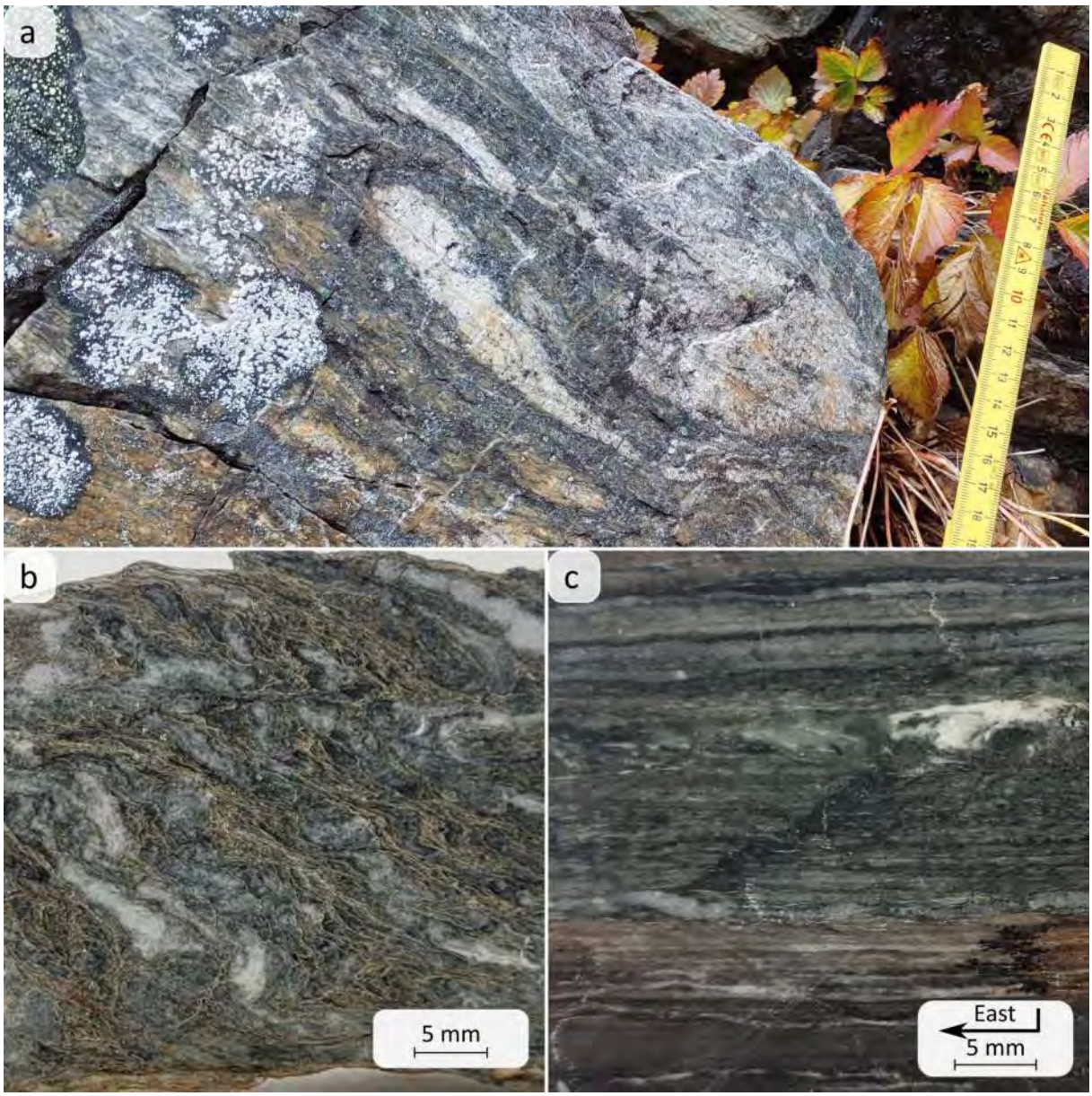


Figure 100: Photos of the green-hued very fine-grained metasandstone observed immediately above the lower boundary of the Nappe. (a) Weakly weathered surface showing the distinct green hue and white patches of the lithology. (b) Cut surface of sample collected within 1 m of the lower nappe boundary, unoriented. The matrix is green-hued with white patches and the highly deformed foliation is marked by $<$ 1mm layers of micaceous minerals. (c) Cut surface of sample collected whithin 10 m of the lower boundary of the nappe, 250 m south along strike from (b). Sample is cut parallel to the stretching lineation. In contrast to samples collected of the same lithology further north, the foliation is planar and the mylonitic texture is strong.



Figure 101: Photos of metasandstone observed at higher structural levels. (a) Light grey weathering surface of metasandstone with planar foliation, showing the well developed stretching lineation. (b) Cut surface of collected sample visible in (a). The composition is quite homogeneous, with the foliation marked by slight compositional variation in the layering. The grain size, while still fine-grained, is coarser than the samples shown in figure 100.



Figure 102: Photo of interfolded semipelitic micaschist and metasandstone with displacement caused by brittle deformation visible towards the top of the exposure. The sketch outlines metasandstone in light grey and micaschist in dark grey.

7.5.2 Semipelitic micaschist

Semipelitic micaschist is common in the Offerdal Nappe exposures, and is often interlayered and folded with metasandstone (Figure 102). The weathering surface is typically striped dark gray and brown, with crenulated foliation immediately apparent. Fine-grained to very fine-grained with thin alternating layers rich in quartz or mica. Small garnets up to 1 mm are found in one locality close to the base of the Ullådalen ski lift, in a semipelitic micaschist with abundant epidote (Figure 103). Up to 0.5 m thick metasandstone layers are present as intercalations, and the micaschist in places seem transitional with the metasandstone. Thin section of semipelitic micaschist sample OF2334 is summarized in table 5.

7.5.3 Deformation history

Five deformational phases, D1-D5, have been identified in the Offerdal Nappe. D1 has been identified in relict layering observed at a high angle to the main foliation S2 in metasandstone (Figure 106). The main foliation developed during D2, and is primarily marked by quartzofeldspathic microlithons and the preferred orientation of white mica in semipelitic micaschist, and compositional layering in metasandstone. The main foliation was folded and reworked in faint shear fabric, S3, during the deformational phase D3. Microscale crenulation of white mica parallel to the stretching lineation in semipelitic micaschist is also interpreted to relate to D3 (Figure 105). The stretching lineation L1 is poorly to well developed depending on lithology and deformation style, and likely related to the deformation phase D3. Highly deformed and folded metasandstone close to the lower contact displays no stretching lineation, whereas metasandstone with planar foliation shows a well developed L1 marked by grooves and ridges on quartzofeldspathic surfaces (Figure 101a). In semipelitic micaschist, L1 is poorly marked by crenulation planes. The Offerdal Nappe dips eastward towards the center of the synform with the stretching lineation trending east-west (Figure 107). Mesoscale shear-sense indicators are lacking in the observed outcrops, but at the microscale a faint S-C microstructure and mica fish related to D3 indicate a top-to-the-east shear sense (Figure 108). Intense small-scale folding of thin micaceous bands is observed in green-hued metasandstone immediately above the lower tectonic boundary (Figure 100a-b), identified as deformation phase D4. Kink bands at a high angle to the main foliation associated with concentration of chlorite alteration is tentatively



Figure 103: Photo of garnet in crenulated micaschist, close to the lower boundary of the nappe. Photo taken roughly perpendicular to the stretching lineation.

grouped in D4. Following ductile deformation of the nappe, brittle deformation related to D5 can be observed in hand samples and outcrops. Top-to-the-east brittle thrusting slightly oblique to the stretching lineation is illustrated in figure 109.

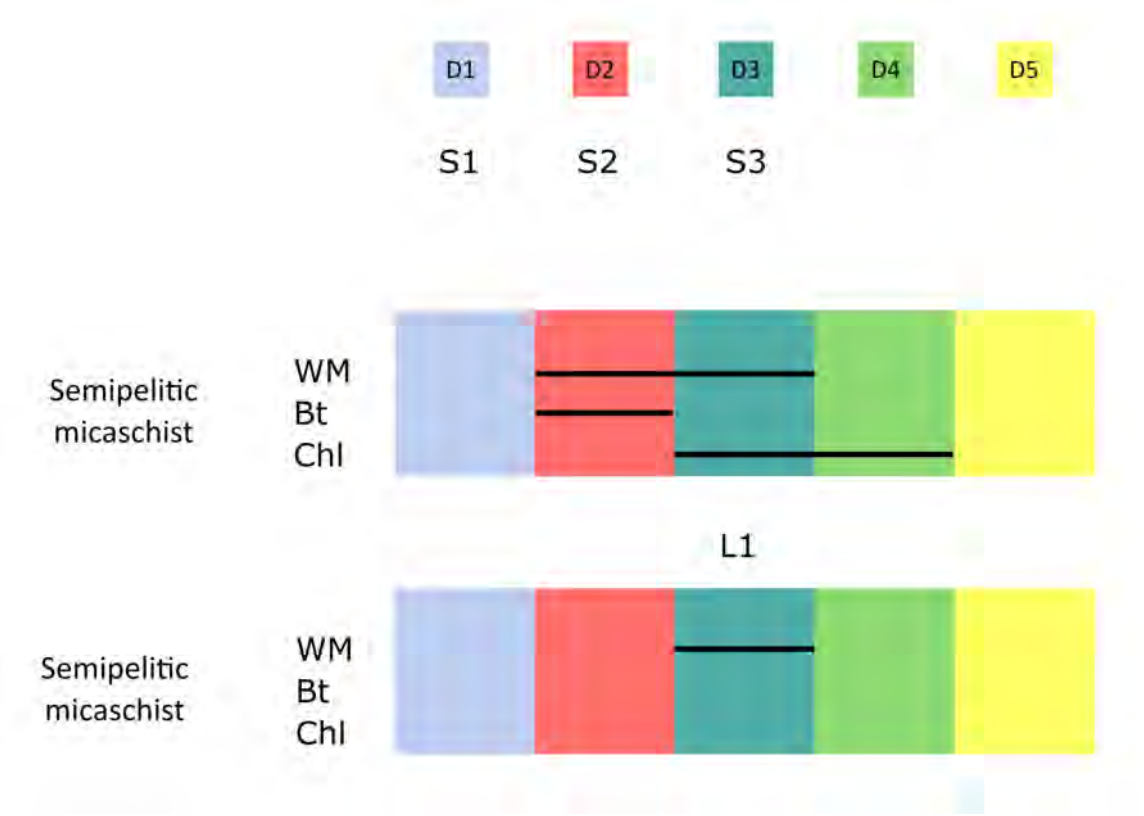


Figure 104: Summary of the deformation history of the Offerdal Nappe. Deformational events D1-D4 are identified and shown based on the succession of minerals marking foliation and stretching lineation.

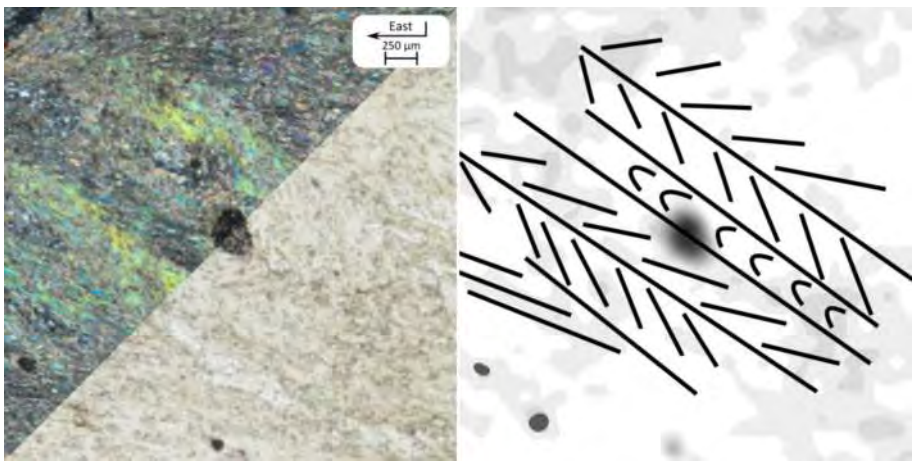


Figure 105: Relict foliation marked by white mica reworked by crenulation. Scan of thin section from semipelitic micaschist sample OF2334. Upper left is displayed in cross-polarized light, lower right in plane-polarized light. The sketch highlights the trace of the relict foliation and crenulation planes.



Figure 106: Photo of relict layering oriented perpendicular to the main foliation in metasandstone with layers of semipelitic micaschist.

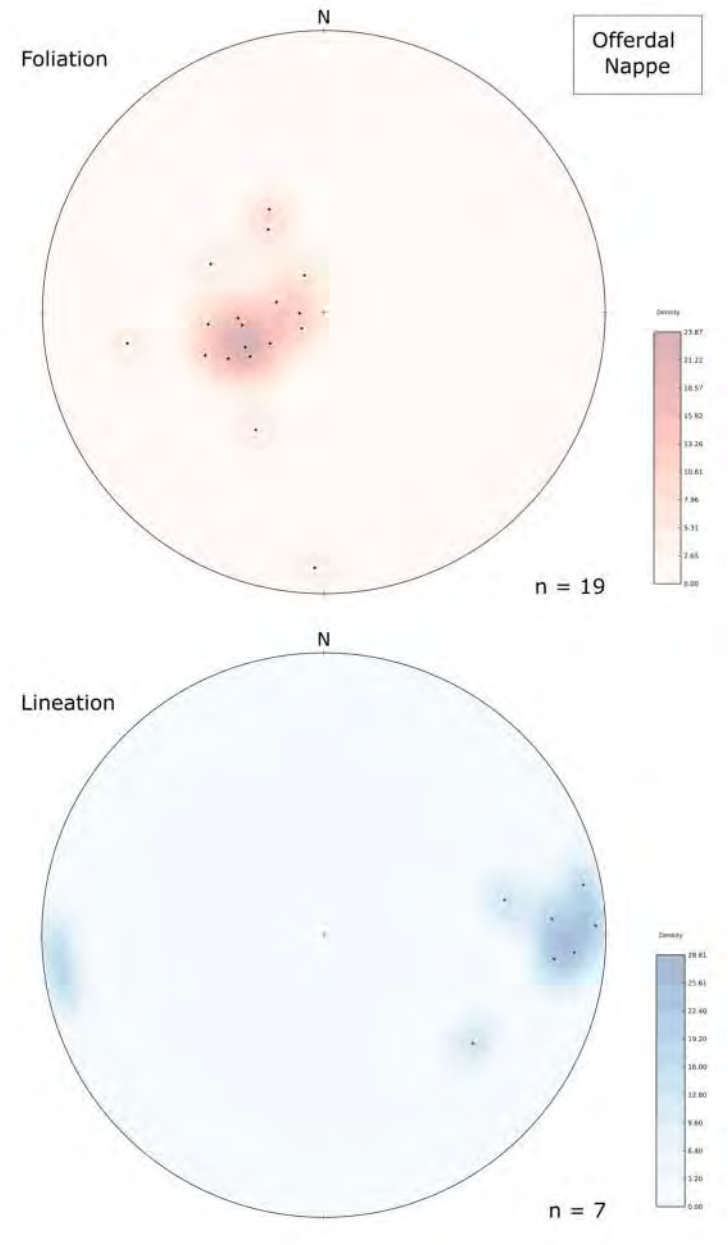


Figure 107: Foliation orientation and stretching lineation measurements of the Offerdal Nappe within the study area, projected in lower hemisphere equal-area stereograms. The distribution of foliation measurements shows subhorizontal to gentle dip towards the east. The stretching lineation dominantly trends east-west. Contours marking the observation density are constructed using Fisher probability distribution in the projection program OpenStereo.

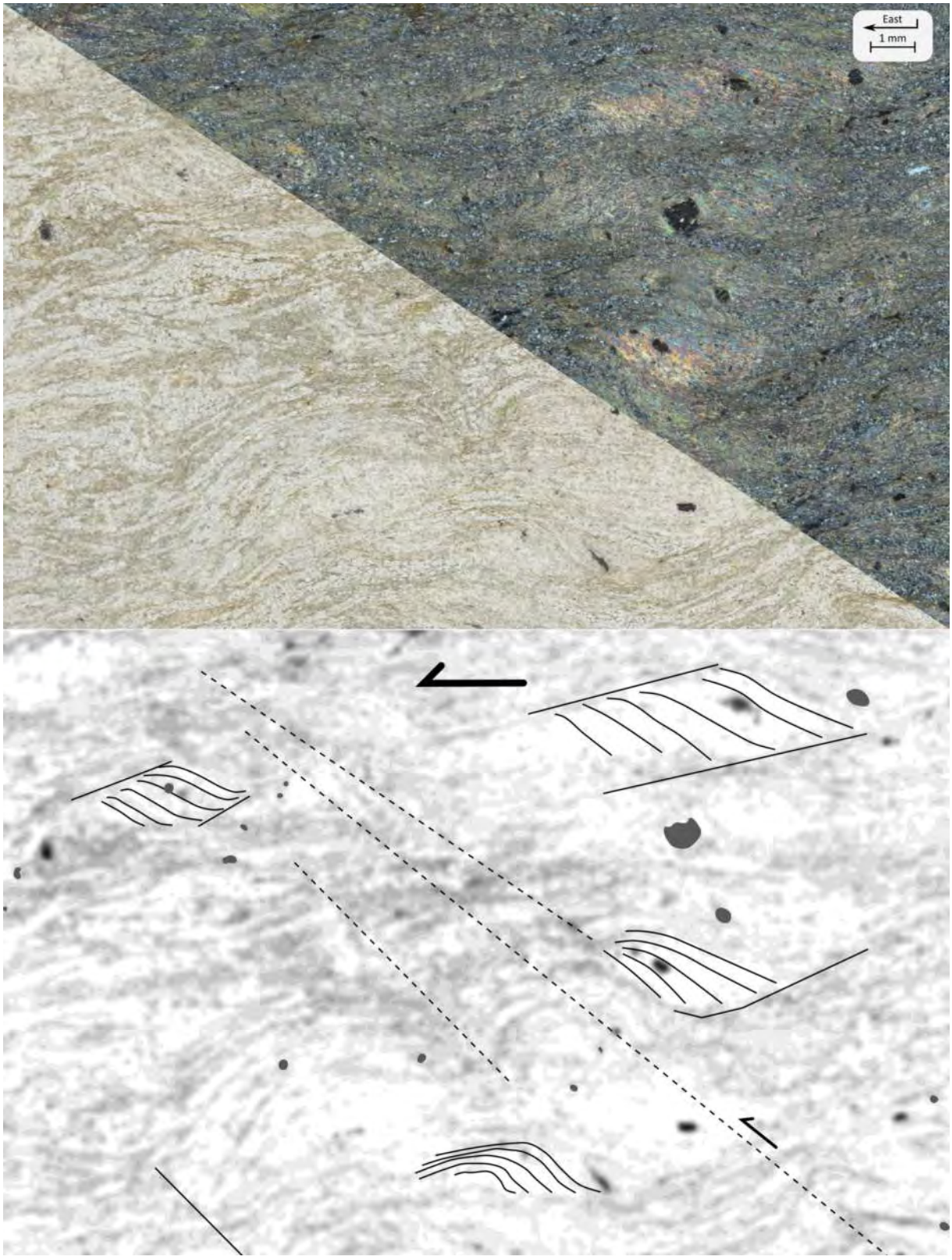


Figure 108: Faint S-C fabric and mica fish in semipelitic micaschist indicating a top to the east shear sense. Scan of thin section from semipelitic micaschist sample OF2334. Lower left is displayed in plane-polarized light, upper right in cross-polarized light. The sketch highlights the deformation fabric. Incipient brittle thrusting is marked by striped lines.

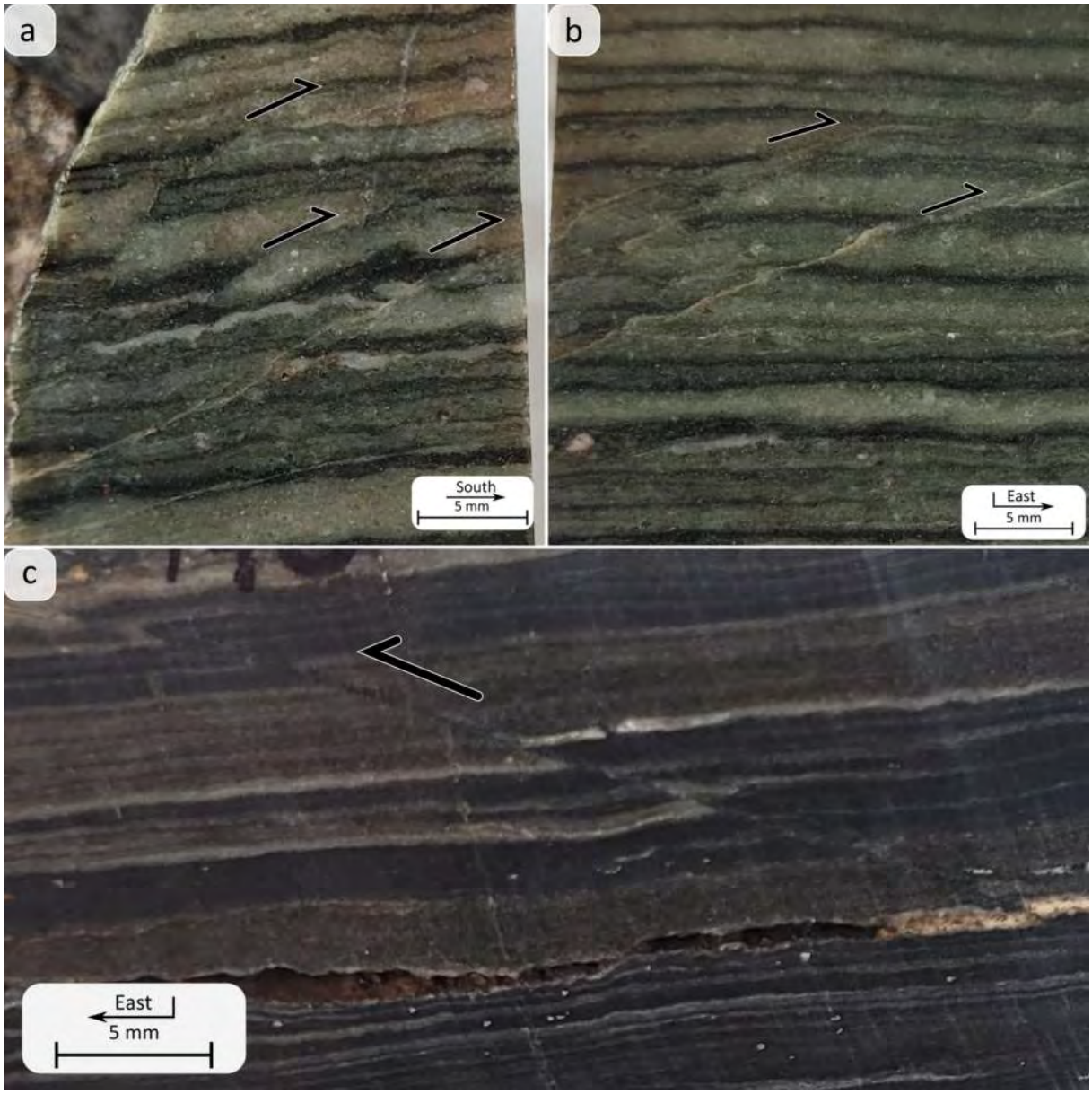


Figure 109: Photos of brittle thrusts in metasandstone samples. (a) and (b) Cut surfaces of metasandstone sample, (a) cut perpendicular and (b) parallel to the stretching lineation, showing top-to-the-southeast thrusting. (c) Cut surface of metasandstone sample showing top-to-the-east brittle thrusting. The sample lacks stretching lineation and is cut along the east-west axis.



Figure 110: Replacement of garnet by chlorite, partial and complete replacement indicated by arrows. Note chlorite elsewhere in the matrix, at the boundary between thin microlithons and domains of white mica and epidote. Scan of thin section from micaschist sample OF2334 displayed in plane-polarized light.

7.5.4 Metamorphic history

The metamorphic grade of the Offerdal Nappe appears to be the lowest of the nappe stack. The first metamorphic phase seen in semipelitic micaschist is the growth of white mica, epidote, small garnets and minor green biotite. Retrogression, M2, is seen through partial to complete replacement of garnet by chlorite (Figure 110).

7.6 Jämtlandian Nappe Complex

The focus of this thesis is a description of the nappes of the Middle Allochton on Åreskutan and as such, little emphasis has been placed on the rocks of the Lower Allochton, which have also been described in detail elsewhere (e.g. Karis and Strömberg, 1998). Black shale dominates from the Ullån river up to the lower boundary of the Offerdal Nappe (Figure 111). The weathering surface is light to dark grey, and the fresh surface is black with lighter bands (Figure 112). No thin section has been made of the shale, and so no detailed description of mineral content can be provided. In the strongly deformed shale close to the boundary with the Middle Allochton, fine-grained quartz- and carbonate-rich layers and thin micaceous layers alternate. The shale of the Jämtlandian Nappe Complex dips east towards beneath the overthrust Middle Allochton (Figure 113). Foliation is well developed, marked by compositional layers and the preferred orientation of micaceous minerals. The stretching lineation is poorly developed, but increases in definition when approaching the Middle Allochton boundary, trending east-west. Compared to the rocks of the overlying nappes, the shale shows a very low, if any, metamorphic grade.



Figure 111: Shale beds exposed along Ullån, $\sim$ 200 m structurally below the basal thrust of the Middle Allochton. Above the pictured waterfall the tributary Tvärån joins Ullån from the east. 400 m upstream along Tvärån the tectonic boundary is exposed.



Figure 112: Grey and lichen-covered weathering surface of the highly fissile shale at the top of the Jämtlandian Nappes on Åreskutan.

7.7 Tectonic Boundaries

Boundaries between nappes are typically mylonite zones, where the metamorphic conditions allow ductile deformation. Where the tectonic contact is obscured, different nappes can be distinguished by differing lithologies, structure or metamorphic grade. All of the Middle Allochton nappes identified on Åreskutan display ductile deformation through all deformation phases except the last of each nappe which is related to minor brittle deformation. Mylonite zones are thus expected to mark the contacts. However, the high degree of deformation has led to large parts of the nappes developing proto-mylonitic to mylonitic fabric internally as well. Below the tree-line there is generally vegetation and thick quaternary sediments covering the rock surface, so the tectonic contacts between the Offerdal, Särv and Kall Nappes are inferred from the above mentioned differing lithologies, structure and metamorphic grade. The basal thrust of the Middle Allochton separating the Offerdal Nappe and the Jämtlandian Nappe Complex is exposed in one location, and the tectonic boundary between the Kall and Åreskutan Nappes is visible in river cuts and other outcrops on all sides of Åreskutan. A profile along the stream Tvärån provides the best exposure of tectonic boundaries in the study area. The stream drains the Tväråvalvet cirque running from east to west and passes all tectonic boundaries described below. Along its length are excellent exposures of the boundary between the Kall and Åreskutan Nappe, as well as the Jämtlandian Nappe Complex and the Offerdal Nappe, i.e. the Lower-Middle Allochton boundary.

7.7.1 The Kall-Åreskutan Nappe boundary

The tectonic boundary between the Kall and Åreskutan Nappes is easily recognisable in the field, and can often be followed in the morphology of the mountain (Figure 114). The width of the mylonite zone related to the contact is difficult to estimate due to the complicated geometry and deformation of the nappes, though a minimum thickness of up to 50 m on either side of the contact is likely. Mylonitic paragneiss on the Åreskutan side of the contact shows an assemblage of garnet and biotite ± sillimanite. Of note is that sillimanite marking the foliation has also been observed in mylonite underlying the basal retrogression zone. On the Kall Nappe side of the contact the fabric is ultramylonitic with mafic boudins up to 10 cm. Quartz is highly recrystallised through grain-size reduction in bands, and small grains of recrystallised

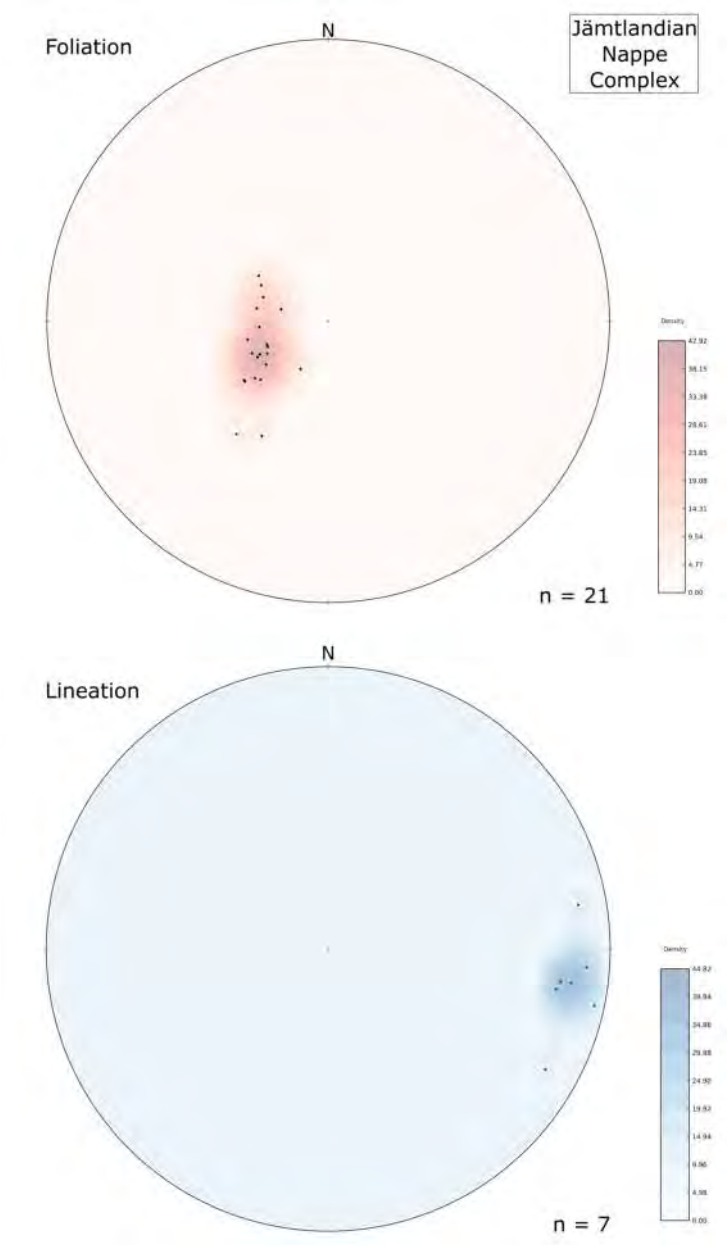


Figure 113: Foliation orientation and stretching lineation measurements of the Offerdal Nappe within the study area, projected in lower hemisphere equal-area stereograms. The distribution of foliation measurements shows subhorizontal to gentle dip towards the east. The stretching lineation dominantly trends east-west. Contours marking the observation density are constructed using Fisher probability distribution in the projection program OpenStereo.

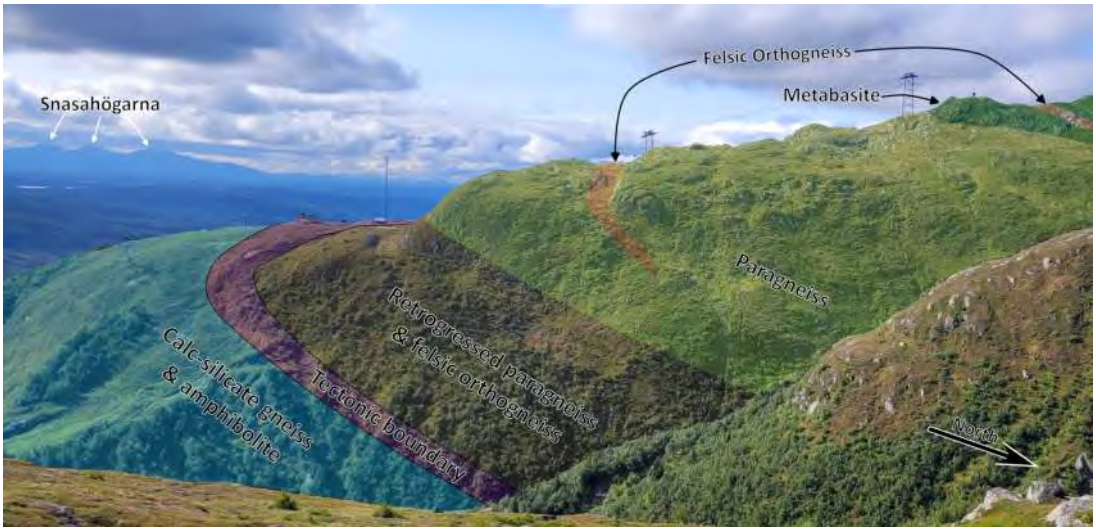


Figure 114: Photo of the tectonic boundary between the Åreskutan and Kall Nappes exposed on Mörvikshummeln. Across the mountain, the restistant rocks of the Åreskutan Nappe are marked by an increase in slope angle and are often exposed in rocky crags. The photo is taken on the south-east ridge of Åreskutan looking west. To the left in the background the Snasahögarna Massif is marked, the location of the related Snasahögarna Nappe.

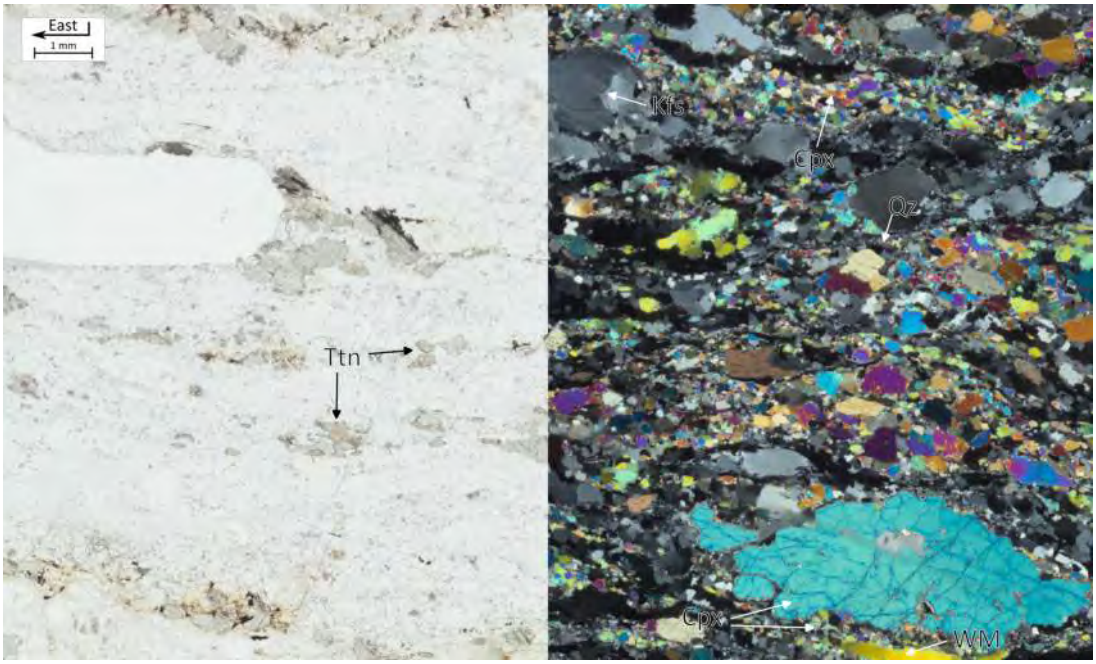


Figure 115: Scan of thin section from ultramylonite sample MS23118 collected at the tectonic boundary between the Åreskutan and Kall Nappes on Mörvikshummeln. The assemblage shows the ultramylonitic fabric of reworked calc-silicate gneiss. Grain-size reduction of quartz is concentrated in bands, and recrystallisation of a large clinopyroxene grain can be seen in the lower right corner. Compared to mylonitic calc-silicate gneiss further down in the Mörvikshummeln formation, this sample contains significantly more titanite. The left side is displayed in plane-polarised light, the right in cross-polarised light.

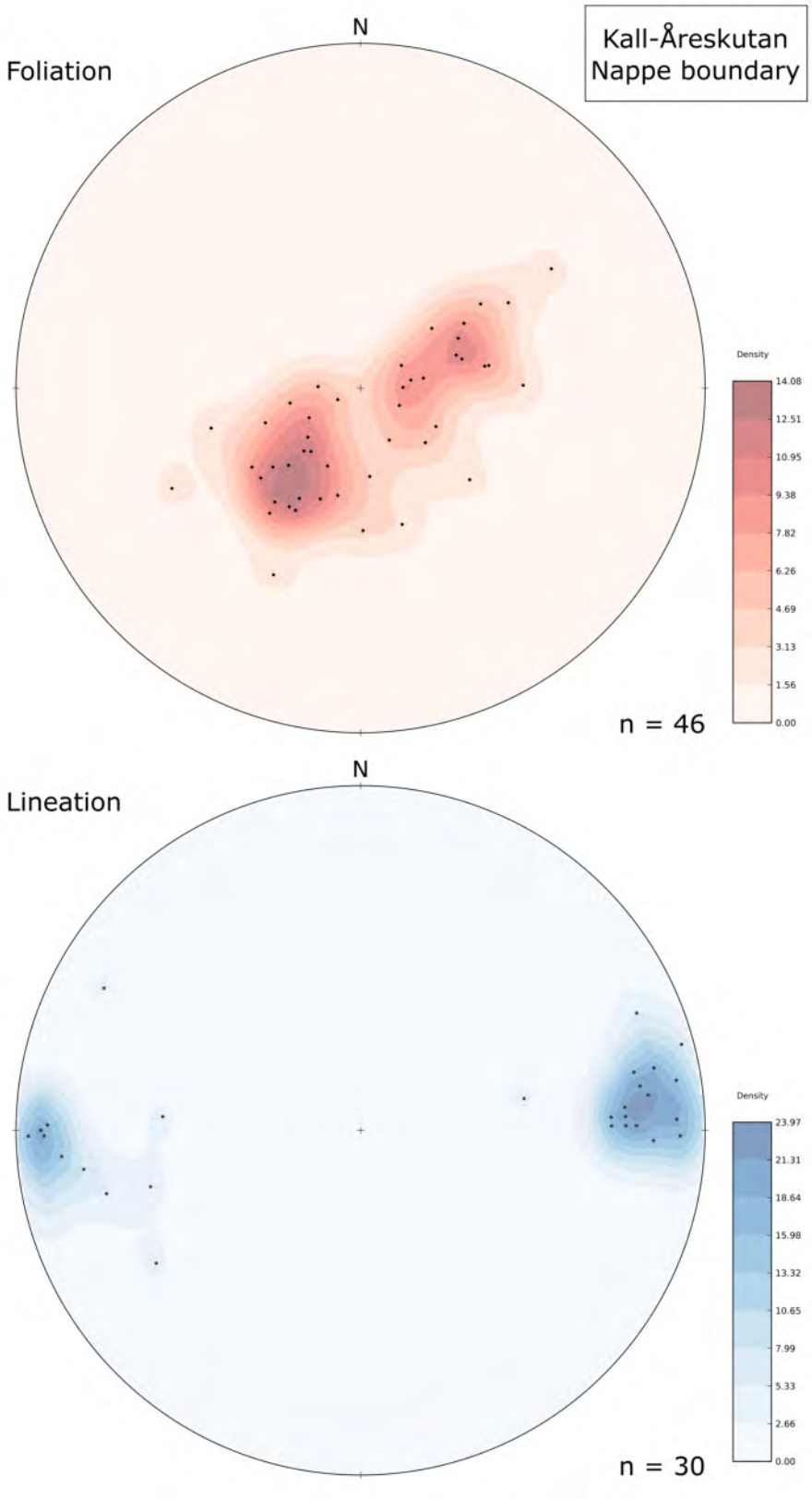


Figure 116: Foliation orientation and stretching lineation measurements of the tectonic boundary between the Kall and Åreskutan Nappe and immediately surrounding mylonites, projected in lower hemisphere equal-area stereograms. The distribution of foliation measurements shows two centers of distribution, dip directions northeast and west-southwest. The stretching lineation dominantly trends east-west. Contours marking the observation density are constructed using Fisher probability distribution in the projection program OpenStereo.

clinopyroxene are common in the matrix (Figure 115). Compared to mylonitic calc-silicate gneiss further down in the Kall Nappe, the ultramylonite at the contact lacks garnet. There are no signs of partial melting above or below the boundary related to the development of the mylonitic foliation of the contact. On the calc-silicate gneiss side of the boundary, boudinage of amphibolite and competent leucogranite is common. The transition from the Åreskutan Nappe to the Kall Nappe is generally sharp, but at Mörvikshummeln a repeat sequence of intercalated garnet paragneiss and ultramylonitic calc-silicate gneiss marks the boundary.

The mylonitic folation of the Kall-Åreskutan nappe boundary is concordant with the large-scale orientation of the upper Kall Nappe, but the foliation of the Åreskutan Nappe more or less quickly becomes discordant. The boundary dips in towards the center of the synform, with clear stretching lineation trending east-west (Figure 116). The stretching lineation is marked by mineral aggregates, sillimanite and biotite in the Åreskutan Nappe, and mineral aggregates and the preferred orientation of rare elongated clinopyroxene or amphibole porphyroblasts. No shear sense indicators can be seen at the microscale of the highly mylonitised fabric. At the mesoscale, indicators show a top-to-the-east shear sense.

7.7.2 Internal boundary in the Kall Nappe?

Previous mappers have made distinctions of the upper and lower part of the Kall Nappe, either by interpreting them as two separate nappes or dividing it into two lithological units. The difference in lithology and rheology between the Rödkullen and Mörvikshummeln Formations is apparent in the field, and the transition is only fully exposed in one location, a blasted roadcut on the south face of Mörvikshummeln. Going upwards in the Rödkullen Formation, calcsilicate minerals start to appear in mafic pods in mylonitic biotite-rich metasandstone just below the transition. The transition itself is quite eroded, and just above it is calc-silicate gneiss with characteristic isoclinal folds, compositional layers marked by grossular garnet and metasomatic reactions around mafic layers. Using diluted HCl, the presence of carbonate can typically be detected in the rocks of the Mörvikshummeln Formation, but not in the Rödkullen Formation. Distinction can also be made by the different textures of amphibolite in the two formations. No compelling evidence is found in the field to support the division into two different nappes. The transition is instead marked as an internal lithological boundary, made clear by the rheological difference of the two formations.

7.7.3 The Särv-Kall Nappe Boundary

The boundary between the Särv and Kall Nappes is not exposed in the field, and thus inferred from differences between the rocks of each nappe. Going downwards in the Kall Nappe, the strain and retrogression of the amphibolite, micaschist and metasandstone of the Rödkullen Formation increases. Close the contact, mylonitic and ultramylonitic fabrics are common. The boundary is diffuse, due to the sometimes high degree of retrogression in the Kall nappe, and the similarity of the lithologies between the nappes. The amphibolite-facies character of the Kall Nappe is evident in micaschists, where garnets close to the base grow to ~ 10 mm, with staurolite observed at the microscale. The retrogressive overprint of the Kall Nappe is commonly seen at outcrop scale through increasing chlorite replacement of e.g. biotite and amphibole, and epidote alteration of feldspars. In contrast with the mylonitic fabric, retrogression is not pervasive across outcrops close to the base, it is not uncommon with little to no retrogression visible by the eye. In the Särv Nappe the mylonitic foliation is not as well developed as in the Kall Nappe when approaching the boundary. Protomylonitic to mylonitic metasandstone, micaschist and metadolerite are all observed just below the inferred contact. In comparison with the Kall Nappe lithologies, those in the Särv Nappe are of clearly lower metamorphic grade and don't show the same degree of grain-size reduction. Micaschist in the Särv Nappe is distinguished by the lack of garnet and by large fish-scale-like flakes of white mica and chlorite; metasandstone and metadolerite is often interlayered, with thin ribbons of chlorite and amphibole marking the foliation and shear fabric. The stretching lineation related to the development of mylonite at

the boundary is marked by amphibole, biotite, white mica and chlorite in the Kall Nappe, and amphibole, white mica and chlorite in the Särv Nappe

7.7.4 The Offerdal-Särv Nappe boundary

The Offerdal-Särv Nappe boundary is not exposed in the field, like the Särv-Kall Nappe boundary. The distinction between the nappes is based on lithology, primarily the lack of metadolerite intrusions and the presence of garnet in the metasediments of the Offerdal Nappe. When approaching the boundary from the Särv Nappe, there is not a marked increase in deformation until a few meters remain. At this point isoclinal folding of metasandstone and metadolerite with the fold axes parallel to the stretching lineation mark the transition to the boundary. Also observed close to the boundary are outcrops of mylonitic chlorite schist interlayered with metasandstone. The thin slice of the Offerdal Nappe present at Åresutan can largely be described as mylonitic throughout, so no distinct increase in deformation is observed when approaching the contact from below. Both thin-layered isoclinally folded metasandstone and thick-layered metasandstone with planar layers are observed just below the contact. The presence or absence of mafic intrusions is the key indicator to distinguish the different nappes; however, dark micaceous layers in the Offerdal Nappe and chlorite schist layers in the Särv Nappe may be difficult to tell apart in the field, and even in cut hand samples. Stretching lineations on the Särv Nappe side of the boundary are marked by chlorite (and amphibole?), and mineral aggregates, white mica and chlorite in the Offerdal Nappe.

7.7.5 The Lower-Middle Allochton boundary

The boundary between the Jämtlandian Nappe Complex and the Offerdal Nappe is clearly exposed in the waterfall Tväråfallet, close to where the stream Tvärån joins Ullån (Figure 117). It is also very nearly exposed in a small stream along the Ullådalen road, just northwest of the entrance to the Rödkullen ski area. As mentioned above, the Offerdal Nappe is mylonitic throughout, but the lithology most often found above the boundary is a green-hued very fine-grained metasandstone. Where the metasandstone has been found whithin up to a few meters of the boundary the fabric is folded, but no distinct shear fabric has been observed. On the Jämtlandian Nappe Complex side of the boundary highly deformed black shale is found, with stronger stretching lineation closer to the boundary. The fissile shale is of a markedly lower metamorphic grade compared to the compact metasandstone and micaschist of the Offerdal Nappe. Stretching lineation is often poorly developed in the metasandstone on the Offerdal Nappe side of the boundary, likely due to the massive nature and difficulty of separating the rock on the foliation plane. Where stretching lineation is observed it is marked by chlorite and white mica. Stretching lineation is well developed in the shale underlying the Middle Allochton, marked by unknown micas.

7.8 Geological maps and cross-sections

On the basis of the observations above, multiple geological maps and cross-sections have been produced, each highlighting different aspects of the geology of Åreskutan. They are provided in appendices A-D, with a short description below:

1. Appendix B: Tectonostratigraphic map with foliation orientation and cross-section traces on a hillshaded topographic background.
2. Appendix C: Tectonostratigraphic map with foliation orientation and cross-section traces on a simple topographic background.
3. Appendix D: Lithological map with outcrops and foliation orientation on a hillshaded topographic background.
4. Appendix E: Lithological map with outcrops and foliation orientation on a simple topographic background.



Figure 117: Photo of the basal thrust of the Middle Allochton exposed at Tväråfallet. Above is the massive very-fine-grained green-hued metasandstone of the Offerdal Nappe, below is the fissile black shale of the top of the Lower Allochton. The boundary is partially marked by a striped line on the right side of the photo.

8 Discussion

8.1 Geological map

As described earlier in this thesis, geological mapping of Åreskutan has been done intermittently over the past 150 years, and it may well be the most mapped singular mountain in the Scandinavian Caledonides. Despite of this, investigations focused on the West Jämtland nappe stack and the geometry of the Åre Synform in the past 15 years has highlighted the need for a thorough mapping effort to meet the needs of modern research, e.g. a internal structural frameworks for comparison of petrological data. Geological maps are key components in describing the subsurface geometry of the bedrock, in addition to describing what can be observed on the surface. The mapping effort made in this thesis has had a great advantage compared to what has been done before on Åreskutan: access to specialized digital field mapping tools, both when gathering data in the field and when processing and interpreting the gathered data. Georeferenced field data and detailed elevation models enables both faster and more precise map compilation. The digital medium also simplifies the production of figures and, as it is not constrained by printing space, allows the full amount of relevant figures to be included in contrast to only a select few.

The high degree of deformation of the nappe stack on Åreskutan, especially folding, boudinage and interlayering of different lithologies, makes it difficult to accurately portray the distribution and variation of the lithologies at map scale. In particular the migmatised Åreskutan Nappe proved hard to interpret as abrupt truncation of rock layers and formations through shear zones, folds or melt patches are common, with the added complication of large-scale displacement along the late shear zones. The tectonostratigraphic map with outcrops marked is the most accurate of the produced maps, but also the least informative of rock type distribution. However, the lithological map is highly interpretative outside of observed areas, but should also be seen as a work in progress for future mappers to improve upon. The limited lithological map is weighed up by the many field photos included in this thesis, meant to illustrate the great variety of the nappe stack on Åreskutan.

In broad strokes, the tectonostratigraphic map produced in this thesis is consistent with the profiles of Törnebohm (1872) and Högbom (1909), and the geological maps made throughout the 1900's. The identified nappe units above the basal thrust of the Middle Allochton, and the placement of tectonic boundaries, has varied throughout the years, as described in the section on previous maps of Årskutan.

The basal thrust of the Middle Allochton has been identified at the same location described by Högbom (1909) and Helfrich (1967). Immediately above the boundary is a thin slice of the Offerdal Nappe, an interpretation made based on the lack of mafic intrusions, the presence of small garnets in semipelitic micaschist and the high similarity of the different metasandstone types to those in the Offerdal Nappe type area further northwest (Stephens et al., 1993b). Just north of Åreskutan in Huså, Karis and Strömberg, 1998 describes the continuation of this slice, also identifying it as the Offerdal Nappe. In the regional map by Strömberg et al. (1984) the Offerdal Nappe has been mapped at the same structural position on Åreskutan and northwards along strike, but apart from locating the base of the nappe in Tväråfallet, the thickness and geometry differs significantly. In an alternate interpretation, Arnbom (1980) identified the outcrop in Tväråfallet as the Cambrian Vemdalen Quartzite, separating the Silurian shales from the overthrust nappes.

In agreement with many previous mappers, the Särv Nappe has been identified underlying the Seve Nappe Complex (Helfrich, 1967; Arnbom, 1980; Strömberg et al., 1984). Neither the lower nor the upper boundary of the nappe is exposed at the surface, and there is disagreement between all geological maps, including the one presented here, on where the boundaries are located. The Särv Nappe is significantly more eroded at the surface compared to the Kall Nappe, and the difficulty of observing it is exacerbated by the cover of Quaternary sediments and vegetation below the treeline.

The placement of the lower boundary of the Kall Nappe is not consistent between mappers, but the upper boundary of both Helfrich (1967) and Arnbom (1980) quite closely resembles what is presented here. Both Helfrich (1967) and Arnbom (1980) also subdivide the Kall Nappe into a basal amphibolite-micaschist unit and an upper calc-silicate gneiss unit, the latter of which covers the eastern slope of Åreskutan. Arnbom (1980) in particular maps the Mörvikshummeln Formation in the western limb of the synform as a thin slice whose boundaries closely match those of the new map.

The easily distinguishable lower boundary of the Åreskutan Nappe is mapped quite consistently from Helfrich (1967) and onwards, with only minor alterations. In the regional map by SGU, based on Strömberg et al. (1984), the nappe boundary is displaced in regards to the morphology of the mountain, likely caused by either erronous georeferencing of the original map material, or mistakes made when constructing the original map.

When considering lithologies, there is some variation over time. Old maps and outcrop data from this thesis are seldom in agreement, though large formations are quite consistently mapped, e.g. the coherent amphibolite domain on Totthummeln and Getvalen, or the thick amphibolite sequence on Rödkullen. The interpretative nature of these maps seems evident, especially when lithological lenses are placed where thick Quaternary sediments cover the bedrock. The lithologies themselves however are quite consistently described across time.

8.2 Geometry of the nappe stack

The cross-sections made in this thesis are key to understand the geometry of nappe stack on Åreskutan, coupled with the subsurface data from the COSC-1 project which provides a view into the nappe stack that previous mappers did not have. In order to test the consistency of the field data gathered here with the observations made around Fröå and available core data (Hedin et al., 2012; Hedin et al., 2014; Hedin et al., 2016; Lorenz et al., 2019), a cross section was made connecting the study area with the seismic profile of Inline 1045 presented by Hedin et al. (2016). There were however too few measurements of the eastern limb of the Mörvikshummeln Formation along this profile to confidently describe the structure, so an east-west cross-section was made further north with a higher density of structural observations (Figure 118). This profile covers the whole nappe stack in order to test the structural consistency along strike in relation to the shape proposed by Hedin et al. (2016), and to investigate the geometry of the Åreskutan Nappe (Figure 119). In addition, a north-south cross-section was constructed (Figure 120). The cross-sections are based on field data projected along a profile extracted from the Digital Elevation Model. The cross-sections presented in this thesis reveal an unusal geometry, supported by structural field data, seismic imaging and lithological field and core-log data.

The geometries of the Offerdal and Särv Nappes are undramatic as they disappear beneath the overlying nappes, dipping east towards the hinge of the synform. The reflectors U3 and U2 identified by Hedin et al. (2016) are interpreted to represent the lower boundary of the Offerdal and Särv Nappe respectively. However, the relative thickness of the two nappes in the western limb (i.e. the thin slice of the Offerdal Nappe compared to the relatively thick Särv Nappe) leave room for alternate interpretations.

The geometry of the Kall Nappe is peculiar when only the field data presented here is considered, and even more so when combined with subsurface data. Field measurements show the Rödkullen Formation dips consistently eastwards, and is not seen again in the eastern limb of the synform within the study area. Observerations of the Mörvikshummeln Formation show it is extremely asymmetric around Åreskutan: in the western limb the thickness is estimated at $\sim$ 50 m, while in the eastern limb it dips consistently to the west across a distance of 3.5 km and an elevation drop of 200 m from the base of the Åreskutan Nappe to the eastern boundary of the study area, greatly exceeding the thickness in the western limb. Lithological and geochemical data from the COSC-1 drill core indicates there is a transition from calc-silicate rich gneiss and amphibolite in the upper part of the core to a basal section dominated by micaschist and mylonites consisting

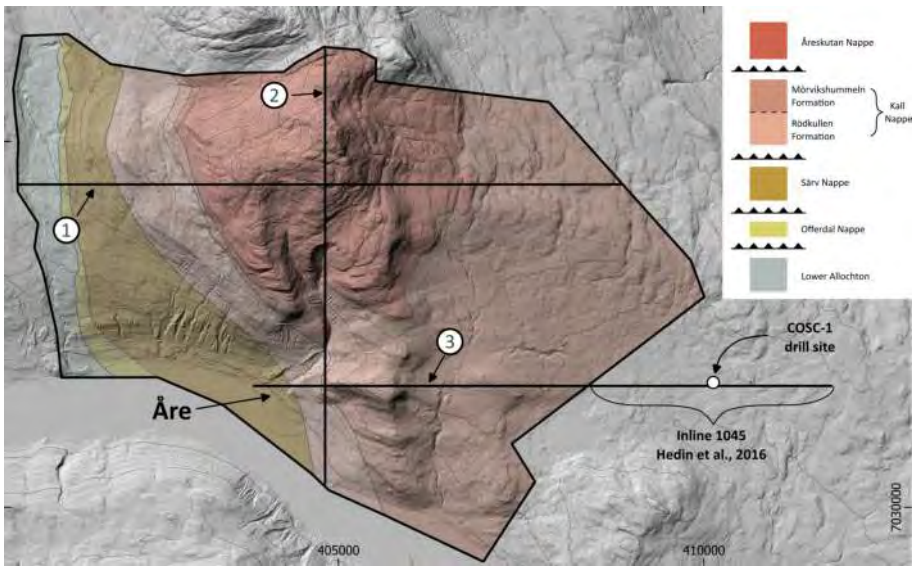


Figure 118: Tectonostratigraphic map of the study area with cross-section traces marked. The location of the COSC-1 drill site and the extent of Inline 1045 from Hedin et al. (2016) are also marked. The DEM is the 2 m tile dataset provided by Lantmäteriet. Grid and projection is SWEREF99 TM.

of CaO-poor lithologies between 1700-1800 m, referred to as the basal shear zone by Hedin et al. (2016). The complete lithology log of the COSC-1 core is shown in figure 121 and a detailed section containing the transition to the basal zone in figure 122, based on data from Lorenz et al. (2019). The lithologies named in the core log data of Lorenz et al. (2019) are inconsistent with field data, though a closer look at the detailed descriptions of core sections, i.e. mineralogy and structure, much better conforms to the data presented here. A visualization of lithologies in the COSC-1 core is also provided by Jeanneret et al. (2022), which matches well with observations of the Mörvikshummeln and Rödkullen Formations, apart from the abundance of orthogneiss interpreted in the lower section of the core (Figure 121). The source of the data is unfortunately not disclosed. Hedin et al. (2016) report several west-dipping reflectors dipping $\sim$ 10-15°, coinciding with mafic bodies in the COSC-1 core. It is further reported that reflectors in the calc-silicate gneiss and amphibolite section dip east when approaching the basal shear zone. When the subsurface data is combined with field data in a cross-section, it is evident that the basal shear zone of Hedin et al. (2016) likely correspond to the Rödkullen Formation outlined in this thesis, and the calc-silicate rich package above corresponds to the Mörvikshummeln Formation (Figure 124). From the boundaries outlined in the geological maps, a consistent dip of $\sim$ 25°is needed to connect the different formations with the subsurface profile, which is within the realm of possibilities and supported by structural measurements at the surface. The synformal hinge of the Kall Nappe is then placed east of the COSC-1 drill hole, likely visible at the eastern edge of Inline 1045. The basal shear zone of Hedin et al. (2016), from here on referred to as the Rödkullen Formation, shows an estimated thickness of $\sim$ 700 m, compared to the estimated $\sim$ 450 on the western flank of Åreskutan. On the eastern side of Åreskutan, the Mörvikshummeln Formation can now be shown to be a minimum of $\sim$ 2000 m thick roughly perpendicular to the west-dipping foliation, i.e. an aspect ratio (R = X/Y) of R = 40 when compared to the western limb (Figure 124).

The Åreskutan Nappe shows a complex internal geometry defined by internal shear zones, both high-grade parallel to the main foliation and late intermediate grade cutting across foliation at a high angle. The high-grade shear zones in the Snasahögarna Nappe to the west have been treated in earlier studies (e.g. Ma et al., 2022), but the geometry and implications of the south-southeast-dipping late shear zones have never previously been discussed. For a discussion on the timing of the late shear zones, see the section on P-T path and nappe stack assembly. The

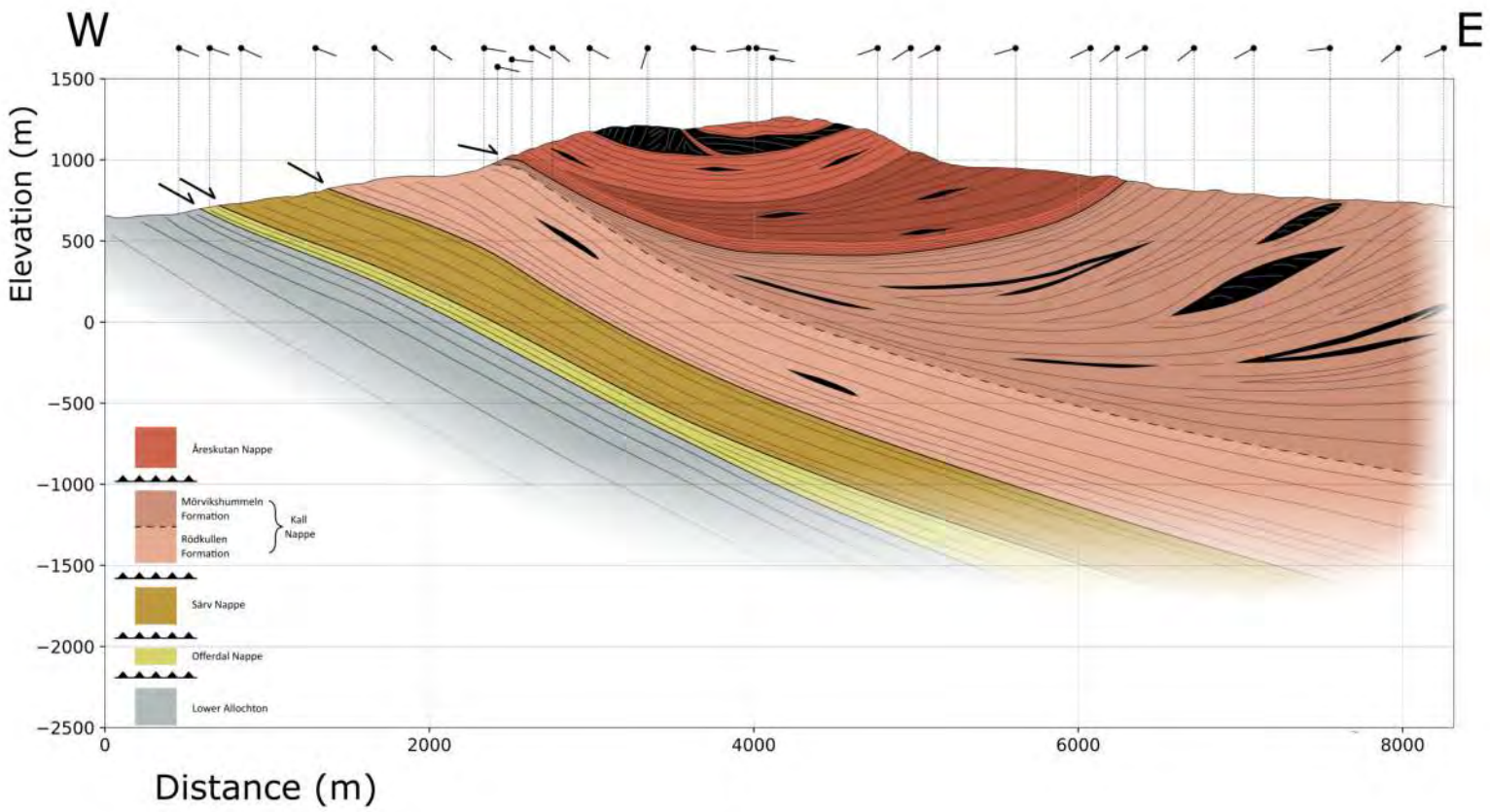


Figure 119: Cross-section 1, a semi-idealised cross-section of the Åreskutan nappe stack along an elevation profile extracted from the DEM, with a vertical to horizontal ratio of 1:1. The profile trends east-west, parallel to the general trend of stretching lineations across the nappe stack. Structural form lines mark the estimated apparent orientation of the foliation. The apparent dip estimated from structural measurements extrapolated to the profile is displayed above the cross-section. The dark red patch at the base of the Åreskutan Nappe indicates the extent of the basal retrogression zone. Dark layers and boudins are purely illustrative, except the two large black-coloured domains at the top of the Åreskutan Nappe, and are included to highlight the deformation mode of the nappe units. The topmost black-coloured domains of the Åreskutan Nappe are extrapolated from large coherent metabasite bodies with discordant foliation. Note the highly asymmetric shape of the Mörvikshummeln Formation and the wedge-shaped form lines at the base of the Åreskutan Nappe.

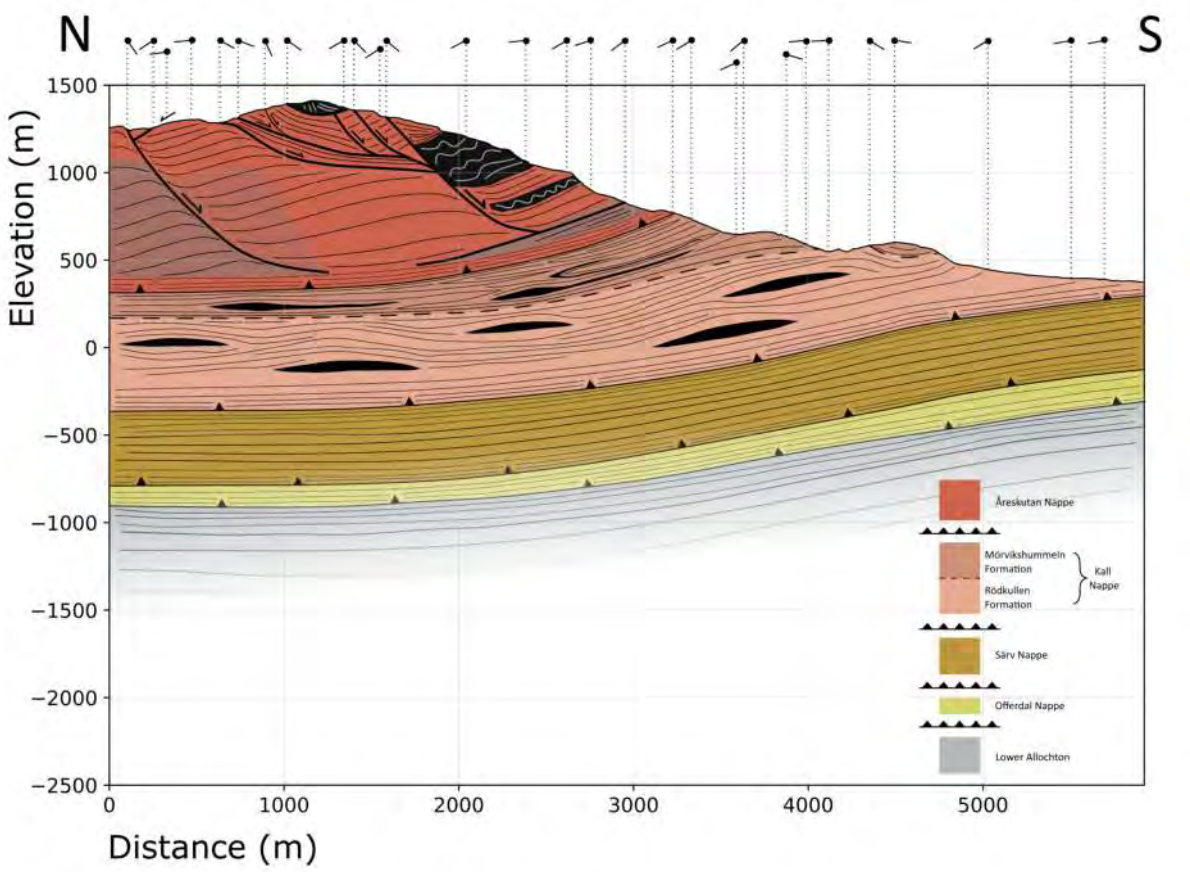


Figure 120: Cross-section 2, a semi-idealised cross-section of the Åreskutan nappe stack along an elevation profile extracted from the DEM, with a vertical to horizontal ratio of 1:1. The profile trends north-south, perpendicular to the general trend of stretching lineations across the nappe stack. Structural form lines mark the estimated apparent orientation of the foliation. The apparent dip estimated from structural measurements extrapolated to the profile is displayed above the cross-section. The grey patches at the base of the Åreskutan Nappe indicates the extent of the basal retrogression zones. Dark layers and boudins in the Kall Nappe are purely illustrative and are included to highlight the deformation mode of the nappe units. The black-coloured domains of the Åreskutan Nappe are extrapolated from large coherent metabasite bodies with discordant foliation.

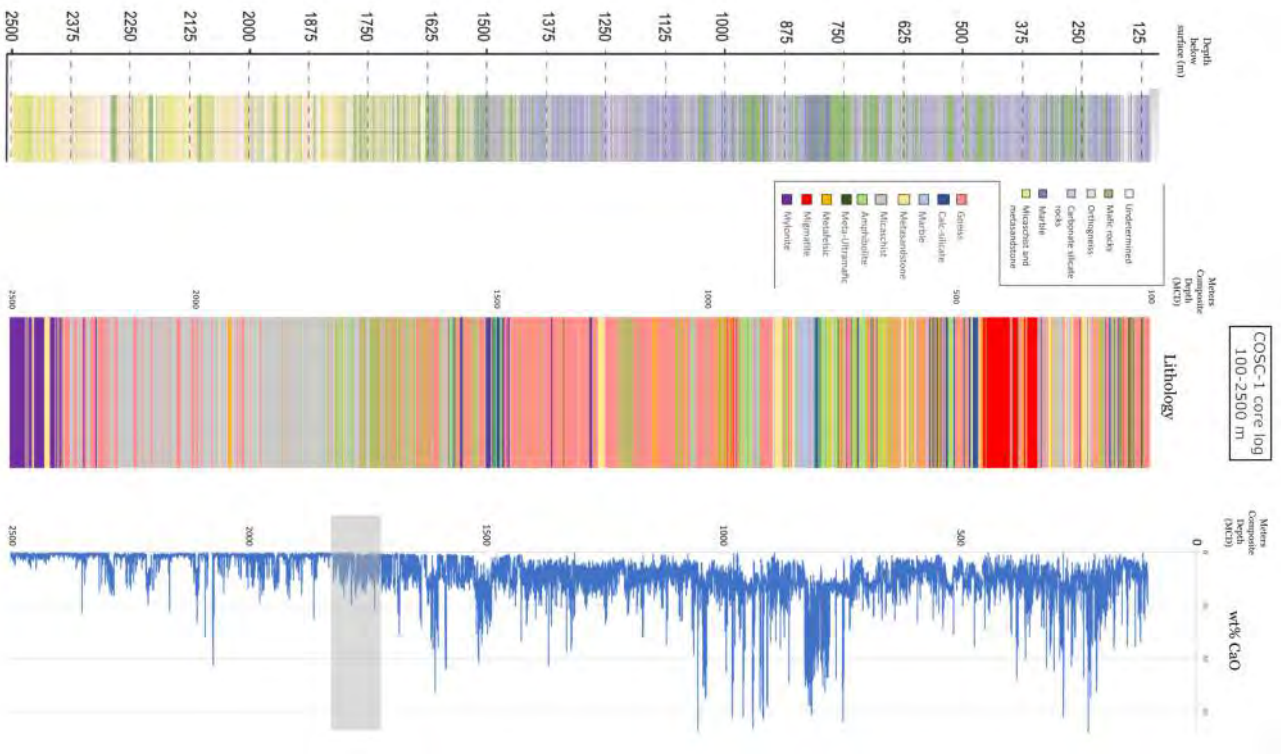


Figure 121: Diagrams visualising the COSC-1 core from core log data. The leftmost core log is modified from Jeanneret et al. (2022), showing lithologies closely matching those observed in the field, except perhaps the amount of orthogneiss indicated towards the bottom of the core. The source of the interpretation is not stated. The central core log is constructed from lithologies in the core log data set provided by Lorenz et al. (2019). Note that the depth scale of the lithology core log is not linear due to limitations of Excel, which was used for visualisation. Each line is an observation at a stated depth, and the distance between depth markers is controlled by the number of observations. The lithologies in the available dataset are inconsistent with field observations when not too vague to draw any conclusions, i.e. "gneiss". The most anomalous observation may be the large migmatite domain logged towards the top of the core; going through high-resolution photos of the core shows the typical highly plastically deformed calc-silicate gneiss of the Mörvikshummeln Formation. The rightmost diagram shows the weight percentage of CaO through the core, measured with XRF every 10 cm along with other major elements. Below 1800 m depth there is a drop in the CaO fraction, which may signify a transition from the Mörvikshummeln to the Rödkullen Formation between 1700-1800 m. XRF data for the COSC-1 core is provided by Lorenz et al. (2019).

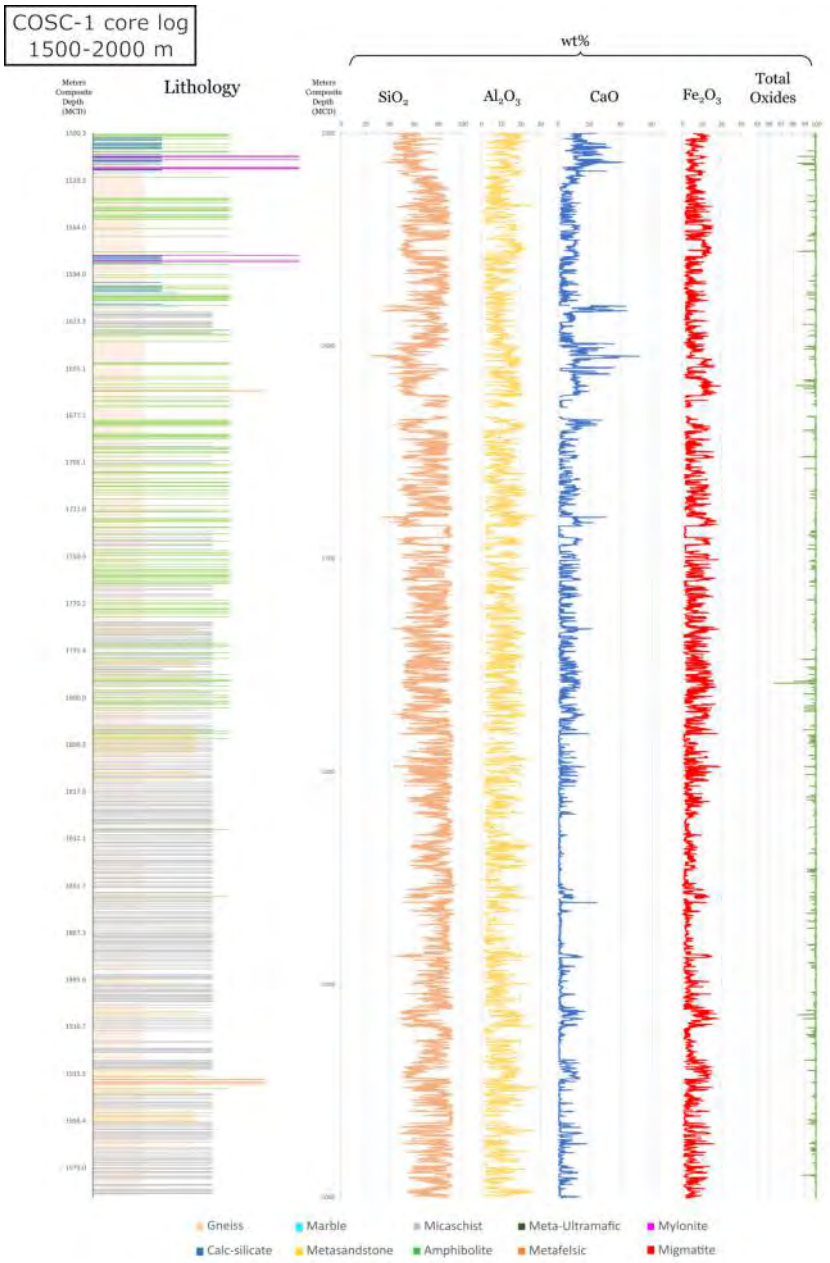


Figure 122: Detailed log of the COSC-1 core between the depths 1500-2000 m. Lithologies are displayed as bars of different length to help with differentiation. Note that the depth scale of the lithology core log is not linear due to limitations of Excel, which was used for visualisation. Each line is an observation at a stated depth, and the distance between depth markers is controlled by the number of observations. Weight percentage of the major oxides SiO_2, Al_2O_3, CaO and Fe_2O_3 are shown to the right, measured with XRF every 10 cm of the core along with other major elements. Total oxides comprise further components not shown here. The drop in CaO content below 1800 m is evident in the detailed log. This is interpreted as the lower boundary of the transition zone between the Mörvikshummeln and Rödkullen Formations.

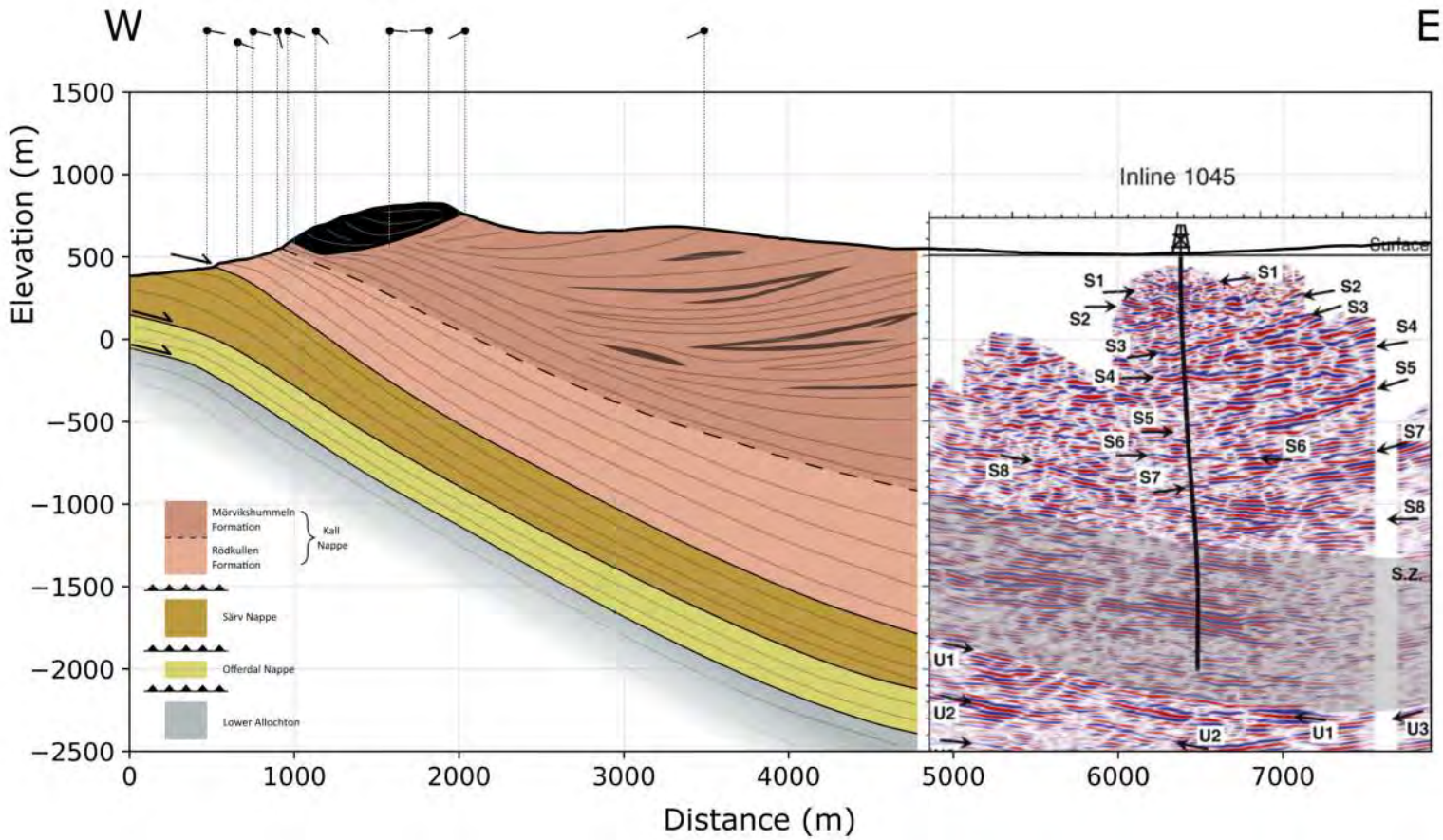


Figure 123: Cross-section 3, a semi-idealised cross-section of the Åreskutan nappe stack along an elevation profile extracted from the DEM, with a vertical to horizontal ratio of 1:1. The profile trends east-west, parallel to the general trend of stretching lineations across the nappe stack, and connects to the east-west trending seismic profile of Inline 1045, adapted from Hedin et al. (2016). Structural form lines mark the estimated apparent orientation of the foliation. The apparent dip estimated from structural measurements extrapolated to the profile is displayed above the cross-section. The large coherent amphibolite domain on Totthummeln at the highest point of the profile is coloured solid black, otherwise folds, dark layers and boudins in the Kall Nappe are purely illustrative and are included to highlight the deformation mode.

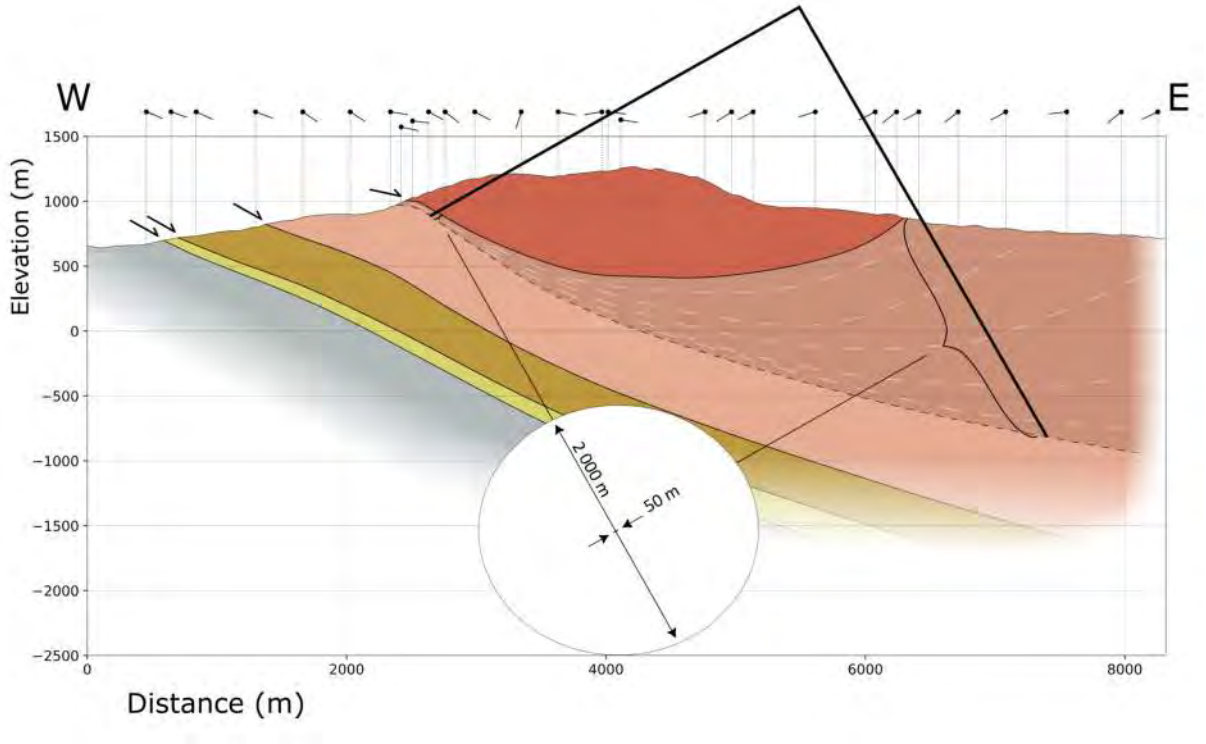


Figure 124: Simplified version of cross-section 1, with foliation traces shown in the Mörvikshummeln Formation to highlight the shortening of the western limb and thickening of the eastern limb. An estimated aspect ratio of R = 40 indicates unusually high strain accomodated by the Mörvikshummeln Formation.

amount of displacement along the late shear zones has not been estimated due to the complex lithological boundaries in the Åreskutan Nappe, but the formation of a 20-40 m wide shear zone in Tväråvalvet indicates it locally may have been significant. The east-west-trending cross-section 1 (Figure 119) crosses one major late shear zone which seems to delineate the basal retrogression zone, while the north-south-trending cross-section B-B' shows several late shear zones cutting across the main foliation of the Åreskutan Nappe. The vertical displacement along late shear zones may further complicate the already complicated internal structure of the nappe and petrological comparisons between different structural domains. Just as observed in the Snasahögarna Nappe by Ma et al. (2022), high-grade shear zones parallel to the main foliation of the nappe separate zones of highly folded migmatites. In addition, the structure presented here indicates large-scale asymmetric strain within the nappe, evident by the wedge shaped structure of the lower half of the nappe (discussion continued in section on P-T path and nappe assembly).

In comparison with previous cross-sections made of Åreskutan, the cross-section presented here is consistent with the those drawn by Törnebohm (1872) and Högbom (1909) at the larger scale, as the overthrust relationship between the Middle and Lower Allochtons is evident. Excepting Helfrich (1967), subsequent cross-sections are structurally simplified to the point where the tectonostratigraphic point the authors want make is clear, but with a geometry inconsistent with the field data presented in this thesis. Typically, the Kall Nappe is presented as a relatively flat sheet of almost uniform thickness from west to east (e.g. Arnbom, 1980; Karis and Strömberg (1998)). Tectonostratigraphically, the cross-section presented here is in agreement with the schematic cross-section by Karis and Strömberg (1998), whereas the other cross-sections described in previous mapping of Åreskutan leave out either the Offerdal or Särv Nappe (Helfrich, 1967; Arnbom, 1980, Bender et al., 2018; Gee et al., 2020). Structurally, the cross-section of this thesis is largely in agreement with the beautiful cross-section made by Helfrich (1967). It closely matches the field data presented here, but is not fully consistent.

Helfrich (1967) estimates roughly the same thickness of the Åreskutan Nappe and the tapering structure of the nappe from east to west is noted; he also noted the marked asymmetry of the Mörvikshummeln Formation, referred to as the Fröå-Bjelke Nappe, which is interpreted as thickening of the nappe in the eastern limb explained through imbrication of internal thrusts. Helfrich (1967) further seems to note the progressive eastward shift of the synform hinge at lower structural levels. Unfortunately, he did not have access to the subsurface data from from the COSC project, so the thickness of the Mörvikshummeln Formation is underestimated by roughly 800 m, and the thickness of the whole Kall Nappe by 1500 m. Helfrich (1967) also mapped an internal thrust separating an upper garnet-pyroxene amphibolite subunit from migmatitic garnet gneiss below (topmost thrust package of the Åreskutan Nappe in figure 5b). This is not supported by the field data presented here, but the location where the cross-section intersects the thrust below the hypothesised garnet-pyroxene amphibolite in the map of Helfrich (1967) coincides precisely with the wide late shear zone cutting through Tväråvalvet, and the eastern terminus of the thrust appears to be located at one of the two late shear zones further south (all three shear zones pictured in figure , the leftmost is the western terminus of the hypothesized thrust, on of the two rightmost the eastern terminus). Excepting the interpretation of an internal thrust bounding a large garnet-pyroxene amphibolite unit at the top of Åreskutan, the cross-section by Helfrich (1967) is in agreement with that presented here; the thickening of the Mörvikshummeln Formation is discussed in the section on boudinage of the Åreskutan Nappe.

8.3 P-T path and assembly of the nappe stack

The P-T paths indicated by rocks of the displaced nappes reflects the tectonic history which resulted in the displacement. Reconstructing the P-T path of the nappe stack at Åreskutan is therefore a window into the past, hinting at the processes which built the Scandinavian Caledonides. At Åreskutan, the metamorphic grade of the individual nappes decrease going downwards in the nappe stack, and the tectonic boundary between the Kall and Åreskutan Nappe shows a distinctly higher metamorhic grade than those below. In this section, gathered field and petrographic data will be used to estimate the conditions experienced by the different nappe units. As no petrological data has been produced for this thesis (e.g. bulk rock chemistry, microprobe analysis of minerals), the path will be estimated using generalized petrogenetic grids for metapelites, which are found in all described nappe units, and through integration of previous P-T estimates of the nappes on Åreskutan (Figure 125). The related nappes to the west of the Mullfjället Antiform, 30-40 km southwest in the Sylan-Vålådalen area, will also be considered as they likely represent the westward continuation of the nappe stack on Åreskutan (Figure 2).

8.3.1 Åreskutan Nappe

The Åreskutan Nappe has long been of interest to tectonic reconstructions, due to the distinctly high metamorphic grade. The mineral succession outlined in the deformation and metamorphic history of the Åreskutan Nappe indicate a path first from high to low pressure, followed by a path of decreasing temperature. Signs of the pre-anatectic history of the nappe are not obvious in the field, and an investigation of palaeosomes may be needed to gain further knowledge, in addition to the thermodynamic modelling that has been performed by previous studies.

Anatexis is inferred to have been contemporaneous with the development of the main foliation, placing the beginning of the path in the kyanite stability and partial melt field (Figure 126), past the $Ms + Ab = Ky + Kfs + L$ reaction line of Spear et al. (1999). No orthopyroxene was found in the investigated paragneiss samples, which together with abundant biotite in paragneiss restite indicates that the biotite-out reaction line was not crossed. The lack of corroded texture of biotite in restite further indicates that biotite consumption would have been low (Kriegsman and Álvarez Valero, 2010). In samples MS2305, MS2310, Ms2320, MS2321 and MS2332C, bioite is primarily found in association with, and replacing, sillimanite. In four of the samples garnet is consumed by sillimanite (Figure 40b; Table 3), pointing to melt-consuming reactions causing the observed disequilibrium, and a path partly defined by cooling decompression (e.g. Groppo et al.,

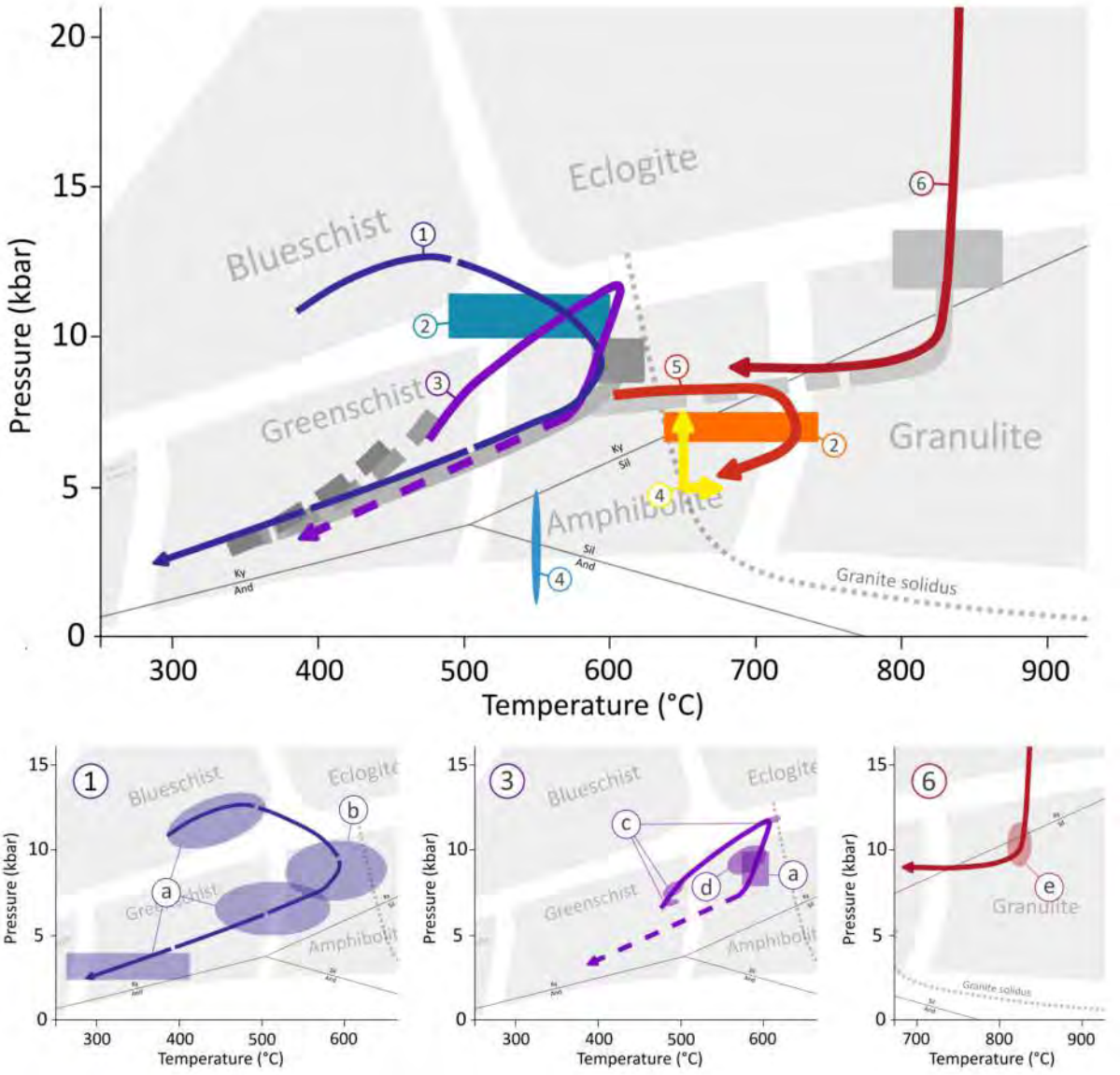


Figure 125: P-T paths and estimates for the Åreskutan Nappe and Kall Nappe displayed together with the P-T path proposed in this thesis for the entire nappe stack (gray outline). P-T estimates for the Kall and Blåhammarfjället Nappes are blue and purple, and the Åreskutan and Snasahögarna Nappes are red, orange and yellow. In the figure are estimates from (1) Giuntoli et al. (2020), (2) Bergman (1992), (3) Jeanneret et al. (2022), (4) Arnbom (1980), (5) Li et al. (2020) and (6) Klonowska et al. (2017). Summaries of all P-T estimates in the Åre-Vålådalen-Sylan area are compiled in table 2. Insets from paths (1), (3) and (6) show the range of estimates along proposed paths and the methods used. (a) Phase equilibrium diagram modelling, (b) amphibole-plagioclase thermobarometry, (c) combined quartz-in-garnet geobarometry and titanium-in-quartz geothermometry, (d) garnet-biotite-muscovite-plagioclase geobarometry, (e) combined phase equilibrium diagram modelling and titanium-in-quartz geothermometry. Approximate fields of metamorphic facies are modified from Liou and Zhang (2003) and Winter (2021), with low-pressure facies omitted.

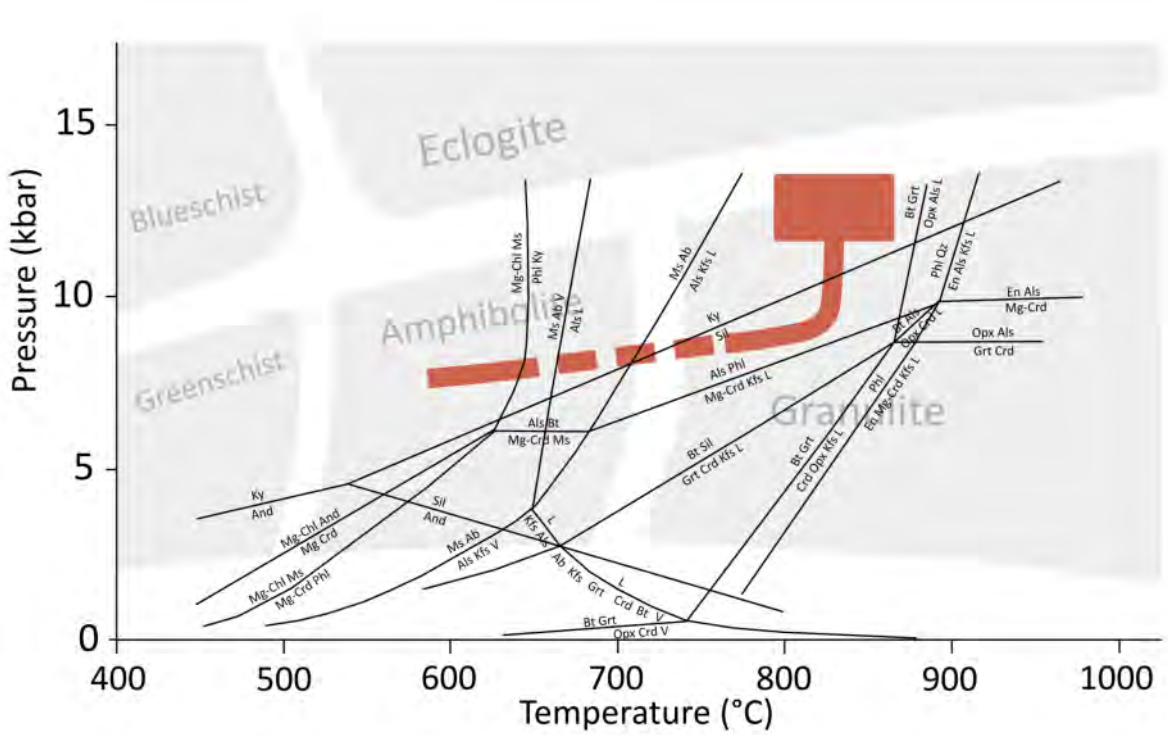


Figure 126: Proposed P-T path for the Åreskutan Nappe based on field and petrographic observations. Simplified petrogenetic grid in the NKFMASH system for anatectic metapelites, redrawn after Spear et al. (1999). Approximate fields of metamorphic facies are modified from Liou and Zhang (2003) and Winter (2021), with low-pressure facies omitted.

2012). The amphibole observed in pyroxene amphibolite does not display any melt corrosion and observed metabasite outcrops generally display greater degrees of partial melting near or in contact with paragneiss. Felsic segregations in metabasite have been shown to postdate partial melting in migmatitic paragneiss, so it can be inferred that fluid flux from partially melted paragneiss likely mediated partial melting in metabasite (Ladenberger et al., 2014).

The P-T path favoured in this thesis based on the discussion above and the metamorphic history of the Åreskutan Nappe outlined previously begins at a temperature range between 800-875°C and a pressure range of 11 - 13 kbar. The dominance of sillimanite over kyanite and the absence of cordierite indicates the kyanite - sillimanite isograd was significantly overstepped (Foster, 1990), but not the cordierite-in reaction line. No kyanite has been observed to replace sillimanite along the cooling path, instead replacement by biotite affects sillimanite aggregates and prismatic crystals. The most common assemblage of metabasite on Åreskutan is rich in primary amphibole, and while amphiboles such as hornblende can be stable over a large range of conditions in the granulite facies, high-pressure assemblages typically include garnet and clinopyroxene (e.g. Forshaw et al., 2019; Zou et al., 2024). Why non-melted metabasite doesn't show a high-pressure assemblage when it is pervasive in migmatitic paragneiss remains to be investigated on Åreskutan. Peritectic garnet and pyroxene in metabasite leucosome also await investigation, as it they may help constrain conditions at anatexis (e.g. Hansen et al., 2015).

Field observations show a high degree of partial melting in pyroxene amphibolite and particularly in paragneiss. Assessing the melt fraction is outside the scope of this thesis, but rare observations of isolated palaeosome pods, and the absence of matrix muscovite predating retrogression indicate it indeed was significant (White and Powell, 2002). Quantitative data is lacking however, and further investigation is needed to accurately constrain the degree of partial melting. The significance of the melt fraction is apparent when considering thermodynamic modelling of the past P-T conditions of the Åreskutan Nappe. Phase equilibrium forward modelling, i.e. P-T pseudosection modelling, is a powerful tool to investigate the thermobarometric history of

a rock sample, but it is dependent on the bulk rock composition reflecting that of the protolith (Powell and Holland, 2008). At the threshold melt fraction of 7 %, inter-connectivity of melt films around grains is enough to redistribute the melt under differential stress (Rosenberg and Handy, 2005). When constructing phase equilibrium diagrams for highly deformed migmatites, such as those on Åreskutan, careful reintegration of the lost melt fraction is needed for a correct analysis of melt-depleted rocks (e.g. Groppo et al., 2012; Li et al., 2021a).

Textural evidence of retrogression is pervasive across the nappe. The predominant retrogressive reaction identified in paragneiss is the replacement of sillimanite by biotite. Pervasive retrogression of partially melted rocks rocks is common, e.g. through back reactions during isothermal decompression, hydration reactions caused by fluids released from crystallised melt, or fluids from an external source (e.g. Kriegsman, 2001; Topuz and Altherr, 2004). The melt produced during anatexis of the Åreskutan Nappe was likely rich in H_2O due to dehydration of muscovite. Unless the produced melt is removed from the system before the melt begins to crystallize, rehydration of the anhydrous assemblage will occur (White and Powell, 2002). Assuming garnet + kyanite + K-feldspar + liquid ± biotite was the first assemblage in migmatitic paragneiss (M2, see metamorphic history of the Åreskutan Nappe), the ubiquity of retrogressive hydrous phases in paragneiss and metabasite indicate that melt escape from the nappe unit was low to negligable (White and Powell, 2002). The high degree of strain recorded in the rocks instead acted to redistribute the melt, particularly H_2O as the melt crystallized when approaching and passing the wet solidus on the cooling path. The continuation of the P-T path is constrained by the juxtaposition of the Åreskutan Nappe over the Kall Nappe, which is discussed further below.

Arnbom (1980) made the first petrological investigation of the rocks of the Åreskutan Nappe, using garnet-biotite geothermometry to constrain the peak temperature conditions and infer pressure from temperature and index mineral assemblages. For the granulite-facies assemblage Arnbom (1980) only provides a minimum estimate, suggesting that conditions exceed 5-7 kbar and 650°C. Of note is that cordierite is reported to occur in the paragneiss of the Åreskutan Nappe, but no subsequent study, including this thesis, has identified cordierite in the rocks of the nappe. Further inconsistencies with petrographic investigation in this thesis is the reported overgrowth of sillimanite and kyanite on biotite towards the base of the nappe, the opposite relationship of what is presented here (Table 3).

The decompressional P-T path proposed by Klonowska et al. (2017) coincides with the estimate of the P-T path presented here. However, Klonowska et al. (2017) reports ultra-high pressure metamorphism in the diamond stability field preceding exhumation and decompression melting, which is not supported by field observations. The estimate is based on phase equilibrium diagram modelling and the presence of metamorphic diamond inclusions in garnet (Table 2). As pointed out by Li et al. (2021c), the thermodynamic modelling of Klonowska et al. (2017) does not account for melt escape, so the validity of the model is uncertain. At the larger scale, ultra-high-pressure metamorphism has been reported in several nappes of the Seve Nappe Complex, including in the diamond field, and the presence of metamorphic microdiamond at Åreskutan is thoroughly verified (Klonowska et al., 2017; Klonowska et al., 2021; Slupski, 2023). If the Åreskutan microdiamonds can not be shown to have formed at low pressures, as suggested by Li et al. (2020), the discrepancy between the observed lithologies of the Åreskutan Nappe and ultra-high-pressure metamorphism must be explained. Such conditions can not be reconciled with the mineral assemblage observed in partially preserved, pre-anatectic metabasite and melt-extraction from biotite-rich paragneiss. Further investigation is needed both to constrain timing and conditions of diamond formation in the Åreskutan Nappe, and the metamorphic conditions leading into partial melting in the kyanite stability field.

Li et al. (2020) presented a conflicting result on the P-T history of the Åreskutan Nappe, based on phase equilibrium modelling. The peak P-T conditions before decompressional melting at high temperature were constrained to 8 - 8.5 kbar and 700°C, and peak T reached at 6.5 kbar

and 725°C. This is lower than what is proposed in this thesis, and the observations of Li et al. (2020) are not consistent with field and petrographic data presented here. It is claimed by the authors that the investigated outcrop contains no leucosome and is minimally affected by partial melting (Li et al. (2020)). However, the outcrop in question is observed to contain abundant leucosome and other evidence of partial melting, i.e. large secondary K-feldspar grains and peritectic garnet (Figure 13c). While it is possible that the collected sample did not experience partial melting, it is highly unlikely when compared to the large-scale pattern in the Åreskutan Nappe. As a consequence, melt escape is not corrected for in the modelling, with implications for the validity of the model. Secondly, the inferred anatectic assemblage differs from field observations presented here, as Li et al. (2020) only include kyanite as a stable phase prior to partial melting. Compared to domains where anhydrous phases are better preserved (see sample MS2332C, figure 30, figure 40a), the sample presented by Li et al. (2020) more closely resemble paragneiss where fluid-assisted re-equilibration at lower grade has been strong, e.g. no large kyanite grains marking the migmatitic foliation. The sample comes from a significantly higher structural level compared to the sample presented by Klonowska et al. (2014), but better preserved paragneiss has been found at all structural levels outside of the retrogression zones. The most compelling argument against the P-T path proposed by Li et al. (2020) is assembly of the Seve Nappe Complex; following the proposed path, even completely isobarically cooled, would place the juxtaposition of the Årskutan Nappe in the middle greenschist-facies field, which is inconsistent with the amphibolite-facies assemblage of the tectonic boundary presented here.

Slupski (2023) corroborates ultra-high-pressure metamorphism at 40-45 kbar and 850-900°C through experimental re-homogenisation of former melt inclusions in garnet from paragneiss in the Åreskutan Nappe. However, a serious flaw in the approach is that re-homogenisation was only tested in the expected pressure range, i.e. 40 and 45 kbar, and not at lower pressures. As nanogranitoid inclusions don't exclusively form at ultra-high pressure (e.g. Cesare et al., 2009), the confirmation bias of the study may invalidate any conclusions drawn about peak metamorphic conditions and it will not be considered further in this discussion.

The Snasahögarna Nappe, situated 30-40 km southwest of Åreskutan in the Sylan and Vålådalen area, shows almost identical paragenesis to the Åreskutan Nappe (Sjöström, 1983; Bergman, 1992; Ma et al., 2022). Sjöström (1983), similar to Arnbom (1980), report occasional cordierite in the paragneiss of the Snasahögarna Nappe, but no subsequent studies have identified cordierite. There is only one published P-T estimate for the Snasahögarna Nappe based on petrological data. Bergman, 1992 constrain peak metamorphic conditions at 6.5-7.5 kbar and 630-740°C based on garnet-biotite geothermometry and garnet-biotite-muscovite-plagioclase geobarometry, reaching a result similar to Arnbom (1980) and Li et al. (2020). However, similar to the Åreskutan Nappe, metamorphic microdiamond has been identified in paragneiss in the Snasahögarna Nappe, indicating much higher peak metamorphic conditions at some point in the history of the nappe (Rosén, 2014; Majka et al., 2014b).

8.3.2 Kall Nappe

The Kall Nappe has a distinct amphibolite facies assemblage of garnet-biotite-staurolite at the base of the Rödkullen Formation and garnet-diopside in the overlying Mörvikshummeln Formation. The calc-silicate parageneses are difficult to model in P-T space, and T-X_CO2 phase equilibrium modelling is needed to constrain the temperatures related to form the assemblage. Winter (2014) likens the assemblage garnet-diopside-anorthite to the Barrovian sillimanite zone, as diopside forms from dehydration of Ca-amphibole, indicating relatively high temperatures were reached. Recrystallisation but not retrogression of clinopyroxene at the upper tectonic boundary also indicates that juxtaposition of the Åreskutan Nappe occurred at close-to-peak temperatures. Metamorphism in the kyanite stability field is confirmed by a kyanite-bearing pod in the Rödkullen formation, but the composition of the pod appears too divergent from the rocks of the Kall Nappe to draw any further conclusions. Further, there are no compelling signs of partial melting in the Kall Nappe, restricting the peak temperature conditions to below

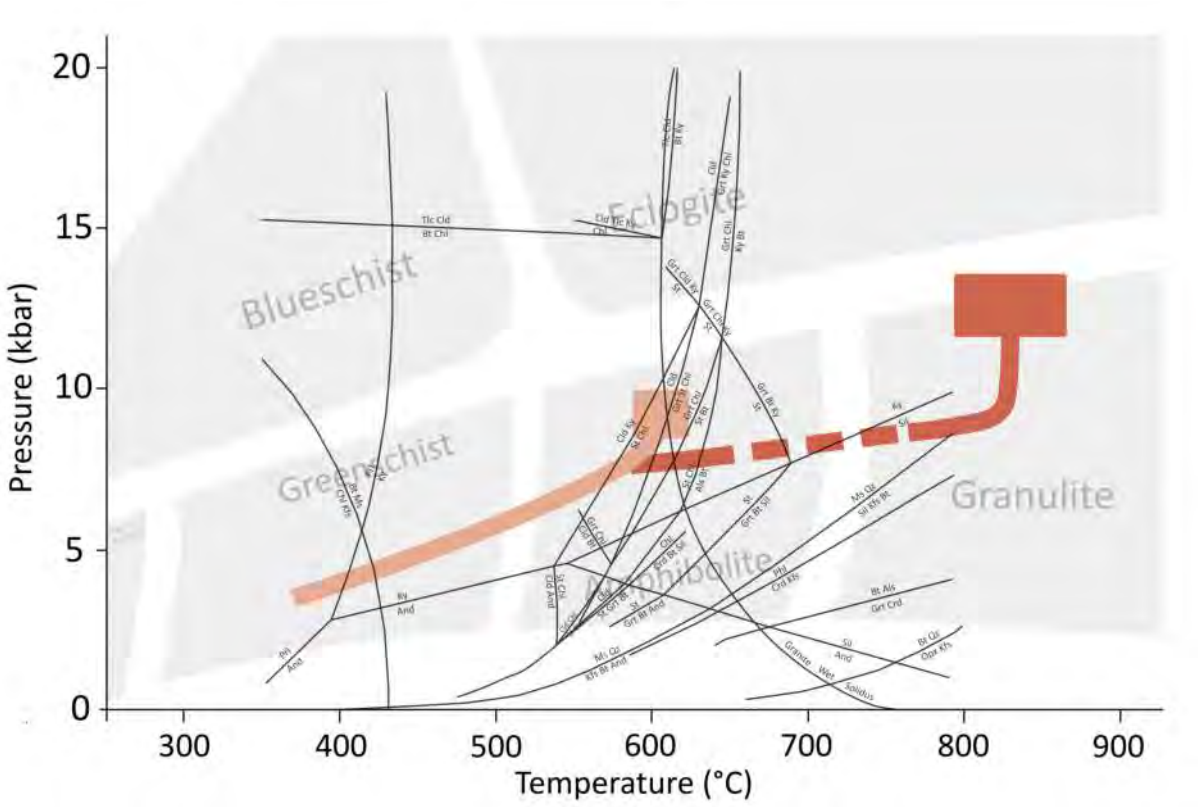


Figure 127: Proposed P-T path for the Kall Nappe based on field and petrographic observations. Simplified petrogenetic grid in the KFMASH system for metapelites, redrawn after Winter (2014, itself modified after Spear and Cheney, 1989, and Spear et al., 1999). Approximate fields of metamorphic facies are modified from Liou and Zhang (2003) and Winter (2021), with low-pressure facies omitted.

the wet solidus of Spear et al. (1999). Investigation of the common leucogranite intrusions in the Mörvikshummeln Formation by Li et al. (2021d) shows two different sources, recycled crustal rocks with an age range of 2.5-2.8 Ga and more mafic and depleted rocks with an age range of 1.6-2.3 Ga. The source(-s) is speculated to be partial melting of Svecokarelian and Sveconorwegian basement, but also raise the possibility of an internal source of the melt. Excluding Caledonian and Baltoscandian Dike Swarm ages, detrital zircons of the Kall Nappe in Åre are shown to have a dominant population in the 1-1.8 Ga age range, and a smaller population between 2.6-2.8 Ga, which also matches the source ages of the leucogranite (Gee et al., 2014; Li et al., 2021d). Incidentally, this is also the age range of detrital zircons in the Åreskutan Nappe (Ladenberger et al., 2014). The indications of incipient partial melting presented in this thesis are too inconclusive to propose an internal source of melt for the leucogranite (see section on metamporphic history of the Kall Nappe), but must be further investigated to rule out this scenario. Recrystallisation but not retrogression of clinopyroxene in the Kall - Åreskutan tectonic boundary In summary, the favoured P-T path for the Kall Nappe is placed outside the partial melt field of Spear et al. (1999). The estimated conditions at the beginning of the P-T path are 8-10 kbar and 580-630°C, constrained by the mineral assemblage garnet-staurolite-biotite-white mica, and the juxtaposition of the Åreskutan Nappe at amphibolite-facies conditions.

Giuntoli et al. (2020) proposed a P-T path based on thermodynamic modelling of amphibolite and micaschist from the Rödkullen Formation and the lowest part of the Mörvikshummeln Formation in the COSC-1 drill core. The modelling included analysis of relic assemblages in micaschist and the P-T conditions during the development of deformational fabrics in micaschist and amphibolite. After a proposed high-pressure phase, the mylonitic fabric in amphibolite developed at progressively lower pressure and temperature, from 8-10 kbar and 600-650°C to 5-8 kbar and 500-600°C (Giuntoli et al., 2020; Table 2). Giuntoli et al. (2020) notes that the mylonitic fabric in micaschist developed during the latter stage, possibly reflecting re-equilibration at lower metamorphic grade. Jeanneret et al. (2022) proposes a similar retrograde path, but with a hairpin curve for the prograde path and peak P-T conditions (Figure 125; Table 2). Field observations and petrographic data presented in this thesis is in good agreement with the results of Giuntoli et al. (2020) and Jeanneret et al. (2022), with a retrograde path through the lower-temperature region of the amphibolite facies.

The Blåhammarfjället Nappe occupies the same structural position as the Kall Nappe in the Sylan and Vålådalen area, 30-40 km southwest, but with a slightly different lithological distribution and paragenesis (Sjöström, 1983). Bergman (1992) estimated P-T conditions for the upper part of the Blåhammarfjället Nappe at 10-11.5 kbar and 480-600°C, wich covers a section of the decompressional heating path of Giuntoli et al. (2020) and parts of both the prograde and retrograde path of Jeanneret et al. (2022). Li et al. (2021b) place peak metamorphic conditions for the Blåhammarfjället Nappe at 9-10.2 kbar and 745-775°C, and the retrograde path at 7-9 kbar below temperatures of 750°C. This temperature estimate is much higher than any previous estimate for both the Blåhammarfjället Nappe and the Kall Nappe, and a closer look at the sample and sampling site may explain why. The mylonitic paragneiss sample investigated by Li et al. (2021b) is taken from an outcrop mapped relatively close to the upper tectonic boundary of the Seve Nappe Complex close to Handöl, and the coordinates provided (63°14'48.7"N, 12°26'15.4"E) point to a large outcropping mapped as a tectonic lens of the high-grade Snasahögarna Nappe (Sjöstrand, 1999). In the local geological map made by Sjöstrand (1999), the outcrop and area around it has been thoroughly mapped. Further, the parageneses and fabric of the sample shown by Li et al. (2021b) does not match anything described previously for either the Blåhammarfjället or Kall Nappes, and would imply a significant internal inverted metamorphic gradient for sillimanite to form at the upper boundary of the nappe. It can be concluded that Li et al. (2021b) investigated a mylonitic paragneiss from the Snasahögarna Nappe or possibly the Täljstensvalen Complex, which also explains the similar P-T estimate to Li et al. (2020), and their P-T estimate will not be taken into consideration.

8.3.3 Särv and Offerdal Nappes

The Särv and Offerdal Nappes reached a relatively low metamorphic grade compared to the overlying nappes, with the index minerals biotite + white mica corresponding to the Barrovian biotite zone. It can be speculated that any chlorite present in the prograde path reacted to form biotite and muscove through the reaction $Chl + Kfs = Bt + Ms$, which consumed all chlorite due to the likely abundance of K-feldspar in the arkosic protoliths. There are clear differences in the parageneses of the nappes; micaschist in the Särv Nappe is rich in both biotite and white mica but lacks garnet, whereas semipelitic micaschist in the Offerdal Nappe is dominated by white mica and epidote with only accessory amounts of biotite, but with abundant small garnets. The Barrovian biotite zone corresponds roughly to the upper greenschist facies (Winter, 2014), and the peak metamorphic conditions of the Särv Nappe is tentatively suggested to lie in the range of 5-8 kbar and 450-550°C (Figure 128.

The peak metamorphic conditions of the Offerdal Nappe is more difficult to place in P-T space due to the conflicting index mineral assemblage; rare low-grade biotite indicates the nappe barely passed into the bioite zone, while abundant small garnets mean the garnet isograd was crossed, i.e. upper greenschist facies or transitional to amphibolite-facies conditions (Winter, 2014). The offerdal Nappe is however a case where petrogenetic grids of metapelite may not be applicable. The studied semipelitic micaschist has too low mica content to be considered a true metapelite, and the high mode of epidote in the sample indicates high calcium content in the protolith. Further, it has been shown that the KFMASH-system of the petrogenetic grid used to constrain metamorphic conditions in this thesis stabilizes garnet at much higher metamorphic conditions compared to systems where Mn activity is considered (e.g. Wei et al., 2004). In systems where garnet stability is chemically controlled by the activity of Mn, the stability field may extend to temperatures below 450°C for a wide range of pressures (Wei et al., 2004). As no chemical analysis has been made of the samples in this thesis, it can only be speculated that the apparent middle greenschist-facies assemblage + garnet in the Offerdal Nappe in fact developed at middle greenschist-facies conditions, with formation of garnet in Mn-rich semipelite. The fact that garnets have only been observed in a set of outcrops at a single location, but not in micaceous layers elsewhere in the nappe, supports this conclusion. Peak metamorphic conditions likely fall in the range of 5-7 kbar and 425-500°C (Figure 129). The P-T paths for the Särv and Offerdal Nappe will hopefully be further investigated in the future and described in better detail. Unfortunately, the high-grade rocks of the Seve Nappe Complex has proven a much bigger draw for petrological studies until now, and will likely continue to overshadow the underlying nappes in the future.

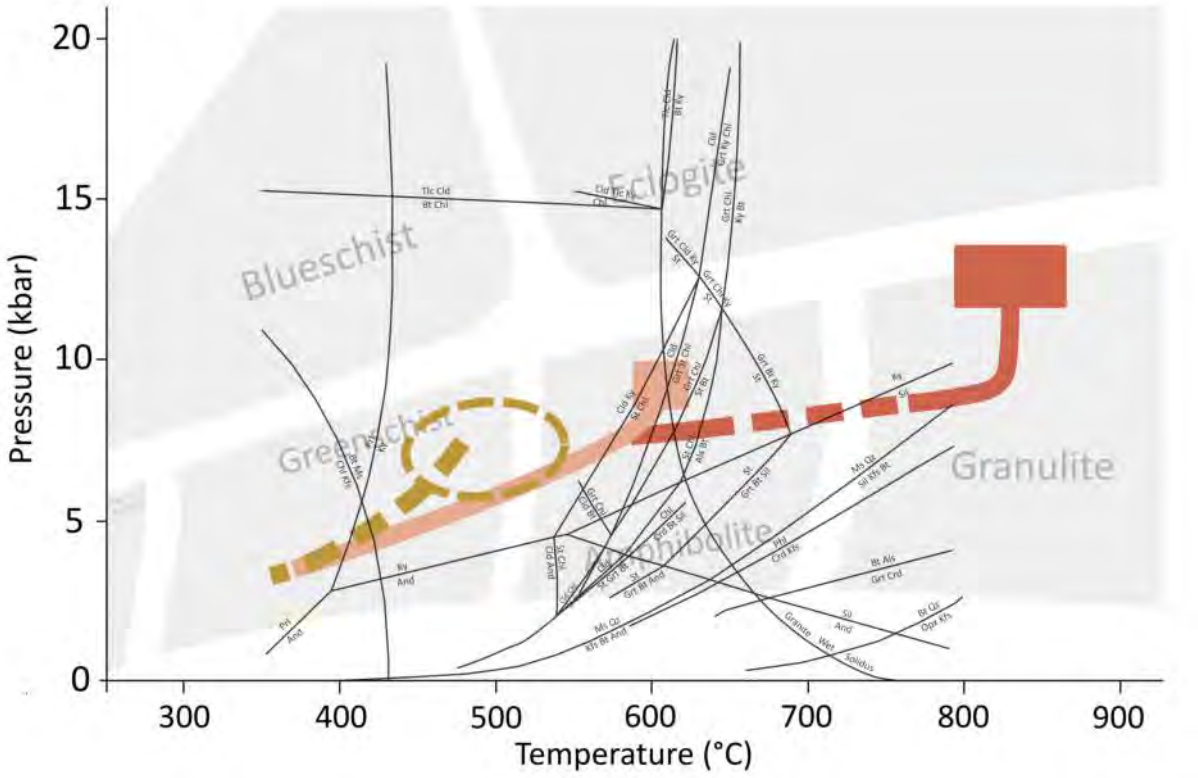


Figure 128: Proposed P-T path for the Särv Nappe based on field and petrographic observations. Both the peak metamorphic conditions and exhumation path are are poorly constrained. Simplified petrogenetic grid in the KFMASH system for metapelites, redrawn after Winter (2014, itself modified after Spear and Cheney, 1989, and Spear et al., 1999). Approximate fields of metamorphic facies are modified from Liou and Zhang (2003) and Winter (2021), with low-pressure facies omitted.

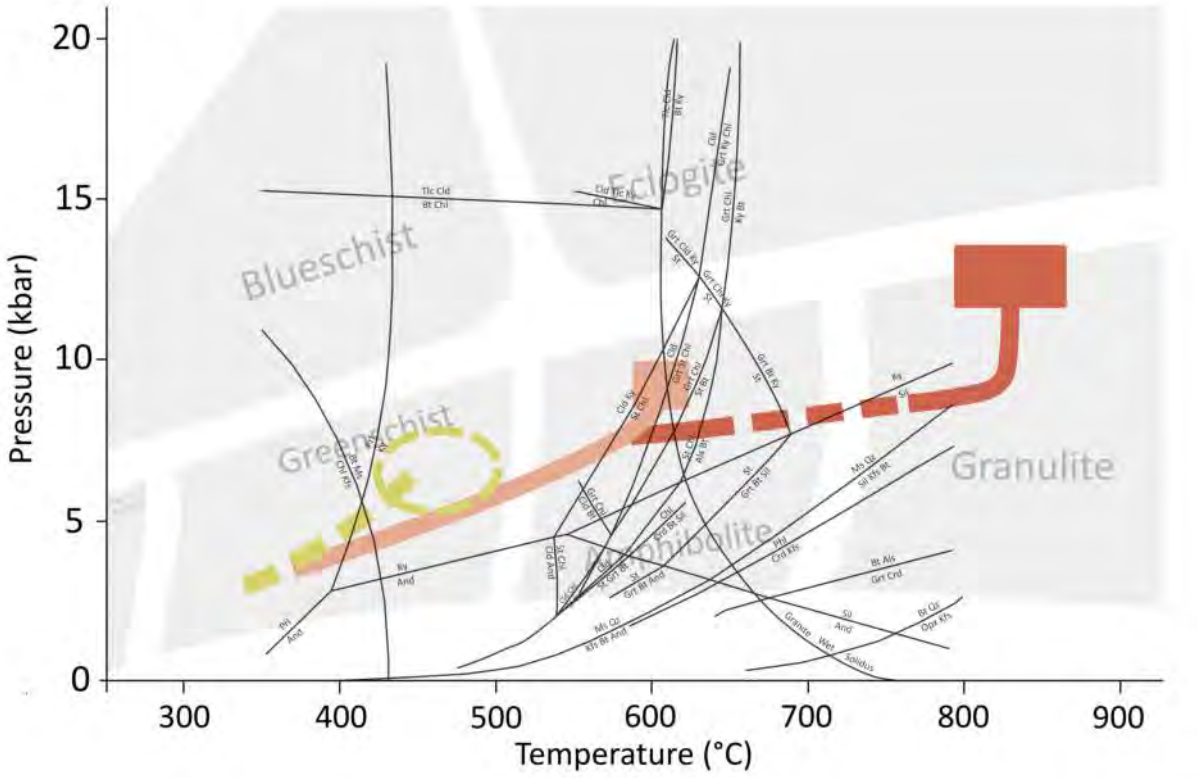


Figure 129: Proposed P-T path for the Offerdal Nappe based on field and petrographic observations. Both the peak metamorphic conditions and exhumation path are are poorly constrained. The path of the Särv Nappe is omitted for clarity. Simplified petrogenetic grid in the KFMASH system for metapelites, redrawn after Winter (2014, itself modified after Spear and Cheney, 1989, and Spear et al., 1999). Approximate fields of metamorphic facies are modified from Liou and Zhang (2003) and Winter (2021), with low-pressure facies omitted.

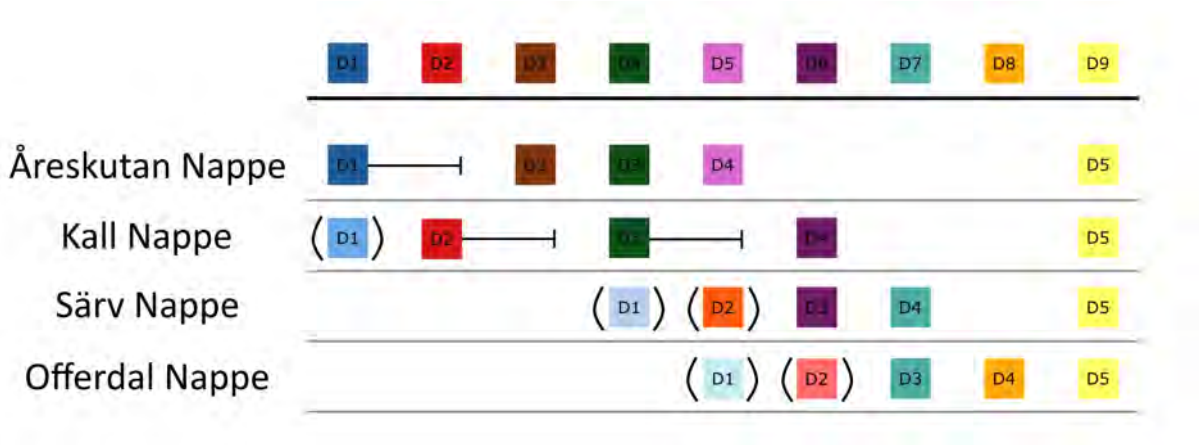


Figure 130: Compilation of the deformation phases of each nappe, synthesised in an overarching deformation history of the nappe stack.

8.3.4 Assembly of the nappe stack

The history of the assembly of the nappe stack at Åreskutan stretches back long before the Scandian phase of the Caledonide Orogen, as indicated by abundant geochronological data. A minimum of eight discrete deformational phases have been identified and correlated across the nappe stack, which serve as the base for describing the joint history of Åreskutan (Figure 130). The deformation phase D5 could be regarded as a subset of D4, but is included as a separate phase (discussed below), bringing the total number of deformation phases to nine. The D1 phase incorporates inclusions and relict foliation that is difficult determine the relative age of between different nappes without geochronological investigation. In the Kall Nappe, and particularly in the Särv and Offerdal Nappes, where the early history is not as studied as in the Åreskutan Nappe, D1 is placed within a parenthesis without its own deformation phase designation. The D2 phases of the Särv and Offerdal Nappes also lack timing constraints and are put within parentheses as well. A summary of geochronological studies and ages of the nappe stack on Åreskutan and the related Sylan-Vålådalen area is compiled in table 6, correlated with inferred deformation phases. Dating by Claesson (1982) which confirmed metamorphism related to the Caledonian Orogeny in the Åreskutan Nappe will not be discussed in the following section due to wide errors. In the discussion below, D1-D9 refers to the overarching phases of figure 130, unless noted.

As described in the geological setting, the history of the Middle Allochton is a history of subduction, exhumation and foreland-directed thrusting. The juxtaposition of higher-grade over lower-grade nappes indicates that the higher nappe was subducted first and thrust over the lower during exhumation or foreland-directed thrusting. As such, younging of metamorphic- and deformation ages are expected going downwards from the topmost nappe. This is generally, but not entirely, the case for the nappe stack on Åreskutan (Figure 131). The difficulty of describing the history of Åreskutan partially lies in the lack of age constraints for metamorphism and deformation in the Särv and Offerdal Nappes where no petrological or geochronological investigations have been made in Jämtland. The other complication is the potentially polycyclic history of the Seve Nappe Complex, where age constraints are poor and pre-Caledonian history is overprinted. The deformation fabrics associated with each phase are highlighted in figure 132 and figure 133, showing the downwards progression of deformation in the nappe stack.

Absolute geochronological ages of the pre-anatectic history of the Åreskutan Nappe, D1, show a large spread, and may include more than one tectonothermal event. In the related Snasahögarna Nappe an ultra-high-pressure event is interpreted to have occurred at 482.6 ± 3.8 Ma, and rare zircons of similar age occurs in the Åreskutan Nappe (Ladenberger et al., 2014; Walczak et al., 2022). Dallmeyer et al. (1985) potentially described cooling after this event at ~ 465-455

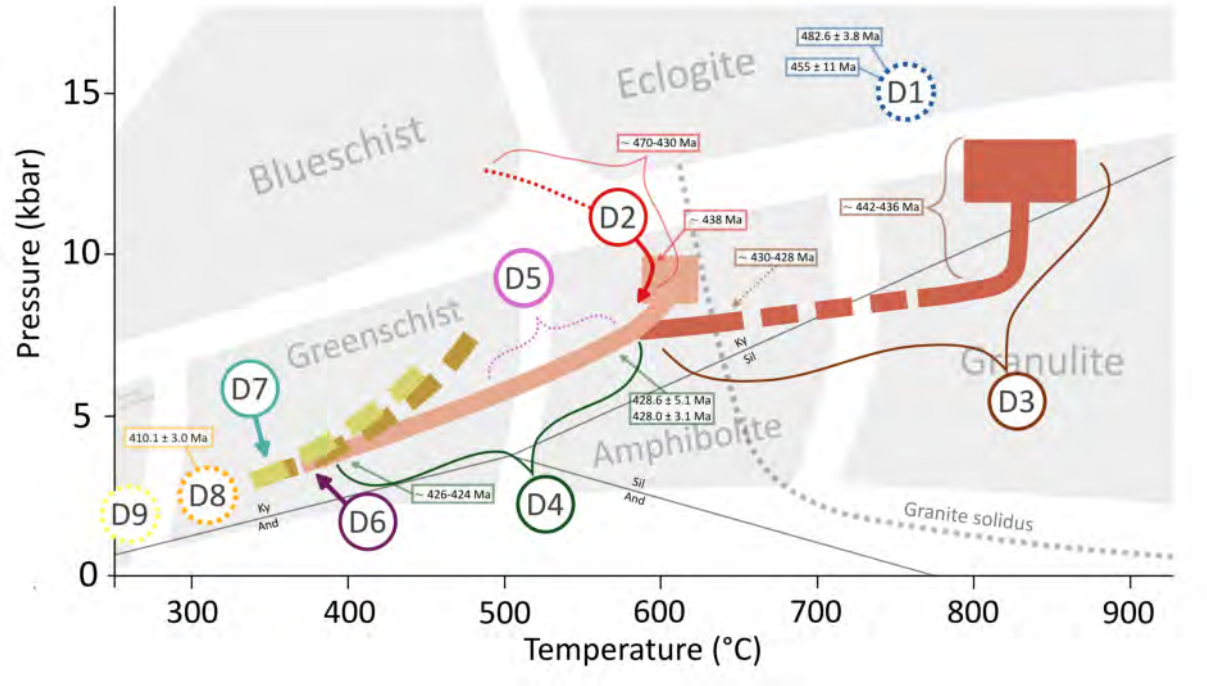


Figure 131: Proposed combined P-T-t path for West Jämtland nappe stack. The deformation phases outlined in this thesis shown where they are inferred to have occurred in P-T space. The displayed ages are explained in the text. Approximate fields of metamorphic facies are modified from Liou and Zhang (2003) and Winter (2021), with low-pressure facies omitted.

Ma. The timing of events and metamorphism leading into partial melting at granulite-facies conditions in the Årskutan Nappe is poorly constrained. Burial and prograde evolution is estimated at 463 ± 12 Ma and 457.5 ± 6.7 Ma (Li et al., 2020), and at 455 ± 11 Ma (Majka et al., 2012). As described in the section on the P-T path of the Åreskutan Nappe above, exhumation from ultra-high pressure conditions have been proposed to precede the granulite-facies overprint (Klonowska et al., 2017), but field observations can not be reconciled with this sequence of events as biotite in paragneiss restite and hydrous minerals in pyroxene amphibolite would not be present in an ultra-high-pressure assemblage.

Overlapping with D1, the first mylonitic foliation was developing in the Kall Nappe during phase D2. During this phase, there are indications of the Kall Nappe being exhumed from high-pressure conditions while heating during decompression, which produced the amphibolite-facies mineral assemblage seen in the field (Giuntoli et al., 2020). The duration of D2 is poorly constrained between 461 ± 21 Ma and 429 ± 20 Ma (Giuntoli et al., 2020). Prior to this the first of two leucogranite generations intruded the Kall Nappe, constrained at 470 ± 1.7 Ma and 468 ± 1.9 Ma (Li et al., 2021d), which is either related to an earlier phase in the history of the nappe, or shows protracted deformation during phase D2, within error of the constraints provided by Giuntoli et al. (2020). The second leucogranite generation intruded at ∼ 443 Ma, though with a large spread of zircon ages (Li et al., 2021d). Glodny et al. (2017) report an age of ∼ 438 Ma for the late phase of the amphibolite-facies overprint, i.e. the beginning the P-T path for the Kall Nappe proposed here. Li et al. (2021d) speculate that amphibolite-facies metamorphism intrusion of leucogranite in the Kall Nappe may be tied to juxtaposition of a hot Åreskutan Nappe, which potentially could have caused partial melting in the lower nappe. As described in the P-T path of the Kall Nappe, there is no textural evidence for partial melting in the metasedimentary rocks, and only sparse indications in amphibolite. There would likely have been a significant flux of CO_2 released from the calcareous rocks in the Mörvikshummeln formation, and signs of partial melting at the tectonic boundary, which is not supported by field observations.

Table 6: Geochronology of the nappe stack on Åreskutan and adjacent areas.

Nappe	Method	Age	Author's interpretation	Author	Notes
D1					
Snasahögarna	Zircon depth profiling	482.6 ± 3.8 Ma	Ultra-high-pressure event.	Walczak et al. (2022)	
Åreskutan	U-Pb zircon dating	489 ± 10 Ma 479 ± 10 Ma 461 ± 10 Ma 455 ± 8 Ma 453 ± 10 Ma 451 ± 8 Ma	Single-zircon populations, speculated to be related to early event, not statistically significant.	Ladenberger et al. (2014)	
Åreskutan	$^{40}Ar/^{39}Ar$ dating	465-455 Ma	Cooling after high-grade metamorphic event.	Dallmeyer et al. (1985)	Cooling of hornblende (500 C)
Åreskutan	U-Th-Pb monazite dating	463 ± 12 Ma 457.5 ± 6.7 Ma	Prograde evolution.	Li et al. (2020)	
Åreskutan	Monazite U–Th–total Pb chemical geochronology	455 ± 11 Ma	High-grade metamorphic event, subsolidus crystallisation of monazite.	Majka et al. (2012)	
D2					
Kall	$^{40}Ar/^{39}Ar$ dating	484 ± 9 Ma 458 ± 9 Ma 457 ± 9 Ma	Cooling after high-grade metamorphic event.	Dallmeyer et al. (1985)	Cooling of hornblende.
Kall	U-Pb zircon dating	470 ± 1.7 Ma 468 ± 1.9 Ma	Intrusion of leucogranite.	Li et al. (2021d)	Igneous zircon age in leucogranite.
Kall	U-Pb titanite dating	461 ± 21 Ma 429 ± 20 Ma	Incipient development of mylonitic foliation in amphibolite.	Giuntoli et al. (2020)	Authors interpret the range 460 - 430 Ma for development of mylonitic fabric prior to Scandian thrusting.
Kall	$^{40}Ar/^{39}Ar$ dating	444 ± 7 Ma	Cooling after high-grade metamorphic event, author speculates about Ar contamination of biotite.	Dallmeyer et al. (1985)	Cooling of biotite.
Kall	U-Pb zircon dating	∼ 443 Ma	Second generation of leucogranite intrusion.	Li et al. (2021d)	Igneous zircon age in leucogranite. Mean of a spread between 452 ± 3 Ma and 435 ± 3 Ma.
Kall	Rb-Sr mineral age	∼ 438 Ma	End of high-grade metamorphic stage.	Glodny et al. (2017)	Sampling in the COSC-1 core.
D3					
Åreskutan	U-Pb zircon dating	442 ± 4 Ma 442 ± 3 Ma 441 ± 4 Ma	Peak temperature conditions and partial melting in migmatitic paragneiss and felsic orthogneiss.	Ladenberger et al. (2014)	
Åreskutan	Monazite U–Th–total Pb chemical geochronology	439 ± 4 Ma 438 ± 4 Ma	Partial melting during decompression.	Majka et al. (2012)	
Snasahögarna	Zircon depth profiling	439.3 ± 3.6 Ma	Decompression melting, granulite-facies overprint.	Walczak et al. (2022)	
Snasahögarna	Multi-mineral Rb-Sr isochron age	437.8 ± 3.9 Ma	Crystallisation of leucosome.	Bender et al. (2019)	
Åreskutan	U-Pb zircon dating	436 ± 2 Ma	Felsic segregation in pyroxene amphibolite.	Ladenberger et al. (2014)	
Åreskutan	U-Pb zircon dating	430 ± 3 Ma 428 ± 4 Ma	Pegmatite intrusion, cutting the main foliation.	Ladenberger et al. (2014)	

Table 6: (continued)

Nappe	Method	Age	Author's interpretation	Author	Notes
D4					
Kall Nappe	$^{40}Ar/^{39}Ar$ dating	429 ± 8 Ma	Post-metamorphic cooling	Dallmeyer et al. (1985)	Cooling of biotite
Kall	Rb-Sr mineral age	∼ 429 Ma	Age of mylonitic overprint towards the base of the nappe.	Glodny et al. (2017)	
Snasahögarna Nappe	Multi-mineral Rb-Sr isochron age	428.8 ± 5.3 Ma	End stage of ductile deformation.	Bender et al. (2019)	
Snasahögarna - Blåhammarfjället Nappe boundary shear zone	Multi-mineral Rb-Sr isochron age	428.6 ± 5.1 Ma 428.0 ± 3.1 Ma	End of amphibolite-facies ductile deformation.	Bender et al. (2019)	
Åreskutan Nappe	$^{40}Ar/^{39}Ar$ dating	428 ± 7 Ma 427 ± 7 Ma	Post-metamorphic cooling	Dallmeyer et al. (1985)	Cooling of biotite
Blåhammarfjället Nappe, within the shear zone at the lower tectonic boundary.	Multi-mineral Rb-Sr isochron age	426.3 ± 3.2 Ma	End of ductile deformation at the Blåhammarfjället - Särv Nappe boundary.	Bender et al. (2019)	
Åreskutan - Kall Nappe boundary shear zone	Monazite U–Th–total Pb chemical geochronology	424 ± 6 Ma	Fluid-assisted growth of monazite within or in association with a shear zone.	Majka et al. (2012)	
Kall Nappe	40Ar/39Ar dating	423.4 ± 2.4 Ma 423.0 ± 5.0 Ma	Age of white mica and biotite recrystallised at greenschist facies conditions, from lower part of the Kall Nappe,	Jeanneret et al. (2022)	Ages from micaschist samples collected at 2500 m and 1880 m depth in the COSC-1 core, respectively.
Kall Nappe	U-Pb titanite dating	417 ± 9 Ma	Development of mylonitic foliation in micaschist at 5-8 kbar and 500-600°C.	Giuntoli et al. (2020)	
D6					
Kall Nappe	Inference	> 400 Ma, < 417 ± 9 Ma	Brittle-to-ductile deformation along discrete C - C' fabric at the base of the Kall Nappe. Neocrystallisation of chlorite and white mica at lower greenschist facies conditions. Exhumation of the Särv Nappe, juxtaposition of the Kall Nappe	Giuntoli et al. (2020)	
D8					
Jämtlandian Nappe Complex	Multi-mineral Rb-Sr isochron age	410.1 ± 3.0 Ma	Age of fine-grained deformation fabric, overthrusting of Middle Allochton.	Bender et al. (2019)	Quartzite sample from the eastern limb of the Skardøra Antiform, close to the basal thrust of the Middle Allochton.

The D3 phase overlaps with D2, pointing towards contemporaneous exhumation of the Åreskutan and Kall Nappes. D3 begins with partial melting of paragneiss in the kyanite stability field, constrained at ∼ 442-438 Ma (Majka et al., 2012; Ladenberger et al., 2014; Bender et al., 2019; Walczak et al., 2022). Crystallisation of paragneiss leucosome is dated to 437.8 ± 3.9 Ma, followed by slightly later by crystallisation of metabasite leucosome at 436 ± 2 Ma. Relatively unstrained leucosome can be observed in metabasite, meaning either reduced strain with time, or that the relatively rigid metabasite deflected strain around larger bodies, leaving undeformed leucosome within. The succession of kyanite-sillimanite-biotite marking D3 structures shows protracted deformation at progressively shallower depths and partial rehydration of migmatitic paragneiss. Crystallisation of pegmatites cutting the main foliation of the nappe can be interpreted as the end of melt presence, due to neocrystallisation along the cooling path and concentration of volatiles in the remaining melt. Pegmatite intrusion is dated at 430 ± 3 Ma and 428 ± 4 Ma (Ladenberger et al., 2014), close to the beginning of the next phase. Pegmatite has been described by Arnbom (1980) to be deflected into the lower tectonic boundary, meaning intrusion pre-dated the joint exhumation of the Kall and Åreskutan Nappes.

D4 ends the overlapping phases D2 and D3 by juxtaposition of the Åreskutan and Kall Nappes and joins the exhumation history of the Seve Nappe Complex. The assemblage at the tectonic boundary indicates it was active at amphibolite-facies conditions, and recrystallisation of clinopyroxene at the Kall Nappe side of the boundary constrain the active phase to near-peak-temperature conditions of the Kall Nappe. Retrogression of garnet further down in the Mörvikshummeln formation, though still close to the boundary, may signify juxtaposition at slightly lower than peak metamorphic conditions, though this may be a retrogressive overprint mediated by fluid flow and a high degree of recrystallisation. Both Arnbom (1980) and Majka et al. (2012) document two generations of garnet close the tectonic boundary in the Åreskutan Nappe, inferring growth of small idoblastic garnets when the tectonic boundary was active. Petrographic investigation in this thesis does not identify multiple garnet generations, but there is a high variety of colour in garnets across the nappe; from light pink and purple to deep burgundy red, with light pink garnets often found at lower structural levels. The asymmetry of the Kall Nappe likely formed during early D4, discussed below in the section on boudinage of the Åreskutan Nappe and strain partitioning within the Kall Nappe.

The end of amphibolite-facies ductile deformation in the Snasahögarna Nappe is dated at 428.8 ± 5.3 Ma, and in the Snasahögarna - Blåhammarfjället Nappe tectonic boundary at 428.6 ± 5.1 Ma and 428.0 ± 3.1 Ma (Bender et al., 2019). With the pre-juxtaposition intrusion of pegmatite in the Åreskutan Nappe described above, D4 can be inferred to have begun at ∼ 430-428 Ma. Growth of monazite is documented within the tectonic boundary shear zone in the Åreskutan Nappe at 424 ± 6 Ma (Majka et al., 2012), but it is not clear whether active deformation at the boundary or subsequent fluid circulation was dated. D4 continued through retrogression at greenschist-facies conditions, until the Seve Nappe Complex was stacked on top of the Särv Nappe which marks the beginning of the next deformation phase. The end of D4 is poorly constrained due to uncertainties of the metamorphic conditions during exhumation of the Särv Nappe and the juxtaposition of the Seve Nappe Complex. The fine-grained greenschist-facies fabric in mylonites close to the lower tectonic boundary of the Blåhammarfjället Nappe is dated to 426.3 ± 3.2 Ma and in the Kall Nappe to 423.4 ± 2.4 Ma and 423.0 ± 5.0 Ma (Bender et al., 2019; Jeanneret et al., 2022). These ages are interpreted either as stacking of the Seve Nappe Complex on top of the Särv Nappe (Jeanneret et al., 2022), or more generally as the end of ductile deformation in the nappe (Bender et al., 2019). Alternatively, Giuntoli et al. (2020) propose an age of 417 ± 9 Ma for the development of mylonitic fabric in the upper greenschist facies and put the juxtaposition of the Seve Nappe Complex between 417-400 Ma. This age is not included in the P-T-t path as it overlaps within error with both the amphibolite-facies deformation of the Åreskutan - Kall Nappe boundary and the age of deformation fabric of quartzite in the Lower Allochton at 410.1 ± 3.0 Ma (Bender et al., 2019).

D5 is an isolated deformation phase overlapping with D4, included as a discrete phase due to

the difficulty of relating the late shear zones cutting through the Åreskutan Nappe with the D4 deformation fabric. The primary deformation of the shear zones is top-to-the-east shearing, indicating differential transport speed of the blocks separated by the south to southeast-dipping major shear zones. Deflection of D3 foliation and subhorizontal to steep east-trending stretching lineation in the steep shear zones also show that there was appreciable vertical displacement. At the large scale, the deflection zone into the major late shear zones is small enough to give the appearance of large rigid blocks displaced by brittle faults. The major shear shear zones are envisioned to join the mylonitic foliation at the lower tectonic boundary, but there are indications that they postdate the active phase of the boundary at amphibolite-facies conditions, i.e. the plastic deformation of quartz but semi-brittle deformation of feldspar, meaning the shear zones were active at conditions below 500°C and $\sim$ 5 kbar (e.g. Fossen and Cavalcante, 2017). The late shear zones do not however seem to cross or displace the tectonic boundary, and are therefore interpreted to join it.

D6 has not been directly dated, and is constrained by developing after the fine-grained fabric in the lower Kall Nappe at $\sim$ 424-423 Ma, and prior to thrusting onto the Baltoscandian platform before $\sim$ 410 Ma. D6 can be related to the exhumation of the Särv Nappe and juxtaposition of the Seve Nappe Complex at lower greenschist-facies conditions. In the Särv Nappe, D6 overprints an earlier deformation phase likely related to burial and prograde metamorphism. Due to the lack of geochronological studies of the Särv Nappe, this early phase can only be constrained by the intrusion of the Baltoscandian Dyke Swarm at $\sim$ 600 Ma.

D7 is related to the exhumation of the Offerdal Nappe and juxtaposition of the Särv Nappe. Similar to D6, the D7 phase has not been directly dated and is constrained between the same ages with a slight delay of the beginning of the phase, as it developed after D6. The fabric related to D7 does not penetrate far into the Särv Nappe, and is mainly observed in the underlying unit. As in the Särv Nappe, the deformation during exhumation overprints a prior fabric which has not been dated. In the case of the Offerdal Nappe, the upper bound of the age of the early fabric is only constrained by deposition, as the nappe was not intruded by the Baltoscandian Dyke Swarm.

D8 is the final ductile deformation phase observed in the nappe stack, affecting the lower part of the Offerdal Nappe and the top of the Jämtlandian Nappes. The phase relates to the thrusting of the Middle Allochton onto the Baltoscandian platform and over the Jämtlandian Nappes of the orogenic foreland. The fine-grained deformation fabric at the top of the Jämtlandian Nappes in the Sylan area is dated to 410.1 $\pm$ 3.0 Ma (Bender et al., 2019), at which point the nappe stack observed at Åreskutan was likely fully assembled and on its way to its final resting place.

D9 is the final observed deformation phase, recorded in brittle deformation during thrusting across the nappe stack. There may be a large spread in ages and conditions during brittle deformation, and the D9 phase may overlap with earlier phases through brittle deformation of the higher nappes while the lower still deformed plastically. Slickensides in the Åreskutan Nappe are coated in white mica, not seen in nappes below, which could indicate brittle deformation and fluid circulation at least in the lower greenschist facies. D9 is not included in the deformation phase cross-sections (Figure 132; Figure 133) due to the minor deformation along each fault plane and distribution through the nappe stacke.

In summary, the deformation phases D1-D9 record the history of the Åreskutan nappe stack from the mid- to early Ordovician history of the Seve Nappe Complex through assembly of the Middle Allochton of the orogenic wedge to thrusting of the nappe stack over the orogenic foreland. Some phases are better constrained in time and P-T space than others, and it is clear our understanding of the Caledonide Orogen is far from complete.

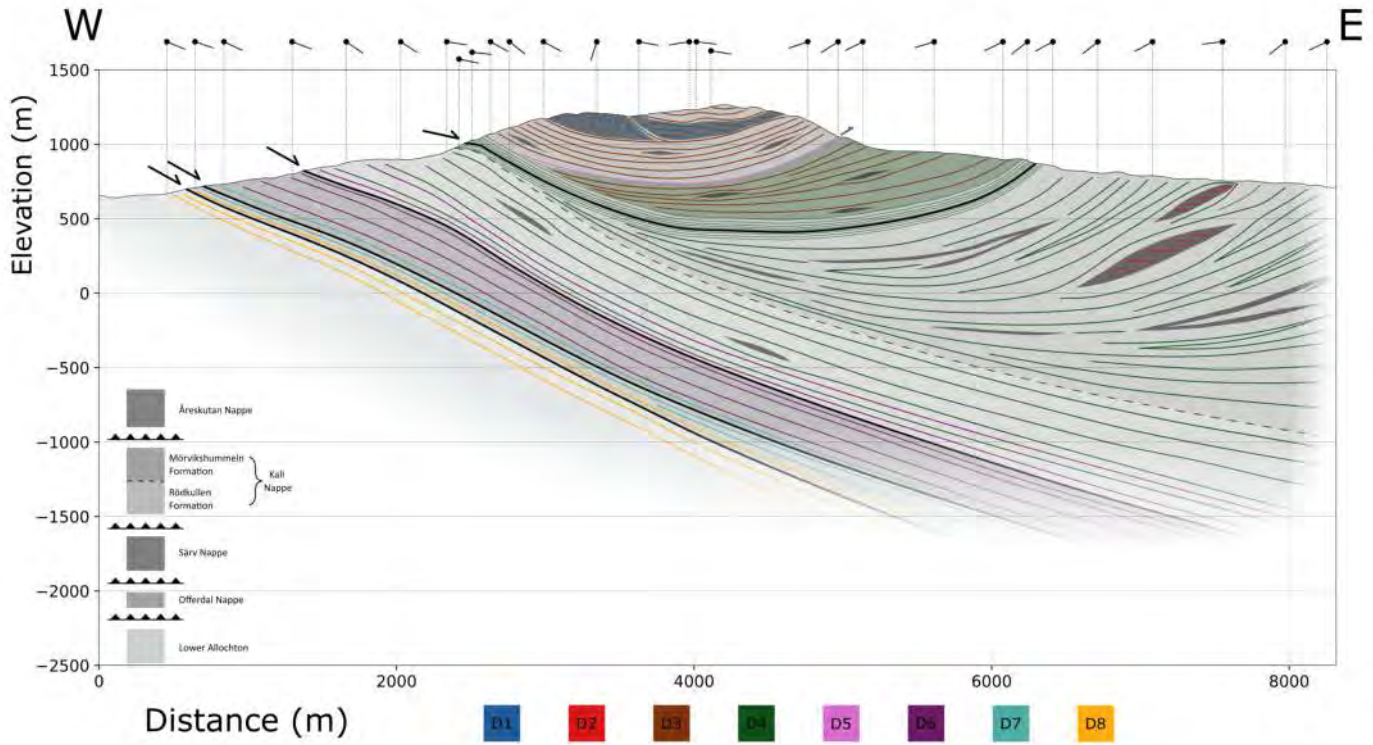


Figure 132: Cross-section 1 modified to show the structural locations of deformation fabrics developed during the deformation phases D1-D8.

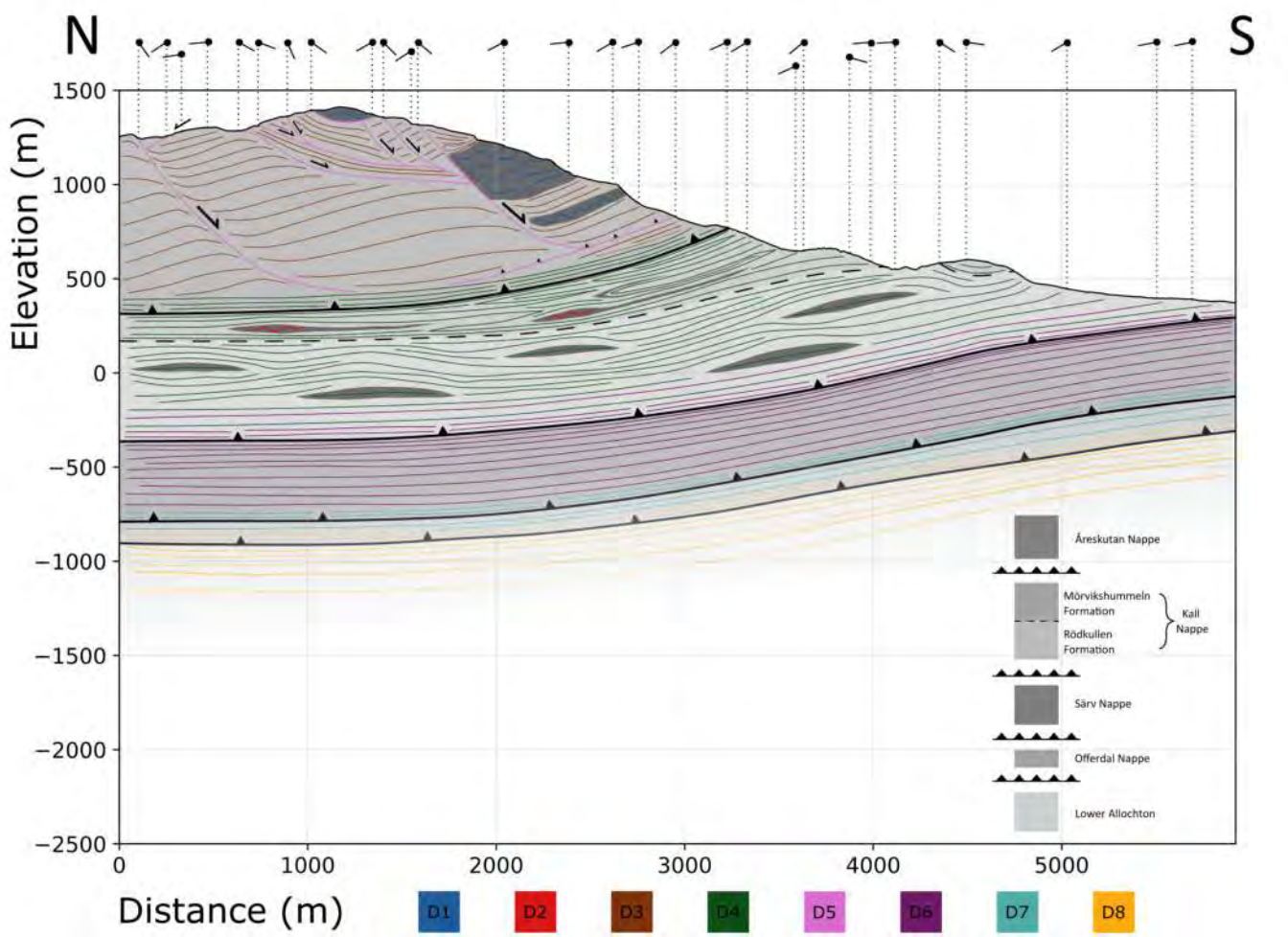


Figure 133: Cross-section 2 modified to show the structural locations of deformation fabrics developed during the deformation phases D1-D8.

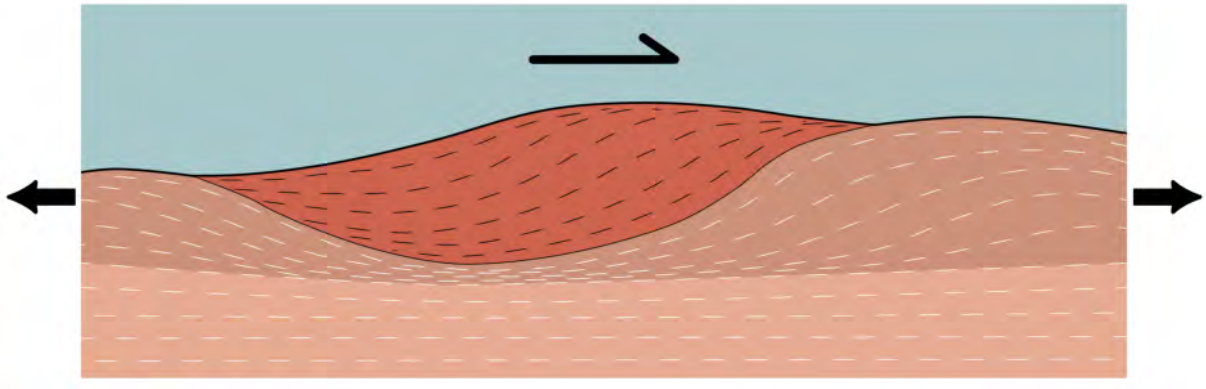


Figure 134: Conceptual sketch, parallel to the shear direction, of boudinage of the Åreskutan Nappe during exhumation of the Seve Nappe Complex through top-to-the-foreland thrusting and vertical ductile thinning. The shear zone separating the Middle and Upper Allochtons was active in the West Jämtland Nappe stack at this approximate time, and it's plausible the overriding rock package is the base of the Köli Nappe Complex (Bender et al., 2019). Legend for colours of the Seve Nappe Complex in figure 119.

8.3.5 Boudinage of the Åreskutan Nappe

The extreme asymmetry of the Kall Nappe is interpreted to have evolved during D4, which saw protracted shearing at progressively lower metamorphic grade. Exhumation of the Seve Nappe Complex in West Jämtland is attributed to subsimple shear, i.e. combination of protracted top-to-the-foreland thrusting and vertical ductile thinning, in contrast to further north in Västerbotten where the structure of the Seve Nappe Complex indicates extrusion wedge exhumation (Grimmer et al., 2015; Bender et al., 2018; Ma et al., 2022). Extensional regimes may cause crustal-scale boudinage of rheologically competent crustal packages, e.g. $>$ 10 km long granulite boudins deformed through a combination of top-to-the-west shear and ductile thinning during crustal extension and the exhumation of the Western Gneiss Region (Labrousse et al., 2002). The Åreskutan Nappe was relatively stiff during D4, evidenced by brittle veins cutting the foliation at high metamorphic grade and internal displacement of rigid blocks along late ductile shear zones, while the carbonate-rich Mörvikshummeln Formation of the Kall Nappe has been shown to be extremely plastically deformed. Foliation and tectonic boundary traces parallel to the stretching lineation shows that boudinage of the Åreskutan and Snasahögarna Nappe is likely the cause of the extreme deformation of the Kall Nappe at Åreskutan, as well as the large-scale dispersion of $>$ 10 km bodies and thinner lenses of the high-grade nappes within the Kall and Blåhammarfjället Nappes. Field observations integrated with subsurface data show that boudinage of the stiff Åreskutan Nappe was accommodated by the highly ductile Mörvikshummeln Formation of the Kall Nappe. Shortening below the Åreskutan Nappe caused highly ductile calc-silicate gneiss to flow outwards from the developing depression. Thickening primarily appears to have occurred in the direction of shear, but signs of strain accommodation can also be seen along the north-south cross-section (Figure 120). Boudinage and isoclinal folds are the primary modes of deformation observed in the Mörvikshummeln Formation, and the Åreskutan Nappe may have acted as a plow during exhumation, causing the Mörvikshummeln Formation to pile up in front of it through isoclinal folding of calc-silicate gneiss and boudinage of competent amphibolite bodies (Figure 134).

By contrast the Rödkullen Formation does not display the same degree of asymmetric deformation, though it is noted that only the western limb of the subunit has been observed, including in subsurface data. The rheological contrast and difference in accomodated strain between the Mörvikshummeln and Rödkullen Formations can be explained by sufficient calcite content in the upper unit. Calcite, which has been the most useful indicator to distinguish the Mörvikshummeln Formation in the field, deforms much more readily than quartzite, particularly at high differential

stress (Brodie and Rutter, 2000). The Rödkullen Formation is dominated by quartzofeldspathic metasandstone and amphibolite with subordinate micaschist, which likely could not flow as readily as the rocks of the Mörvikshummeln Formation.

8.4 Regional significance and implications

The observations and analysis presented in this thesis sets the Seve Nappe Complex in West Jämtland apart from nappes at the same structural position further north in northern Jämtland, Västerbotten and southern Norrbotten (Table 1). In all of these, high- or ultra-high-pressure metamorphism has been inferred from the presence of preserved high-pressure lithologies, e.g. eclogite, or metamorphic microdiamond (e.g. van Roermund, 1985; Majka et al., 2014a; Fassmer et al., 2021). In West Jämtland, ultra-high-pressure metamorphism has only been inferred from thermodynamic modelling and discoveries of metamorphic microdiamond; no high-pressure lithologies have been recorded in the field. Three explanations can be applied to this scenario: (1) No ultra-high-pressure metamorphism has occurred in the Åreskutan and Snasahögarna Nappe, as proposed by Li et al. (2020); (2) Ultra-high-pressure metamorphism occurred immediately prior to decompression melting in the kyanite stability field, with indicative lithologies completely overprinted in the granulite facies, as proposed by Klonowska et al. (2017); (3) Ultra-high-pressure metamorphism occurred at an earlier time, followed by exhumation and repeated subduction, as proposed by Brueckner and Van Roermund (2007). The 'Jämtlandian Orogeny' leading to eclogite-facies metamorphism in northern Jämtland described by Brueckner and Van Roermund (2007) is dated to $\sim$ 458 Ma, coinciding with estimates of prograde metamorphism in the Årskutan Nappe (Majka et al., 2012; Li et al., 2020). This event post-dates ultra-high-pressure metamorphism dated in Västerbotten and southern Norrbotten by $\sim$ 25-30 Ma (Barnes et al., 2022, *and references therein*). The recent find of an interpreted $\sim$ 380 Ma ultra-high-pressure event in the Snasahögarna Nappe (Walczak et al., 2022) might well indicate that a long stretch of the extended Baltoscandian margin, from Jämtland to Norrbotten today, was deeply subducted in the late Cambrian to early Ordovician, and that an isolated portion was involved in a subsequent subduction event $\sim$ 25-30 Ma later. However, why high-pressure lithologies were preserved in northern Jämtland and not on Åreskutan remains to be uncovered. Also, if a polycyclic history of the Åreskutan Nappe is used to explain a prior ultra-high-pressure event through preservation of metamorphic microdiamond in polycyclic garnet, such multi-stage garnets are easily recognized through new growth in fractures and overgrowth rims (e.g. Manzotti et al., 2024), something not reported in garnet in the Åreskutan or Snasahögarna Nappes.

This thesis also highlights our poor understanding of the assembly of the Middle Allochton after the exhumation of the Seve Nappe Complex. While researching the current understanding of the Caledonide Orogen, no absolute dating studies were been found which directly target the Särv or Offerdal Nappe in regards to timing of metamorphism, exhumation or incorporation in the orogenic wedge. Doing this would help refine our understanding of the incipient orogeny and the timing of thrusting onto the Baltoscandian platform.

9 Conclusions

- This study shows that careful geological field mapping through outcrop observation, structural measurements and field photography is an important tool to understand the structure and metamorphic history of orogens. The production of geological maps enables drawing of cross-sections, which in turn are a key to visualize geometry, deformation and metamorphism. The area around Åreskutan in particular has been of interest for geologists for over 150 years, and the cross-sections presented in this thesis provide a much-needed structural framework for the West Jämtland nappe stack.
- In orogens with complex deformation, such as the Scandinavian Caledonides, geological field mapping alone is insufficient to explain structural anomalies that only can be partially described at the surface. Subsurface surveys, e.g. seismic investigations, are likewise insufficient to explain the subsurface geometry without a structural framework developed by looking at the surface geology.
- There is no field evidence for "hot" juxtaposition of the West Jämtland nappe stack. The metamorphic grade of the nappes is inverted in relation to Barrovian metamorphic zonation, but the tectonic boundaries investigated in this thesis indicate that each subsequent stacking event occurred at metamorphic conditions lower than the peak of the nappes on either side of the tectonic boundary.
- The local geometry of the Seve Nappe Complex was primarily controlled by strain partitioning in the calc-silicate-rich Mörvikshummeln Formation of the Kall Nappe during exhumation at amphibolite facies conditions. The Åreskutan Nappe is proposed to have been exhumed as a semi-rigid boudin accomodated by the ductile Kall Nappe in a subsimple shear regime. This model also explains the spotty distribution of the related Snasahögarna Nappe in the Sylan Area; as the West Jämtland nappe stack was assembled, boudins of the Middle Seve Nappes may already have separated and not formed a continuous, now eroded, unit.

10 Proposals for future research

- To further our understanding of the pre-anatectic history of the Åreskutan Nappe, petrological investigation of palaesome pods may give clues to prior events and conditions.
- Absolute age dating of the Kall - Särv Nappe boundary and the Särv - Offerdal Nappe boundary as well as petrological investigation into conditions when the boundaries were active will refine our understanding of all the building blocks of the Middle Allochton.
- Petrological and microstructure deformation studies of the Kall Nappe immediately below and the Åreskutan Nappe immediately above the tectonic boundary may help constrain conditions at juxtaposition and joint exhumation of the Seve Nappe Complex.

11 References

References

Abdelmalak, M. M., Andersen, T. B., Planke, S., Faleide, J. I., Corfu, F., Tegner, C., Shephard, G. E., Zastrozhnov, D., and Myklebust, R. (2015). The ocean-continent transition in the mid-Norwegian margin: Insight from seismic data and an onshore Caledonian field analogue. *Geology*, 43(11):1011–1014.

Albrecht, L. (2000). *Early structural and metamorphic evolution of the Scandinavian Caledonides a study of the eclogite-bearing Seve Nappe Complex at the Arctic Circle, Sweden*. PhD Thesis, Lund University.

Andersen, T. B., Jakob, J., Kjøll, H. J., and Tegner, C. (2022). Vestiges of the Pre-Caledonian Passive Margin of Baltica in the Scandinavian Caledonides: Overview, Revisions and Control on the Structure of the Mountain Belt. *Geosciences*, 12(2):57.

Andreasson, P. (1978). Aspects of the lithology and structure of the Leksdalsvann Group, Tömmerås window, Central Norwegian Caledonides. *Norsk Geologisk Tidsskrift*, 58:109–112.

Andreasson, P. G. and Lagerblad, B. (1980). Occurrence and significance of inverted metamorphic gradients in the western Scandinavian Caledonides. *Journal of the Geological Society*, 137(3):219–230.

Andréasson, P.-G. (1987). Early evolution of the Late Proterozoic Baltoscandian margin: Inferences from rift magmatism. *Geologiska Föreningen i Stockholm Förhandlingar*, 109(4):336–340.

Andréasson, P.-G. (2020). The continent-ocean (Seve-Köli) boundary in the Sarek-Padjelanta Mts. revisited: Swedish Caledonides. *Geologiska Föreningen i Stockholm Förhandlingar*, 142(2):125–138.

Andréasson, P.-G. and Albrecht, L. (1995). Derivation of 500 Ma eclogites from the passive margin of Baltica and a note on the tectonometamorphic heterogeneity of eclogite-bearing crust. *Geological Magazine*, 132(6):729–738.

Andréasson, P.-G., Allen, A., Aurell, O., Boman, D., Ekestubbe, J., Goerke, U., Lundgren, A., Nilsson, P., and Sandelin, S. (2018). Seve terranes of the Kebnekaise Mts., Swedish Caledonides, and their amalgamation, accretion and affinity. *Geologiska Föreningen i Stockholm Förhandlingar*, 140(3):264–291.

Andréasson, P.-G., Svenningsen, O., Johansson, I., Solyom, Z., and Xiaodan, T. (1992). Mafic dyke swarms of the Baltica-Iapetus transition, Seve Nappe Complex of the Sarek Mts., Swedish Caledonides. *Geologiska Föreningen i Stockholm Förhandlingar*, 114(1):31–45.

Andréasson, P.-G., Svenningsen, O. M., and Albrecht, L. (1998). Dawn of Phanerozoic orogeny in the North Atlantic tract; Evidence from the Seve-Kalak Superterrane, Scandinavian Caledonides. *Geologiska Föreningen i Stockholm Förhandlingar*, 120(2):159–172.

Arnbom, J.-O. (1980). Metamorphism of the Seve Nappes at Åreskutan, Swedish Caledonides. *Geologiska Föreningen i Stockholm Förhandlingar*, 102(4):359–371.

Asklund, B. (1962). Berggrunden inom fjällkedjan och dess randområden. In *Ba 16 Beskrivning till karta över Sveriges berggrund*, pages 171–224. Sveriges Geologiska Undersökning.

Baird, G. B., Figg, S. A., and Chamberlain, K. R. (2014). Intrusive age and geochemistry of the Kebne Dyke Complex in the Seve Nappe Complex, Kebnekaise Massif, arctic Sweden Caledonides. *Geologiska Föreningen i Stockholm Förhandlingar*, 136(4):556–570.

Barnes, C., Majka, J., Schneider, D., Walczak, K., Bukała, M., Kośmińska, K., Tokarski, T., and Karlsson, A. (2019). High-spatial resolution dating of monazite and zircon reveals the timing

of subduction–exhumation of the Vaimok Lens in the Seve Nappe Complex (Scandinavian Caledonides). *Contributions to Mineralogy and Petrology*, 174(1):5.

Barnes, C. J., Bukała, M., Callegari, R., Walczak, K., Kooijman, E., Kielman-Schmitt, M., and Majka, J. (2022). Zircon and monazite reveal late Cambrian/early Ordovician partial melting of the Central Seve Nappe Complex, Scandinavian Caledonides. *Contributions to Mineralogy and Petrology*, 177(9):92.

Barnes, C. J., Gilio, M., Bukała, M., Włodek, A., Majka, J., and Smit, M. (2023). Garnet–Quartz Inclusion Thermobarometry and Lu–Hf Chronology Detail the Pre-Ultra-High Pressure Metamorphic History of the Grapesvare Nappe, Scandinavian Caledonides. *Journal of Petrology*, 64(12):egad086.

Beckholmen, M. (1978). Geology of the Nordhallen—Duved—Greningen area in Jämtland, central Swedish Caledonides. *Geologiska Föreningen i Stockholm Förhandlingar*, 100(4):335–347.

Bender, H., Glodny, J., and Ring, U. (2019). Absolute timing of Caledonian orogenic wedge assembly, Central Sweden, constrained by Rb–Sr multi-mineral isochron data. *Lithos*, 344-345:339–359.

Bender, H., Ring, U., Almqvist, B., Grasemann, B., and Stephens, M. (2018). Metamorphic Zonation by Out-of-Sequence Thrusting at Back-Stepping Subduction Zones: Sequential Accretion of the Caledonian Internides, Central Sweden. *Tectonics*, 37:3545–3576.

Bergman, S. (1992). P-T paths in the Handöl area, central Scandinavia: record of Caledonian accretion of outboard rocks to the Baltoscandian margin. *Journal of Metamorphic Geology*, 10(2):265–281.

Bergman, S. (1993). Geology and geochemistry of mafic-ultramafic rocks (Köli) in the Handol area, central Scandinavian Caledonides. *Norsk Geologisk Tidsskrift*, 73:21–42.

Be'eri-Shlevin, Y., Gee, D., Claesson, S., Ladenberger, A., Majka, J., Kirkland, C., Robinson, P., and Frei, D. (2011). Provenance of Neoproterozoic sediments in the Särv nappes (Middle Allochthon) of the Scandinavian Caledonides: LA-ICP-MS and SIMS U–Pb dating of detrital zircons. *Precambrian Research*, 187(1-2):181–200.

Bingen, B., Demaiffe, D., and Breemen, O. (1998). The 616 Ma Old Egersund Basaltic Dike Swarm, Sw Norway, and Late Neoproterozoic Opening of the Iapetus Ocean. *The Journal of Geology*, 106(5):565–574.

Blomdin, R., Peterson Becher, G., Smith, C. A., Regnell, C., Öhrling, C., Goodfellow, B. W., and Mikko, H. (2021). *K 705 Beskrivning till geomorfologiska kartan, Jämtlands län.* Sveriges Geologiska Undersökning, Uppsala.

Brodie, K. H. and Rutter, E. H. (2000). Deformation mechanisms and rheology: why marble is weaker than quartzite. *Journal of the Geological Society*, 157(6):1093–1096.

Brueckner, H. K. and Van Roermund, H. L. (2007). Concurrent HP metamorphism on both margins of Iapetus: Ordovician ages for eclogites and garnet pyroxenites from the Seve Nappe Complex, Swedish Caledonides. *Journal of the Geological Society*, 164(1):117–128.

Bryhni, I. and Andreasson, P. (1985). Metamorphism in the Scandinavian Caledonides. In Gee, D. G. and Sturt, B. A., editors, *The Caledonide Orogen - Scandinavia and Related Areas.* Wiley, Chichester.

Bukała, M., Barnes, C. J., Jeanneret, P., Hidas, K., Mazur, S., Almqvist, B. S. G., Kośmińska, K., Klonowska, I., Šurka, J., and Majka, J. (2020a). Brittle Deformation During Eclogitization of Early Paleozoic Blueschist. *Frontiers in Earth Science*, 8:594453.

Bukała, M., Klonowska, I., Barnes, C., Majka, J., Kośmińska, K., Janák, M., Fassmer, K., Broman, C., and Luptáková, J. (2018). UHP metamorphism recorded by phengite eclogite from the Caledonides of northern Sweden: *P–T* path and tectonic implications. *Journal of Metamorphic Geology*, 36(5):547–566.

Bukała, M., Majka, J., Walczak, K., Włodek, A., Schmitt, M., and Zagórska, A. (2020b). U-Pb Zircon Dating of Migmatitic Paragneisses and Garnet Amphibolite from the High Pressure Seve Nappe Complex in Kittelfjäll, Swedish Caledonides. *Minerals*, 10(4):295.

Callegari, R., Kośmińska, K., Klonowska, I., Barnes, C. J., and Majka, J. (2023). Magmatism and metamorphism of the Mårma Terrane, Kebnekaise region, northern Swedish Caledonides. In *Proceedings of EGU General Assembly 2023*, Vienna, Austria.

Carter, I. S. M., Cuthbert, S. J., Walczak, K., Ziemniak, G., Kooijman, E., and Majka, J. (2023). Cambrian ages for metavolcanic rocks in the Lower Köli Nappes, Swedish Caledonides: implications for the status of the Virisen arc terrane. *Journal of the Geological Society*, 180(6):jgs2022–130.

Cesare, B., Ferrero, S., Salvioli-Mariani, E., Pedron, D., and Cavallo, A. (2009). "Nanogranite" and glassy inclusions: The anatectic melt in migmatites and granulites. *Geology*, 37(7):627–630.

Claesson, S. (1982). Caledonian metamorphism of Proterozoic Seve rocks on Mt. Åreskutan, southern Swedish Caledonides. *Geologiska Föreningen i Stockholm Förhandlingar*, 103(3):291–304.

Claesson, S., Stephens, M. B., and Klingspor, I. (1988). U-Pb zircon dating of felsic intrusions, Middle Kali Nappes, central Scandinavian Caledonides. *Norsk Geologisk Tidsskrift*, 67:89–97.

Corfu, F., Andersen, T. B., and Gasser, D. (2014). The Scandinavian Caledonides: main features, conceptual advances and critical questions. *Geological Society, London, Special Publications*, 390(1):9–43.

Dallmeyer, R. D., Andréasson, P. G., and Svenningsen, O. (1991). Initial tectonothermal evolution within the Scandinavian Caledonide Accretionary Prism: constraints from ^{40} Ar/ ^{39} Ar mineral ages within the Seve Nappe Complex, Sarek Mountains, Sweden. *Journal of Metamorphic Geology*, 9(2):203–218.

Dallmeyer, R. D., Gee, D. G., and Beckholmen, M. (1985). ^{40} Ar/ ^{39} Ar mineral age record of early Caledonian tectonothermal activity in the Baltoscandian miogeocline, Cental Scandinavia. *American Journal of Science*, 285:532–568.

DesOrmeau, J. W., Gordon, S. M., Kylander-Clark, A. R., Hacker, B. R., Bowring, S. A., Schoene, B., and Samperton, K. M. (2015). Insights into (U)HP metamorphism of the Western Gneiss Region, Norway: A high-spatial resolution and high-precision zircon study. *Chemical Geology*, 414:138–155.

Fassmer, K., Froitzheim, N., Janák, M., Strohmeyer, M., Bukała, M., Lagos, M., and Münker, C. (2021). Diachronous collision in the Seve Nappe Complex: Evidence from Lu–Hf geochronology of eclogites (Norrbotten, North Sweden). *Journal of Metamorphic Geology*, 39(7):819–842.

Fassmer, K., Klonowska, I., Walczak, K., Andersson, B., Froitzheim, N., Majka, J., Fonseca, R. O. C., Münker, C., Janák, M., and Whitehouse, M. (2017). Middle Ordovician subduction of continental crust in the Scandinavian Caledonides: an example from Tjeliken, Seve Nappe Complex, Sweden. *Contributions to Mineralogy and Petrology*, 172(11-12):103.

Forshaw, J. B., Waters, D. J., Pattison, D. R. M., Palin, R. M., and Gopon, P. (2019). A comparison of observed and thermodynamically predicted phase equilibria and mineral compositions in mafic granulites. *Journal of Metamorphic Geology*, 37(2):153–179.

Fossen, H. (2010). Extensional tectonics in the North Atlantic Caledonides: a regional view. *Geological Society, London, Special Publications*, 335(1):767–793.

Fossen, H. and Cavalcante, G. C. G. (2017). Shear zones – A review. *Earth-Science Reviews*, 171:434–455.

Foster, T. (1990). Control of material transport and reaction mechanisms by metastable mineral assemblages: An example involving kyanite, sillimanite, muscovite and quartz. In Spencer, R. and Chou, I.-M., editors, *Fluid-Mineral Interactions: A Tribute to H.P. Eugster.* The Geochemical Society.

Gee, D. G. (1975a). *A geotraverse through the Scandinavian Caledonides-Östersund to Trondheim.* Number C 717 in Sveriges Geologiska Undersökning Ser C Avhandlingar och uppsatser. Sveriges Geologiska Undersökning, Stockholm.

Gee, D. G. (1975b). A tectonic model for the central part of the Scandinavian Caledonides. *American Journal of Science*, 275:468–515.

Gee, D. G., Andréasson, P.-G., Lorenz, H., Frei, D., and Majka, J. (2015). Detrital zircon signatures of the Baltoscandian margin along the Arctic Circle Caledonides in Sweden: The Sveconorwegian connection. *Precambrian Research*, 265:40–56.

Gee, D. G., Fossen, H., Henriksen, N., and Higgins, A. (2008). From the Early Paleozoic Platforms of Baltica and Laurentia to the Caledonide Orogen of Scandinavia and Greenland. *Episodes*, 31(1):44–51.

Gee, D. G., Guezou, J.-C., Roberts, D., and Wolff, F. (1985). The central-southern part of the Scandinavian Caledonides. In Gee, D. G. and Sturt, B. A., editors, *The Caledonide Orogen - Scandinavia and Related Areas.* Wiley, Chichester.

Gee, D. G., Juhlin, C., Pascal, C., and Robinson, P. (2010). Collisional Orogeny in the Scandinavian Caledonides (COSC). *Geologiska Föreningen i Stockholm Förhandlingar*, 132(1):29–44.

Gee, D. G., Klonowska, I., Andréasson, P.-G., and Stephens, M. B. (2020). Middle thrust sheets in the Caledonide orogen, Sweden: the outer margin of Baltica, the continent–ocean transition zone and late Cambrian–Ordovician subduction–accretion. *Geological Society, London, Memoirs*, 50(1):517–548.

Gee, D. G. and Kumpulainen, R. (1980). *An excursion through the Caledonian mountain chain in central Sweden from Östersund to Storlien: guide to excursion no. 003A of the 26th International Geological Congress, Paris, 1980.* Number C 774 in Sveriges Geologiska Undersökning Ser C Avhandlingar och uppsatser. Sveriges geologiska undersökning, Uppsala, Vällingby. OCLC: 10380870.

Gee, D. G., Ladenberger, A., Dahlqvist, P., Majka, J., Be'eri-Shlevin, Y., Frei, D., and Thomsen, T. (2014). The Baltoscandian margin detrital zircon signatures of the central Scandes. *Geological Society, London, Special Publications*, 390(1):131–155.

Gee, D. G. and Stephens, M. B. (2020a). Lower thrust sheets in the Caledonide orogen, Sweden: Cryogenian–Silurian sedimentary successions and underlying, imbricated, crystalline basement. *Geological Society, London, Memoirs*, 50(1):495–515.

Gee, D. G. and Stephens, M. B. (2020b). Regional context and tectonostratigraphic framework of the early–middle Paleozoic Caledonide orogen, northwestern Sweden. *Geological Society, London, Memoirs*, 50(1):481–494.

Ghosh, S. K., Roy, A. B., and Troëng, B. (1979). Superposed folding and metamorphism in the Seve nappe around Åreskutan in the Swedish Caledonides. *Geologiska Föreningen i Stockholm Förhandlingar*, 101(2):85–103.

Gilotti, J. A. (1989). Reaction progress during mylonitization of basaltic dikes along the S irv thrust, Swedish Caledonides. *Contributions to Mineralogy and Petrology*, 101:30–45.

Gilotti, J. A. and Kumpulainen, R. (1986). Strain softening induced ductile flow in the Särv thrust sheet, Scandinavian Caledonides. *Journal of Structural Geology*, 8(3-4):441–455.

Giuntoli, F., Menegon, L., Warren, C., Darling, J., and Anderson, M. (2020). Protracted Shearing at Midcrustal Conditions During Large-Scale Thrusting in the Scandinavian Caledonides. *Tectonics*, 39(e2020TC006267).

Giuntoli, F., Menegon, L., and Warren, C. J. (2018). Replacement reactions and deformation by dissolution and precipitation processes in amphibolites. *Journal of Metamorphic Geology*, 36(9):1263–1286.

Glodny, J., Hierold, J., and Harms, U. (2017). Direct dating of ductile deformation within the Caledonian nappe stack: Rb-Sr mineral data and element mapping from the COSC-1 drill core. In *Proceedings of EGU General Assembly 2017*, Vienna, Austria.

Greiling, R. O., Kathol, B., and Kumpulainen, R. A. (2018). Nappe units along the Caledonian margin in central Scandinavia (Grong–Olden to Nasafjället): definition, distinction criteria and tectonic evolution. *GFF*, 140(1):66–89.

Greiling, R. O., Kathol, B., and Kumpulainen, R. A. (2023). An early Cambrian post-rift basin within the Baltica–Iapetus passive margin (north-central Scandinavian Caledonides). *International Journal of Earth Sciences*.

Greiling, R. O., Oszczypko, N., and Garfunkel, Z. (2013). A comparison of two orogenic margins: central Scandinavian Caledonides and western Outer Carpathians. *Zeitschrift der Deutschen Gesellschaft für Geowissenschaften*, 164(1):9–32.

Grimmer, J. C., Glodny, J., Drüppel, K., Greiling, R. O., and Kontny, A. (2015). Early- to mid-Silurian extrusion wedge tectonics in the central Scandinavian Caledonides. *Geology*, 43(4):347–350.

Grimmer, J. C. and Greiling, R. O. (2012). Serpentinites and low-K island arc meta-volcanic rocks in the Lower Köli Nappe of the central Scandinavian Caledonides: Late Cambrian–early Ordovician serpentinite mud volcanoes in a forearc basin? *Tectonophysics*, 541-543:19–30.

Groppo, C., Rolfo, F., and Indares, A. (2012). Partial Melting in the Higher Himalayan Crystallines of Eastern Nepal: the Effect of Decompression and Implications for the 'Channel Flow' Model. *Journal of Petrology*, 53(5):1057–1088.

Hansen, E., Johansson, L., Andersson, J., LaBarge, L., Harlov, D., Möller, C., and Vincent, S. (2015). Partial melting in amphibolites in a deep section of the Sveconorwegian Orogen, SW Sweden. *Lithos*, 236-237:27–45.

Hedin, P., Almqvist, B., Berthet, T., Juhlin, C., Buske, S., Simon, H., Giese, R., Krauß, F., Rosberg, J.-E., and Alm, P.-G. (2016). 3D reflection seismic imaging at the 2.5km deep COSC-1 scientific borehole, central Scandinavian Caledonides. *Tectonophysics*, 689:40–55.

Hedin, P., Juhlin, C., and Gee, D. G. (2012). Seismic imaging of the Scandinavian Caledonides to define ICDP drilling sites. *Tectonophysics*, 554-557:30–41.

Hedin, P., Malehmir, A., Gee, D. G., Juhlin, C., and Dyrelius, D. (2014). 3D interpretation by integrating seismic and potential field data in the vicinity of the proposed COSC-1 drill site, central Swedish Caledonides. *Geological Society, London, Special Publications*, 390(1):301–319.

Helfrich, H. K. (1967). *Ein Beitrag zur Geologie des Åregebietes.* Number C 612 in Sveriges Geologiska Undersökning Ser C Avhandlingar och uppsatser. Sveriges Geologiska Undersökning, Uppsala.

Hisinger, W. (1819). *Anteckningar i Physik och Geognosi under resor uti Sverige och Norrige. First Compendium.* Palmblad & C, Uppsala.

Hollocher, K., Robinson, P., Van Nostrand, M., and Walsh, E. (2022). The Blåhø Nappe, central Norwegian Scandinavian Caledonides: An oceanic arc–back-arc assemblage distinct from the Seve Nappe Complex. In Kuiper, Y. D., Murphy, J. B., Nance, R. D., Strachan, R. A., and Thompson, M. D., editors, *New Developments in the Appalachian-Caledonian-Variscan Orogen*, pages 315–334. Geological Society of America.

Hollocher, K., Robinson, P., Walsh, E., and Roberts, D. (2012). Geochemistry of amphibolite-facies volcanics and gabbros of the Støren Nappe in extensions west and southwest of Trondheim, western gneiss region, Norway: A key to correlations and paleotectonic settings. *American Journal of Science*, 312(4):357–416.

Hollocher, K., Robinson, P., Walsh, E., and Terry, M. P. (2007). The Neoproterozoic Ottfjallet dike swarm of the Middle Allochthon, traced geochemically into the Scandian Hinterland, Western Gneiss Region, Norway. *American Journal of Science*, 307(6):901–953.

Högbom, A. G. (1909). Studies in the post-Silurian thrust region of Jämtland. *Geologiska Föreningen i Stockholm Förhandlingar*, 31(5):289–346.

Högbom, A. G. (1920). *Geologisk beskrivning över Jämtlands Län.* Number C 140 in Sveriges Geologiska Undersökning Ser C Avhandlingar och uppsatser. Sveriges Geologiska Undersökning, Uppsala, 2 edition.

Jakob, J., Andersen, T. B., and Kjøll, H. J. (2019). A review and reinterpretation of the architecture of the South and South-Central Scandinavian Caledonides—A magma-poor to magma-rich transition and the significance of the reactivation of rift inherited structures. *Earth-Science Reviews*, 192:513–528.

Jakob, J., Andersen, T. B., Mohn, G., Kjøll, H. J., and Beyssac, O. (2022). Revised tectonostratigraphic scheme for the Scandinavian Caledonides and its implications for our understanding of the Scandian orogeny. In Kuiper, Y. D., Murphy, J. B., Nance, R. D., Strachan, R. A., and Thompson, M. D., editors, *New Developments in the Appalachian-Caledonian-Variscan Orogen*, pages 335–374. Geological Society of America.

Janák, M., Van Roermund, H., Majka, J., and Gee, D. (2013). UHP metamorphism recorded by kyanite-bearing eclogite in the Seve Nappe Complex of northern Jämtland, Swedish Caledonides. *Gondwana Research*, 23(3):865–879.

Jeanneret, P., Klonowska, I., Barnes, C., Majka, J., Holmberg, J., Gilio, M., Nachlas, W., Alvaro, M., Kośmińska, K., Lorenz, H., Zack, T., Ladenberger, A., and Koyi, H. (2022). Deciphering the tectonometamorphic history of subducted metapelites using quartz-in-garnet and Ti-in-quartz (QuiG–TiQ) geothermobarometry—A key for understanding burial in the Scandinavian Caledonides. *Journal of Metamorphic Geology*, 41(2):235–270.

Juhojuntti, N., Juhlin, C., and Dyrelius, D. (2001). Crustal reflectivity underneath the Central Scandinavian Caledonides. *Tectonophysics*, 334:191–210.

Karis, L. and Strömberg, A. G. B. (1998). *Beskrivning till berggrundskartan över Jämtlands län. Del 2: Fjälldelen.* Number Ca 53:2 in SGU series Ca, Research papers, SGU series Ca, Forskningsrapporter. Sveriges Geologiska Undersökning, Uppsala.

Kjøll, H. J. (2020). Late Neoproterozoic basin evolution of the magma rich Iapetus margin of Baltica. *Norwegian Journal of Geology*, 100:202005.

Kjøll, H. J., Andersen, T., Corfu, F., Labrousse, L., Tegner, C., Abdelmalak, M. M., and Planke, S. (2019). Timing of Breakup and Thermal Evolution of a Pre-Caledonian Neoproterozoic Exhumed Magma-Rich Rifted Margin. *Tectonics*, 38:1843–1862.

Klonowska, I., Janák, M., Majka, J., Froitzheim, N., and Kośmińska, K. (2016). Eclogite and garnet pyroxenite from Stor Jougdan, Seve Nappe Complex, Sweden: implications for UHP metamorphism of allochthons in the Scandinavian Caledonides. *Journal of Metamorphic Geology*, 34(2):103–119.

Klonowska, I., Janák, M., Majka, J., Petrík, I., Froitzheim, N., Gee, D. G., and Sasinková, V. (2017). Microdiamond on Åreskutan confirms regional UHP metamorphism in the Seve Nappe Complex of the Scandinavian Caledonides. *Journal of Metamorphic Geology*, 35(5):541–564.

Klonowska, I., Majka, J., Janák, M., Gee, D. G., and Ladenberger, A. (2014). Pressure–temperature evolution of a kyanite–garnet pelitic gneiss from Åreskutan: evidence of ultra-high-pressure metamorphism of the Seve Nappe Complex, west-central Jämtland, Swedish Caledonides. *Geological Society, London, Special Publications*, 390(1):321–336.

Klonowska, I., Majka, J., Janák, M., Petrík, I., Froitzheim, N., Gee, D. G., and Cuthbert, S. (2021). Comment on the paper: "Evolution of a gneiss in the Seve nappe complex of central Sweden – Hints at an early Caledonian, medium-pressure metamorphism" by. *Lithos*, 400-401:106067.

Kriegsman, L. M. (2001). Partial melting, partial melt extraction and partial back reaction in anatectic migmatites. *Lithos*, 56(1):75–96.

Kriegsman, L. M. and Álvarez Valero, A. M. (2010). Melt-producing versus melt-consuming reactions in pelitic xenoliths and migmatites. *Lithos*, 116(3-4):310–320.

Krill, A. G. (1980). Tectonics of the Oppdal area, central Norway. *Geologiska Föreningen i Stockholm Förhandlingar*, 102(4):523–530.

Kumpulainen, R. (1980). Upper Proterozoic stratigraphy and depositional environments of the Tossåsfjället Group, Särv Nappe, southern Swedish Caledonides. *Geologiska Föreningen i Stockholm Förhandlingar*, 102(4):531–550.

Kumpulainen, R. and Nystuen, J. P. (1985). Late Proterozoic basin evolution and sedimentation in the westernmost part of Baltoscandia. In Gee, D. G. and Sturt, B. A., editors, *The Caledonide Orogen - Scandinavia and Related Areas*. Wiley, Chichester.

Kumpulainen, R. A. (2017). Guide for geological nomenclature in Sweden. *Geologiska Föreningen i Stockholm Förhandlingar*, 139(1):3–20.

Kumpulainen, R. A. and Greiling, R. O. (2011). Evidence for late Neoproterozoic glaciation in the central Scandinavian Caledonides. *Geological Society, London, Memoirs*, 36(1):623–628.

Kumpulainen, R. A., Hamilton, M. A., Söderlund, U., and Nystuen, J. P. (2021). U-Pb baddeleyite age for the Ottfjället Dyke Swarm, central Scandinavian Caledonides: new constraints on Ediacaran opening of the Iapetus Ocean and glaciations on Baltica. *Geologiska Föreningen i Stockholm Förhandlingar*, 143(1):40–54.

Kylander-Clark, A., Hacker, B., and Mattinson, J. (2008). Slow exhumation of UHP terranes: Titanite and rutile ages of the Western Gneiss Region, Norway. *Earth and Planetary Science Letters*, 272(3-4):531–540.

Labrousse, L., Jolivet, L., Agard, P., Hébert, R., and Andersen, T. B. (2002). Crustal-scale boudinage and migmatization of gneiss during their exhumation in the UHP Province of Western Norway. *Terra Nova*, 14(4):263–270.

Ladenberger, A., Be'eri-Shlevin, Y., Claesson, S., Gee, D. G., Majka, J., and Romanova, I. V. (2014). Tectonometamorphic evolution of the Åreskutan Nappe – Caledonian history revealed by SIMS U–Pb zircon geochronology. *Geological Society, London, Special Publications*, 390(1):337–368.

Li, B., Massonne, H.-J., Hartmann, L. A., Zhang, J., and Luo, T. (2021a). Kyanite-garnet granulite from the Andrelândia nappe system, Brasília belt, registers two late Neoproterozoic metamorphic cycles. *Precambrian Research*, 355:106086.

Li, B., Massonne, H.-J., and Yuan, X. (2021b). Pressure-Temperature Evolution of a Mylonitic Gneiss from the Lower Seve Nappe in the Handöl Area, Central Sweden. *Journal of Earth Science*, 32(6):1496–1511.

Li, B., Massonne, H.-J., and Zhang, J. (2020). Evolution of a gneiss in the Seve nappe complex of central Sweden – Hints at an early Caledonian, medium-pressure metamorphism. *Lithos*, 376-377:105746.

Li, B., Massonne, H.-J., and Zhang, J. (2021c). Reply to the comment by Klonowska et al. on the paper "Evolution of a gneiss in the Seve nappe complex of central Sweden – Hints at an early Caledonian, medium-pressure metamorphism" by. *Lithos*, 400-401:106384.

Li, Y., Gee, D. G., Ladenberger, A., and Sjöström, H. (2021d). Timing of deformation, metamorphism and leucogranite intrusion in the lower part of the Seve Nappe Complex in central Jämtland, Swedish Caledonides. *Geologiska Föreningen i Stockholm Förhandlingar*, 143(1):55–70.

Liou, J. and Zhang, R.-Y. (2003). Ultrahigh-Pressure Metamorphic Rocks. In *Encyclopedia of Physical Science and Technology*, pages 227–244. Elsevier.

Lorenz, H., Rosberg, J.-E., Juhlin, C., Bjelm, L., Almqvist, B., Berthet, T., Conze, R., Gee, D. G., Klonowska, I., Pascal, C., Pedersen, K., Roberts, N., and Tsang, C. (2019). COSC-1 operational report - Operational data sets (V. 1.2). Technical report, GFZ Data Services.

Lorenz, H., Rosberg, J.-E., Juhlin, C., Bjelm, L., Almqvist, B. S. G., Berthet, T., Conze, R., Gee, D. G., Klonowska, I., Pascal, C., Pedersen, K., Roberts, N. M. W., and Tsang, C.-F. (2015). COSC-1 – drilling of a subduction-related allochthon in the Palaeozoic Caledonide orogen of Scandinavia. *Scientific Drilling*, 19:1–11.

Ma, C., Majka, J., Benowitz, J. A., Barnes, C., Sjöström, H., Gee, D. G., and Steltenpohl, M. G. (2022). Exhumation of continental margin rocks from mantle depths to orogenic foreland: example from the Seve Nappe Complex of the central Scandinavian Caledonides. *International Journal of Earth Sciences*, 111(8):2925–2950.

Magnusson, N., Thorslund, P., Brotzen, F., Asklund, B., and Kulling, O. (1962). *Ba 16 Beskrivning till karta över Sveriges berggrund*. Sveriges Geologiska Undersökning.

Majka, J., Be'eri-Shlevin, Y., Gee, D., Ladenberger, A., Claesson, S., Konečný, P., and Klonowska, I. (2012). Multiple monazite growth in the Åreskutan migmatite: evidence for a polymetamorphic Late Ordovician to Late Silurian evolution in the Seve Nappe Complex of west-central Jämtland, Sweden. *Journal of Geosciences*, 57:3–23.

Majka, J., Janák, M., Andersson, B., Klonowska, I., Gee, D. G., Rosén, , and Kośmińska, K. (2014a). Pressure–temperature estimates on the Tjeliken eclogite: new insights into the (ultra)-high-pressure evolution of the Seve Nappe Complex in the Scandinavian Caledonides. *Geological Society, London, Special Publications*, 390(1):369–384.

Majka, J., Rosén, , Janák, M., Froitzheim, N., Klonowska, I., Manecki, M., Sasinková, V., and Yoshida, K. (2014b). Microdiamond discovered in the Seve Nappe (Scandinavian Caledonides) and its exhumation by the "vacuum-cleaner" mechanism. *Geology*, 42(12):1107–1110.

Manzotti, P., Regis, D., Petts, D. C., Graziani, R., and Polivchuk, M. (2024). Formation of multistage garnet grains by fragmentation and overgrowth constrained by microchemical and microstructural mapping. *Journal of Metamorphic Geology*, 42(4):471–496.

March, S., Hand, M., Tamblyn, R., Carvalho, B. B., and Clark, C. (2022). A diachronous

record of metamorphism in metapelites of the Western Gneiss Region, Norway. *Journal of Metamorphic Geology*, 40(6):1121–1158.

Nilsen, O. and Wolff, F. (1989). Berggrunnskart Røros og Sveg.

Nilsson, L.-P. and Roberts, D. (2014). A trail of ophiolitic debris and its detritus along the Trøndelag-Jämtland border: correlations and palaeogeographical implications. *Norges geologiske undersøkelse Bulletin*, 453:29–41.

Nordgulen, , Braathen, A., Corfu, F., Osmundsen, P., and Husmo, T. (2002). Polyphase kinematics and geochronology of the late-Caledonian Kollstraumen detachment, north-central Norway. *Norwegian Journal of Geology*, 82:299–316.

Nystuen, J. P. (1980). Stratigraphy of the Upper Proterozoic Engerdalen Group, Kvitvola Nappe, southeastern Scandinavian Caledonides. *Geologiska Föreningen i Stockholm Förhandlingar*, 102(4):551–560.

Nystuen, J. P., Andresen, A., Kumpulainen, R. A., and Siedlecka, A. (2008). Neoproterozoic basin evolution in Fennoscandia, East Greenland and Svalbard. *Episodes*, 31(1):35–43.

Palm, H. (1991). *A reflection seismic image of Caledonian structure in central Sweden*. Number Ca 75 in Sveriges Geologiska Undersökning Serie Ca, Avhandlingar och uppsatser. Sveriges Geologiska Undersökning, Uppsala.

Pease, V., Daly, J., Elming, S.-, Kumpulainen, R., Moczydlowska, M., Puchkov, V., Roberts, D., Saintot, A., and Stephenson, R. (2008). Baltica in the Cryogenian, 850–630 Ma. *Precambrian Research*, 160(1-2):46–65.

Petroleum Experts (2020). FieldMove User Guide.

Petrík, I., Janák, M., Klonowska, I., Majka, J., Froitzheim, N., Yoshida, K., Sasinková, V., Konečný, P., and Vaculovič, T. (2019). Monazite behaviour during metamorphic evolution of a diamond-bearing gneiss: a case study from the Seve Nappe Complex, Scandinavian Caledonides. *Journal of Petrology*, 60(9):1773–1796.

Plink-Björklund, P., Björklund, L., and Loorents, K. (2005). Sedimentary documentation of the break-up of Rodinia, Offerdal Nappe, Swedish Caledonides. *Precambrian Research*, 136(1):1–26.

Powell, R. and Holland, T. J. B. (2008). On thermobarometry. *Journal of Metamorphic Geology*, 26(2):155–179.

Rice, A. H. N. and Anderson, M. W. (2016). Restoration of the external Scandinavian Caledonides. *Geological Magazine*, 153(5-6):1136–1165.

Roberts, D. and Gee, D. G. (1985). An introduction to the structure of the Scandinavian Caledonides. In Gee, D. G. and Sturt, B. A., editors, *The Caledonide Orogen - Scandinavia and Related Areas*. Wiley, Chichester.

Robinson, P. (1995). Extension of Trollheimen tectono-stratigraphic sequence in deep synclines near Molde and Brattvåg, Western Gneiss Region, southern Norway. *Norsk Geologisk Tidsskrift*, 75:181–198.

Robinson, P. and Roberts, D. (2008). A tectonostratigraphic transect across the central Scandinavian Caledonides, Storlien-Trondheim-Lepsøy. Part II: Excursion guide in Norway. Technical Report Report 2008.064, Norges Geologiske Undersøkelse.

Root, D. and Corfu, F. (2012). U–Pb geochronology of two discrete Ordovician high-pressure metamorphic events in the Seve Nappe Complex, Scandinavian Caledonides. *Contributions to Mineralogy and Petrology*, 163(5):769–788.

Rosenberg, C. L. and Handy, M. R. (2005). Experimental deformation of partially melted granite revisited: implications for the continental crust. *Journal of Metamorphic Geology*, 23(1):19–28.

Rosén, (2014). *Metamorphic Evolution of the Middle Seve Nappe in the Snasahögarna area, Scandinavian Caledonides*. Master Degree, Uppsala Universitet, Uppsala.

Röshoff, K. (1978). *Structures of the Tännas augen gneiss Mappe: and its relation to under- and overlaying units in the central Scandinavian Caledonides*. Number C 739 in Sveriges Geologiska Undersökning Ser C Avhandlingar och uppsatser. Sveriges Geologiska Undersökning, Stockholm.

Saalmann, K., Bjerkgård, T., Slagstad, T., Sandstad, J., Lutro, O., Keiding, J., Snook, B., and Angvik, T. (2021). Revised tectonostratigraphy and structural evolution of the Köli Nappe Complex, Central Caledonides in Nordland, Norway. *Journal of the Geological Society*, 178(5):jgs2020–214.

Sawyer, E. W. (2008). *Atlas of Migmatites*, volume Special Publication 9. Canadian Science Publishing, Ottawa, Ontario.

Siedlecka, A., Roberts, D., Nystuen, J. P., and Olovyanishnikov, V. G. (2004). Northeastern and northwestern margins of Baltica in Neoproterozoic time: evidence from the Timanian and Caledonian Orogens. *Geological Society, London, Memoirs*, 30(1):169–190.

Sjöqvist, A. S. L., Arthursson, M., Lundström, A., Calderón Estrada, E., Inerfeldt, A., and Lorenz, H. (2015). An innovative optical and chemical drill core scanner. *Scientific Drilling*, 19:13–16.

Sjöstrand, T. (1999). Bedrock map 19C Storlien SV, scale 1:50 000.

Sjöström, H. (1983). The Seve—Köli Nappe Complex of the Handöl—Storlien—Essandsjøen area, Scandinavian Caledonides. *Geologiska Föreningen i Stockholm Förhandlingar*, 105(2):93–117.

Sjöström, H., Bergman, S., and Sokoutis, D. (1991). Nappe geometry, basement structure and normal faulting in the central Scandinavian Caledonides; kinematic implications. *Geologiska Föreningen i Stockholm Förhandlingar*, 113(2-3):265–269.

Slagstad, T., Pin, C., Roberts, D., Kirkland, C. L., Grenne, T., Dunning, G., Sauer, S., and Andersen, T. (2014). Tectonomagmatic evolution of the Early Ordovician suprasubduction-zone ophiolites of the Trondheim Region, Mid-Norwegian Caledonides. *Geological Society, London, Special Publications*, 390(1):541–561.

Slupski, P. (2023). *Former melt inclusions in garnet from UHP gneisses of the Seve Nappe Complex, Scandinavian Caledonides*. PhD Thesis, University of Padova, Padova.

Smith, D. C. (1984). Coesite in clinopyroxene in the Caledonides and its implications for geodynamics. *Nature*, 310(5979):641–644.

Solyom, Z., Andréasson, P.-G., and Johansson, I. (1979). Geochemistry of amphibolites from Mt. Sylarna, Central Scandinavian Caledonides. *Geologiska Föreningen i Stockholm Förhandlingar*, 101(1):17–25.

Spear, F. S. and Cheney, J. T. (1989). A petrogenetic grid for pelitic schists in the system SiO2-Al2O3 - FeO - MgO - K2O - H2O. *Contributions to Mineralogy and Petrology*, 101:149–164.

Spear, F. S., Kohn, M. J., and Cheney, J. T. (1999). P - T paths from anatectic pelites. *Contributions to Mineralogy and Petrology*, 134(1):17–32.

Stephens, M. B. (2020). Upper and uppermost thrust sheets in the Caledonide orogen, Swe-

den: outboard oceanic and exotic continental terranes. *Geological Society, London, Memoirs*, 50(1):549–575.

Stephens, M. B. and Gee, D. G. (1985). A tectonic model for the evolution of the eugeoclinal terranes in the central Scandinavian Caledonides. In Gee, D. G. and Sturt, B. A., editors, *The Caledonide Orogen - Scandinavia and Related Areas*. Wiley, Chichester.

Stephens, M. B., Kullerud, K., and Claesson, S. (1993a). Early Caledonian tectonothermal evolution in outboard terranes, central Scandinavian Caledonides: new constraints from U-Pb zircon dates. *Journal of the Geological Society*, 150(1):51–56.

Stephens, M. B., Stejskal, V., and Antal, L. (1993b). Geologiska och geofysiska undersökningar i Landögssjöområdet, Jämtlands län. Technical Report BRAP rapport 93017, Sveriges Geologiska Undersökning.

Strömberg, A. G. B., Karis, L., Zachrisson, E., Sjöstrand, T., and Skoglund, R. (1984). Ca 53 Berggrundskarta över Jämtlands län utom förutvarande Fjällsjö kommun.

Svenningsen, O. (2001). Onset of seafloor spreading in the Iapetus Ocean at 608 Ma: precise age of the Sarek Dyke Swarm, northern Swedish Caledonides. *Precambrian Research*, 110(1-4):241–254.

Tegner, C., Andersen, T. B., Kjøll, H. J., Brown, E. L., Hagen-Peter, G., Corfu, F., Planke, S., and Torsvik, T. H. (2019). A Mantle Plume Origin for the Scandinavian Dyke Complex: A "Piercing Point" for 615 Ma Plate Reconstruction of Baltica? *Geochemistry, Geophysics, Geosystems*, 20(2):1075–1094.

Thelander, T. (2009). *K 222 Description to the bedrock map the Caledonides in northern Sweden*. Sveriges geologiska undersökning, Uppsala.

Topuz, G. and Altherr, R. (2004). Pervasive rehydration of granulites during exhumation - an example from the Pulur complex, Eastern Pontides, Turkey. *Mineralogy and Petrology*, 81(1-2):165–185.

Tucker, R. D., Robinson, P., Solli, A., Gee, D. G., Thorsnes, T., Krogh, T. E., Nordgulen, , and Bickford, M. E. (2004). Thrusting and extension in the Scandian hinterland, Norway: New U-Pb ages and tectonostratigraphic evidence. *American Journal of Science*, 304(477-532).

Törnebohm, A. (1877). *Om Sveriges vigtigare diabas- och gabbro-arter*, volume 14 of *Kongliga Svenska Vetenskaps-Akademiens Handlingar*. Kongliga Svenska Vetenskaps-Akademien.

Törnebohm, A. E. (1872). *En geognostisk profil öfver den skandinaviska fjällryggen mellan Östersund och Levanger*. Number C 6 in Sveriges Geologiska Undersökning Serie C, Avhandlingar och uppsatser. Sveriges Geologiska Undersökning.

Törnebohm, A. E. (1888). Om fjällproblemet. *Geologiska Föreningen i Stockholm Förhandlingar*, 10(5):328–336.

Törnebohm, A. E. (1896). Grunddragen af det centrala Skandinaviens bergbyggnad. *Kungliga Svenska Vetenskapsakademiens Handlingar*, 28(5):212 pp.

van Roermund, H. (1985). Eclogites of the Seve Nappe, central Scandinavian Caledonides. In Gee, D. G. and Sturt, B. A., editors, *The Caledonide Orogen - Scandinavia and Related Areas*. Wiley, Chichester.

Walczak, K., Barnes, C. J., Majka, J., Gee, D. G., and Klonowska, I. (2022). Zircon age depth-profiling sheds light on the early Caledonian evolution of the Seve Nappe Complex in west-central Jämtland. *Geoscience Frontiers*, 13(2):101112.

Wei, C. J., Powell, R., and Clarke, G. L. (2004). Calculated phase equilibria for low- and medium-

pressure metapelites in the KFMASH and KMnFMASH systems. *Journal of Metamorphic Geology*, 22(5):495–508.

White, R. W. and Powell, R. (2002). Melt loss and the preservation of granulite facies mineral assemblages. *Journal of Metamorphic Geology*, 20(7):621–632.

Whitney, D. L. and Evans, B. W. (2010). Abbreviations for names of rock-forming minerals. *American Mineralogist*, 95(1):185–187.

Williams, I. S. and Claesson, S. (1987). Isotopic evidence for the Precambrian provenance and Caledonian metamorphism of high grade paragneisses from the Seve Nappes, Scandinavian Caledonides. *Contributions to Mineralogy and Petrology*, 97:205–217.

Winter, J. D. (2014). *Principles of igneous and metamorphic petrology*. Pearson Education, Harlow, 2. ed., pearson new internat. ed edition.

Winter, J. D. (2021). Metamorphic Grades, Zones, Facies and Facies Series. In *Encyclopedia of Geology*, pages 439–444. Elsevier.

Yngström, S. (1969). *Åretraktens metamorfa berggrund*. Unpublished PhD Thesis, Stockholm University.

Zachrisson, E. and Sjöstrand, T. (1990). Berggrundskartorna 22E.

Zou, L., Guo, J., Zhang, L., Huang, G., Jiao, S., Tian, Z., Wang, D., and Liu, P. (2024). Paleoproterozoic ultrahigh-temperature mafic granulites with a high-pressure prograde path from the Alxa Block: Implications on the tectonic evolution of the Khondalite Belt, North China Craton. *Journal of Metamorphic Geology*, 42(4):551–581.

Zwart, H. (1974). Structure and metamorphism in the Seve-Köli Nappe Complex (Scandinavian Caledonides) and its implications concerning the formation of metamorphic nappes. *Centenaire de la Société Géologique de Belgique*, pages 129–144.